Analysing Efficacy of Padded Clothing in Rugby using Finite Element Analysis

S A IMAM

PhD 2021

Analysing Efficacy of Padded Clothing in Rugby using Finite Element Analysis

SYED ADIL IMAM

A thesis submitted in partial fulfilment of the requirements of

Manchester Metropolitan University

for the degree of Doctor of Philosophy

Department of Engineering

Manchester Metropolitan University

in collaboration with World Rugby™

2021

Abstract

World Rugby™ allows players to wear padded clothing to reduce the risk of soft tissue injuries, such as cuts and lacerations. Such padding must meet the requirements of World Rugby™ Regulation-12, which limits its density (45 + 15 kg·m^{-3}), thickness (10 + 2 mm) and impact attenuation performance (acceleration >150 g for a 14.7 J impact). Regulation-12 was critiqued and areas for improvement were identified. From the findings from this PhD, alternative tests to replace the material density criterion in Regulation-12 were investigated and a suitable hardness test (adapted from ISO 2439) was identified. Hertzian contact modelling was used to define a suitable hardness[1] limit (750 N) recommended for future testing.

To assess the efficacy of the rugby padding in reducing the risk of cuts and lacerations, a silicone based surrogate model (mimicking simplified shoulder anatomy with bone, muscle and skin layer) was developed by a PhD student at the University of Sheffield. In this study, a finite element model mimicking the shoulder surrogate was generated and compared against experimental impact testing at energies of 4.9, 9.8 and 14.7 J. Material modelling of the surrogate silicone was carried out using quasi-static compression and stress relaxation testing. Different hyperelastic models were compared against experimental impact data and a 5-parameter Mooney-Rivlin material model along with the 2-term Prony series was found to be the best predictor of performance over the three impact energies.

The validated model was used to predict damage to the silicone using novel FE modelling techniques. These techniques involved defining an element deletion criterion, whereby elements on the surface of the surrogate were deleted if the principal stress of the element reached a predefined value. Stud impacts were carried out at three different energies (2, 4 and 6 J), at three angular orientations (0°, 15° and 30°) and compared to simulations to analyse the validity of the FE model

---

[1] Hardness defined as per ISO:2439-Indentation Technique

(difference < 15 % for force at tear and < 30 % for time to tear). The novel FE model developed was shown to predict damage for raking simulations and for testing different padding structures. The modelling techniques developed in this research can be applied to different skin simulants to assess the extent of skin injuries and assess the efficacy of PPE used to protect against such injuries. For future work, the model can be further developed into a tool for assessing efficacy of PPE in reducing skin injuries.

Outputs from this thesis

1. **Imam, S**., Driscoll, H., Winwood, K., Venkatraman, P. and Allen, T., 2020. Efficacy of Density in Predicting the Protective Properties of Padded Clothing in Rugby. In *Multidisciplinary Digital Publishing Institute Proceedings* (Vol. 49, No. 1, p. 38).

2. Dr Tom Allen, Prof Matt Carré, Dr Heather Driscoll, Angus Hughes and **Adil Imam**. *Review of World Rugby™ Regulation-12 – Update on Report III following Manufacturers Meeting 2020*. Submitted to World Rugby™- January 2021.

3. Dr Tom Allen, Prof Matt Carré, Dr Heather Driscoll, Angus Hughes and **Adil Imam**. *Review of World Rugby™ Regulation-12 – Report III - Recommendations for Regulation-12 Update*. Submitted to World Rugby™- September 2020.

4. Dr Tom Allen, Prof Matt Carré, Dr Heather Driscoll, Angus Hughes and **Adil Imam**. *Review of World Rugby™ Regulation-12 – Padded Clothing- Report II - Update and Testbed Development*. Submitted to World Rugby™- February 2020.

5. Dr Tom Allen, Dr Matt Carré, Dr Heather Driscoll, Angus Hughes and **Adil Imam**. *Report I - Regulation-12: Critique, Assessment and Recommendations*. Submitted to World Rugby™- January 2019.

6. Dr Tom Allen, Dr Matt Carré, Dr Heather Driscoll, Angus Hughes and **Adil Imam**. *Literature Review of Injuries relevant to padded clothing used in rugby union*. Submitted to World Rugby™- April 2018.

Invited / Conference Talks

25th March 2021: MMU-UNAM Binational Seminar: Oral Presentation.

6th January 2021: Oral Presentation: FE-Analysis of padded clothing in Rugby- MMU Biomedical Seminar.

17th November 2020: Oral Presentation: World Rugby™ Regulation-12 Research- World Rugby™ Manufacturers Meeting 2020.

25th June 2020: Oral Presentation: Density or Compliance? - Material Property of padded clothing in Rugby. 13th conference of the International Sports Engineering Association, Tokyo, Japan.

30th January 2019: Oral Presentation: Analysis of Rugby padding using Finite Element Analysis 3rd Sport Engineering Seminar Day – Loughborough University.

Scientific Talks

7th March 2018: MMU PGR Conference- Poster Presentation: Analysis of rugby padding using finite element modelling.

16th May 2018: MMU 3MT- Science and Engineering Heat.

13th September 2018: Poster Presentation- Science and Engineering Symposium- MMU -Analysing protective properties of padded clothing rugby.

6th March 2019: MMU PGR Conference –Poster and Oral Presentation.

13th May 2019: MMU 3MT- Science and Engineering Heat.

12th September 2019: Oral Presentation- MMU Science and Engineering Symposium.

20th February 2020: 3-Minute Lightning Talk- 4th Sport Engineering Seminar Day – Advance Wellbeing Research Centre-Sheffield.

4th March 2020: MMU PGR Conference- Roots and Reach- 3- Minute Lightning Talk.

6th July 2020: MMU 3MT- University Finals.

Acknowledgements

I would like to start by thanking World Rugby™, for funding this research and providing me the opportunity to pursue my research, and Marc Douglas for his guidance.

I would like to thank my supervisors, Drs Tom Allen, Heather Driscoll, Keith Winwood and Prabhuraj Venkatraman for their support throughout this PhD. Thank you to Prof. Matt Carré and Angus Hughes at University of Sheffield for fabricating and providing samples of silicones used in this study. Special thanks to the technicians, Mike Green, Stephen Moyle, Bob Bamford, John Penfold and Tony Dickenson, without them, no testing would have been possible.

To my colleagues: Ruth, Chloe, Laila, Ola, George, Todd, Gemma, Will & Matteo, you all have made this journey memorable, and I will always be grateful to you. To my adopted family in the UK, Georgia, Ben, Sabiah, Cath, Fateha, Juan, James and everyone at Styal CC, thank you for keeping me sane and being there for me at all times.

Mary & Mason, thank you for everything you both do. Words can't describe what y'all mean to me.

Ammi & Baba

ہر چیز کے لیے آپ کا بہت شکریہ. امید ہے کہ آپ کو میرے کام پر فخر ہے.

Lubna (Aapi), Bushra (Baaji) and Hajra (Bajjo), Faisal, Hassan and Mosharraf Bhai, thank you for the most wonderful gifts in my life: Suhaib, Aarifah, Ayesha, Zainab, Yusra and Yumna.

Sana, thank you for changing my life for good, being a pillar of support and being your amazing self.

Contents

Table of Figures

Table of Tables

Acronyms, Definitions & Terminologies used

Term	Definition / Explanation
PPE	Personal Protective Equipment
Rugby	Rugby Union
World Rugby™	The governing authority of the sport of Rugby Union
Regulation-12	Sections of the World Rugby™ pertaining to rules and regulations regarding shoulder / body padding
Cut and Laceration[2]	A cut is a break or opening in the skin. It is also called a laceration. A cut may be deep, smooth, or jagged.
Abrasion	a wound caused by friction or scraping, part of the skin is missing
In-Vivo	experimentation using a whole, living organism as opposed to a partial or dead organism
In-Vitro	studies conducted using components of an organism that have been isolated from their usual biological surroundings in order to permit a more detailed or more convenient analysis than can be done with whole organisms
Ex-Vivo	experimentation or measurements done in or on tissue in an artificial environment outside the organism with the minimum alteration of natural conditions.
CAD	Computer Aided Design
FE	Finite Element- used in different terms such as FE-Modelling and FE-Analysis

---

[2] U.S National Library of Medicine : https://medlineplus.gov/ency/article/000043.htm

ISO	International Organization for Standardization
BSi	British Standards Institution
ASTM	American Society for Testing and Materials
HSV	High Speed Video
E	Young's Modulus
v	Poisson's Ratio
SD	Standard Deviation

1.   Introduction, Aim and Objectives

This thesis documents the assessment of current regulations on padded clothing in rugby and the development of a finite element (FE) model capable of simulating injuries such as cuts and lacerations on the human skin tissue. The findings of this research will be used to provide recommendations to World Rugby™ to help improve the regulations on padding clothing. This chapter outlines the research questions posed by World Rugby™ along with the aim and objectives of this PhD project.

1.1   Introduction to Research Questions

The origins of rugby lay in different types of football games and other sports such as Ki-o-Rahi (New Zealand), Marn Grook (Australia) and Caid (Ireland). The first reports of the game of rugby date to 1823, where a 16-year-old supposedly ran with a football in his arms at Rugby school. From the formation of the Rugby football union in 1871 to the Six nations in 2000, rugby has grown considerably with participation rates increasing from 7.7 to 8.5 million within 2016 (World Rugby™, 2017). Some of the targets set out under the World Rugby™ Strategic Plan for 2021-2025 (World Rugby™, 2021) state:

"Lead targeted research informing and advancing injury prevention and mental wellbeing" and

"Advance player welfare law review and trials to further protect players"

Chadwick et al. (2011) stated that the rugby merchandise market was worth USD 18.5 billion in Japan (host nation for the 2019 Rugby World Cup). With the plans of World Rugby™ to expand and involve more players, the market value of equipment used in rugby is likely to increase. With the number of players increasing, there is a broader spectrum of skill and level of competition. Sinclair (2009) claims that at the semi-professional and professional levels, incentives and monetary benefits have made the game more competitive while increasing the risk

of injury. To combat this increased injury risk, they also claim that more players now wear some form of padded clothing. Sinclair (2009) also states that while there are more studies on rugby PPE, both to ensure the protection of players and to substantiate manufacturers' claims, it is unclear as to whether it does reduce the risk of injuries.

To govern the padded clothing used, World Rugby™ have defined a set of specifications and directives in the World Rugby™ Handbook, specifically Regulation-12. Regulation-12 is further divided into three schedules; this research was focused on Schedule 1: *Specifications relating to Players' Dress-Shoulder Pads.* Schedule 1 focusses on padded clothing, providing guidelines for i) design and construction; ii) material specifications, and iii) performance requirements and test methods. With continual technological and material advancements, there is a need to review the regulations monitoring the performance requirements of padded clothing.

The aim of the overarching project defined by World Rugby™ was: "To create a new Regulation-12, with respect to padded clothing, to reflect the developing game of rugby." As part of the project, two postgraduate researchers (i.e. PhD students) at the University of Sheffield and the Manchester Metropolitan University, worked in collaboration, to critique Regulation-12 based on the scientific literature and to develop test methodologies to analyse padded clothing using novel techniques. The research questions that were raised by World Rugby™ to be addressed were as follows:

RQ1) Is the current requirement for padded clothing appropriate for the modern game of rugby, how and why?

RQ2) Is the current requirement for padded clothing appropriate in permitting the use of modern technology, how and why?

RQ3) Considering that the intention for padded clothing is to continue to protect against cuts and lacerations only, devise an updated regulation with testing procedures that permits the latest technology.

RQ4) If no restriction were placed on the performance of padded clothing by World Rugby™, what would the development of such clothing look like?

The researcher at the University of Sheffield focused on defining the injury biomechanics and developing a mechanical test to emulate an event causing an injury such as a cut or laceration. The researcher also investigated the use of a synthetic shoulder surrogate, incorporating a skin and soft tissue simulant, to test if padding material can reduce the risk of a cut or laceration to skin tissue. Meanwhile, this research, at the Manchester Metropolitan University, investigated padding materials and the development of a FE model for simulating impact scenarios, to assess the efficacy of padding material in reducing the risk of injuries such as cuts and lacerations (Figure 1-1).
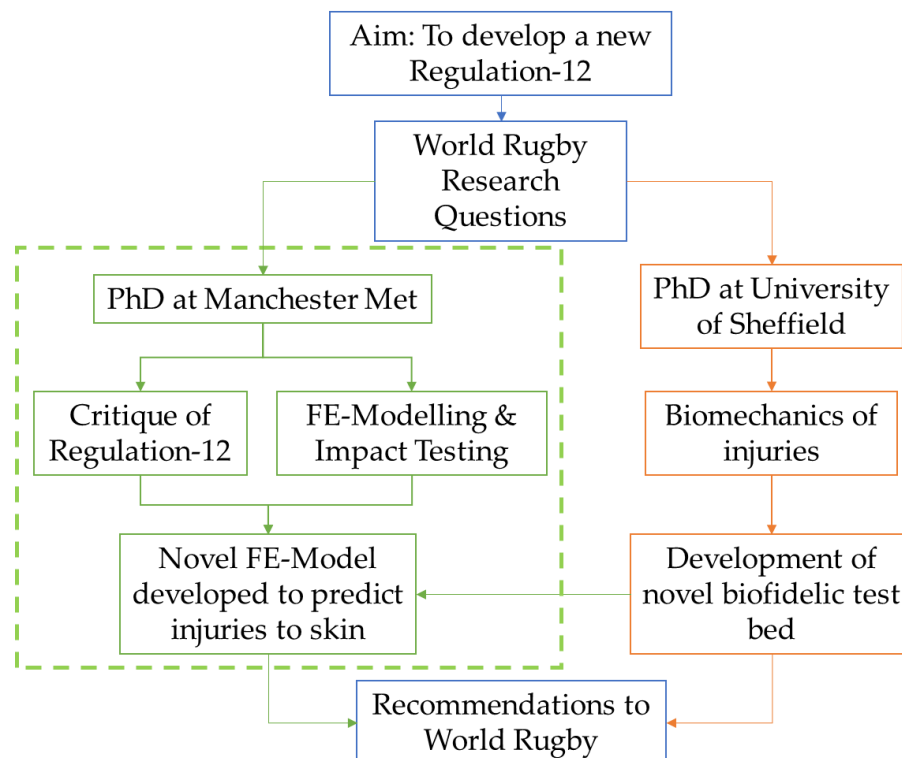
Figure 1-1: Overall layout of the project and the two PhD researches carried out.

This PhD research had two phases: (i) critiquing the current regulations, testing methodologies and materials used for padded clothing in rugby and (ii) developing an FE model capable of predicting injuries to the human skin tissue. The intention of this PhD research was to assess the padded clothing for protection specifically against cuts and lacerations only and not as an equipment to reduce injuries such as fractures and dislocations, which is a common misconception of the intention of such clothing. An FE model of the human skin tissue based on the research at the University of Sheffield was to be developed. Using novel simulation techniques, the FE model would be the first to predict injuries such as cuts and lacerations on the human skin tissue and hence the ability of an item of padded clothing to reduce the risk of such injuries. The findings of this research will inform recommendations provided to World Rugby™, to help them draft and create a new Regulation-12.

1.2 Aim and Objectives

The aim of this thesis was to develop a FE model capable of analysing the efficacy of paddings used in rugby specifically against injuries such as cuts and lacerations.

1. To review current literature relating to injury mechanisms in rugby, protective sports clothing, FE modelling of PPE and skin tissue, and advances in apparel and material technologies.

2. To critically review current regulations for padded clothing (Schedule 1-Players Dress - Shoulder padding, only) in rugby to identify gaps and areas of improvement.

3. To identify materials that could be used to prevent cuts and lacerations in rugby and identify any unintended consequences of permitting these materials.

4. To develop and validate an FE model to predict the performance of a biofidelic impact surrogate mimicking the human skin, fat and muscle layer.

5. To apply the developed model to predict injury to human skin tissue which could then be used to analyse current and futuristic materials in their ability to prevent injuries such as cuts and lacerations.

6. To recommend methods for testing padded clothing designed to reduce cuts and lacerations in rugby.

1.3 Thesis Structure

The PhD project was focused on developing novel FE models, capable of predicting injuries such as cuts and lacerations, which will help inform the Regulation-12 updates on shoulder pads. The project followed a problem-oriented approach (Lawrence, 1992), wherein the literature and Regulation-12 were critiqued, and the problems identified. The research then focused on finding solutions based on the literature and developing novel test methods to fill gaps. FE modelling techniques were used to model and test injury scenarios as there are ethical considerations associated with testing on human skin. While physical testing of skin surrogates would require regular change of simulant, validated FE models would allow repeatable testing of various designs of padded clothing in a controlled manner without the need for prototyping every design. FE models can also provide a wealth of information which may not be easily available during physical testing, such as full-field strain mapping or the physical response at any given location.

Using the problem-oriented approach can help in resolving the issues faced, but the real-world application of the regulation needs to be controlled. Changes to the regulations can lead to a change in interpretation of the ruling, by PPE manufacturers and test houses, leading to miscommunication and complications. During this research, by cooperating with the padding manufacturers and test house facilities, under the support and guidance of World Rugby™, the hope is to ensure that the recommendations are easily adopted and that they do not alter the nature of the game.

Figure 1-2 showcases the content of the thesis and the path followed during this research. The literature on injuries in rugby and associated PPE, along with existing FE based studies, will be reviewed in Chapter 2. Regulation-12 documentation will be critiqued, and the impact testing methodology will be studied using World

Rugby™ approved samples of padding (Chapter 2). The findings of the review in Chapters 2 and 3 will be summarized at the end of Chapter 3 as areas of concern and research foci, which will then shape the rest of the research.
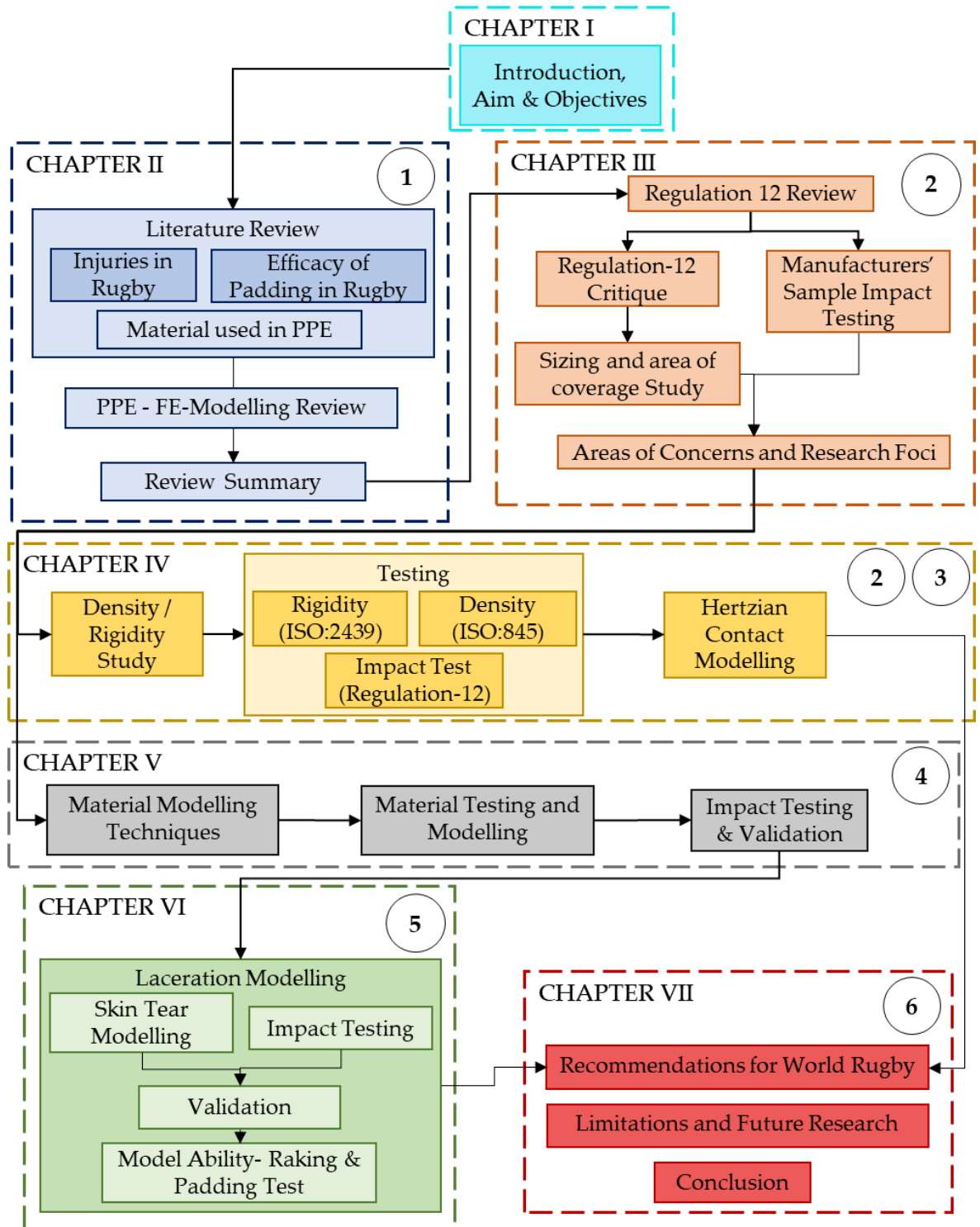
Figure 1-2: Schematic indicating the thesis layout and content of each chapter (colour coded and denoted in dashed boxes). Circled number corresponds to the objective number.

Study of a potential alternate physical property to replace the density criterion (padding $\leq$ 60 kg·m^{-3}) for padded clothing in Regulation-12, which is hard to measure, will be carried out in Chapter 4. Chapters 5 and 6 will focus on developing the FE model capable of mimicking injuries such as cuts and lacerations. Chapter 5 will focus on the different material models and then details the development of the biofidelic shoulder surrogate FE model followed by validation against impact testing. Chapter 6 will detail the testing and validation of the biofidelic surrogate against both stud impact and raking tests. Based on the findings in each of the chapters, the recommendations to World Rugby™ for updating the regulation along with limitations and future research will be presented in Chapter 7. Chapter 2 will present a review of the literature on injuries in rugby, materials used in PPE (rugby and other industries) and the study of FE based research.

2.   **Literature Review**

The aim of this review is to assess the literature relating to injury in rugby union and to establish the associated injury mechanisms. When assessing sports personal protective equipment (PPE), it is important to consider the anatomy it aims to protect. In the following chapter, the incidence and severity of injuries in rugby union will be reviewed, with close attention to shoulder injuries. Current knowledge is collated to understand the extent of injuries in rugby, especially those to the skin tissue, like cuts and lacerations, as well as how padded clothing may prevent and reduce the severity of injury.

2.1   **Introduction**

Injury prevention research has been described by Van Mechelen et al. (1992) as a four-step process (Figure 2-1), and this review will cover the first two.
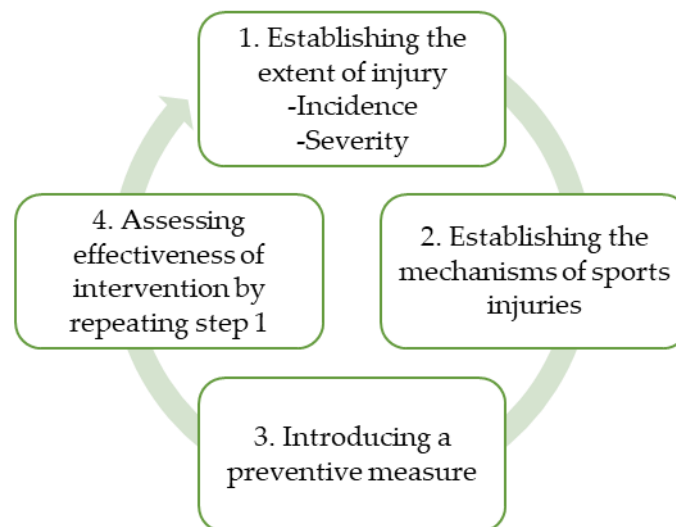
Figure 2-1: Four-step sequence of injury prevention research (adapted from Van Mechelen, 1992).

To assess and better understand the use of PPE in sports, the epidemiology and mechanisms of injury must be considered (Payne et al., 2016). Extant research is aimed at exploring the regulations (World Rugby™ Regulation-12) and technical advancements with regards to padded clothing in rugby union, with a focus on jerseys. While the regulations permit padding on any part of the

jersey, the tests and requirements tend to focus on shoulder padding, as do many commercial products. Research into shoulder padding in rugby union has found that it can attenuate impact force and may therefore reduce the chance and severity of injury (Harris and Spears, 2010). As World Rugby™ specifically identifies padded clothing to reduce injuries on the human skin only, the focus of this review is to assess the extent of injuries such as cuts and lacerations in rugby union.

2.2   Injury Definition and Occurrence in rugby union

Injuries in sports are common, but the trauma is often less severe than an automotive crash or ballistic injuries for example (Payne et al., 2013). The regular occurrence but often low severity of sports injuries is thought to be because athletes can experience multiple loads to the same location during competition or training (Tsui, 2011). To report injury, definitions must be made, although this can be complex as they can vary within and between sports and between researchers (Hodgson et al., 2007). A consensus statement regarding injury definition in rugby union has been published, which splits injury into two categories, a 'medical-attention' injury (less severe) and a 'time-loss' injury (more severe) (Fuller et al., 2007:329), as follows:

"*An injury that results in a player receiving medical attention is referred to as a 'medical-attention' injury and an injury that results in a player being unable to take a full part in future rugby training or match play as a 'time-loss' injury.*"

Despite its popularity and widespread appeal, rugby has one of the highest injury occurrences amongst contact sports (Marshall et al., 2002). There is much research into the surveillance and understanding of rugby injuries (Brooks et al., 2005a; Freitag et al., 2015; Orr and Cheng, 2016; Yeomans et al., 2018). There are different ways of reporting sports injuries, such as the number per game or the incidence of injury. Reporting injuries per game or the number of incidences is not recommended, as this approach does not account for the number of

players or exposure hours. Injury reporting, to be comparable across sports, should be reported as rates or per player hours to account for exposure time to risk (Phillips, 2000). Williams et al. (2013) carried out a meta-analysis of injury occurrences amongst team sports, concluding that on average there are 81 injuries per 1,000 player match hours (PMH) in rugby union, which is higher than reported for tennis (31 injuries per 1,000 PMH), cricket (48 injuries per 1,000 PMH), field hockey (25-58 injuries per 1,000 PMH) and soccer (65-76 injuries per 1,000 PMH) (Brooks and Kemp, 2008; Levi et al., 2020; Moore et al., 2015; Nicholl et al., 1995).

Eighty-one injuries per 1,000 PMH, between the years 1995 and 2012, as reported by is lower than the 90 injuries per 1,000 PMH at the 2015 World Cup (Fuller, 2016), but similar to 79 injuries per 1,000 PMH at the 2019 World Cup (Fuller et al., 2020). Fuller et al. (2020) also states that the incidence, severity, and nature of the injuries at Rugby World Cup 2019 were similar to those reported at previous World Cups. West et al. (2020) studied the pattern of injuries in elite rugby clubs for 1.5 million hours between 2008 and 2018 (11 seasons). Their findings suggest that the incidence rate over 11 seasons did not change significantly, but the severity of injuries associated with training increased in each season barring two (2009-2010 and 2013-2014).

Moore et al. (2015) state that injury rates may be underreported if data is collated across different teams. Their study of injuries in the Welsh national team over a period of three years (2012-2104) reported injury rates of 263 per 1,000 PMH, which was three times higher than those reported by Fuller et al., across all teams in different tournaments, between 2012 and 2017. The injury rates reported by Moore and colleagues were similar to those for the England national team during the 2003 Rugby World Cup, where match injury incidence was reported at 218 injuries per 1,000 PMH (Brooks et al., 2005a) (excluding training which was 6 per 1,000 PMH). The differences in incidence rates

between studies highlights that even though the injury incidence rates in rugby are higher than for other sports, the true values may be higher still.

Understanding what types of injuries occur in sport can direct injury prevention research (Bahr and Krosshaug, 2005). Injury research in rugby union has grouped types of injury into bone (4-9%), joint / ligament (28-52%), muscle / tendon (33-46%), skin (0-3%) and brain / peripheral nervous system / spinal cord (5-9%) (Fuller et al., 2013; Fuller et al., 2008; Brooks et al., 2005a; Fuller et al., 2011; Fuller et al., 2010). Injury severity has also been grouped, based on time loss: minimal, 2-3 days (19.1%), mild, 4-7 days (28.9%), moderate, 8-28 days (26.0%), severe, >28 days (26.0%).

Lacerations, abrasions and contusions can be classified as mild and may be considered less severe than many other rugby union injuries. Brooks et al. (2005a) found laceration and skin injuries to cause on average 5.3 days of time loss, meanwhile Fuller et al. (2008) found contusions to cause on average 5.0 days of time loss. When compared to joint and ligament injuries (20.6 days), or bone stress and fractures (50.2 days), the lower time loss for lacerations and abrasions suggests that they are less severe. Any time loss in a player's training regime may reduce performance and for the professional game, incur a financial loss. Cuts and lacerations can also be highly visual (i.e. blood / bleeding), which may negatively influence public perception of rugby.

Table 2-1 summarizes the laceration, abrasion and contusion rates reported in sixteen articles. Twelve articles measured injury rates at the elite level, three at amateur level and one at all levels. Laceration injury rates (cuts and lacerations were grouped together) per 1,000 PMH range from 0 - 21 (0 - 27% of injuries), abrasions 0 - 2 (0 – 2% of injuries) and contusions 0 – 20 (5 – 24% of injuries). The inter-study variance in reported incidence for lacerations, abrasions and contusions is thought to be due to differing injury definitions and estimating the true rate of these injuries can be problematic.

Table 2-1: Laceration, Abrasion and Contusion injury statistics (Adapted from the work of Angus Hughes).

Study	Playing Level / Competition	Injury Definition	Total Recorded Injuries	Lacerations		Abrasions		Contusions / Haematomas	
				Overall Incidence Rate	% Total Injuries	Overall Incidence Rate	% Total Injuries	Overall Incidence Rate	% Total Injuries
Jakoet and Noakes (1998)	International – Rugby World Cup RWC 1998	Leave the field	70 M	8.64	27.00	-	-	7.68	24.00 (All muscle injuries)
Bathgate et al. (2002)	International – Australia	Leave the field or miss subsequent game	143 M	15.87	23.00	-	-	6.90	10.00
Junge et al. (2004)	School Boy – New Zealand	Physical Complaint	340 M+T	1.45	2.90	-	-	10.60	21.50
Best et al. (2005)	International – RWC 2003	Leave the field or miss subsequent game	189 M	21.24	21.70	1.57	1.60	19.68	20.1
Brooks et al. (2005a)	English Premiership	Time loss	1534 M	1.55	1.17	-	-	16.30	17.91

Brooks et al. (2005b)	English Premiership	Time loss	395 T	0.02	1.01	-	-	0.09	4.50
Brooks et al. (2005c)	International – England	Time loss	145 M+T	0.23	1.38	-	-	2.46	14.48
Collins et al. (2005)	High School - USA	Time loss & medical attention	594 M+T	-	-	-	-	0.47	9.10
Fuller et al. (2008)	International – RWC 2007	Time loss 24hrs +	161 M	0	0	0	0	14.60	17.40
			582 M	0.94	5.50	-	-	-	-
Kerr et al. (2008)	Collegiate Rugby - USA	Time loss 24hrs +	265 T	0.25	4.53	-	-	-	-
Fuller (2009)	Elite – Super 14	Time loss 24hrs +	345 M	3.95	4.10	-	-	-	-
Fuller et al. (2013)	International – RWC 2011	Time loss 24hrs +	171 M	1.60	1.80	0	0	16.10	18.07
Thomson (2014)	Elite – Super 15	Time loss 24hrs +	160 M+T	6.00	4.00	-	-	-	-
Fuller et al. (2016)	International – RWC 2015	Time loss 24hrs +	173 M	1.87	1.70	0	0	12.21	11.00

Sabesan et al. (2016)	Level 1 – Elite – USA	Athlete went to hospital	128,813	-	-	-	-	-	14.40
Fuller et al. (2020)	International-RWC-2019	Time loss 24 hrs +	168 M + T		2.80	-	0		13.30

M is match & T is training.

Overall incidence rate is reported in injuries per 1,000 player hours.

Using the definition "*that a player must leave the field of play for an injury to be counted*", Best et al. (2005) reported 21 lacerations per 1,000 PMH (22% of total injuries). Whereas, Fuller et al. (2013) reported only 1.6 lacerations per 1,000 PMH (2% of all injuries) using the stricter definition of time loss over one day; meaning players could temporarily leave the field of play and then return after medical attention without the injury being counted.

Another way of tracking injury is through insurance claims. In New Zealand, Accident Compensation Corporation (ACC) is a compulsory, personal injury insurance scheme. Ken Quarrie et al. (2020) studied 635,657 rugby injury insurance claims, made through ACC, for players aged 5–40 years over the period 2005–2017. Their findings showed that cuts and lacerations accounted for 6.3% of all reported injuries with 49% of these occurring on the face / head region. They also found that ~14% of all claims were related to shoulder injuries.

As noted by Oudshoorn et al. 2017, using a 'Time-loss' injury definition in rugby research can lead to underestimation of less severe injuries, like lacerations, abrasions and contusions, that do not stop a player from competing. Injury definitions may vary and provide skewed results, especially in terms of cuts and lacerations and epidemiology studies are largely carried out at the elite level, as shown in Table 2-1.

2.3 **Injury Causation and Location**

When forming injury prevention strategies, it is important to understand the events that cause injury (Usman et al., 2011). Rugby includes four main phases of play; tackle, ruck and maul, set piece (scrum and lineout) and open play. The main cause of injury in rugby is the tackle (36 – 56%) (Best et al., 2005; Brooks et al., 2005b; Fuller et al., 2013; Thomson, 2014). Whether a tackle in rugby union causes injury depends on four factors, i) the amount of energy transferred, ii) the contact area over which the force is distributed, iii) the direction of the force and iv) the biomechanical properties of the body structures to which the energy is transferred to and from.

These factors may be influenced by any padding worn by the players. As the tackle is a key injury causing event in rugby union, the biomechanics of injury causing tackles should be further explored to direct injury prevention methods (Bahr and Krosshaug, 2005).

A high proportion of injuries also come from collisions (12 to 20%) (Best et al., 2005; Brooks et al., 2005; Fuller et al., 2013; Thomson, 2014). Many injury surveillance reports do not define what a collision is in rugby union, making it hard to draw conclusions. Fuller et al. (2007) defines a collision as the event in which the "tackler attempts to stop the ball-carrier without the use of his arm(s)". Fuller reported that while less frequent, a collision was almost twice as likely to cause an injury than a tackle. As well as player-to-player interactions, stud-to-player interactions are prevalent (5 lacerations per 1,000 PMH). Oudshoorn et al. (2016) found the ruck to be associated with 56% of stud injuries, with 35% of these caused by stamping from an opponent. It is therefore clear that the ruck is a major cause of stud induced lacerations.

Oudshoorn et al. (2016) surveyed 191 players to better understand the causes of stud induced lacerations during match play. Of those surveyed, i) 97% had experienced minor skin injuries due to studs, which did not hamper their participation in that game; and ii) 71% had experienced major skin injuries due to studs, leading to loss of playing time. Determining the body locations of these stud induced injuries would benefit the current padded clothing research.

Shoulder injuries occur often in rugby union, at 12 per 1,000 PMH (Usman et al., 2015), and have been reported to be the most injured body part during a game (Moore et al., 2015). Despite the regular occurrence of shoulder injuries, little attention has been given to preventing them in comparison to other injury types, like spinal injuries, where consideration has led to the modification of scrum laws (Quarrie et al., 2002). Few studies have focussed solely on shoulder injuries in rugby union despite their frequency and severity. The tackle is thought to be the main

cause of shoulder injuries (25-79%) (Usman et al., 2015; Fuller et al., 2007; Quarrie and Hopkins, 2008). In the men's rugby union World Cup (RWC) and rugby 7s, a player has a similar risk of shoulder injury when both being tackled and making a tackle. It is therefore important to consider shoulder injury mechanisms in the ball carrier as well as the tackler. Contrary to this, in international u20s rugby union the tackler (46-50%) (Fuller et al., 2018; Headey et al., 2007) has been reported to be more in danger of receiving a shoulder injury than the ball carrier (23%) (Headey et al., 2007), which was supported by Usman et al. (2015) who found the tackler (5 per 1,000 PMH) has almost double the chance of shoulder injury than the ball carrier (3 per 1,000 PMH). Usman et al. (2015) reported that over half of shoulder injuries were caused by direct impact to the shoulder, either from a player or the playing surface.

Table 2-2 summarises the types of injuries that occur at the shoulder / clavicle in elite rugby union. Joint sprains and ligament injury are most prevalent (30-45%), followed by dislocations (25-34%). Shoulder padding is not designed to limit the range of movement at the shoulder joint and, therefore, is unlikely to prevent sprains, dislocations and ligament injuries. Contusion is the third most common injury (4-10%) to the shoulder region, which may warrant the use of shoulder padding to limit the severity of such injuries (Pain et al., 2008). Lacerations and abrasions are not reported to occur in the shoulder region, which suggests that wearing shoulder padding to prevent these types of injuries is unwarranted, although the widespread use of the time loss injury definition suggests they may be underreported.

Table 2-2: Match shoulder/ clavicle injury statistics.

Match Injury	Proportion (%)			
	RWC 2007, 2011, 2015 (n=55)	International U20 2008 – 2017 (n=117)	International Rugby 7s 2008 – 2017 (n=117)	Overall Mean
Abrasion	0	0	0	0
Dislocation	25.0	25.4	33.9	28
Bone Injury	3.8	0.9	0.9	2
Haematoma / Contusions	9.6	7.0	4.3	7
Laceration	0	0	0	0
Lesion Meniscus	3.8	3.5	9.6	6
Muscle Rupture	1.9	2.6	4.3	3
Nerve Injury	3.8	7.0	3.5	5
Sprain / Ligament	44.2	44.7	30.4	40
Tendon Injury	5.8	7.0	13.0	9
Other	1.9	1.8	-	2

(Fuller, 2018)

Increased use of artificial pitches in rugby union has led to more skin related injuries. Williams (2015) reported 119 abrasions per 1,000 PMH for elite play on artificial turf, and the most prevalent locations were the knee (74%), lower leg (9%), elbow (7%) and forearm (4%). In this instance, an abrasion did not have to induce time loss to be reported, which may explain the high incidence rate compared with those in Table 2-1. It was also found that abrasions occur 15 times every 1,000 PMH on natural turf, suggesting previous studies may have underestimated this injury type. Shoulder injuries have been reported to be a consistent issue within rugby (Headey et al., 2007; Harris and Spears, 2010; Usman et al., 2011; Crichton et al., 2012; Moore et al., 2015; Quarrie et al., 2020). Moore et al. (2015) state that the protective pads worn in rugby need to be investigated and improved, with a view to reducing the risk of shoulder injury.

2.4   Efficacy of Padding in Rugby

With the literature suggesting an increasing rate of injuries in rugby, and more specifically skin tissue injuries such as cuts, lacerations and abrasions, it is necessary to understand the mechanics of these injuries. Studies have investigated the impact force attenuation of PPE such as headgear used in rugby (Marshall et al., 2001; Marshall et al., 2002; Marshall et al., 2005; Mcintosh et al., 2009). Research has tended to focus on headgear (McIntosh et al., 2009 and McIntosh et al., 2001) with limited work on shoulder padding (Gabbett, 2005).

Research on the performance of padded clothing has provided mixed results. Usman et al. (2011) measured the forces acting through a padded (Canterbury's Flexi Lite) and unpadded shoulder when tackling a 45 kg tackle bag instrumented with pressure sensors (ELF Tekscan™). Their findings suggest that wearing padding does not change the forces acting on the shoulder during a tackle on a bag. A meta-analysis by Gerrard (1998) on the use of shoulder padding in rugby union and American football also found little evidence towards pads decreasing the incidence of severe shoulder injuries. On the other hand, Harris and Spears (2010)

showed shoulder padding can reduce peak impact force by up to 70% during simple laboratory-based impact tests (compared to a bare impact between the impactor and force plate). Testing involved dropping impactors of varying mass and stiffness (2 kg medicine ball and 1 kg hockey ball) onto padding (consumer products of different thicknesses approved by World Rugby™ – Canterbury (10 mm), Kooga (8 mm), Gilbert (8 mm) and Terminator Clothing (4 mm)) that was placed on a force plate. Drop heights were adjusted to give impact energies of 3, 7, 12.5 and 32 J. Impact forces varied between pads, probably due to differences in their thickness and material properties. When forces were normalised to impacts without padding, the padding was more effective at limiting force from an impact with the smaller and stiffer hockey ball than for the heavier medicine ball. Harris and Spears stated that the lower stiffness medicine ball deformed more than the hockey ball upon impact with a bare force plate, and hence adding padding had less effect on force attenuation than for the stiff hockey ball.

Pain et al. (2008) also dropped objects of different mass, size and stiffness (7.26 kg indoor shot put (stiffest), 10 kg medicine ball (intermediate stiffness), and 5 kg weight belt (softest)) onto shoulder padding resting on a force plate. The findings were similar to those of Harris and Spears (2010), with the padding performing better under a stiffer impactor (shot put). Following the drop tests, the rugby pads were instrumented with thin film force sensors (Tekscan F-Socket 9811 force sensor, Boston, MA) to measure impact forces during tackles, involving participants with and without pads. Their findings suggested that shoulder pads on average reduced peak forces by 40% for all tackles. The impact force reduction was localised above the acromioclavicular joint and forces in other regions were not reduced.

The test method in World Rugby™ Regulation-12 states that shoulder padding must be impacted with a flat faced metal disc (115 mm Ø). Research has shown that the stiffness of the impactor can affect the performance of pads, which were more effective at reducing impact force from stiffer impactors (Pain et al., 2008; Harris

and Spears, 2010). Hence, suggestions have been made to use more biofidelic (more human-like) impactors and anvils, so the resulting impact trace during testing matches an actual rugby tackle more closely (Harris and Spears, 2010; Pain et al., 2008). Authors have called for a study with more participants with a view to better understand the force attenuation capabilities of shoulder padding in rugby tackles (Harris and Spears, 2010; Usman et al., 2011).

Due to the lack of research on a range of padding and its performance using appropriate testing methods, there is a need for detailed research investigating the efficacy of shoulder padding used in rugby. Such research could cover the material properties, design and testing of PPE, with a focus on rugby padding.

2.5 Materials Used In PPE

PPE designs can vary between sports depending on the intent of the protection. Sporting protective equipment is intended to reduce the risk of injuries and can be a part of the playing environment (i.e., landing mats or barriers) or be a part of the athletes' attire. PPE used by athletes can be embedded into the garment / attire (i.e., padded clothing in rugby, padded gear in cycling, motor racing or fencing) or worn as an additional item (i.e., helmets, body protection in cricket, shin pads). PPE is typically designed to provide impact protection and reduce peak forces / accelerations, but the intention of World Rugby™ is that rugby shoulder padding is only meant to reduce the risk of superficial injuries of the skin tissue in the form of cuts and lacerations.

Sporting PPE often contains layers of different materials (Figure 2-2). The outer layer of PPE is often a stiff material, or shell, to help distribute the impact force and reduce the pressure acting on the body. PPE also usually has one or more layers of compliant material, typically closed cell foam, for absorbing impact energy and reducing forces / accelerations (Duncan et al., 2018). The specific reduction of forces is dependent on the nature of the padding material and how it deforms under

impact. Gradual deformation of foam under impact can increase the impact duration, lower the impulse, and hence increase the level of protection.

Stiff Material

Padding Material

Fabric
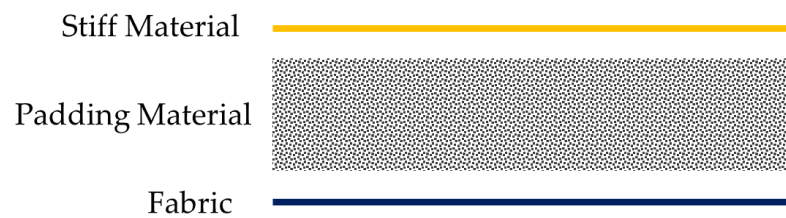
Figure 2-2: Schematic of a typical cross section of a PPE showing the different materials.

With improvements in manufacturing and associated technologies, like additive manufacturing and moulding, researchers can make new materials with varied mechanical properties. Such materials can be made to perform differently in different situations or scenarios. Currently Regulation-12 limits padding material density to a maximum of 60 kg·m^{-3}. Researchers are also able to ensure material properties remain consistent while manipulating the density of padding material. To be able to test the suitability of new and emerging materials for use in rugby it is important to understand their properties. The following sections summarise materials that could be applied to padded clothing for rugby, including those that could be used if the regulations were changed.

2.5.1   Auxetic Materials

Auxetic materials have a negative Poisson's ratio (Evans, 1991), meaning they expand laterally when stretched axially (Figure 2-3). Poisson's ratio is the product of negative one and the ratio of lateral to axial strain.
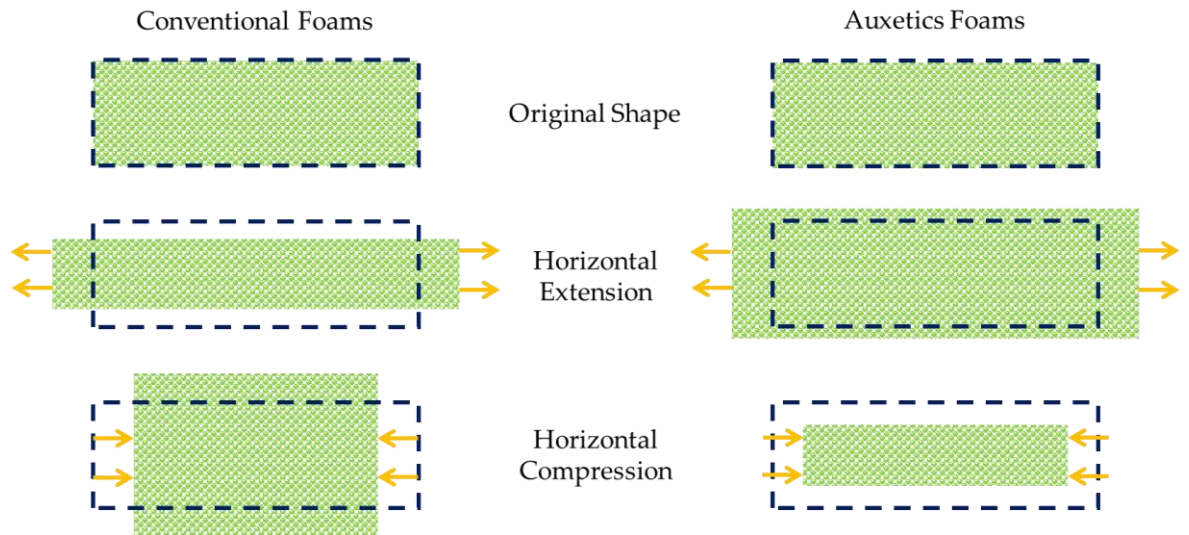
Figure 2-3: Schematic showing comparison between conventional and auxetic foam under deformation due to axial (horizontal) loading. Arrows show load applied and dotted outline depict original shape for reference. Adapted from the work of Duncan et al. (2018).

Auxetic materials / structures have been used in some sporting PPE, including helmets (D3O® Trust, Madillo Helmet Designs, Trail Skills Auxagon), American Football gear (Auxadyne) and running shoes (Nike Flyknit). Reviews on auxetic materials and their current and potential applications in the sports industry have been presented by Duncan et al. (2018) and Kelkar et al. (2020). These reviews highlight enhanced indentation resistance and synclastic curvature as key benefits of auxetic materials and structures. Duncan and colleagues suggest that with development and testing, auxetic materials could bring benefits to rugby tops. Conventional foams can be converted into auxetics foams (e.g., thermo-mechanical process) or auxetic patterns / structures can be cut into them, and these modified foams have shown benefits. Moroney (2021) showed commercial shoulder padding that has been approved by World Rugby™ to contain auxetic patterns / structures (Figure 2-4). It is likely that the auxetic pattern was intended for improved conformability of the padding to the body of the wearer.
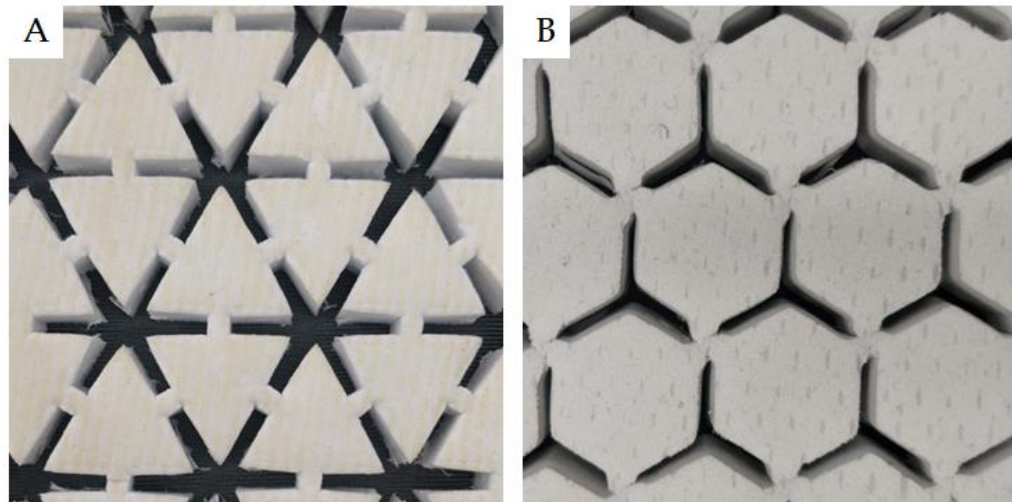
Figure 2-4: Pictures of two samples of commercial rugby paddings showing different auxetic structures.

Chan and Evans (1998) showed auxetic foams (density range: 69-95 kg·m^{-3}) to have improved indentation resilience over conventional foams. Scarpa et al. (2005) converted polyurethane (PU) foam (density: 27 kg·m^{-3}) into auxetic foams, with densities ranging from 75 to 254 kg·m^{-3}. 2-D FE simulations of these foams under indentation predicted lower stresses in the auxetic than the conventional foam. Testing of auxetic foam under impact, at energies between 2 and 15 J (comparable to the 14.7 J impact in the regulation), has shown between ~3 and ~8 times lower peak forces than conventional foams (Allen et al., 2015; Duncan et al., 2016).

While most of the reported auxetic foams had densities above the Regulation-12 limit of 60 kg·m^{-3}, the density (42-52 kg·m^{-3}) of the auxetic foam of Allen et al. (2015) was within this limit. Suggestions by Allen et al. (2015) and Duncan et al. (2018), backed up by evidence of improved properties, such as impact protection and indentation resistance, suggests that auxetic foams may soon be used in rugby padding. More research in this area may result in a wider variety of auxetic foams that meet the Regulation-12 density requirement. With researchers being able to change the physical response of auxetic foams by manipulating the cellular structure, limiting the density of shoulder padding materials in Regulation-12 may become ineffective as these novel materials become commercialised.

2.5.2 Dilatant Materials

Newton's law of Viscosity states that the shear stress between adjacent fluid layers is proportional to the velocity gradients between these layers. The ratio of shear stress (τ) to shear rate is a constant, for a given temperature and pressure and is defined as the coefficient of viscosity (Equation 2-1),

$$\tau = \mu \frac{du}{dy}$$

<div align="right">Equation 2-1</div>

where, μ is viscosity and $\frac{du}{dy}$ is the rate of shear deformation.

For many fluids, the viscosity is independent of the strain rate. Fluids that demonstrate increased viscosity under higher strain rates are termed as dilatant fluids. Since the commercialisation of D3O®'s dilatant material (Energy absorbing material, US Patent 7794827), other brands, such as RHEON™ Reflex (Patent no: US20120021167A1) and Dow Corning-Deflexion™ (Patent no: US20110039087A1), have used similar technologies, with claims of improved impact protection in products for sports like American Football (e.g. Schutt Sports D3O® Liner, Shadow XR), boxing (e.g. OPRO mouthguards), lacrosse (GameBreaker headgear) and field hockey. When impact testing rugby headgear incorporating dilatants (Poron XRD® & D3O® AERO & DECELL), Kajtaz and Subic (2015) reported a 10% reduction in peak force values in comparison to traditional (EVA) foams. Though these materials provided improved force attenuation properties, their use in rugby is restricted as they exceed the density criterion.

Currently, the commercially available dilatant materials have densities starting from 140 kg·m^{-3} (Poron-XRD®) or 500 kg·m^{-3} (D3O®), which is much higher than the 60 kg·m^{-3} limit in Regulation-12. Most of the brands marketing dilatants (D3O® products particularly) claim that their products are abrasion resistant, which could make them effective in reducing injuries such as cuts and lacerations, although this has not been demonstrated nor tested specifically in the scientific literature. While

there is potential for dilatants materials to bring improvements to rugby padding, they are currently not allowed as they are too dense.

2.5.3   Bio-inspired / Biomimetic Materials

Polymer foams are widely used in applications where the mechanical function is important (Svagan et al., 2008). Due to concern over climate change, and our impact on the environment in general, there is a strong motivation to replace petroleum-based polymers with alternatives from renewable resources. For example, starches like Polysaccharide are available from wheat, corn, potato or other plant sources and are of interest as they are widely available and potentially low cost. The properties of starch-based foams have been shown to improve through reinforcement by cellulosic fibres (Soykeabkaew et al., 2004). Regular polymer foams can be modified by adding metal nanoparticles into the cell walls and hence by varying the density of the foam properties can be tailored to meet specific applications (Svagan et al., 2008). The addition of functional nanometre sized elements to biopolymer foams may enhance the mechanical and physical properties, while reducing the mass and gas diffusivity of the polymer film (Zeng et al., 2003).

Svagan et al. (2008) studied the mechanical properties of biomimetic nanocomposite foams by varying the micro fibrillated cellulose (MFC) content. Figure 2-4-A & Table 2-3 show that Svagan and colleagues were able to vary the compressive stress vs. strain response of the foam by varying the MFC content. Sehaqui et al. (2010) developed a plant-inspired biopolymer foam, by adding MFC found in plant cell walls, during the foam fabrication process. They were able to change the compressive stress vs. strain response of the foam by varying the cellulose content, while maintaining a constant density of $21 \pm 1 \ kg \cdot m^{-3}$ (by varying the foam content). They also state that the energy absorption of the foam under quasi-static compression is higher than expanded Polystyrene (EPS) foam.
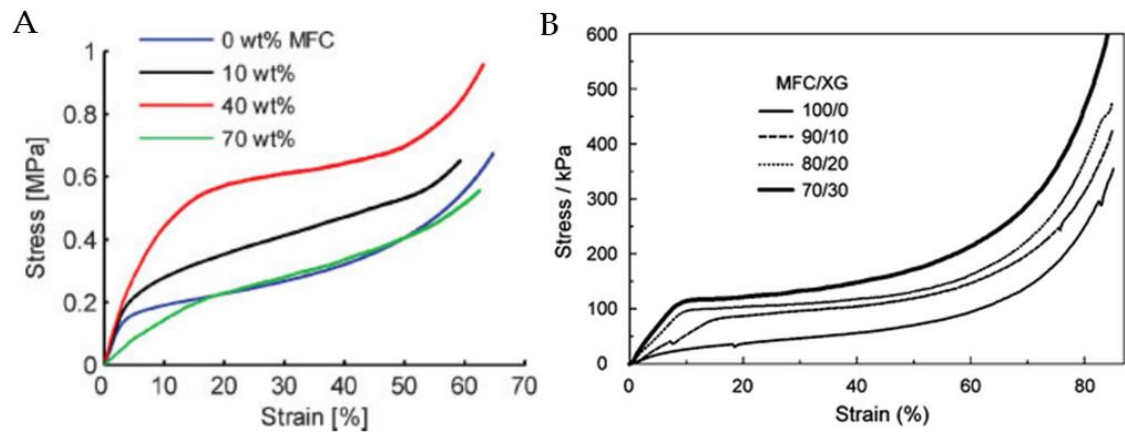
Figure 2-5: Typical quasi-static compressive stress–strain curves for (A) MFC-reinforced amylopectin foam with varying MFC contents (Svagan et al., 2008) and (B) foams with different MFC / XG content ratio and a constant density of 21 ± 1 kg·m⁻³ (Sehaqui et al., 2010).

Table 2-3: Physical and mechanical properties of MFC reinforced amylopectin-based foam with varying MFC contents. Values are Mean ± SD (Svagan et al., 2008).

MFC (wt%)	Young's Modulus (MPa)	Yield Strength (kPa)	Density (kg·m⁻³)
0	4.9 ± 1.1	170 ± 25	103 ± 2
10	5.0 ± 1.0	310 ± 91	109 ± 3
40	7.0 ± 0.6	510 ± 21	95 ± 1
70	1.7 ± 0.4	110 ± 78	87 ± 1

Foam density values reported by Svagan et al. (2008) ranged from 87 to 103 kg·m⁻³. Sehaqui et al. (2010) claim that their biopolymer foams can be tailored to have densities ranging from 7 to 103 kg·m⁻³, with capabilities to alter the stress vs. strain response at a given density. This suggests that if a bio-inspired / biomimetic foam is used as shoulder padding in rugby, measuring the density of the material would unlikely provide any useful information about the hardness response of the material.

While the intention of World Rugby™ is to restrict the impact force attenuation capabilities of shoulder padding, the above-mentioned (especially dilatant and auxetics) materials have been reported to have high indentation resistance, which

may help reduce the risk of cuts and lacerations. Aside from protective padding materials, there are materials specifically designed to provide indentation or penetration resistance, such as stab proof materials, which will now be discussed.

2.6 Stab Proof Materials and Prevention Techniques

Advances in manufacturing techniques and materials have led to the development of highly engineered and lightweight products that offer protection to vital organs. Modern-day body armour is often made using ceramic, Polycarbonate or aramid-based fibres, like Cordura® (Figure 2-6) or Kevlar® (Zhou et al., 2005). The fibres are known to "catch" the impactor in its web and reduce the impact energy, while the other layers work towards additional energy absorption until the impactor is stopped. The ceramic layers shatter around the region of impact and are capable of dispersing the impact energy. This shattering of the ceramic layers does however reduce the capacity of the vest to offer protection against further impacts, eventually rendering it ineffective.

Figure 2-6: Commander™ tactical vest, manufactured using Cordura® with pockets for ceramic inserts.

Further research has led to the development of high-performance polymer fibres called "ultra-high molecular weight polyethylene fibre" (UHMWPE), like Dyneema® & Spectra®. UHMWPEs are lightweight high performance polymer

fibres (Van Dingenen, 1989) that have a density around eight times lower than steel (Greenhalgh et al., 2013). UHMWPE fibres are high modulus and high strength, abrasion-resistant fibres, described as 10 and 50 times stronger than steel and Kevlar, respectively (Van Dingenen, 1989). Studies have shown that these fibres have a high cut, abrasion, and puncture resistance and can provide protection against lacerations (Karbalaie et al., 2012) and impacts (Van Dingenen, 1989; Greenhalgh et al., 2013). Because of their lightweight and high-resistance characteristics, UHMWPE fibres have been used for various forms of protective clothing (e.g. body armour, gloves, chainsaw protection, and fencing suits).

Whitmarsh et al. (2019) investigated whether backing neoprene rubber with UHMWPE would reduce the risk of injury from a shark attack. Testing included puncture (single axis compression to mimic a shark bite) and laceration (multi axis compression and translation, to mimic a shark head shake) tests with a shark tooth. The UHMWPE backed neoprene withstood higher forces before failure. Whitmarsh and colleagues noted that even though the UHMWPE backed neoprene was resistant to damage, further research is needed to check if the same applies to the underlying skin tissues or any protective equipment being worn.

In a review of stab resistant materials, Johnson (2013) predicted future uptake of materials like Carbon Nanotubes (CNTs) and MagnetoRheological (MR) fluids in body armour, and recent studies have shown promising results (Shanmugam et al., 2019; Ruan and Bao, 2014). While CNTs are thinner (typically one thousandth of the width of a human hair) and reported to have higher Young's Modulus (1-1.28 TPa) than Kevlar (100 GPa), MR liquid-based armour benefits from improved shear resistance. Ruan and Bao (2014) reported that adding a CNT coating on UHMWPE fibres improves the compressive and bending strength. Similar findings were reported by Shanmugam et al. (2019), who stated that adding multiple coatings of CNTs increased the compressive strength of the fibre by up to 42%.

MagnetoRheological fluids have iron particles dispersed in a non-magnetic viscous solution (Figure 2-7-A), which form dipole columns when magnetised (Figure 2-7-B).
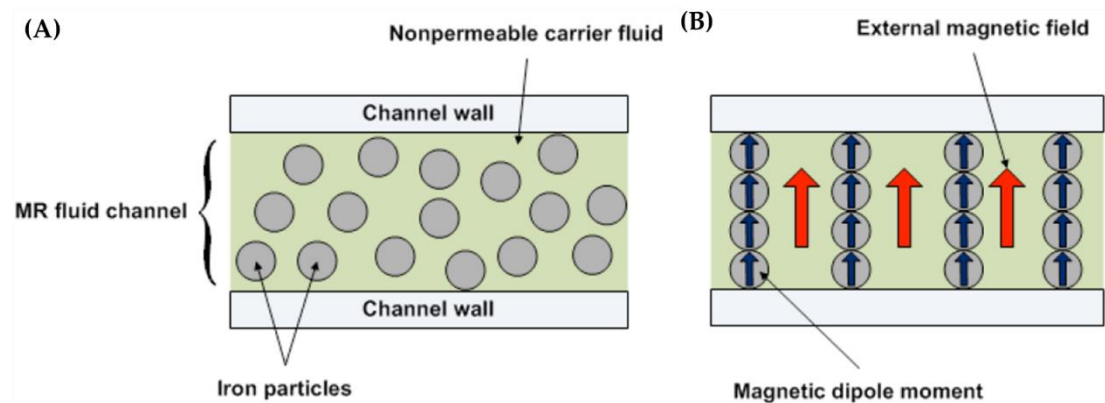
Figure 2-7: MagnetoRheological Fluid- (A) Non-magnetised and (B) magnetised.

In MagnetoRheological fluid-based armour, upon impact, the fluid molecules align to the magnetic field and harden to spread the impact force over a larger area, increasing penetration resistance and decreasing the pressure felt underneath the protective layer. Johnson et al. (2013) states that combining MagnetoRheological fluid with Kevlar™ layers can improve impact and penetration resistance of PPE.

Materials like UHMWPE in combination with dilatants have shown potential for reducing the risk of injuries like cuts and lacerations, suggesting they could bring benefits to PPE in rugby jerseys. Much of the research into the performance of body armour is focused on the impact protection (as is also the case of research into other materials used in PPE) and stab resistance capabilities. As Regulation-12 limits the impact force attenuation of rugby padding (acceleration ≤ 150 g under 14.7 J impact), it is important to understand techniques aside from impact force reduction that could be applied to reduce the risk of cuts and lacerations.

There are different mechanisms for reducing the risk of cuts and lacerations. Johnson et al. (2013) states two methods for reducing the risk of life-threatening injuries caused by knife or ballistic attacks: i) absorbing and dissipating the impact energy, and ii) deflecting the striking implement.

Scott (2005) describes the different ways the impact energy can be absorbed or dissipated to prevent the impactor / striker from penetrating the protective equipment. For a bladed / sharp impact threat, damaging the tip of the blade may reduce the risk of injury, as it increases the chances of it breaking or getting caught in the protective material. Scott (2005) suggests that the protective material could apply a high frictional load to the blade to limit the level of penetration. Similar techniques have been seen when studying the mechanical properties of armoured fish (Song et al., 2011). To achieve minimal penetration from a sharp object two mechanical strategies may be used, either together or in isolation: i) deforming or fracturing the penetrating threat and ii) dissipating the penetrating energy via deformation or cracking of the armour.

Johnson et al. (2013) states that the damage to the human body from a sharp object can be reduced by either using materials that prevent armour penetration by deflecting an impactor or by absorbing impact energy. As the intention of World Rugby™ Regulation-12 is to not permit padding with excessive impact force attenuation properties, there may be benefits from using materials that can deflect an impactor. Such materials may, however, be too stiff for use as rugby padding and may increase injury risk to opponents. Johnson et al. (2013) states that to deflect an impactor, armour must have a higher Young's modulus than the impactor. In rugby, taking an impact of a stud on skin as an example, based on the Material Family Chart (Figure 2-8), only a few material groups such as ceramics or metals, have a higher Young's Modulus than a standard aluminium stud and could therefore be used to deflect a stud.
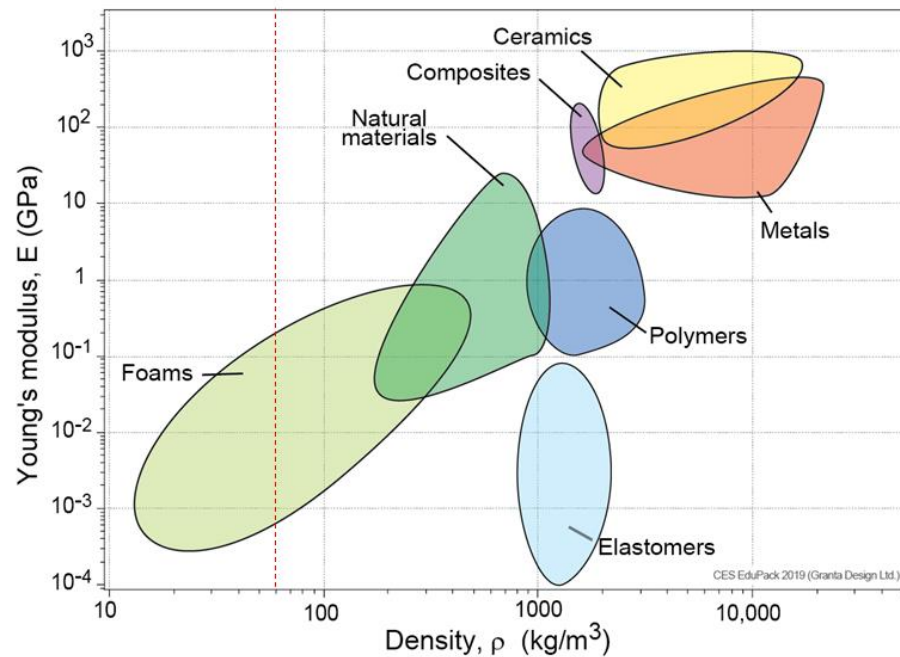
Figure 2-8: Young's Modulus vs Density Chart -Material Family Chart (Chart created using CES EduPack 2019, Ansys© Granta© 2020 Granta Design). Red line marking the 60 kg·m^{-3} maximum density limit.

2.7 Test Methods for Protective Materials

This section reviews established methods for testing materials designed to reduce the risk of soft tissue injuries. Various test methods are summarised, including stab impact, abrasion test, cut resistance and stud impacts onto skin simulants.

The United Kingdom Home Office has defined a *Body Armour Standard* (2017) that outlines the minimum requirements and testing methodologies for various body armour intended for UK law enforcement agencies. There are three classifications based on protection levels: (i) ballistics, (ii) knife and (iii) knife with spike. The setup described in the standard is a drop tower assembly with a knife or spike impactor (Figure 2-9). Testing is carried out at four energy levels (24, 33, 36 and 50 J) with different limits of penetrations allowed at each level.
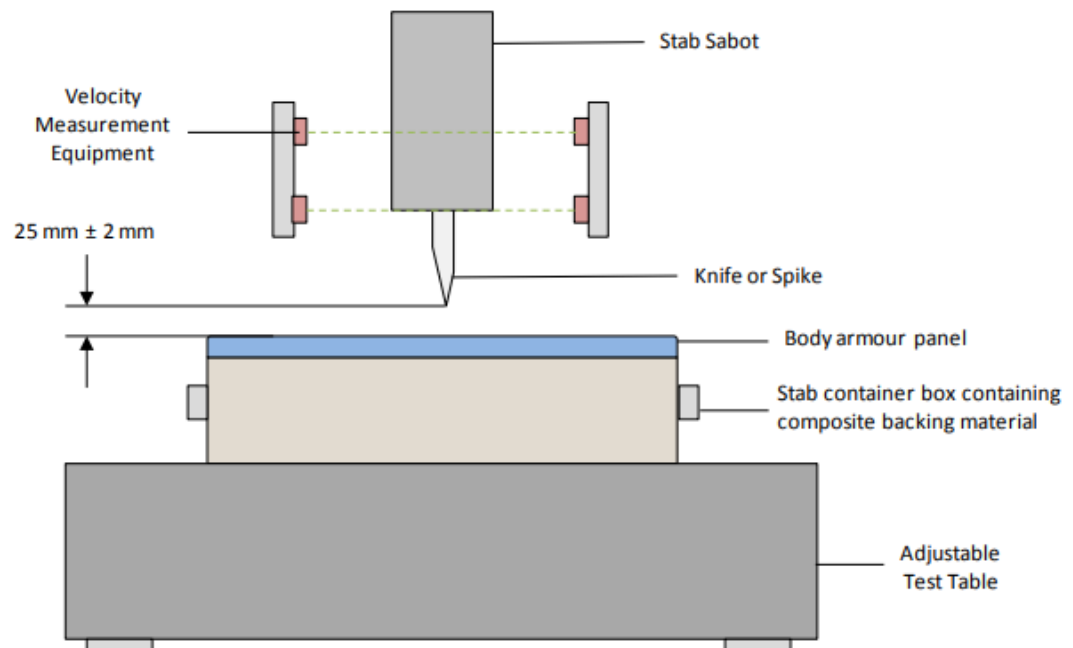
Figure 2-9: Schematic of a typical stab test configuration described by the Home Office Body Armour Standard (2017).

Another standard to test against cuts and abrasions is BS EN ISO 13997: *Protective clothing – Mechanical properties —Determination of resistance to cutting by sharp objects*. The standard complements BS EN 388: *Protective gloves against mechanical risks*. BS 388 defines some tests to determine if the equipment can protect against sharp and abrasive objects. The standard defines a few testing methodologies, including abrasion, blade cut, cut resistance, tear resistance, and puncture resistance.

The abrasion testing, specified in BS EN ISO 13997, is based on EN ISO 12947-1: *Textiles — Determination of the abrasion resistance of fabrics by the Martindale method*. The method requires a specialist testing machine (Figure 2-9-A) consisting of a mass pressing a specimen against an abrasive surface (Figure 2-10-B). The machine applies randomised cyclic loads that cause the sample to rub against the abradant to mimic wear. Assessment is based on either a visual comparison of the material before and after the test or the number of cycles until the material tears.
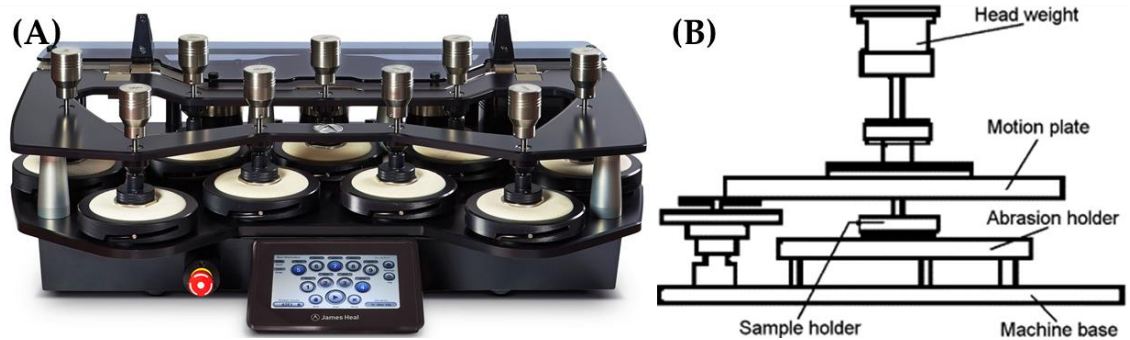
Figure 2-10: (A) Martindale Testing machine (Image courtesy: James Heal) and (B) Testing setup schematic (Wang et al., 2007).

The cut resistance testing in BS EN ISO 13997 involves moving a flat blade (with a defined preload) over a specimen in a linear path (Figure 2-11). The length of the blade path is varied, and the length of any cuts induced in the specimen is measured. The blade cut resistance test is similar, but the blade is circular and rotating, and the measurement noted is the number of load applications before a cut occurs.
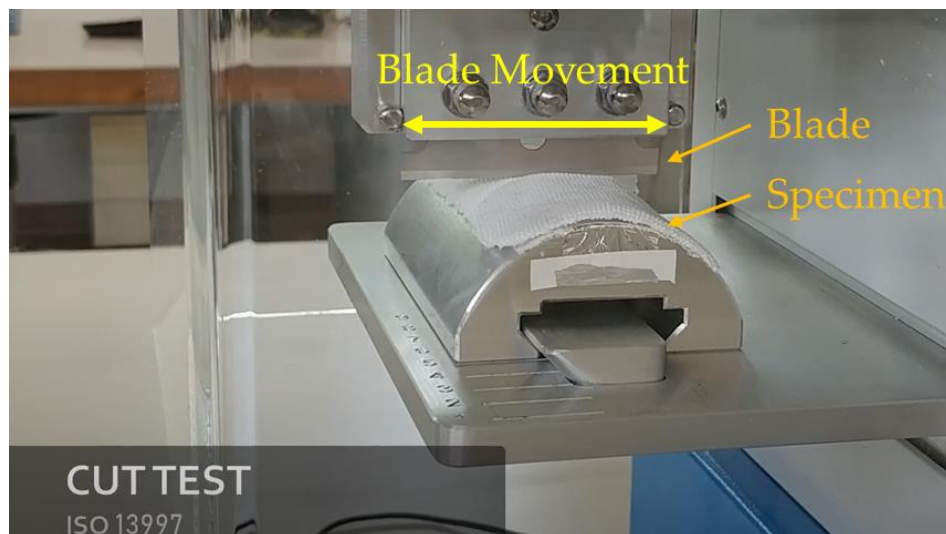
Figure 2-11: Screenshot of cut test carried out by RicoTest Laboratories (Italy) as per ISO 13997.

As well as the body armour testing and BS 13997, there are some other standards for testing protective equipment with respect to prevention of cuts and lacerations. BS EN 13594: *Protective gloves for motorcycle riders — Requirements and test methods*, outlines the test method for determination of impact abrasion resistance. The standard states that "*The test machine is designed such as to allow the test piece to be dropped from a set height with defined energy onto an abrasive belt moving at a fixed speed*

over a rigid horizontal surface". This test is intended to replicate the palmer region of the glove sliding on the road or asphalt during a motorcycle fall / crash.

The standard testing methodologies for prevention against cuts or stabs use sharp objects like knives or blades. While these tests should provide useful insights into the cut resistance of materials, they do not represent rugby scenarios. The Home Office *Body Armour Standard* (2017) states that development of technology over time provides the ability to produce test methods that are more representative of the operational scenarios faced by the end user. Hence while devising a methodology to test against cuts and lacerations it is important to use scenarios representative of those in rugby.

While there is a gap in our knowledge of the mechanics of cut or laceration inducing scenarios in rugby, there is a test methodology in the World Rugby™ Regulation-12 for stud design. Regulation-12 Schedule-2 has five optional tests:

- Test A – Skin glancing / raking test
- Test B – Skin stamping test
- Test C – Stud / Cleat impact test
- Test D – Fitting of replaceable studs / cleats
- Test E – Wear simulation

The regulation states that tests A and B provide a direct method of assessing a stud / cleat's potential to cause injury through glancing, raking or stamping mechanisms. Test A describes a pendulum impactor with a stud impacting a muscle and skin simulant (Figure 2-12). Test B comprises a vertical drop of an impactor (8.5 kg) with a standard stud design from 50 mm (4.17 J impact energy).

For both tests A and B, the standard recommends using "a suitable human flesh simulant is required comprising an artificial skin backed with a thick deformable muscle-like material" (World Rugby™ Handbook, 2015:218). The Handbook suggests using a 1.5 mm thick poromeric shoe upper material having relatively low

abrasion resistance as an artificial skin, and gelatine, moulded into suitable form, as the deformable muscle simulant. The descriptions of the test methods do not include references to literature nor other reasoning to support or otherwise justify the values or the surrogate materials suggested.
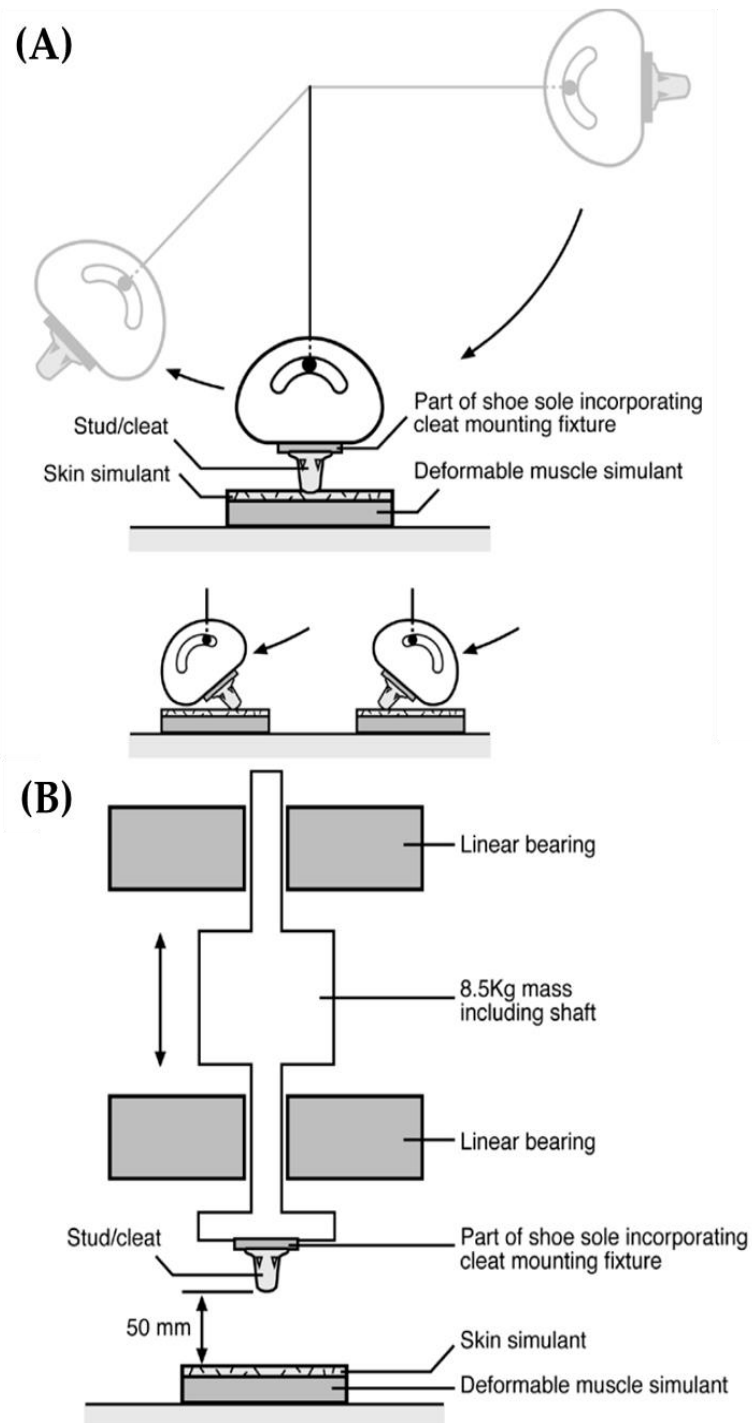
Figure 2-12: Schematic of (A) Skin Glancing/Raking Test & (B) Skin Stamping Test in World Rugby™ Regulation-12 Schedule-2.

The test methods are comparative and are used to compare the damage caused to the skin simulant by stud designs in comparison to the standard stud design defined by the regulation. The test methods use non-rigid materials that may be more representative of human muscle and skin tissue than metal anvils (i.e. more biofidelic), and mimic scenarios similar to those that are likely to occur during a game of rugby.

Fédération Internationale de Football Association (FIFA) in their Handbook for test methods (2012) use 'Silicon Skin L7350' as a simulant to mimic skin to test abrasion against artificial surfaces (turf). The skin simulant defined is only used to determine skin abrasion and not against blunt impact injury scenario. The test method involves sliding a test foot with the silicone skin 7350 attached to, across the turf and note the force readings. Hurtado et al., (2016) compared the Silicone Skin L7350 for tribological performance of mechanical skin equivalents against ex-vivo human skin samples. Their results showed that there were significant differences in the elastic properties of the human skin against skin samples.

As the most likely cause of skin injuries in rugby is stud impacts (Oudshoorn et al. 2016), these methods would be an ideal starting point to test the efficacy of padding materials / designs for reducing cuts and lacerations. Testing for skin injuries could include the experimental tests outlined in this section, and these tests could also be simulated in FE models.

2.8   **Overview of FE based research**

FE analysis is often used to understand an impact between two objects or the forces acting in a physical system. Using CAD and FE analysis allows for testing of product designs virtually, which can reduce the cost of initial development and prototyping. These computer aided analysis techniques can also be used to analyse physical events in sports to understand the physics in detail. FE analysis has been used to understand equipment interaction in various sports, such as tennis (Goodwill et al., 2005; Allen et al., 2009; Banwell et al., 2012) field hockey (Ruznan et al., 2018) and

softball (Biesen and Smith, 2007) amongst others. FE analysis has also been used by researchers to analyse sporting injury (Ankrah and Mills, 2003) and with a view to improving safety standards (Newton-Mann et al., 2018).

Padding materials, such as foams, have been used in PPE to reduce impact forces. Researchers have applied FE analysis to simulate impact involving foams in different industries, such as packaging (Mills and Masso-Moreu, 2005), and in many sports, such as padding in shoes (Verdejo and Mills, 2004) and helmets (Mills et al. 2003, Mills and Gilchrist, 2008 and Toma et al., 2010). Various test methods can be applied to obtain material properties, which can then be incorporated into the FE models by fitting the data to material models. These material models differ depending on the type of material being analysed, and this topic will be covered in Section 5.4 Material Models. Furthermore, any FE-model needs to be validated by comparing the simulation outputs to either the literature or laboratory test data. The typical process for carrying out an FE simulation is depicted in Figure 2-13. Table 2-4 summarises some of the models used by researchers to simulate the materials used in PPE, and the corresponding method of validation.
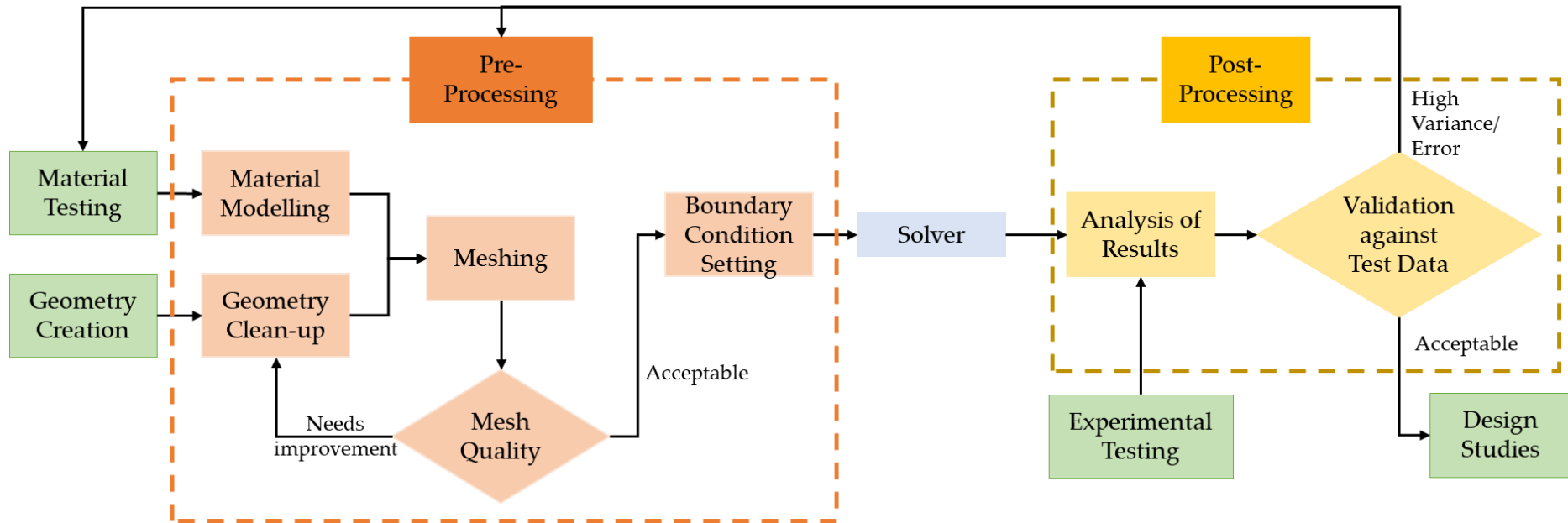
Figure 2-13: Flowchart describing the FE analysis process used to validate the material model against experimental data.

Table 2-4: Summary of researches looking at performance of different materials used in PPE.

Reference	Application	Geometries	Material Models	Validation Method	Software
Ankrah and Mills (2003)	Football shin guards	Tibia was modelled as a hollow cross-section tube and simply supported at each end.	Zotefoams EV30 (EVA) Foam, Leg muscle / soft tissue - **Ogden**, Tibia and shells - **elastic** materials	Impact test - accelerometer in striker, high speed camera. Tekscan FlexiForce™ sensors	ABAQUS
Mills & Gilchrist (2008)	Bicycle helmet impact - comparison of helmet features	Scanned bicycle helmet & head form	Extruded polystyrene foam - **Crushable Foam model**	Experimental	ABAQUS
Price et al. (2008)	Football material and model testing	-	Woven Fabric, EPDM Foam, PU Foam - **Viscoelastic Prony Series**	Series of impact tests - High speed camera	ABAQUS
Mills et al. (2009)	Oblique impacts on motorcycle helmets	CT scan of the helmet	-	-	-
Ranga & Strangwood (2010)	Quasi static and dynamic behaviour of solid sports balls	Simple cylinder drawn in CAD	Hockey Ball material - **viscoelastic Prony Series**	Material testing	ABAQUS

Coto et al. (2012)	Nose Protector impact with solid ball	CT scan of anatomical structures	Bone - **elastic linear**, Soft tissue - **Ogden**, EVA flexible - **Ogden**, EVA rigid	-	LS-DYNA®
Nagaoka et al. (2012)	Material modelling for swimwear	-	Swimwear - Anisotropic hyperelastic model **Mooney-Rivlin** (isotropic part of the strain energy function)	Biaxial test & cyclic loading tests	-
Rueda & Gilchrist (2012)	Design of components of protective equestrian helmets	-	-	Comparison with lab tests on 15 different equestrian helmets - flat anvil impacts at 6.26 ms⁻¹ on 3 impact locations	ABAQUS
Tanabe et al. (2012)	Numerical analysis of competitive swimwear	-	Swimwear - Anisotropic hyperelastic model **Mooney-Rivlin** (isotropic part of the strain energy function)	Material testing & pressure testing (6 sensors around a cylinder)	-
Luo & Liang (2013)	Sport helmet design and virtual impact testing	CT and MRI of the subjects head, geometric shapes for the helmet	Helmet (composite made of carbon fibres and polyester) - **linear orthotropic material**	Experimental data from previous literature.	-
Nevins &	Softball properties	2 softball models	Softball (polyurethane) - Low	-	LS-DYNA®

Smith (2014)	in ball-to-head impacts	created in CAD, 50th percentile adult male Total Human Model for Safety (THUMS) for head and neck	density foam material model (Mat #57)		
Shimana et al. (2013)	Designing compressive sportswear	3D-CG-Human-Model used created by commercial software Autodesk MAYA	Swimwear - Anisotropic hyperelastic model	-	-
Smith & Burbank (2013)	Foam material model in softball impact	Geometry created in CAD	PU Foam - experimentally derived material loading response and phenomenologically developed unloading response using (Mat #57 low density foam)	Impact Test - Load cells, light screen	LS-DYNA®
Thoraval et al. (2013)	Wrist guard effectiveness for snowboarders	Several scans of wrists and a European anthropomorphic database, wrist	Anthropomorphic model - **elastic plastic**, Falling mass - **elastic plastic**, Foam - **general nonlinear strain rate foam**, Wrist guard shell -	Impact test - force plate with 3 uniaxial piezoelectric load cells, laser displacement sensor,	Pamcrash

		guard was digitised using a 3D scanner	**Elastic plastic**	accelerometer mounted in mass	
Mao et al. (2014)	10-year-old forearm injury + wrist protector	Scaled from an adult radiologic image	Bone - isotropic **elastic plastic**, cartilage - **elastic**	No experimental data on 10-year-old paediatric subjects therefore no comparison to experiments for model validation were feasible	LS-DYNA®
Lehner et al. (2014)	Backwards fall in snowboarding	CT data 3D surface of the upper extremity exact bone geometries used	-	Experimental studies described in literature - backwards fall onto a mat	SIMPACK
Senner et al. (2014)	Effectiveness of wrist guards in snowboarding	CT data 3D surface of the upper extremity exact bone geometries used. 20 different CAD models of wrist protectors designed in CATIA	-	-	SIMPACK / Ansys©

		fixed to the model.			
Brolin & Wass (2016)	Equestrian simulation using virtual human body model	Geometries created in CAD, hoof an oval shaped rigid shell plate, simplified safety-vest, horse body generated outer shape as seen from the side with splines & sweeping oval sections	Nylon fabric (safety-vest) - **linear elastic,** foam core (safety-vest) - **low-density foam, viscoelastic**	-	LS-DYNA®
Rinaldi et al. (2016)	Table tennis ball & bat impact	Geometries created in CAD	Ball - **Prony Series**, viscoelastic material	Impact test - camera with stroboscopic lighting	ABAQUS
Smith et al. (2016)	Softball impact (ball on bat)	Template-based 3D shape reconstruction from camera	High density polyurethane ball - MAT 006 **linear viscoelastic**, MAT 057 **low density foam model**, MAT 083 **medium-density foam model** where the hysteretic unloading is a function of rate sensitivity, MAT 181	Impact test - load cells, light screens & video analysis	LS-DYNA®

			hyperelastic model response		
Biesen and Smith (2007)	Softball impact on Aluminium Bat	Hemisphere for the ball and solid cylinder for the bat (Section)	Rigid Aluminium Bat with Viscoelastic Ball	Impact test - load cells, light screens & video analysis	LS-DYNA®
Mills & Masso-Moreu (2004)	Foam Cushion in Package Drop Test	Foam sections used in package boxes	EthaFoam 220 & 400, Elastic (Pre-Yield) Followed by 'crushable foam' Model	Impact Test-Loadcell	ABAQUS
Ozturk and Anlas (2010)	Multiple Loading and unloading of Foam used in packaging	Foam Cube with Spherical Indenter	Expanded-Polystyrene (EPS) ABAQUS-Crushable foam model LS-DYNA®-Low density Foam Material Model	Cyclic Loading	ABAQUS & LS-DYNA®
Newton-Mann et al. (2017)	Palmer Pad for Snowboard wrist protector	Cylinder (off circle) geometry	Ogden Model with Prony Series	Impact test with accelerometer and High-Speed Video to measure impact duration and deformation	LS-DYNA®
Verdejo & Mills (2003)	Running Shoes Mid Soles	Curved Heel on a block of foam with rotational Symmetry- Heel	EVA -Ogden Model	Force Plate and Tekscan Sensors to measure heel shoe pressures	ABAQUS

		Impact (3 co-radial cylinders-Heel Bone, Heel pad and foam)			
Mills et al. (2003)	Polymer foams for Personal protection	Curved Heel on a block of foam with rotational Symmetry- Heel Impact (3 co-radial cylinders-Heel Bone, Heel pad and foam)	Ogden Model- Poly- EVA Foam	Compared against literature and manual calculation	ABAQUS
		Curved foam impact with flat anvil & kerbstone anvil for helmet	Crushable Foam Model- Isotropic Material- Polystyrene Foam		
		Cylinder indenter on a cube of foam	Ogden Model- Polyurethane		

From Table 2-4, it can be seen that FE modelling is an established technique that has been used to analyse impact scenarios in various sporting environments. FE models have been used to simulate the PPE material and analyse the force propagation through it during impact. Simulations have also been carried out to understand the physics between equipment (e.g. ball and bat in baseball, ball and stick in hockey). Contact between equipment and the human body has also been modelled to understand the preventive capability of PPE (cycling helmets, snowboarding wrist protectors). Following validation, these models have allowed researchers to explore PPE design parameters or simulate other scenarios (which may not be easy to test physically) and understand the effect or consequences of them.

Most PPE simulations are carried out with the intention to study the impact force and the protection level the padding provides. Since padding used in rugby is designed to reduce the risk of cuts and lacerations, testing the efficacy of PPE in reducing the risk of injuries on the human tissue could benefit from testing with cadavers. There are, however, many practical and ethical challenges and complications associated with testing with cadavers. For example, cadavers are not readily available, there is considerable variation between individuals, and specialist storage and testing facilities are required.

Physical testing would require new surrogates / cadavers following testing as materials are not durable and undergo degradation (Payne et al., 2015a; Payne et al. 2015b) upon impact creating variability among the results. Using FE simulations to study injuries such as cuts and lacerations, allows testing in a repeatable test scenario with capability to simulate different scenarios. FE simulations would allow easy adaptability when changing testing parameters or scenarios. FE simulations also allow better visualization and analysis of various physical parameters (such as stress, strain) at any location at every time step. Hence using FE simulations could help analyse the extent of shoulder padding in reducing the risk of cuts and lacerations.

2.9   **Human Tissue Modelling**

Skin is the largest single organ of the body and has many roles, including sensing, thermo-regulation, and host defence (Figure 2-14) (Xu et al., 2008; Leveque et al., 1980; Larrabee Jr, 1986). Xu et al. (2008) state that the skin *in vivo* is mechanically heterogeneous, anisotropic, nonlinear, viscoelastic and under tension. Skin properties are dependent on age, gender, site and hydration, amongst other factors (Silver et al., 2001; Panchal et al., 2019; Leveque et al., 1980; Larrabee Jr, 1986; Lapeer et al., 2010).
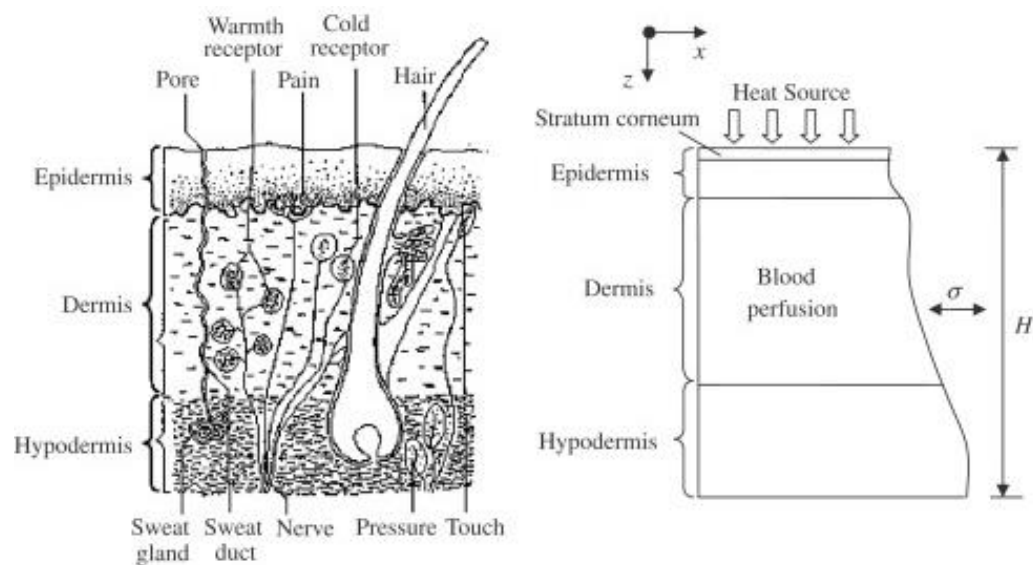
Figure 2-14: Cross-section of a human skin as described by Xu et al. (2008) describing the different sensory functions along with the simplified geometrical breakdown.

To simulate injuries such as cuts and lacerations, the human skin tissue must be studied, and an appropriate model must be made that is capable of mimicking the mechanical properties of the human skin tissue. Various *in vivo* and *in vitro* test methods have been used to characterise the behaviour of human skin. Using the material properties obtained, researchers have defined mathematical models using various linear elastic (e.g., Figure 2-15), hyperelastic and linear viscoelastic techniques (Table 2-5).
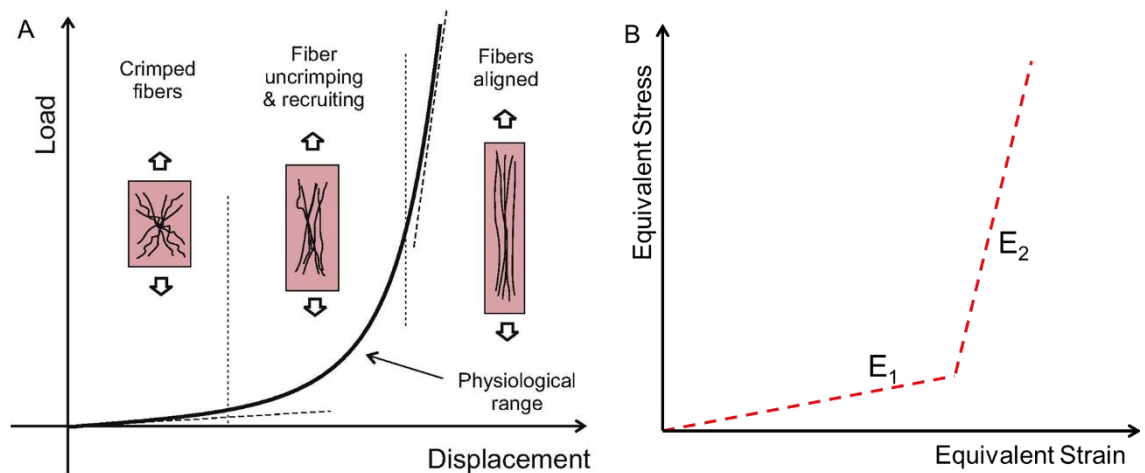
Figure 2-15: (A) Mechanical response of human skin in relation to fibre orientation during loading and (B) non-linear skin response modelled as two straight lines representing low and high stiffness regions, respectively. Adapted from the works of Benítez and Montáns (2017).

The mechanical response of skin can vary based on its location on the body and the underlying fat and muscle layer (Leveque et al., 1980; Lapeer et al., 2010; Hendriks et al., 2003; Flynn et al., 2011). Much of the research on modelling of skin has excluded the underlying anatomy. Researchers have used simulants to mimic the skin, or the anatomy of the areas being considered and applied FE modelling to assess the performance of PPE (Payne et al., 2014). The ability of a material to reduce the risk of cuts and lacerations could be assessed using skin simulants. Researchers have used various silicones to mimic human skin tissue to assess the effect of an impact on the human body (Hrysomallis, 2009; Payne et al., 2014; Payne et al., 2015a and b). These stimulants could help us understand the efficacy of padding in reducing injury risk to the human tissue. Table 2-6 summarises some studies that have included a skin / skin simulant or a physical anatomy simulant in an FE model for predicting the performance of PPE.

Table 2-5: Summary of studies focusing on modelling of skin along with their respective material test method and material model used.

Researchers	Test	Model
Diridollou et al. (1998), Diridollou et al. (2000)	*in vivo* and under suction using Ultrasound	Hookean Linear Elastic
Hendriks et al. (2003)	*in vivo* and under suction using Ultrasound	Mooney–Rivlin Hyper Elastic
Khatyr et al. (2004)	*in vivo* extension, creep and relaxation test of forearm skin	linear Viscoelastic
Jachowicz et al. (2007)	*in vivo* indentation test to measure stress vs. strain	linear Viscoelastic
Leveque et al. (1980), Agache et al. (1980)	*in vivo* (torsion)	Linear Elastic
Dunn and Silver (1983)	*in vitro*	Linear Elastic + Linear Viscoelastic
Silver et al. (2001)	*in vitro*	Viscoelastic
Shergold et al. (2006)	Compression of silicone Rubber (B452 and Sil8800) and pig skin	Mooney-Rivlin does **not** work Ogden provides adequate match
Evans (2009)	Using uniaxial tensile data from Shergold and Fleck (2006) data and Dunn et al. (1983)	Hyper-elastic Ogden
Evans and Holt (2009)	*in vivo* measurement of deformation using Digital Image Correlation (DIC)	Hyper-elastic Ogden- Single Term

Flynn et al. (2011)	*in vivo* skin deformation using 3D Motion capture	Hyper-elastic Ogden & neo-Hookean
Delalleau et al. (2008)	Suction on the forearm to measure deformation in relation to pressure applied	neo-Hookean model and linear elastic model **do not** work Hyper elastic models provide better fit
Groves et al. (2012)	*Ex Vivo* Tensile tests on human and murine skin	Hyper-Elastic Anisotropic
Mahmud et al. (2010)	*In vivo* skin deformation using 3D Motion capture	Hyper-elastic Ogden

Table 2-6: Summary of studies focusing on modelling of skin along with their respective material test method and material model used.

Reference	Application	Geometry	Material Model	Validation	FE-Software
Ankrah and Mills (2004)	Football ankle protection (shin guards)	Fibula modelled as a cylinder with an 8mm hemispherical end and an axis of rotational symmetry	EVA Foam, Leg muscle / soft tissue - **Ogden**, Tibia and shells - **elastic** materials	Impact test - accelerometer in striker, high speed camera. Tekscan FlexiForce™ single point button sensors. Wear ability trials by 18 volunteers	ABAQUS
Lin et al. (2011)	Male leg & sportswear contact pressure and clothing deformation	Reconstruction of geometrical shapes of the commercial 3D anatomic make skin & skeleton model	Sports Tights - **Non-linear elastic, hyperelastic - 3rd order Ogden model**	4 athletes wore sports tights - 7 Flexiforce sensors placed at 7 important muscles that flex or extend when running. Force plates under sensors to track perpendicular force to sensor plane	-

Payne et al. (2015)	Synthetic muscle tissue for sports impact surrogates	-	Comparison of **Ogden**, **Mooney-Rivlin** and **Neo Hookean** to describe incompressible, hyperelastic materials. **Prony Series** used to model the viscoelastic properties of the simulants.	Drop Test - Instron equipped with 3 piezoelectric load cells. High speed camera used to measure displacement	ABAQUS
Marchesseau et al. (2010)	Synthetic Soft tissue model for liver surgery simulation		Hyper-elastic Models along with Visco-Hyperelasticity using Prony Series	DMA on 60 Porcine liver samples	
Panchal et al. (2019)	Vibrational Analysis of Skin	Flat Surface area of 120 mm x 50 mm, containing skin, fat, muscle and bone layer	Assumed as linear isotropic for the defined range of vibration analysis	Experimental data captured using DIC	ABAQUS
Lapeer et al. (2010)	Plastic Surgery Simulation		Hyperelastic Models-General Polynomial, Reduced Polynomial and Ogden	Skin Harvested from female patients undergoing plastic surgery	ABAQUS

Most of the studies in Table 2-6 focused on the force propagation through the skin / soft tissue, rather than injury / damage to the skin itself. Also, most of the research carried out on the isolated skin tissue focussed on low strain rates, without considering impact scenarios. Various material modelling techniques, such as elastic, hyperelastic, viscoelastic, or a combination of different techniques have been used to model the human skin tissue. Hyperelastic modelling in combination with viscoelastic modelling has been shown to be suitable for predicting the skin tissue response during impact (Lapeer et al.,2010; Payne et al.,2015a; Lin et al., 2011).

Studies by Payne et al. (2015b), Payne et al. (2016) and Panchal et al. (2019) were similar to this PhD project, as they focused on developing a surrogate to analyse and simulate the performance of the human tissue and skin. Payne et al. (2015) created material models of silicones, with a view to using these silicones in surrogates. The silicones were characterised in quasi-static compression tests, and hyperelastic material models (Mooney-Rivlin, Ogden and Neo-Hookean) were then fitted to the stress vs. strain data. A Prony series, fitted to stress relaxation data, was combined with the hyperelastic material model to account for strain rate dependency of the silicone. Details of the different hyper elastic models will be presented in Chapter 5.

Payne et al. (2016) developed a thigh surrogate (Figure 2-16). The surrogate contained the structure of the main comprising layers of soft tissues (muscle, adipose and skin) of the thigh, which were moulded together (Figure 2-16). Each layer of the surrogate was fabricated using specific silicone formulations to mimic the respective mechanical properties.
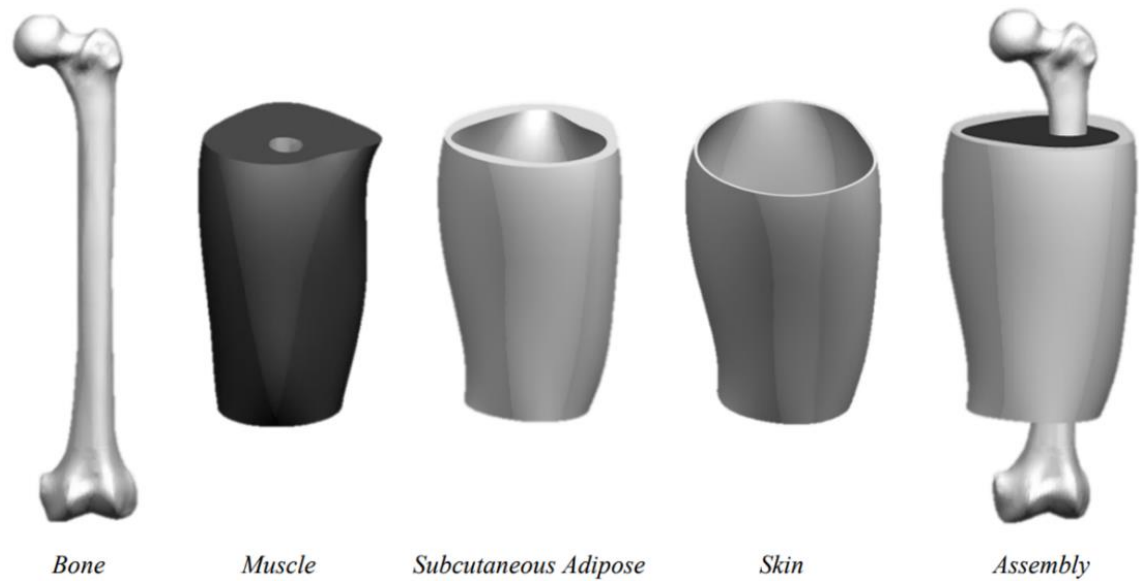
Figure 2-16: CAD model of the substructures used by Payne et al. (2016) to manufacture the thigh surrogate.

Panchal et al. (2019) created an FE model consisting of the cross-sectional anatomy of the forearm to analyse the vibrational properties of the skin. The model consisted of 120 × 50 mm structures of the five layers of the anatomy (Figure 2-17). The skin geometry was assumed to be flat and simulations were carried out to analyse the vibrational properties. The soft tissue materials were modelled as isotropic linear elastic with a different Young's moduli applied to each layer (Table 2-7). The muscle and bone layers were modelled as rigid structures, and adjacent layers were connected using tied contacts. The simulation results were compared against full field strains on the skin surface measured using Digital Image Correlation (DIC).

The values of Poisson's ration used by Panchal et al. (2019) were obtained from Delalleau et al. 2006, who calculated Poisson's ratio by carrying out inverse analysis in combination with indentation tests (*in vivo*). The reported values of 0.48 have been used by researchers to model soft tissue and soft tissue simulants (Xu et al., 2008; Delalleau, 2008; Benitez and Montans, 2017; Panchal et al., 2019).
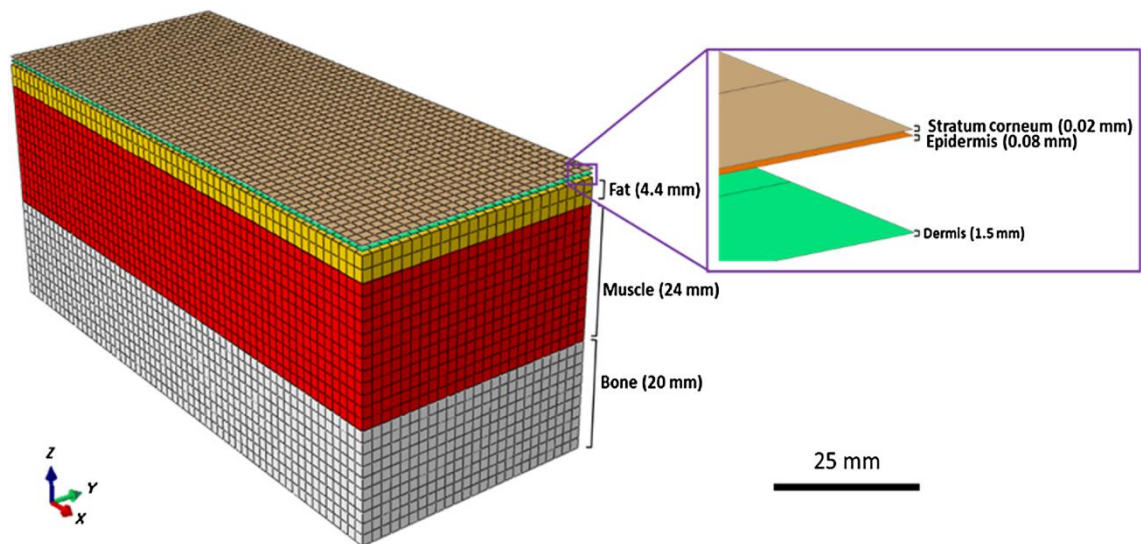
Figure 2-17: The FE model of the human forearm with different layers of skin connected to muscle and bone (Panchal et al. (2019).

Table 2-7: Material properties of different anatomical structures as used by Panchal et al. (2019).

Mechanical properties	Young's modulus (MPa)	Poisson's ratio	Density (kg·m⁻³)
Stratum corneum	1,998	0.48	1,500
Epidermis	102	0.48	1,119
Dermis	10.2	0.48	1,116
Subcutaneous fat	0.01	0.48	971
Muscle	888	0.3	1,200
Bone	17,000	0.3	2,000

The thigh surrogate developed by Payne et al. (2015) and Payne et al. (2016) was developed and tested specifically for evaluating impact protection of PPE. The main role of the surrogate was to analyse the force and pressure distribution within the thigh during an impact, rather than damage to the skin. Conversely, the surrogate model of Panchal et al. (2019) focused solely on the vibrational properties of the skin and underlying fat layer. There is a gap in the literature focusing on impact induced damage to the skin, either in isolation or with the underlying muscle and fat anatomy. During this research project, Hughes et al. (2020) developed a silicone material specifically for use in a test for assessing padded clothing in rugby. The

silicones developed were compared with relaxed organic muscle tissue (porcine) under slow compression ($0.067s^{-1}$), showing similar stress vs. strain response (Figure 2-18).
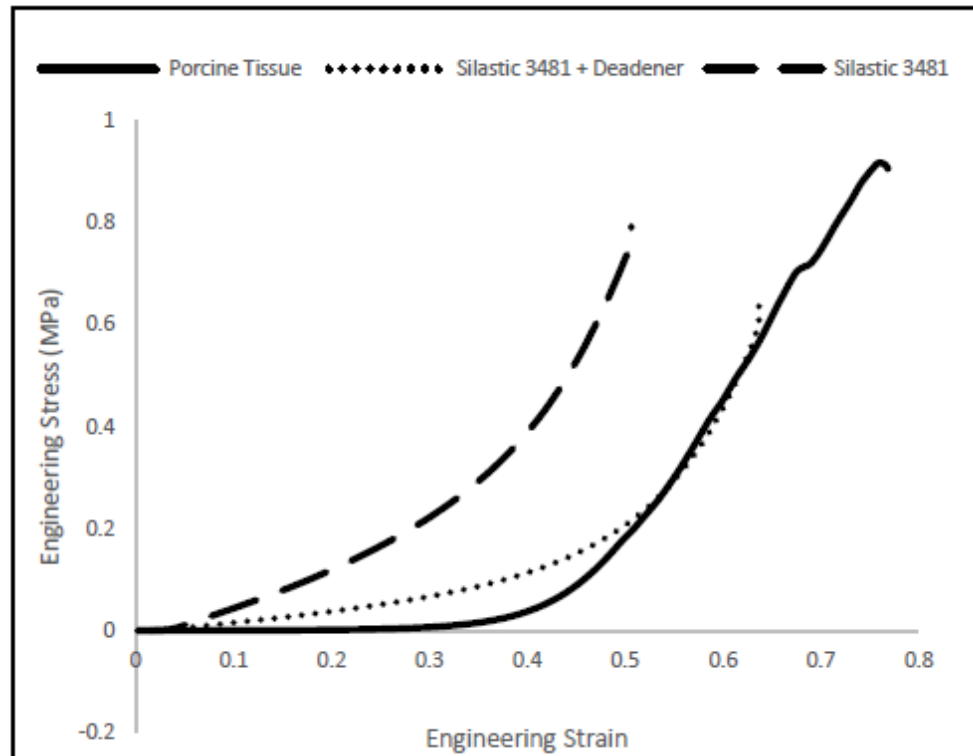
Figure 2-18: Compressive stress vs. strain plot of the different silicones fabricated by Hughes et al. (2020) against porcine tissue at 0.067 s^{-1}.

The combination of silicone used to manufacture the silicone was Silastic 3481, catalyst plus deadener in a 10:1:4 weight ratio. The base material used was similar to the single material silicones (Silastic 3481, 3483 and 3487) developed by Payne et al. (2015b). The silicone developed by Hughes et al. (2020) was incorporated into a shoulder surrogate (defined in Section 2.11). The shoulder surrogate developed by Hughes et al., specifically for assessing padded rugby clothing, will therefore be used as reference for simulating skin injuries.

2.10 Literature Review Summary

There is a high frequency (80-90 injuries per 1,000 PMH) of injuries, including cuts and lacerations, on the human skin tissue during the game of rugby. Skin injuries account for ~5% of match injuries and ~1.5% of training injuries in rugby. The

literature also suggests that skin injuries have been under-reported due to inconsistencies in injury definitions between studies, and the lack of standardised injury definitions. Epidemiology studies show little to no evidence of cuts and lacerations occurring on the shoulder region during rugby, which suggests that wearing shoulder padding to prevent such injuries is unwarranted.

With skin injuries being underreported in rugby and the padded clothing being tested for impact protection, Regulation-12 needs to be improved. As Regulation-12 does not specify the purpose of shoulder paddings, it is often misconstrued as equipment intended for reducing impact force, and hence for preventing serious injuries such as fractures and dislocations. Most impact test studies have provided results in the form of impact force reduction, which is not entirely aligned to World Rugby™'s intended purpose of shoulder padding. Impact testing of shoulder padding has focused on force attenuation properties in relation to scenarios like tackles and collisions. Studies have suggested that using a more biofidelic impact rig would provide a better understanding of the injury preventive properties of padding.

Products and techniques aimed at protection against stabs and cuts were analysed. A review of PPE designed to reduce the risk of cuts and stabs highlighted the need to reduce the impact force or to use stiff materials to reduce risk of skin injuries. The various standard testing methods studied were found to focus on the performance of the protective padding and did not directly consider damage to the underlying skin tissue. These standard testing methods use sharp impactors / indenter, such as blades, which are not replicative of any scenario that may occur in rugby. Skin stamping and raking / glancing test methods used in Regulation-12 to access stud design were analysed. The skin stamping, raking and glancing test provides a more biofidelic surrogate focused on testing the risk of skin injuries, but it excludes testing of padding material. Also, the materials suggested to be used in these biofidelic surrogates have no scientific backing. Though these tests lack the scientific evidence

behind the test parameters and the surrogate materials, they can be adapted as they replicate scenarios that are more likely to occur during a game of rugby.

Literature on FE modelling was reviewed, and FE modelling noted to be an established tool in simulating PPE to assess its performance. Various researchers have modelled (mathematical and / or analytical) the skin layer in isolation or along with the underlying muscle layer. Various silicones have been used to mimic muscle and skin tissues, with a focus on understanding impact force distribution. Little to no research has focused on predicting skin damage within simulation. To assess the role of PPE in preventing cuts and lacerations in rugby, there is a need to develop an FE model that can mimic such injuries.

2.11 Shoulder Surrogate Development

Hughes et al. incorporated the silicone developed into a shoulder surrogate intended for impact testing. Properties of the skin and underlying muscle and fat layers are variable, making modelling these materials complex. As part of this research project, at the University of Sheffield, a commercially available skin and fat (adipose) layer (SynDaver™- tissue plate) was procured and placed on top of the muscle silicone layer as an initial design (Figure 2-19).
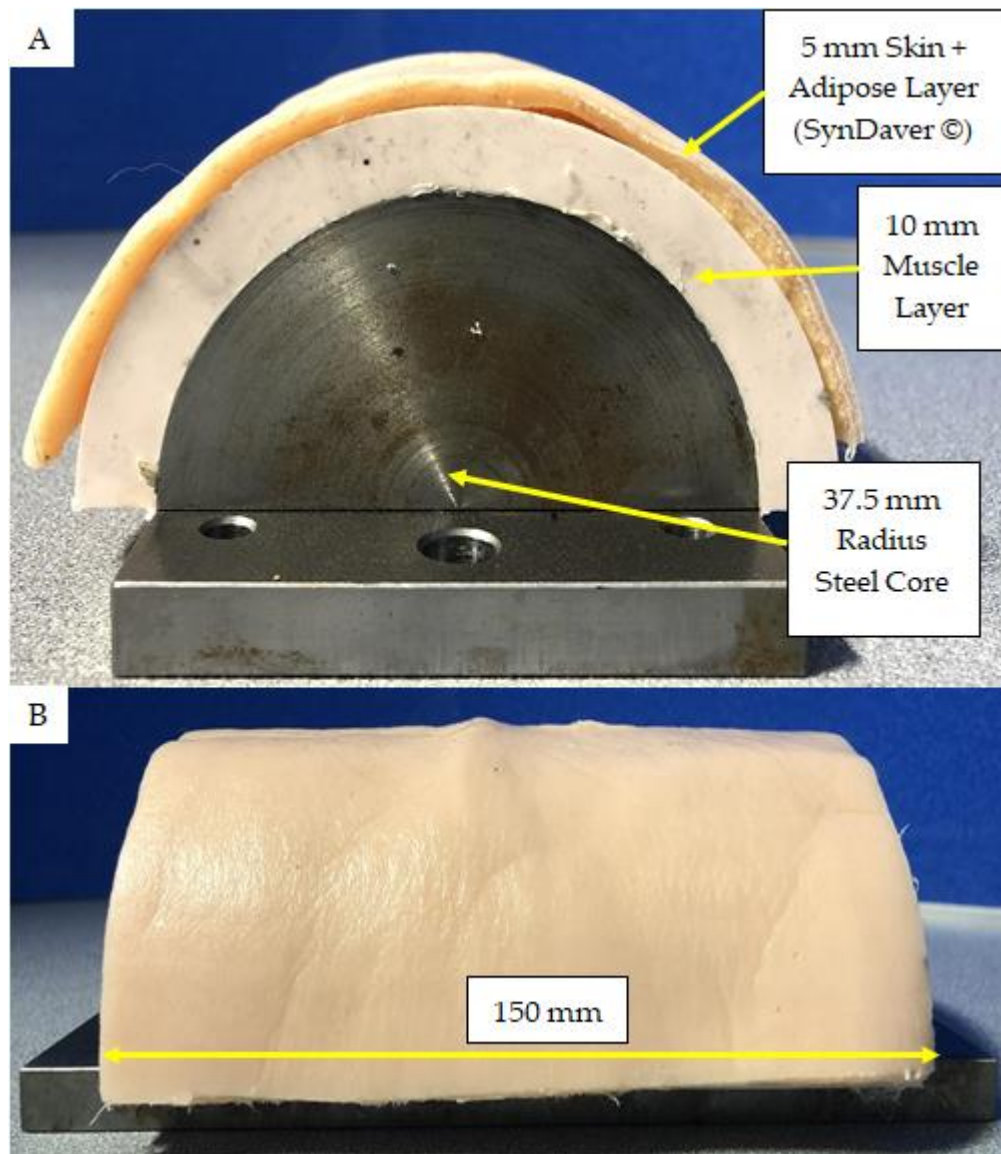
Figure 2-19: (A) cross-sectional view and (B) side view of the initial shoulder simulant developed by Hughes et al. (2020).

The initial shoulder (muscle and fat) simulant layers were then combined into one silicone (Figure 2-20) with a layer of synthetic leather to mimic the skin. The skin layer was made from synthetic chamois (1.5 mm) cross-woven polyvinyl acetate (PVA) (KCIC200, Kent Car Care, Manchester, UK), which has comparable force-deformation and frictional properties to human skin (Dąbrowska et al., 2016).
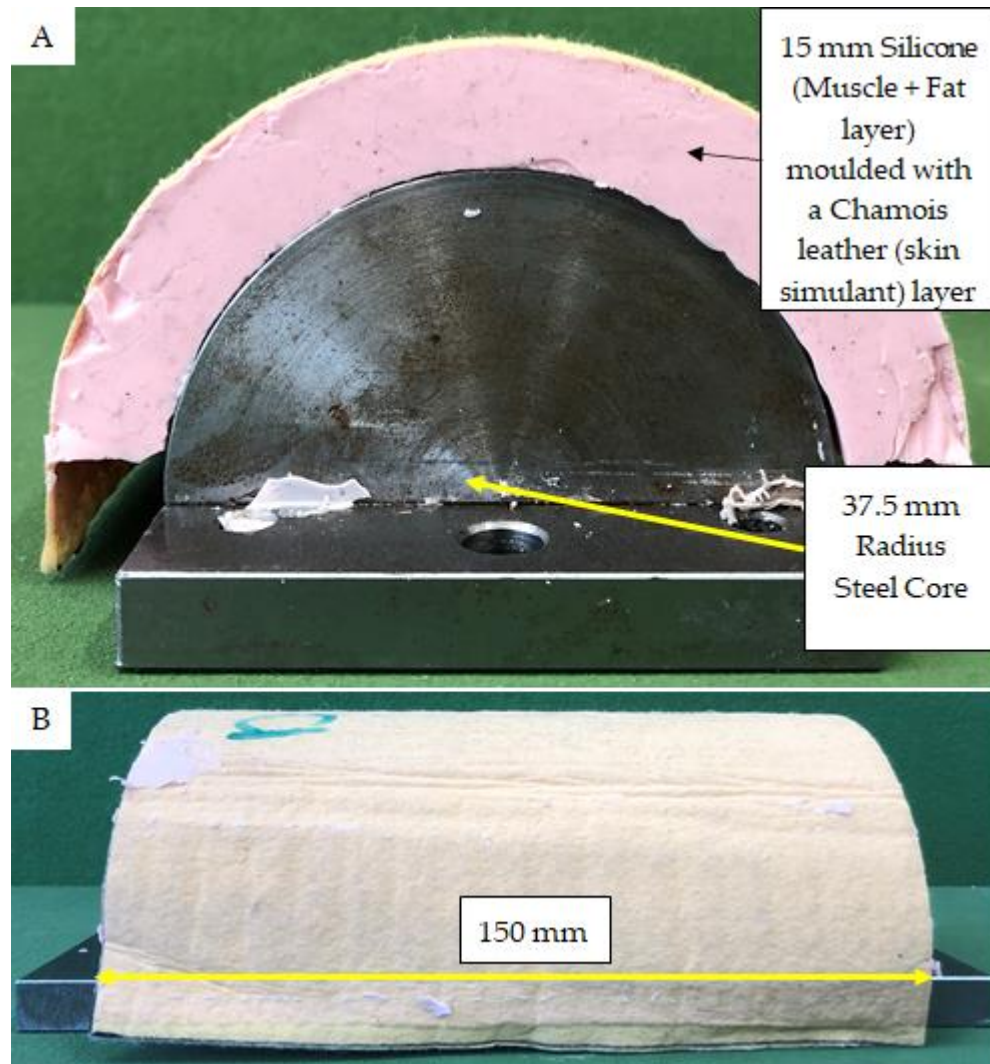
Figure 2-20: (A) cross-sectional view and (B) side view of the final shoulder surrogate - silicone simulant with chamois leather skin layer developed for modelling and validation.

This silicone and chamois leather-based shoulder surrogate has been fabricated for the purpose of testing impacts in rugby, specifically for predicting injuries to the human skin tissue. This simulant material could be incorporated into an FE model capable of mimicking the human skin and underlying muscle and fat tissue. The shoulder surrogate will, therefore, be used to support the development of an FE model capable of predicting skin injury from impact. The development of this model is presented in Chapters 5 & 6.

2.12 Injury Definitions for this research

In sections 2.2 and 2.3 the injuries rates for cuts, lacerations and abrasion were discussed in detail. For this research it is important to identify and define the types of injuries that are going to be studied. Van den Eijnde (2017) defines six types of skin wounds with their respective depth of cut as shown in Table 2-8. Abrasions and blisters are limited to the upper layers of the skin while the others affect the underlying layers.

Table 2-8: Types of skin wounds occurring on the human skin as defined by

Wound	Depth	Clinical Appearance
Abrasion	Epidermal	
Blister	Dermal-Epidermal	
Puncture	Hypodermal	
Laceration/cut	Hypodermal	
Tear	Hypodermal	
Contusion	Hypodermal	

Injuries which do not cause the skin to open up / split such as abrasions, blisters and contusions, were not included in the scope of the study. For this research the injuries which were causing a visible split to the outermost layer, i.e., puncture, cut / laceration or tear were included. This was done to provide a simple and clear visual representation of an injury occurring to the skin layer. In the surrogate developed, there was a clear visual difference in the colour of the Chamois leather (tan/brown) and the underlying silicone (pink). Hence during testing, if the chamois leather tore, and the pink colour of the silicone was visible, it was determined to have caused an injury such as a cut or a laceration. Similarly, in Chapter 6 a cut or laceration was identified when an element from the top layer of the model developed was deleted.

2.13 Chapter Summary

Literature on skin injuries in rugby and impact performance of rugby shoulder padding was reviewed. Literature relevant to protection against cuts and lacerations, such as stab prevention was studied. Standard tests were compared to identify gaps in the current test methods. Based on the literature review, there is a need to alter the regulations to ensure realistic and appropriate testing of materials used as shoulder padding in rugby. There is an identified gap in the literature in modelling skin injuries. The different models that can be used for mimicking the human tissue response have been discussed. Figure 2-21 summarises the main findings of this chapter. A review of the current Regulation-12 (Chapter 3) would help to both identify and understand the gaps and to define a better testing method. In the subsequent chapters (Chapters 5 & 6), details of techniques to model injury on the human skin tissue, such as cuts and lacerations, are presented, alongside validation of the models.

Injuries in Rugby
- Rugby injury rates are usually higher compared to other team sports.
- Varied injury definitions leading to skin injuries being under reported.
- Skin injuries have been reported on various locations on the body and mainly caused by studs.

Shoulder padding efficacy
- Most literature testing done have focused on force attenuation performance.
- Call for biofidelic testing setup, rather than rigid steel impactors.
- No reported testing carried out for efficacy against skin injuries.

Materials used in PPE
- Latest materials such as Auxetics, Dilatants & Bioinspired materials have shown potential for penetration resistance.
- Density criterion is restricting the use of these materials, but there is potential to vary density.

Stab Proof Materials
- Fabrics or UHMWPE fibres are being used in stab resistant clothing.
- Currently not observed in rugby padding, but could have potential application in shoulder padding.
- Most stab proof materials are beyond Regulation-12 limits.

Test Methods
- Test methods in standards use either sharp indenters (knives or blades).
- Stud stamping test available as standard but no rationale behind test parameters.

FE Modelling in Sports
- FE analysis has been used in sports to study the protective properties of various PPE.
- Using FE Analysis may allow to understand and analyse shoulder paddings in rugby.

FE-Modelling of Skin
- Most literature focus only on skin and not the underlaying muscle and fat layer.
- Simulant developed by Payne et al. is focused on thigh anatomy and force propagation, not injury to the human skin

Conclusion
- To predict skin injuries a shoulder surrogate(using skin, muscle and fat simulant) developed in University of Sheffield was developed as part of this project.
- This surrogate will be modelled using novel FE techniques to predict injuries such as cuts or laceration.

Figure 2-21: Summary of work presented in Chapter-2.

3. Review of Regulation-12

Following the literature review in Chapter 2, this chapter will focus on Regulation-12 and critique the relevant sections associated with this current PhD thesis as shown in Figure 3-1. Textual critique followed by detailed studies on understanding the coverage areas and the impact testing method will be presented. The findings of this chapter will help answer RQ1 and RQ2 from World Rugby™ presented in Chapter 1.
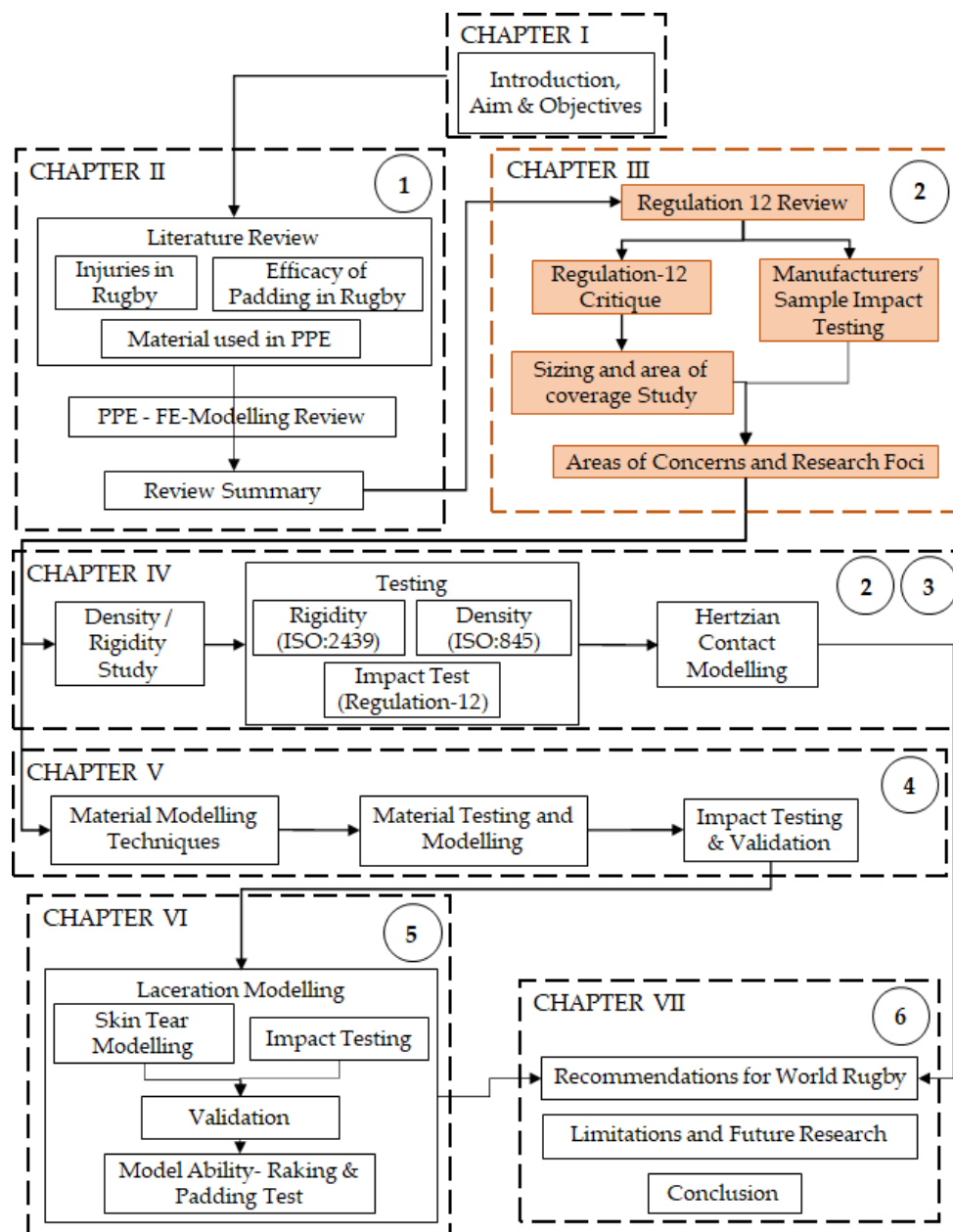
Figure 3-1: Layout of Thesis showing the placement of Chapter 3 with respect to the overall project. Numbers in circles correspond to objectives listed in Chapter 1.

3.1 Overview of Regulation-12

The World Rugby™ Handbook defines all the rules and regulations in the sport of Rugby, with Regulation-12 focusing on Provisions Relating to Players' Dress.

Regulation-12 is divided into three schedules:

- Schedule 1: Specifications Relating to Players' Dress, Law-4- Players Clothing
- Schedule 2: Safety Aspects of Rugby Boot Sole Design. General Design Guidance.
- Schedule 3: World Rugby™ Performance Specifications for Players Monitoring Device.

Schedule 1 is further divided into seven subsections covering design limitations and performance requirements of headgear, shoulder padding and breast padding. Sections 1 and 2 define the scope and the terminologies respectively for each subsequent section. Section 3 defines the requirements for headgear used in rugby whilst section 4 details the test methods and procedures for headgear testing. Section 5 defines the shoulder padding requirements covering ergonomics (5.1), construction (5.2), design (5.3) and performance requirements (5.4). Testing procedures for shoulder padding are defined in Section 6. Finally, Section 7 focuses on breast padding requirements. As this research is focussed only on shoulder padding, only sections 5 and 6 will be critiqued in detail.

3.2 Textual Critique of Regulation-12

Regulation-12 Section 5 details the requirements and test methods of padding materials. The aspects of Regulation-12 Section 5 that do not provide adequate information and need improvement have been explained below.

3.2.1 Section 5.2.1-Material Construction

Section 5.2.1 defines that the material should not be adversely affected by substances such as water, dirt, and perspiration. The regulation states "*It is the*

manufacturer's responsibility that all materials used should not be adversely affected by water, dirt, perspiration, toiletries, household soaps and detergents". However, no standards are cited in relation to how these properties should be tested. Standards such as ISO 15487 - '*Textiles - Method for assessing appearance of apparel and other textile end products after domestic washing and drying*', could be used for testing the fabric against soaps and detergents, while ISO 22958- '*Textiles - Water resistance- Rain tests: exposure to a horizontal water spray*' could provide information on how they are affected by water or perspiration.

3.2.2   Section 5.2.2- Padding Materials

Section 5.2.2 states "*Padding materials must be homogeneous (i.e. padding facing towards the wearer must be the same texture, hardness and density as that facing the opponent). Foam padding of sandwich construction is not allowed*". Homogeneity of the padding material is ambiguous as the pads are usually cut or moulded into non-uniform structures, so they adhere to and fit the body of the wearer better (as seen in manufacturer samples in Section 3.4). The restriction on sandwich constructions has been removed from the World Rugby™ regulations for headgear and replaced with a requirement to test the construct in both directions. Testing padding in both directions could allow manufacturers to use designs with non-homogeneous materials, while ensuring no advantage to the wearer and no increase of injury risk to the opposition.

3.2.3   Section 5.3.1- Zone of Coverage
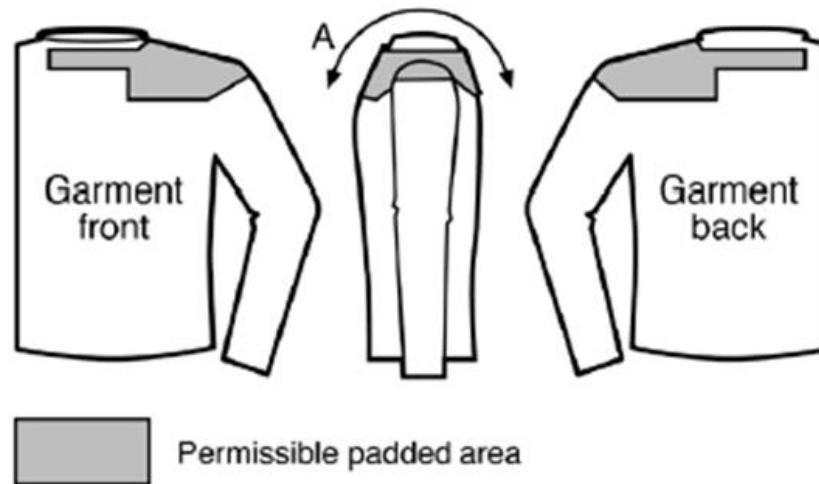
Figure 3-2: Image from Regulation-12: Areas of Coverage.

The zones of coverage (Regulation-12 - Section 5.3.1) describes the areas where padding of the jersey is permitted (Figure 3-2). Section 5.3.1 defines zones of coverage around the shoulder region where padding is allowed (Permissible padded area). In the following text, the regulations state "*Areas outside the designated zones of coverage do not have to meet impact requirements*" which allows manufacturers to place padding outside the shoulder region. Any padding placed outside the shoulder region only needs to meet a thickness criterion (max 5 mm) and the same density restriction ($45 + 15$ kg·m^{-3}).

The padding material density must not exceed $45 + 15$ kg·m^{-3}, thus giving a maximum limit of 60 kg·m^{-3}. Furthermore, density is the only physical material property that is used to regulate the padding material. However, a procedure for testing of material density has not been detailed and can be erroneous if paddings have non uniform structures and are combined with other materials (as they often are). An additional or alternative parameter, such as hardness or indentation resistance, could help restrict hard materials, improving regulation of the padding and ease testing methodology.

Section 5.3.1 therefore, suggests that padding material can be placed in areas other than the specified zones of coverage. As the impact attenuation testing criteria

(Regulation-12 - Section 6.3) only applies to the zones of coverage. Padding material outside these zones does not need to match any impact attenuation performance criteria, thus the effect of which is unknown. Therefore, as padding outside the coverage area does not have to undergo any impact testing, manufacturers can place paddings with improved impact force attenuation performance beyond the allowed limits.

3.2.4 Section 5.4.1-Performance Requirements - Impact Attenuations

The performance requirements section limits the maximum protection a shoulder padding can offer. Section 5.4.1 states "*the peak acceleration of impacts delivered to test locations shall not be less than 150 g*". The minimum peak acceleration value (150 g) does not appear to be underpinned by any supporting research. Also, the 150 g value (~8 kN force) is higher than the impact forces reported during a tackle on an instrumented bag (2-6 kN) (Seminati et al., 2017). Using values that are supported by literature would better define the limiting impact force attenuation value.

As Regulation-12 limits the maximum impact force attenuation, materials with little or no impact protection capabilities or hard materials could pass the impact attenuation performance requirements and be classified as paddings.

3.2.5 Section 6.2- Condition of Specimens

Section 6.2 highlights that test specimens must be acclimatised at temperatures of 20° C and 50° C. However, these temperature values have not been backed up by any scientific evidence. Understanding the ranges and simulating real-life playing conditions might provide more realistic performance scenarios (Meir et al., 2003; West et al., 2014; Brewer and Davis, 1995).

3.2.6 Section 6.3.2 Impact Attenuation Testing Apparatus

This section defines the impact test setup as a flat impactor dropping onto a steel anvil. This rigid setup does not reflect any gameplay interaction between players and or turf. The impact test scenario is not replicative of tackles, or other collisions,

in rugby, especially those that cause injuries such as cuts and lacerations. Using a more biofidelic impactor and anvil would help improve our understanding of the impact and performance of the padding in reducing the risk of injuries such as cuts and lacerations.

For data acquisition the regulation states "*Accelerometer - an accelerometer is mounted at or close to the centre of gravity of the drop mass. The impact shall be recorded and displayed on a storage oscilloscope with specified deflection factor, sweep speed per division and bandwidth for the accelerometer and be capable of resolving the g_{max} of the drop weight. Equivalent instrumentation capable of recording, displaying, and storing the impact signal from the accelerometer shall meet this requirement*"

It has been reported within the literature that using an accelerometer can lead to a variance depending on the mounting technique (Jang et al., 2008; Seimetz et al., 2012). Using a force plate or load cells underneath the anvil may help capture the temporal impact force being transmitted through the padding to the anvil.

3.2.7   Section 6.3.4 - Impacting

Section 6.3.4 details the impact test method but the criterion for acceptable performance has not been defined. The section states "*Each shoulder pad is impacted at two locations providing the size of padding allows a distance of not less than 30mm apart and at least 20mm from the periphery of the padding. Where size of shoulder pad does not allow this then a single location for each padding is permitted.*" The regulation does not specify if each impact or the mean of the impacts needs to meet the 150 g limitation.

Therefore, to identify any further gaps in the regulation, samples of already approved rugby paddings were obtained and tested as per the regulation for this current PhD thesis.

3.3   **Manufacturer Sample Testing**

At the commencement of this PhD, companies were approached who market padded clothing for use in rugby to take part in this research study. A presentation

was carried out to inform the manufacturers at a World Rugby™ Manufacturers meeting of the aims and objectives of the research study. Following the meeting, a notification of interest was sent out to inquire about the willingness of the manufacturers to be a part of this research study. In response to the notification, a total of seven manufacturers expressed interest to take part in the research. They all offered to provide samples and were willing to provide their corresponding test results for comparison (provided the test reports were being dealt with privacy and confidentiality). Following the response, a letter (Appendix A) requesting four samples of each design of the XL size of the padded clothing was circulated amongst the interested manufacturers. Ten designs (four samples of each) were provided by four manufacturers.

3.3.1 Manufacturer Sample Testing as per Regulation-12

To critique the existing testing methodology, 11 different shoulder paddings (ten from manufacturers and one purchased) and one control material (Aortha White Plastazote®-LD-60, Algeos) (meeting the thickness: 10 mm, and density criterion in Regulation-12: LD-60 corresponds to 60 kg·m^{-3}) were impact tested using the impact rig shown in Figure 3-3-A following Regulation-12-Section 6.3.4 specifications and methodology.
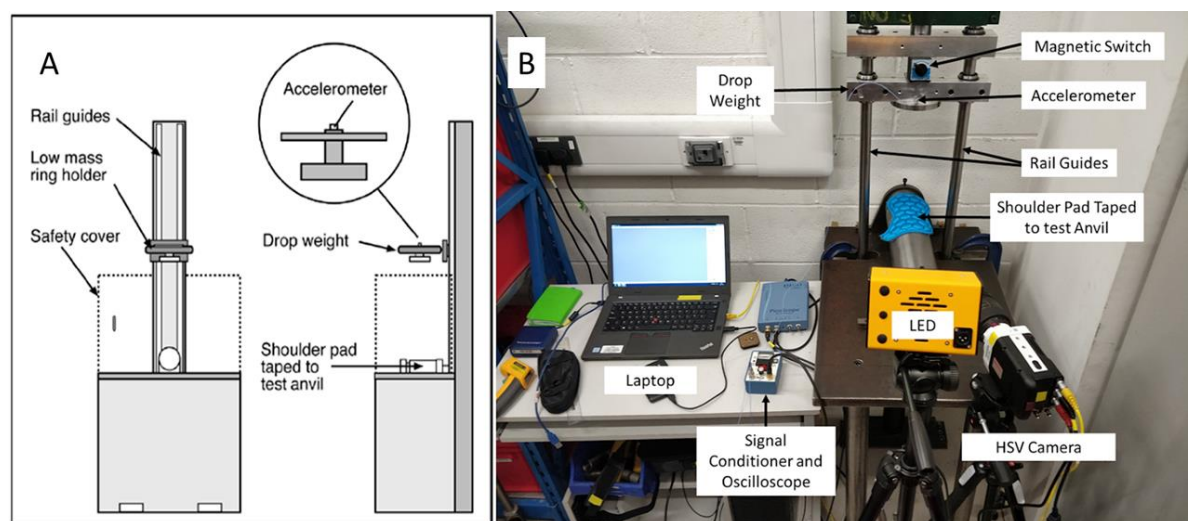
Figure 3-3: (A) Drop rig schematic described in Regulation 12 and (B) Drop rig used for testing manufacturer samples along with data logging equipment.

Method

Two samples (one each for hot and cold conditioning) of the shoulder padding were cut from the jerseys (one of each model provided by the manufacturers) creating a total of 12 samples at each temperature rating. One sample from each design was then acclimatized in an oven (LHT6/30, Carbolite Gabe Ltd, UK) for at least 4 hours at 50 °C[3] (as stated in Regulation-12), while the other sample was maintained at room temperature (20 ± 2 °C). Thickness measurements were obtained at three different locations using a digital Vernier Calliper (Duratool- Carbon Fibre Composite Digital Calliper). Each sample was then tested at an impact energy of 14.7 J using circular flat face (Ø 130 mm) impactor of mass 5 kg from 30 cm drop height on a horizontal steel cylinder (Ø 115 mm) as shown in Figure 3-3-B. The drop mass was fitted with a single axis accelerometer (352B01-ICP-Accelerometer, PCB Piezotronics) sampling at 20 kHz and connected to an oscilloscope software PicoScope® (Version 6, Pico Technology) via an ICP® sensor signal conditioner (480B21, PCB®), to enable temporal acceleration to be obtained throughout impact. The impact was filmed with a High-Speed Video (HSV) Camera (Phantom Miro R111, Vision Research, USA) with a zoom lens (Nikon AF Nikkor 24-85mm 1:2.8-4 D, Nikon Corporation, Japan). The camera was set to a resolution of 512 × 320, a sample rate of 10 kHz and an exposure rate of 99.00 µs. The camera was synchronised with the accelerometer using the PicoScope.

Each sample was impacted three times with a one-minute recovery time between each test. One-minute recovery time allowed hot condition testing to be completed within five minutes of removing the padding from the oven (as stated in Regulation-12 Section 6.2). From the data collected, peak impact acceleration for each impact of the sample was calculated and the results were analysed.

---

[3] Reasoning behind the value has not been provided in Regulation-12. Was used in this research to carry out as per regulation and identify if it provided any added value to testing at 20° C.

Results

Impact testing as per Regulation-12, on eleven samples of rugby padding and one control material (padding 12), showed varied impact force attenuation capabilities across the testing temperature (Table 3-1). Amongst manufacturer samples, on average there was an increase in mean peak acceleration from room temperature to hot temperature testing from 645 to 819 g. All samples met the minimum peak acceleration value of 150 g specified in Regulation-12. The control material at room temperature produced peak acceleration values of 112 g, which was lower than the restricted 150 g value. The same material at the hot temperature testing produced an average peak acceleration of 162 g.

Table 3-1: Thickness and Peak Acceleration results from sample testing at 20 °C and 50 °C (Results shown as Mean ± SD).

Padding No	Testing Temperature 20 ± 2 °C		Testing Temperature 50 ± 2 °C	
	Thickness (mm)	Peak Acceleration (g)	Thickness (mm)	Peak Acceleration (g)
1	9.9 ± 0.1	498 ± 119	9.9 ± 0.2	1,070 ± 18
2	10.9 ± 0.3	361 ± 51	11.0 ± 0.5	587 ± 69
3	10.1 ± 0.1	760 ± 97	9.9 ± 0.1	911 ± 58
4	9.7 ± 0.2	633 ± 101	10.0 ± 0.2	1,112 ± 3
5	9.8 ± 0.4	1,010 ± 156	-	-
6	10.6 ± 0.2	471 ± 80	10.0 ± 0.7	691 ± 133
7	8.1 ± 0.2	427 ± 127	10.8 ± 0.6	592 ± 88
8	8.1 ± 0.2	1,131 ± 20	8.5 ± 0.4	1124 ± 3
9	8.5 ± 0.7	869 ± 177	-	-
10	10.5 ± 0.1	699 ± 258	10.8 ± 0.8	656 ± 142
11	5.7 ± 0.1	230 ± 12	5.7 ± 0.1	629 ± 380
12*	10.1 ± 0.1	112 ± 24	10.1 ± 0.1	161 ± 22
	Mean ± SD	**645 ± 317**	**Mean ± SD**	**819 ± 316**

[c]Control Material *Mean values shown for paddings (Sample 1-11) only, control material excluded from calculations.

Some samples showed signs of degradation / plastic (permanent) deformation on first impact. The deformation occurred at the area of contact between the anvil and the impactor (Figure 3-4).
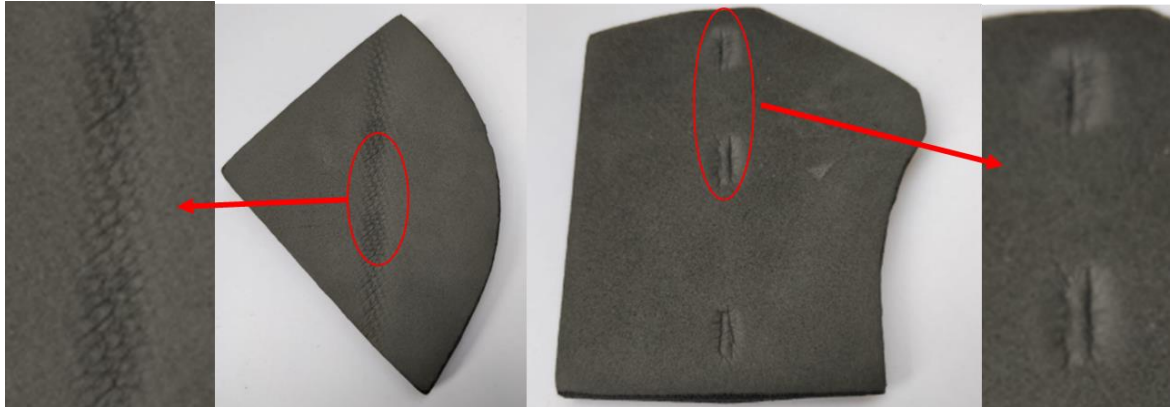
Figure 3-4: Manufacturer samples with areas of plastic deformation highlighted in red.

The acceleration values obtained from the testing showed a large standard deviation value, ranging from 12 to 258 g at 20 °C, and 3 to 380 g at 50 °C. The mean standard deviation excluding the control material, was 109 g at 20 °C, and 99 g at 50 °C. The mean standard deviations account for almost 73% and 66% of the regulation limit set at 150 g.

3.3.2   Study of Padding Variations

Visual inspection of various padded clothing specimens for rugby showed that the areas of padding differed between designs, which has been highlighted in Section 3.2 - textual critique of Regulation-12. A list of approved padded clothing was obtained from the World Rugby™ website (World Rugby™ Approved Equipment List - shoulder padding), which contained a plethora of padding and padding equipment (Figure 3-5). The list was filtered to account for only padded jerseys (eliminating detachable or shoulder pads not incorporated into clothing) and the corresponding images for 24 designs were obtained.

Figure 3-5: Examples of approved designs with varied padding area outside the shoulder region- highlighted in red. (Images obtained from retailers' websites).

Method

Twenty-four male padding designs were studied, and the front and rear images were analysed to identify areas of padding. A numeric grid design was overlaid on the shirt template and then on each design to recognise areas of presence / concentration of padding (Figure 3-6 a). The grids were populated by cumulating the number of different designs having padding in that specific grid (Figure 3-6 b). Similar grids were used to analyse the rear areas of the padded clothing.
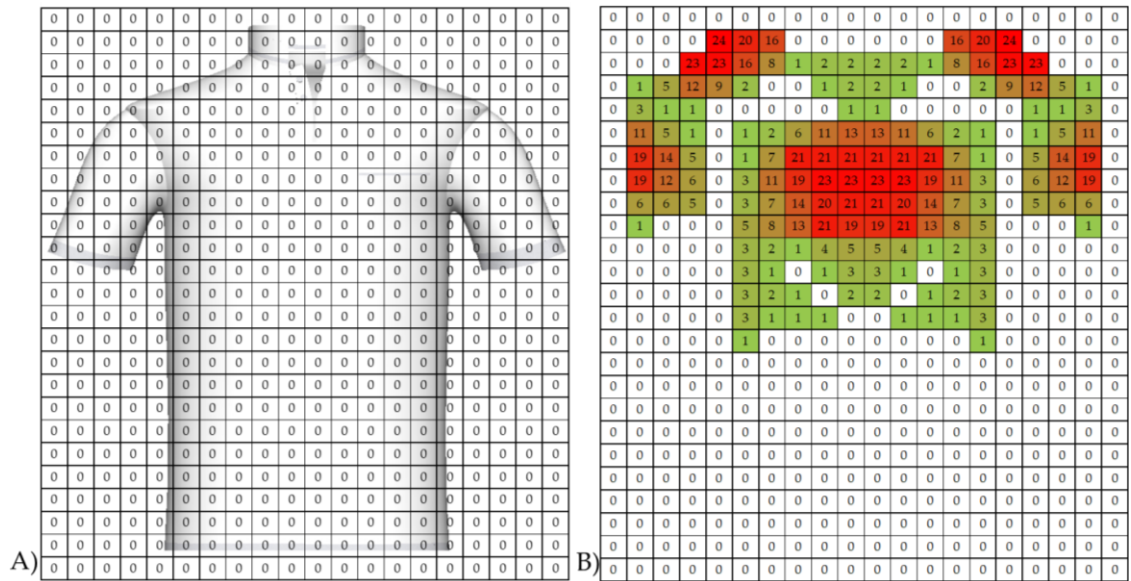
Figure 3-6: Grid used to identify areas of padding on the front of a padded jersey. a) blank grid over template and b) grid after being used to analyse 24 designs. Numbers represent count of different designs having padding in the respective grid.

The areas were then grouped into two sections: (i) areas where padding was present (at least one design) and (ii) areas with high frequency of padding (i.e. at least 14 different designs (60%) having padding in an area).

Results

23 / 24 designs (~96 %) of padded jersey analysed showed presence of padding outside the permissible padded area, highlighting the point raised in the critique of Regulation-12 that padding appears outside the described areas. Areas of high concentration of padding were identified and highlighted (Figure 3-7-B).
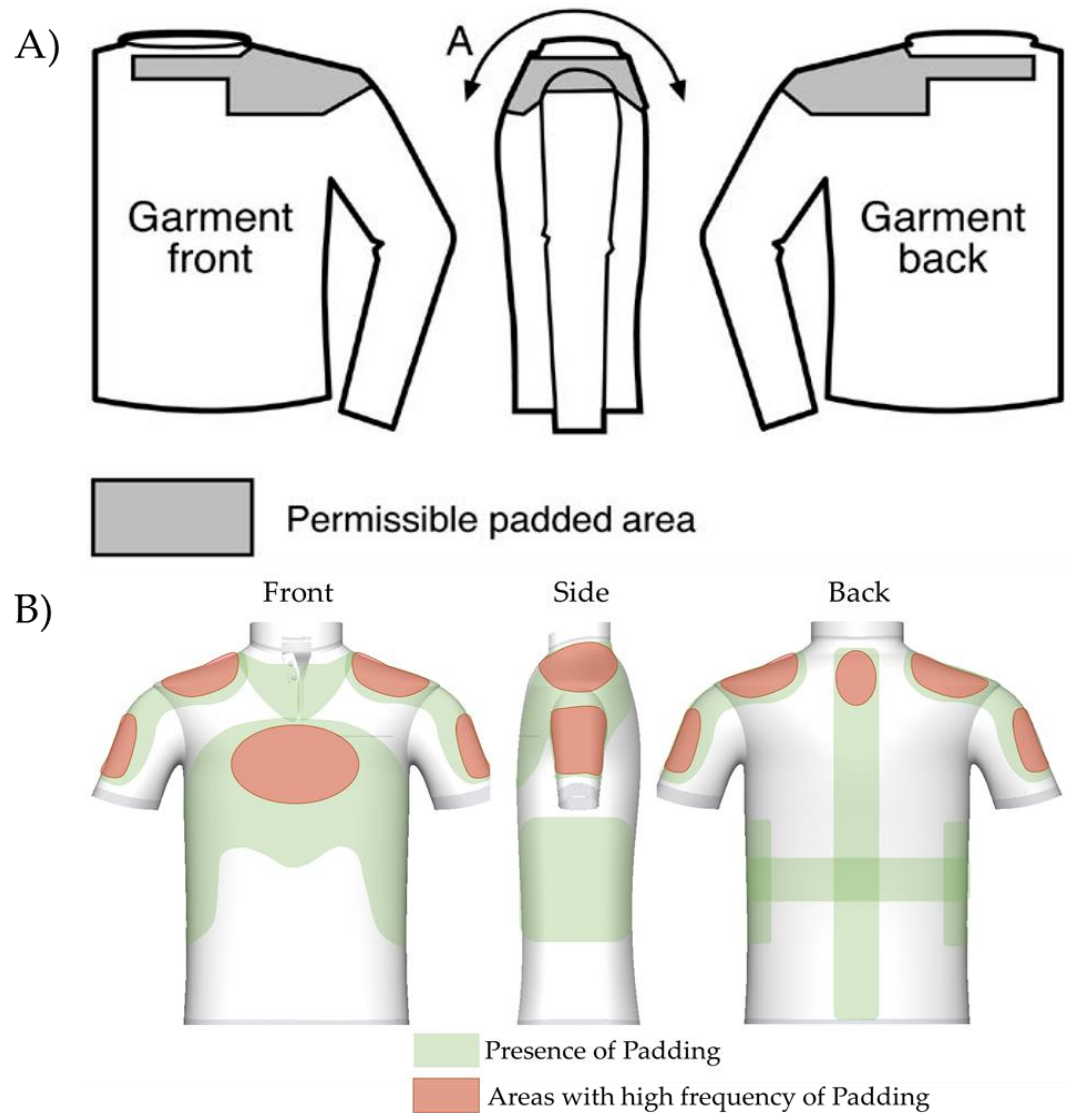
Figure 3-7: (A) Permissible areas of padding as per Regulation-12 compared to (B) Areas of concentration of padding in approved designs, high-frequency area highlighted if padding is present in more than 60% of designs.

3.4 Discussion

The studies and findings carried out within this chapter provide supporting evidence to answer RQ1 and RQ2 from World Rugby™.

RQ1: Is the current requirement for padded clothing appropriate for the modern game of rugby, how and why?

● The Regulation-12 (as per May 2019) did not define the purpose and intended use of the padding, nor require manufacturers to state this on their products, leading to ambiguity of its perception and effectiveness.

- The impact attenuation test outlined in Section 6.3 of Regulation-12 features a cylindrical rigid anvil and a flat faced rigid striker with 15 J of energy. There is no evidence to suggest that this test is representative of a rugby injury scenario, particularly those that put players at risk of sustaining cuts or lacerations.

- Ambiguity in Regulation-12 allows padding to be placed outside of the shoulder region, which has led to jerseys with padding in other locations and these paddings do not have to conform to the impact performance criterion.

- Furthermore, padding placed outside the shoulder region does not need to conform to the impact attenuation criteria, which could allow manufacturers to place padding in these areas with better impact force attenuation properties (e.g. under 150 g limit).

- Sizing mentioned (nominal rather than range) can lead to ambiguity in the designated sizes of jersey between manufacturers, and in turn to the maximum area of shoulder padding coverage (zone of coverage) between different sizes.

RQ2: Is the current requirement for padded clothing appropriate in permitting the use of modern technology, how and why?

- Density is the only defining physical material property for the padding in the current Regulation-12, and with development of technology it is possible to change the hardness (and other properties) of a material while maintaining a constant density (e.g. auxetic foams and other auxetic materials). Due to the moulded design and irregular shape of padding, measuring density is challenging and prone to inaccuracy.

- The requirement for homogeneity of the padding restricts design innovation and could be replaced by testing the padding inside and out (ensuring no increased risk to the opposition). Some non-homogenous padding, such as

3D printed structures, could have varied performance based on the direction of testing.

- The current Regulation-12 also does not provide clear information on the restriction of futuristic materials / technologies (e.g. 3D printed structures, smart clothing / fabrics, bio-inspired clothing) which could form, or be embedded into, the padding and jersey.

- As the impact attenuation test is only carried out at one impact energy scenario (set mass and drop height), the specifications do not account for all materials, such as non-Newtonian materials which can behave differently under different strain rates (e.g. different energies, impact speed, and impactor and anvil geometry and hardness).

3.5   Conclusion

Based on the findings of the studies carried out, the current Regulation-12 needs to be updated to address the areas of concern. The areas of concern identified have been summarized in Table 3-2 and were presented to World Rugby™ as part of the regular updates and to the manufacturers at the World Rugby™ manufacturers meeting held in November-2018. The findings of this chapter were used to make updates to the Regulation-12 and resulted in the release of 'Body Padding performance specifications' in June 2019. The new documentation states that the intention of padding is only to reduce the risk of injuries such as cuts and lacerations. The performance specification has been renamed to cover the different areas of the jersey and not just shoulders but is subject to change based on the findings of the research project. The performance specification still contains the impact test methodologies and material requirements and will be updated following the completion of the research studies and a trial period expected to start in 2022.

Table 3-2: Summary of areas of concern identified in Regulation-12.

Criterion	Details	Recommendation	Reason / Rationale
Density-Defining Parameter	Density is the only defining criteria for the material to be used as padding.	To remove the density criterion and / or add a rigidity test method to test the padding.	With the development in manufacturing techniques and creation of new materials such as auxetics, the density of the material can be kept constant which changing the rigidity
Area of coverage	The areas of permissible padding areas have been defined but the wordings of the regulation allow paddings on the other areas as well.	Rewording the section to specifically identify the areas which require padding and limiting padding use to the specified areas	Currently the padding on the areas apart from the shoulder do not have to meet any impact acceleration criteria. Restricting areas will also allow uniformity of designs and better control over the designs
Performance requirements	Currently only limiting criteria is the minimum impact acceleration protection value of 150 g.	Adding a range of values of impact acceleration could help limit the range of performance of the padding. Addition of other impact testing procedures to test for injuries such as cuts and laceration. Use of synthetic surrogate (instead of the current rigid impactor) to mimic real life scenarios.	The current regulation limits only the maximum protection allowed. This allows any material with very low or no impact protection capabilities to be also classified as padding.

3.6   **Chapter Summary**

Chapter 3 focused on critiquing Regulation-12 and identifying the areas that need to be addressed during this research. Experimental testing of the manufacturer provided samples for impact force attenuation performance were tested at two temperatures, following the guidelines detailed in Regulation-12. Placement of padding material on the jersey was also analysed. The areas of Regulation-12 that need to be assessed and improved along with the reasoning and rationale have been listed in Table 3-2 and future chapters will detail the work carried out in these areas. The findings of this current chapter have resulted in the release of an updated regulation named '*Performance Specifications-Body Padding*', which will be updated following the completion of the research project. A summary of this chapter has been presented in Figure 3-8. The following chapter (Chapter-4) will focus on reviewing efficacy of density (used in Regulation-12) along with other material properties, as the defining material properties.

Regulation - 12
- Defines the rules and limitations on shoulder padding and corresponding test methods to measure these parameters.
- Does not define the intended use of shoulder padding

Defining properties
- Area of Coverage
- Density limitation
- Impact Attenuation Testing & Performance

Area of Coverage
- Limited padding allow on the shoulder area – but wordings allow padding to be put other places too.
- Paddings outside the shoulder area only need to meet thickness, no impact attenuation limit.

Density Limitation
- Limit set at max 60 kgm^{-3} but no testing method defined.
- It limits the use of paddings to foams but is not suitable for futuristic materials.
- Literature suggests foam density can be reduced while maintaining stiffness.

Impact Test Attenuation
- Impact between rigid impactor and anvil- not replicative of any rugby game play scenario.
- Impact energy and limiting acceleration value have no scientific backing.
- Use of accelerometer was noted to be noisy and overestimating the impact acceleration

Areas of Focus
- Need to define the intended use of padding (for cuts and lacerations only).
- Need to defined a better test methodology to check for use of stiff materials.
- Need to define a biofidelic test to test efficacy of shoulder paddings against skin injuries.

Updated Regulation
- During the project, Regulation-12 was revised based on feedback from Chapter 3.
- Shoulder paddings changed to Body padding (no longer limited to shoulder region)
- Intended use of body padding defined as reduction of risk related to cuts and lacerations.

Figure 3-8: Summary of work presented in Chapter-3.

4.   Material Property Regulation for Padded Clothing

4.1   Introduction

As shown in the literature review, the density of a material can be reduced while maintaining hardness. As measuring density does not provide any useful information on material hardness, this chapter investigated the potential of hardness testing as a replacement of the density requirements of rugby padding material. Chapter 4 will, therefore, start forming the basis of the recommendations to be made to World Rugby™ for improving Regulation-12 (Figure 4-1).
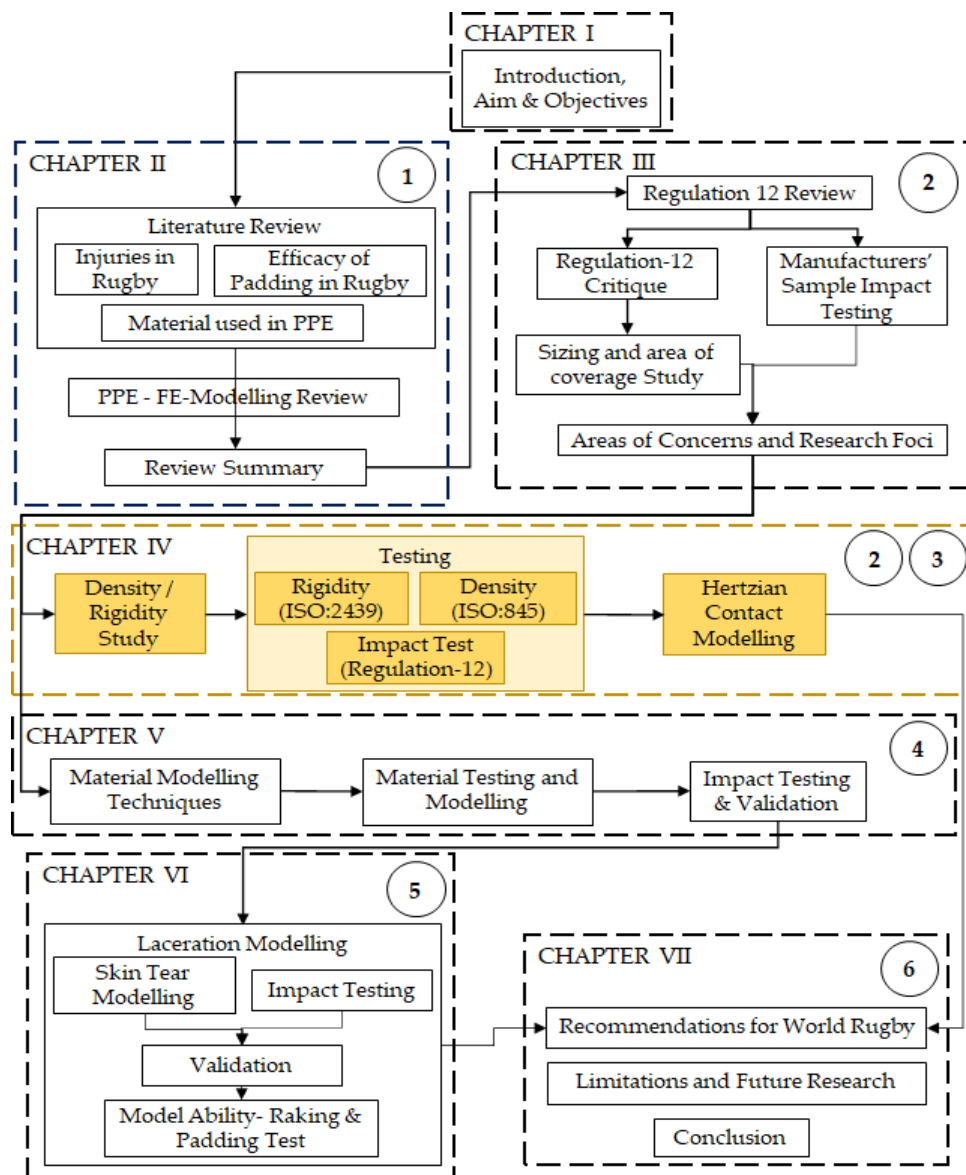
Figure 4-1: Layout of thesis showing the placement of Chapter 4 with respect to the overall project. Numbers in circles correspond to objectives listed in Chapter 1.

Regulation-12 specifies limitations on padding thickness (10 (+2) mm), material density (45 (+15) kg·m⁻³) and impact performance (acceleration >150 g for a 14.7 J impact, referred to as impact attenuation performance in Regulation-12). Regulation-12 does not specify a method for measuring padding density. Rugby padding often combines foam with fabric layers (Figure 4-2-A), typically compressed into regular or irregular geometries (Figure 4-2-B-D). Density measurements according to ISO 845 require foam samples to be cut into a shape such that its volume can be easily calculated. The combination of fabric and foam (typically bonded together) and the varied geometry of padding means density measurements can be challenging, and prone to uncertainty.
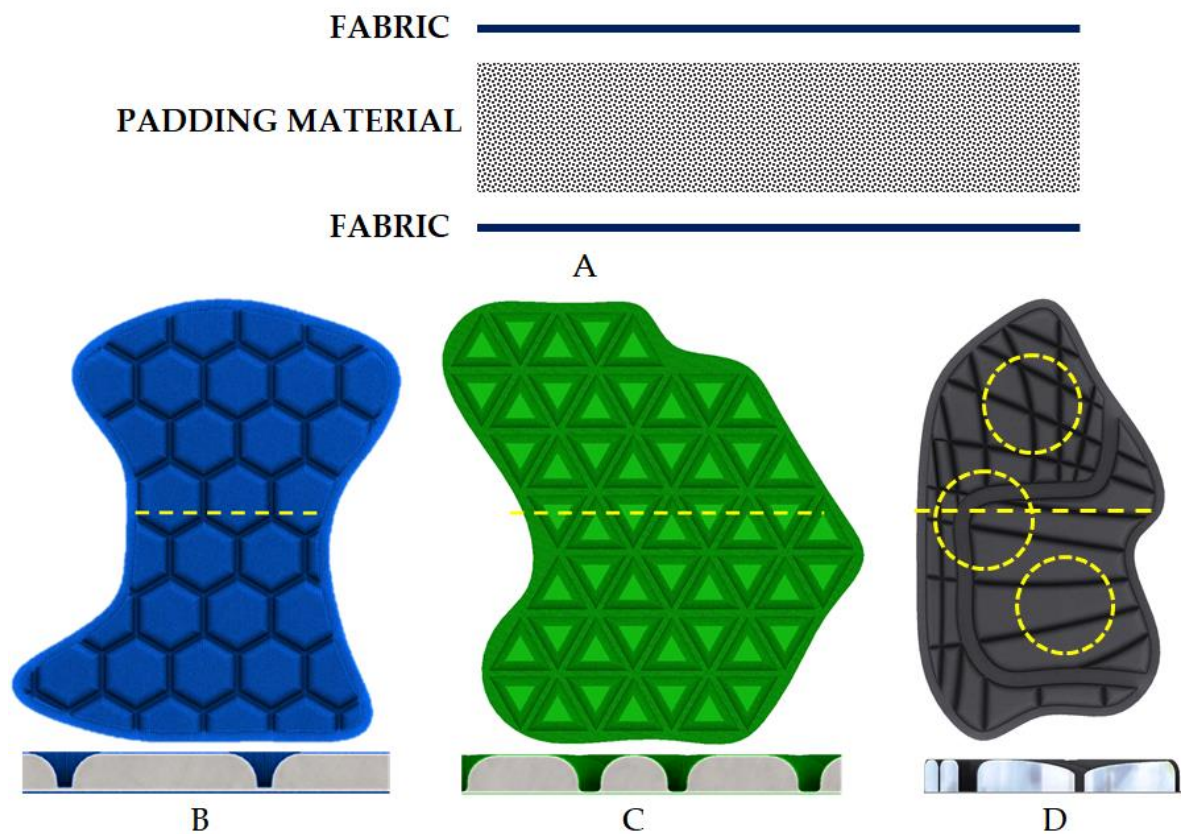
Figure 4-2: (A) Typical cross-sectional makeup of a rugby padding along with computer-aided design reconstructions of approved paddings showing (B) hexagonal, (C) triangular and (D) irregular patterns with enlarged cross-sectional view showing variation within the geometry.

On the other hand, PPE focusing on indentation resistance and impact attenuation usually has a hard outer shell over a padding material (Figure 4-3-A), such as PPE for American football (Figure 4-3-B) and hockey (Figure 4-3-C).
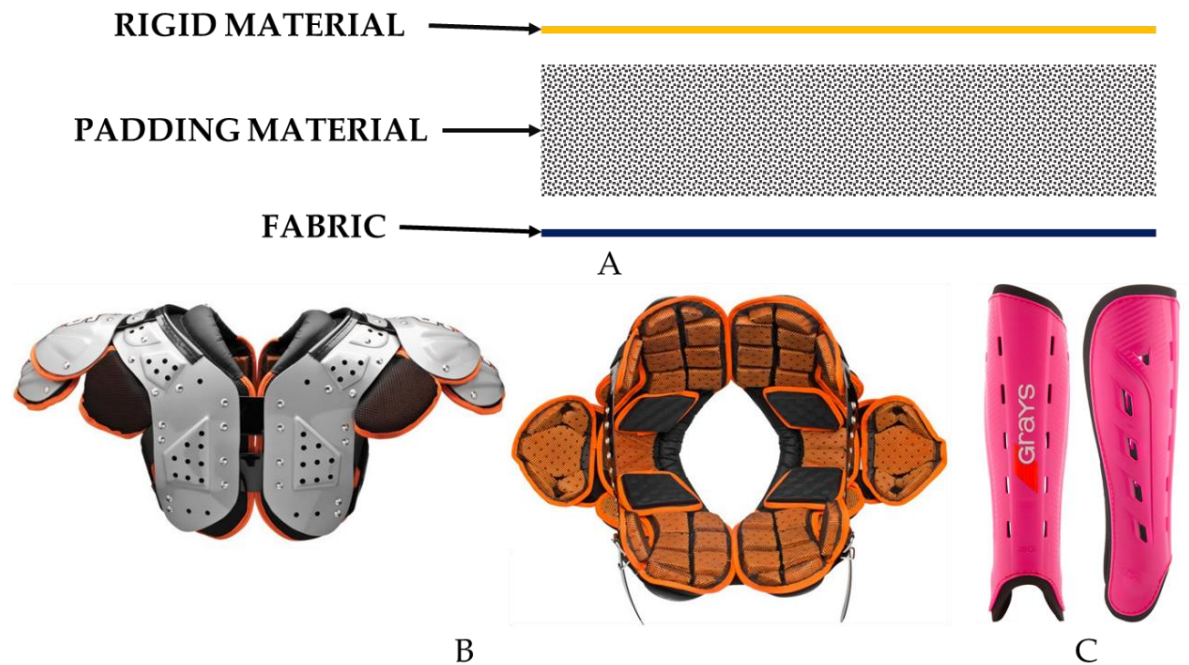
Figure 4-3: (A) Typical cross-sectional make of a PPE focusing on indentation resistance along with example of similar padding equipment for examples (B) American Football - XV HD All Purpose Shoulder Pads-Schutt and (C) Field Hockey Shin Pads- G-600- Grays.

PPE with a hard shell could meet the impact attenuation criterion set in the Regulation-12, which simply limits the maximum acceleration that can be attenuated during an impact (>150 g for a 14.7 J impact). With advances in manufacturing, the impact performance of padding material can be tailored without (substantially) changing density, as with auxetic (Duncan et al., 2018; Chan and Evans, 1998) and biomimetic (Svagan et al., 2008) foams. Currently, hard materials may not meet the density criterion stated in the regulation, but in future there could be a possibility of low density high hardness material. Testing for hardness could be done using different hardness tests defined in ISO 2439 -'*Flexible cellular polymeric materials — Determination of hardness (indentation technique)*'.

Measuring the hardness of rugby padding, following the methods in ISO 2439, would most likely be easier and more accurate and repeatable than measuring its

density. With World Rugby™'s intention to limit impact acceleration attenuation provided by padding (>150 g for a 14.7 J impact), hardness testing could complement the impact test. Hardness testing could be performed at low strain rates and could prevent the use of hard materials, such as plastic shells, which could pass the impact test but change the nature of the game and may put players at risk of other injuries, like cuts, lacerations and abrasions. The edge of a hard shell could become sharp and serrated with wear / use, for example, and then pose a risk to soft tissue damage.

Impact test energies used in this chapter were based on the works of Seminati et al., (2017), who reported that the range of peak force during a shoulder tackle is between 2-6 kN. During pilot testing, 9.8 J impact provided a comparable peak impact force to the median of the range of values reported by Seminati et al. (2017). To analyse the trend between impact energy, density of the material and peak force during impact, three energies 4.9, 9.8 and 14.7 J were used. These values also provided drop heights which were easy to measure using the drop mass of the regulation-12 drop rig and included the Regulation-12 defined test values (14.7 J).

This chapter investigates the potential of hardness tests for replacing the density criterion of padding in World Rugby™ Regulation-12. Following the hardness testing, FE simulations are used to understand the effect of introducing a hard material over a foam padding material, and the ability of the hardness test to detect presence of a hard covering.

4.2 Methods

Eleven designs of World Rugby™ approved jerseys were obtained from five manufacturers. Intact padding samples (size range: 150 × 120 mm to 280 × 220 mm) were taken from the shoulder region. A 220 × 150 mm sample of control material (Aortha White Plastazote®-LD-60, Algeos), which met the thickness and density (LD-60 corresponds to 60 kg·m^{-3}) requirements of Regulation-12, was also tested alongside the padding samples for hardness, impact performance and density.

4.2.1 Hardness Testing

Hardness testing was carried out according to ISO 2439, using a uniaxial testing machine (Hounsfield HK10S) with a 1 kN load cell (0.5% or 5 N accuracy). The sample was compressed with a 62 mm diameter indenter (Figure 4-4) at a rate of 100 mm/min. Sample thicknesses were measured before testing with a height gauge (Dial Gauge, J.E. Baty & Co., UK, accuracy: 0.01 mm) and used to calculate compressive strain. Samples were subjected to the five testing methodologies in the standard:

- A: Force at 40% strain after a 30 s hold;
- B: Forces at 25% (B-25), 40% (B-40) and 65% (B-65) strain, after a 30 s hold at each strain;
- C: Instantaneous force at 40% strain;
- D: Force at 20% compression after a 20 s hold;
- E: Ratio of forces at 25% and 65% strain during the compression cycle.

For Methods A to D, a higher force reading corresponds to a higher Hardness. Method E gives a compression deflection coefficient that only provides information about the load bearing properties of the material and cannot be linked directly to its hardness.
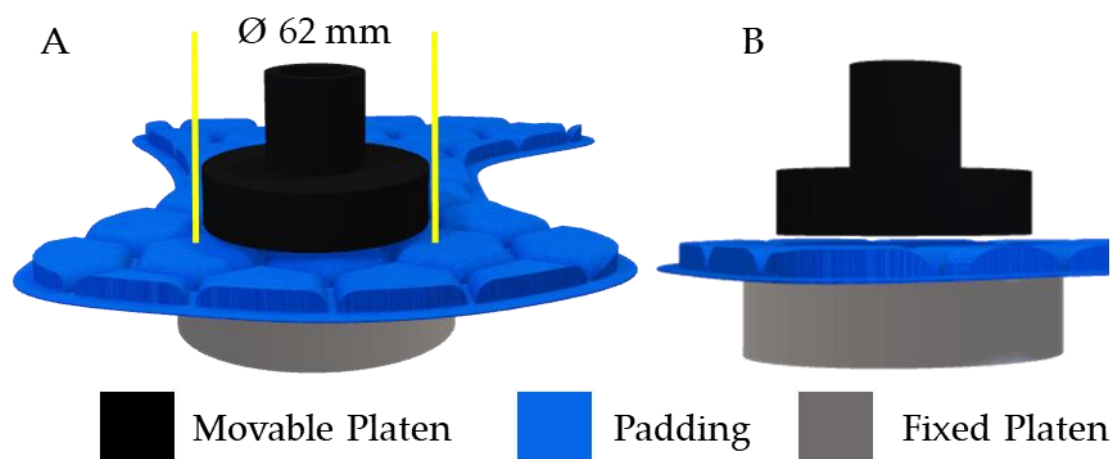
Figure 4-4: (A) front view and (B) side view of CAD reconstruction of the hardness test setup using the Universal testing machine.

4.2.2   Impact Testing

Samples were impacted at energies of 4.9, 9.8 and 14.7 J using a 5 kg mass (flat face, Ø 130 mm) dropped from 0.1, 0.2 and 0.3 m (Figure 4-5-A). The anvil (horizontal steel cylinder, Ø 115 mm) was fixed on four load cells (208C05-Force Sensor, PCB Piezotronics) which sampled at 20 kHz and were connected to an oscilloscope (PicoScope®, Version 6, Pico Technology) via two 3-Channel ICP® sensor signal conditioners (480B21, PCB®) to record impact force. To measure deformation, each impact was filmed with a High-Speed Video (HSV) Camera (Phantom Miro R111, Vision Research, USA) with a zoom lens (Nikon AF Nikkor 24-85mm 1:2.8-4 D, Nikon Corporation, Japan). The camera was set to a resolution of 512 × 320, a sample rate of 10 kHz and an exposure rate of 99.00 μs. The camera and load cells were synchronized using the oscilloscope. Temperature of the laboratory was monitored hourly during testing to ensure the it stayed within the limit (20 ± 2 °C).
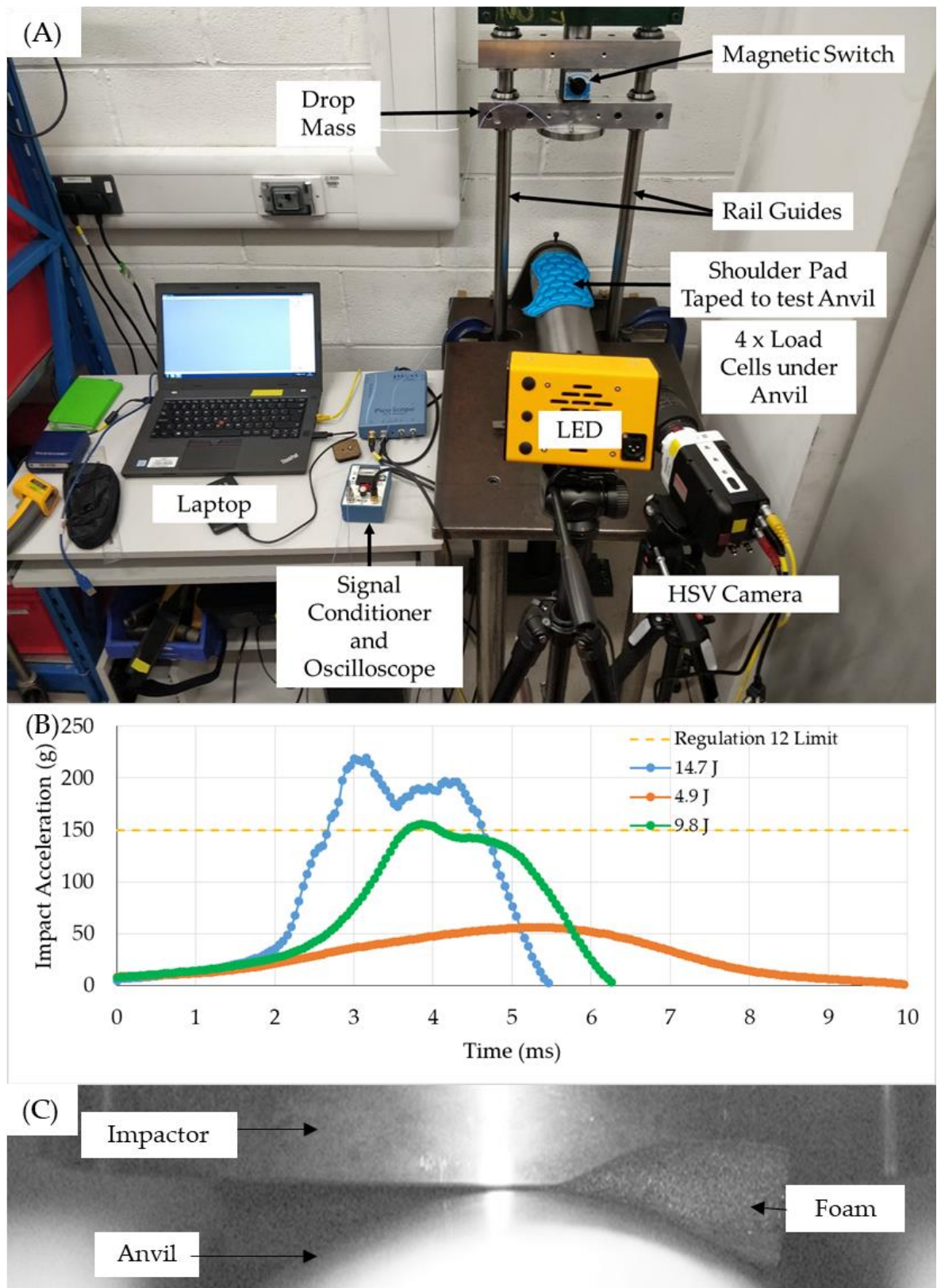
Figure 4-5: (A) Drop rig setup (as per Regulation-12) used for impact testing, (B) sample output graph for impacts at 4.9, 9.8 and 14.7 J and (C) a High-Speed Video (HSV) image at 4.9 J.

Each sample was impacted three times at each energy with at least one minute between impacts. The sample was moved between impacts to change the impact location (as per Regulation-12: 20 mm from the periphery and minimum 30 mm apart). The voltage readings from each load cell were exported in an MS Excel® file and then converted to force using the corresponding calibration factors (range: 0.2214 to 0.2399 mVN^{-1}) provided by the manufacturer. The forces from the four load cells were summed to give the total force at each timestep. Peak force was divided by the weight of the drop mass (5 kg $\times$ 9.81 ms^{-2} = 49 kg·ms^{-2}) to give acceleration in g (as per Regulation-12).

4.2.3 Density Testing

Density measurements were carried out according to ISO 845. Following impact testing, five cylindrical specimens were cut from each padding sample (at varied locations) using a wad punch (Ø 9.8 mm to accommodate padding patterns). The diameter (mean of three locations: two ends and approximate middle) and height of each specimen were measured using a Vernier calliper (Composite Digital Vernier Calliper, Silverline®) and used to calculate the volume. The mass of each cylindrical specimen was measured using a balance (ABS 220-4N, KERN®, Germany). Density of the padding was calculated as the ratio of specimen mass to volume. The mean values for thickness, hardness, density and peak acceleration for each sample were compared using a Spearman's rank correlation at a confidence level of 95% using Minitab® (V18 Statistical software, USA).

4.2.4 Inter and Intra User Error Calculations

The specimens obtained for density testing were warped (Figure 4-6) and were not uniform cylinders. The diameter was noted to change across the height of the sample, which caused variance in density calculations.
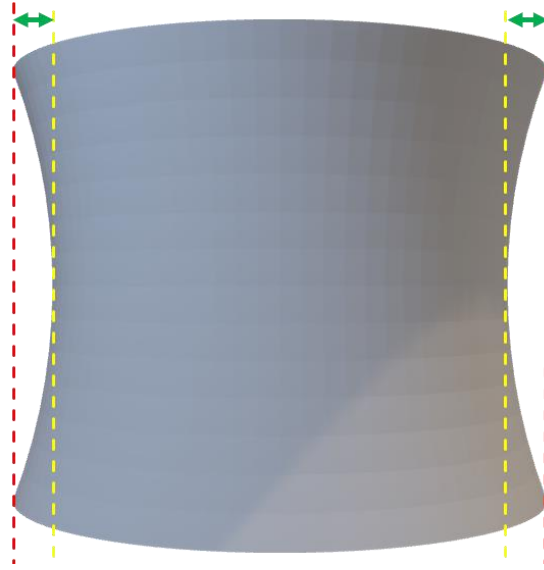
Figure 4-6: CAD representation of warped cylindrical structure of specimens obtained from cutting foams for density measurements Dotted lines and arrows depicting the variance in diameters.

The diameter and height of one cylindrical specimen was measured five times by three operators and the resultant density values were used to estimate the intra operator error (E_{INTRA}), as the coefficient of variation (CV) (Equation 4-1).

$$E_{INTRA} = \left(\frac{\sigma_{op}}{\mu_{op}}\right) \times 100 \%$$
<div style="text-align:right">Equation 4-1</div>

where σ_{op} is the standard deviation and μ_{op} is the mean density for each operator.

Ten cylindrical specimens (5 from Sample 1 and 5 from Sample 6) were measured once by two additional operators (giving three total) to estimate inter-operator error E_{INTER} (Equation 4-2).

$$E_{INTER} = \sqrt{(\sigma_1^2 + \sigma_6^2)}$$
<div style="text-align:right">Equation 4-2</div>

where σ_1 and σ_6 are the CV values for the two sets of five specimens (from Sample 1 and 6) for combined density measurements for all three operators (Equation 4-3).

$$\sigma_n = \left(\frac{\sigma_{sample\_n}}{\mu_{sample\_n}}\right) \times 100, \ (n = 1, 6)$$
<div style="text-align:right">Equation 4-3</div>

where σ_{sample_n} is the standard deviation and μ_{sample_n} is the mean of all density measurements for a sample set.

The height of one sample was measured three times by three operators and the resultant hardness test results (using the universal test machine) were used to estimate intra operator error (E_{INTRA}), as the coefficient of variation (Equation 1). The heights of samples 4 and 7 were measured three times by each operator before being tested for hardness. As done for measuring thickness, each sample was tested for hardness over three locations and the force values were noted. Inter-user error measurements for hardness were calculated using Equations 2 and 3 (Samples 4 and 7 replacing Samples 1 and 6 respectively).

The error propagation (E_{PROP}) during the density calculation was estimated using the accuracy of the measuring instruments for variables in Equation 4-4,

$$E_{PROP} = \sqrt{\left(\frac{A_B}{m}\right)^2 + 2\left(\frac{A_C}{d}\right)^2 + \left(\frac{A_C}{h}\right)^2}$$

<div align="right">Equation 4-4</div>

where A_B is the balance accuracy (0.1 mg), m is the measured mass, A_C is the calliper accuracy (0.01 mm), d is the measured diameter and h is the measured height.

The error in hardness measurement was the accuracy of the load cell which, according to calibration certificate, was under 0.5% (5 N).

4.2.5 Finite Element Modelling of Hardness Testing

To assess the effect of placing a hard shell over a more compliant padding material, a 12 × 75 × 75 mm cuboid was modelled in SolidWorks 2018 (depicting a section of the padding material with the maximum allowable thickness under Regulation-12). The .sldprt was imported into Ansys© Static Structural and the geometry was split into two sections, corresponding to a hard shell and underlying padding (Figure 4-7). The compression plates were modelled as a rigid cylinder with a diameter of 62 mm and a fixed rigid cuboidal (75 mm side and 5 mm thickness) base.
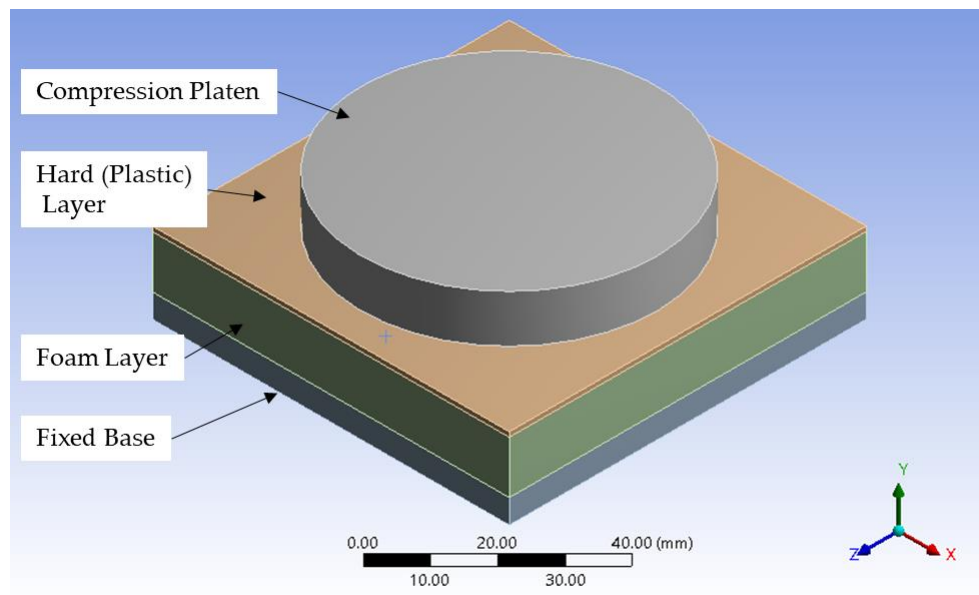
Figure 4-7: Geometry to analyse the change in hardness due to the presence of a hard layer on a foam layer.

The material chosen for the foam was EVA foam (linear elastic: E = 0.24 MPa and v = 0.3) from the Ansys© material library, as the density (60 kg·m^{-3}) of the EVA foam was equal to that of the control material and EVA foam is commonly used in PPE (Foster et al., 2018; Duncan et al., 2016; Casey, 2020). The material used for the hard shell was High Density Polyethylene (HDPE) (E = 1,080 MPa, v = 0.418 & Density = 958 kg·m^{-3}) (Ansys© Material library), which is widely used in a similar way in shoulder pads, shin pads and helmets (Casey, 2020).

The simulation setup was based on the ISO 2439 standard Method C: instantaneous force at 40% strain as the aim was to determine the instantaneous hardness. The compression platen was set to move 4.8 mm (40% of 12 mm) in the y-axis at a rate of 100 mm/min (Figure 8-A). The compression platen and base plate were defined as Steel material (Ansys © library). Mesh definitions for the foam and hard shell were set as hexahedral body sizing of 2 mm and edge divisions to ensure three layers across the (Figure 8-B). The setting ensured constant mesh count quality across the different thicknesses detailed in Table 4-1.

Table 4-1: Mesh properties of different geometries modelled for compression simulation.

Part	Nodes	Elements
Compression Platen	6,508	1,254
Hard shell	22,503	4,332
Foam layer	22,503	4,332
Base Plate	1,515	196

All contacts between the layers and the platens were defined as frictional with static coefficient of friction value 0.3. The thickness of the shell was increased from 0.3 to 1.0 mm, in steps of 0.1 mm, and from 1-10 mm, in steps of 1 mm, while maintaining the overall thickness (foam and shell) at 12 mm. The normal reaction force at the base was noted at maximum compression (Figure 8-C). A simulation was also performed without the shell (foam layer thickness of 12 mm) to obtain a comparison to the control material results from the experiment.
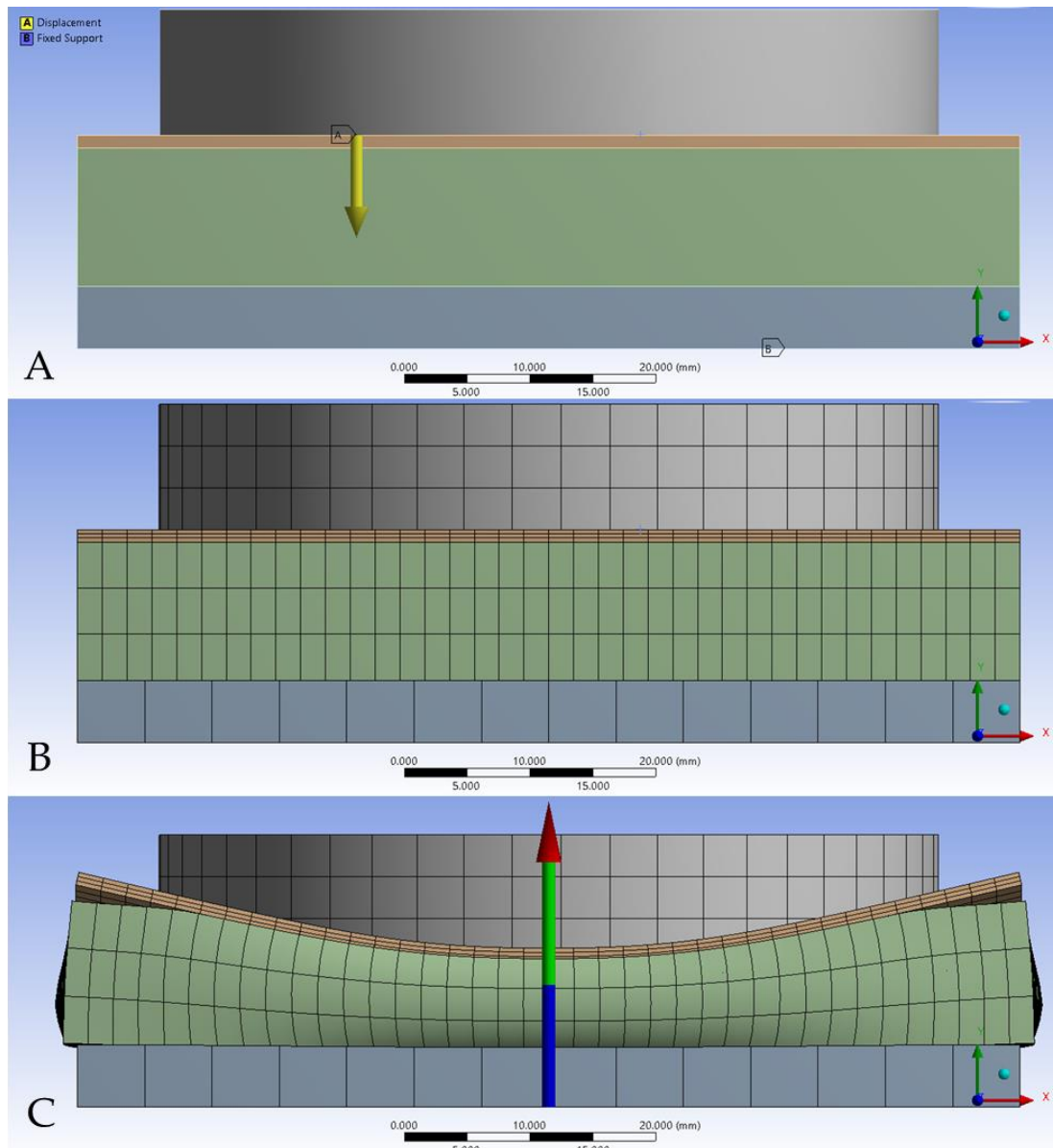
Figure 4-8: (A) Boundary conditions defined as y-axis displacement of the compression platen and fixed support on the base. (B) Mesh definition to ensure at least 3 layers of mesh across the hard shell and foam layer and (C) Ground reaction force measured at maximum compression.

4.3 Results

Force values from the hardness tests on the padding increased with the applied strain (B-65 > B-40 > B-25), and instantaneous readings were typically higher than those after a hold period (C > A) (Table 4-2).

Table 4-2: Force measurements using the five different methods in ISO 2439. (Mean ± SD. * has no unit. ** Control material.)

S. No.	Thickness (mm)	Force values (N)						
		A	B-25	B-40	B-65	C	D	E*
1	10.3 ± 0.2	220 ± 3	129 ± 2	234 ± 1	590 ± 13	248 ± 1	131 ± 7	4.3 ± 0.1
2	10.5 ± 0.3	178 ± 2	97 ± 4	187 ± 8	511 ± 31	175 ± 10	102 ± 2	5.0 ± 0.2
3	9.6 ± 0.2	154 ± 10	90 ± 4	171 ± 9	460 ± 36	184 ± 10	83 ± 5	4.9 ± 0.3
4	10.2 ± 0.1	204 ± 2	111 ± 6	206 ± 9	518 ± 27	236 ± 4	118 ± 1	4.4 ± 0.2
5	9.8 ± 0.1	96 ± 19	45 ± 6	124 ± 5	330 ± 49	201 ± 6	33 ± 4	5.9 ± 0.7
6	11.0 ± 0.2	145 ± 7	76 ± 7	156 ± 6	423 ± 5	162 ± 8	77 ± 5	4.9 ± 0.2
7	10.1 ± 0.3	169 ± 11	102 ± 12	187 ± 13	452 ± 33	189 ± 10	94 ± 3	3.9 ± 0.1
8	7.7 ± 0.3	97 ± 9	44 ± 8	104 ± 14	368 ± 34	105 ± 12	38 ± 3	7.2 ± 0.1
9	8.1 ± 0.4	128 ± 4	60 ± 4	134 ± 4	409 ± 13	112 ± 7	59 ± 3	5.3 ± 0
10	11.0 ± 0.3	196 ± 41	96 ± 10	197 ± 18	577 ± 83	207 ± 38	78 ± 8	4.8 ± 0.3
11	5.8 ± 0.1	46 ± 1	33 ± 1	54 ± 4	174 ± 22	64 ± 4	24 ± 3	6.1 ± 0.4
12 **	10.2 ± 0.2	274 ± 14	202 ± 17	354 ± 19	781 ± 63	337 ± 16	169 ± 1	2.9 ± 0

For all samples, peak acceleration increased with impact energy (Table 4-3). At 14.7 J impact energy, all peak acceleration values were above the Regulation-12 limit of 150 g. All samples at 9.8 and 14.7 J impact energy were observed (through HSV images) to bottom out (over 90% compression) during impact (Figure 4-9).

Table 4-3: Peak impact acceleration at three impact energies (Mean ± SD. ** Control material)

Sample No.	Peak Impact acceleration (g)		
	4.9 J	9.8 J	14.7 J
1	57 ± 1.4	153 ± 2.6	220 ± 1.2
2	57 ± 1.5	151 ± 0.7	221 ± 0.7
3	71 ± 2.1	163 ± 6.3	229 ± 1.1
4	62 ± 0.1	148 ± 4.4	223 ± 2.9
5	106 ± 4.5	171 ± 2.0	232 ± 1.3
6	66 ± 2.3	149 ± 3.0	223 ± 1.4
7	56 ± 2.3	138 ± 4.0	210 ± 5.2
8	113 ± 2.6	181 ± 4.4	222 ± 2.3
9	91 ± 4.2	174 ± 2.5	220 ± 4.4
10	70 ± 7.9	156 ± 6.5	215 ± 7.5
11	84 ± 0.8	146 ± 0.6	183 ± 1.3
12[**]	44 ± 0.7	95 ± 4.2	155 ± 5.7
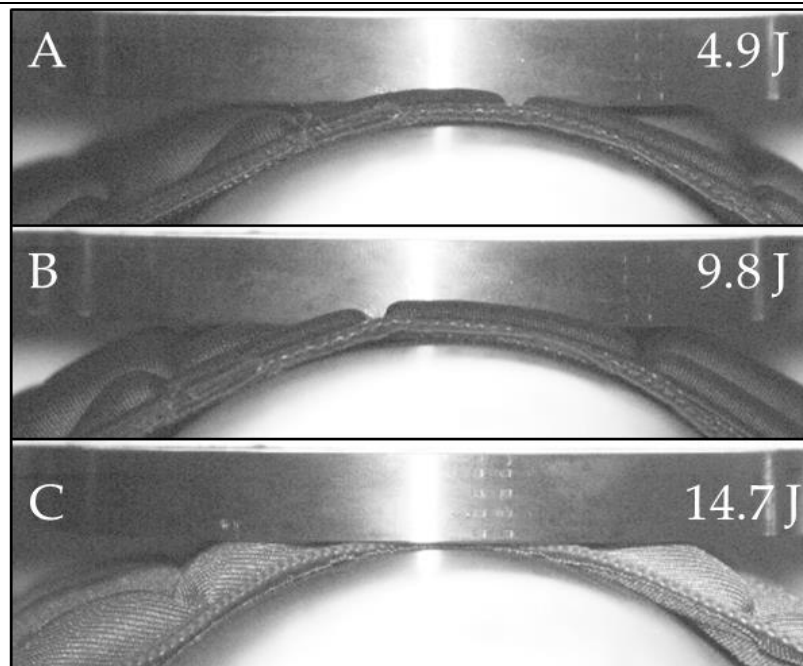
Figure 4-9: Samples at maximum compression (over 90%) at (A) 4.7 J, (B) 9.8J and (C) 14.7 J.

The density of seven out of the 12 padding samples exceeded the Regulation-12 limit of 60 kg·m^{-3} (Figure 4-10).
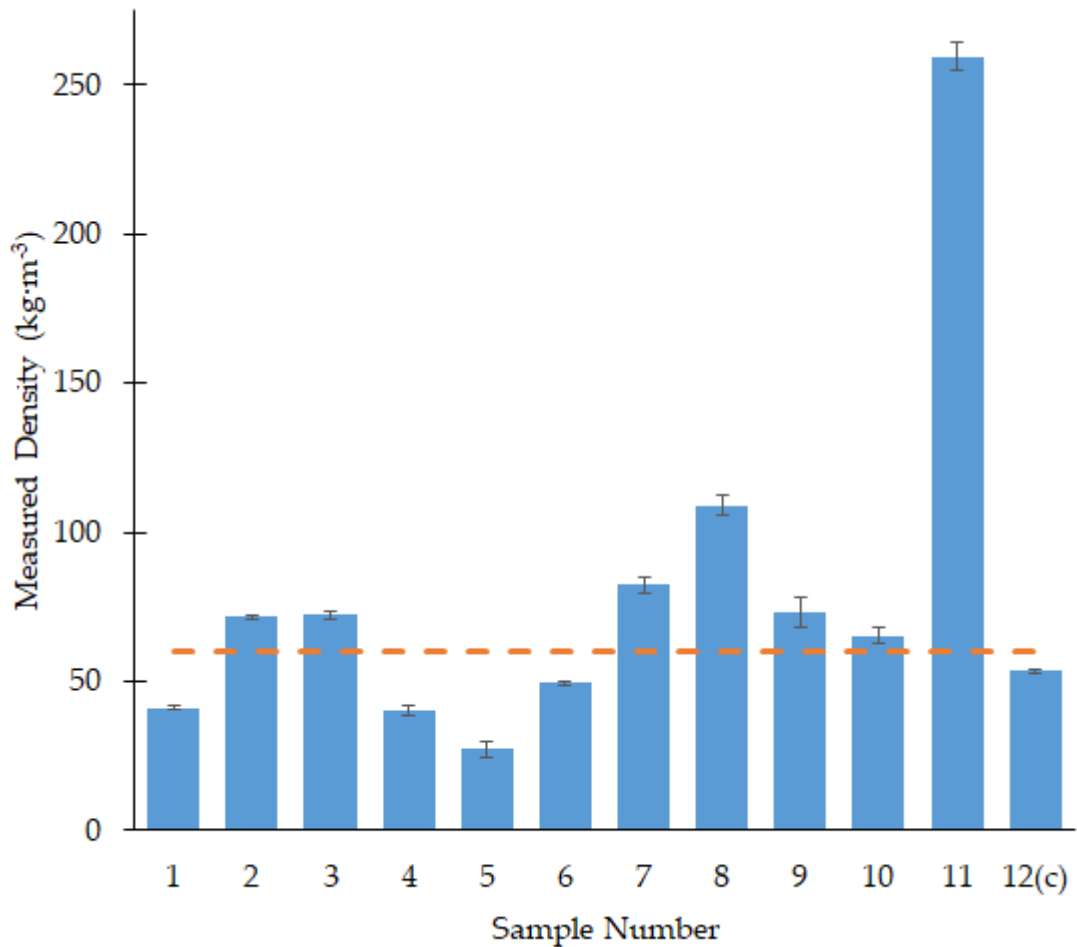
Figure 4-10: Mean density values of the samples along with the Regulation-12 limit line (60 kg·m-3- Orange dotted line). Error bars denote S.D. (c) denotes control material.

When measuring the density of samples, E_{INTRA} values were 1.8%, 2.4% and 5.9% (mean error: 4.1%), E_{INTER} was 16.9% (value range Sample 1: 40.3 to 52.2 kg·m^{-3}, Sample 6: 48.6 to 68.0 kg·m^{-3}), and E_{PROP} was 0.2%.

For hardness testing, E_{INTRA} values were 1.9%, 4.6% and 5.1% (mean error: 3.9%) and E_{INTER} was 7.0% (value range sample 4: 208 to 241 N, sample 7: 170 to 200 N).

All hardness methods (apart from E, which was positive) and thickness had significant negative correlation with peak impact acceleration at 4.9 J (Table 4-4), meaning peak acceleration decreased as sample hardness or thickness increased.

Density was not significantly correlated with peak impact acceleration at any impact energy.

Table 4-4: Spearman's (rho) Correlation Matrix comparing density, hardness and peak acceleration.

	4.9J	9.8J	14.7	Density
Thickness	-0.593*	-0.274	-0.014	-
Density	0.224	0.042	-0.434	-
A	-0.804*	-0.434	-0.294	-0.441
B-25	-0.881*	-0.531	-0.280	-0.455
B-40	-0.816*	-0.462	-0.280	-0.501
B-65	-0.748*	-0.357	-0.280	-0.427
C	-0.601*	-0.336	0.098	-0.713*
D	-0.860*	-0.483	-0.231	-0.392
E-CDC	0.862*	0.630*	0.371	0.378

* indicates significant correlation p <0.05

The results from the correlation testing (Table 4-4), although not significant, indicate that changing the impact energy changed the relationship (positive to negative) between both peak impact acceleration and density and peak impact acceleration and hardness. Figure 4-11 illustrates how the relationship between hardness measured using Method C and peak impact acceleration changed from negative to positive as impact energy increased (without control material).
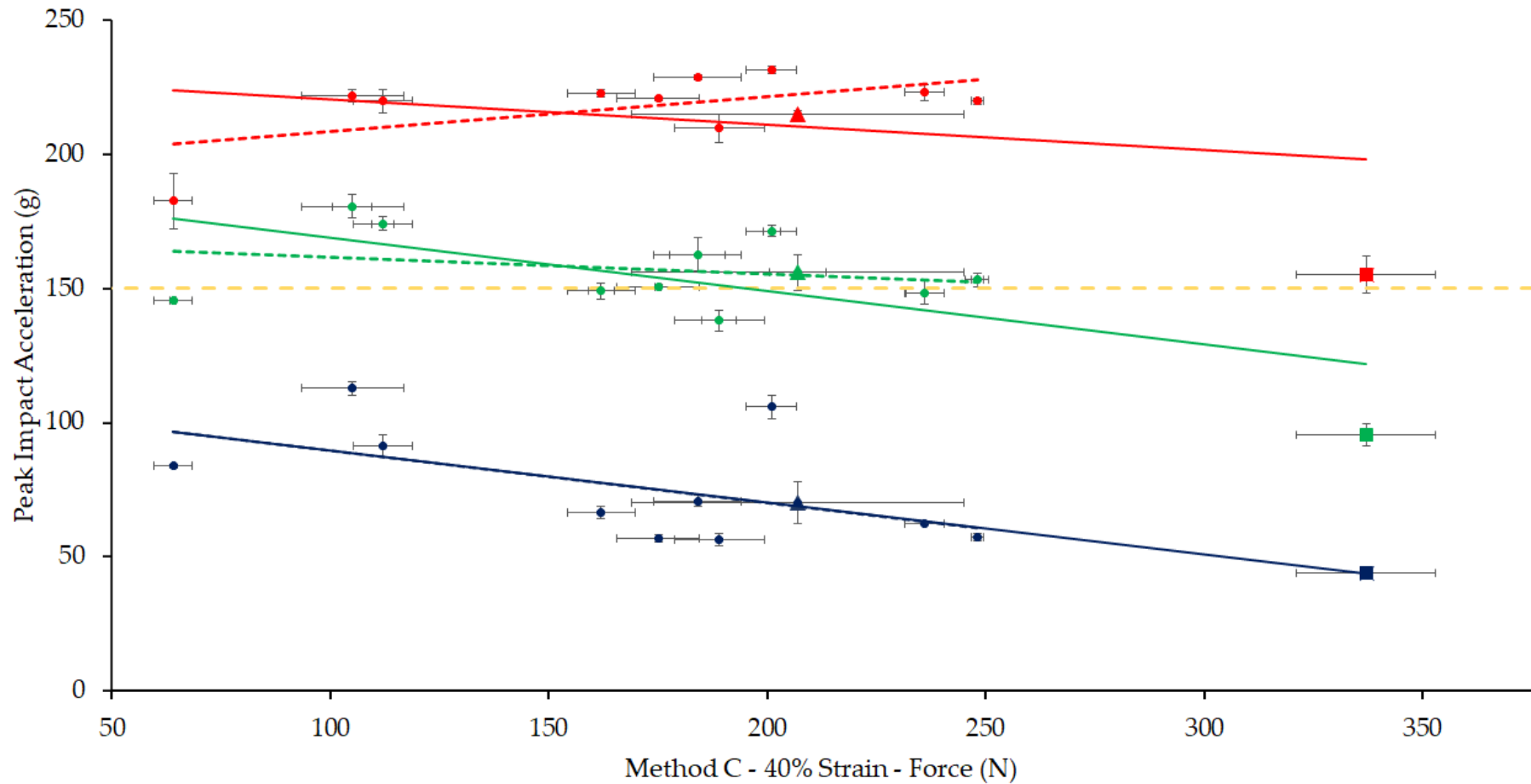
Figure 4-11: Peak impact acceleration vs. hardness at impact energies of 4.9, 9.8 & 14.7 J. Hardness measured using ISO 2439 Method-C. Error bars indicate SD. Linear trend for padding without- (dashed) and with- (continuous) control material (square) shown.

The control material was harder than the rugby padding samples (~100 N higher, using Method C) and had lower peak acceleration at all three energy levels. At 14.7 J, the mean impact acceleration of the control material exceeded the Regulation-12 limit of 150 g by 5 g (~3%). The linear relationship between hardness (Method C) and peak impact acceleration at 14.7 J is skewed due to the lower peak impact acceleration of the control sample, although this is accounted for in Spearman's correlation (which gave a positive correlation).

During simulation, upon introduction of a hard plastic layer on top of the foam padding, the force value at 40% compression increased. The force at 40% compression, and hence hardness, increased with the plastic thickness (Figure 4-12).
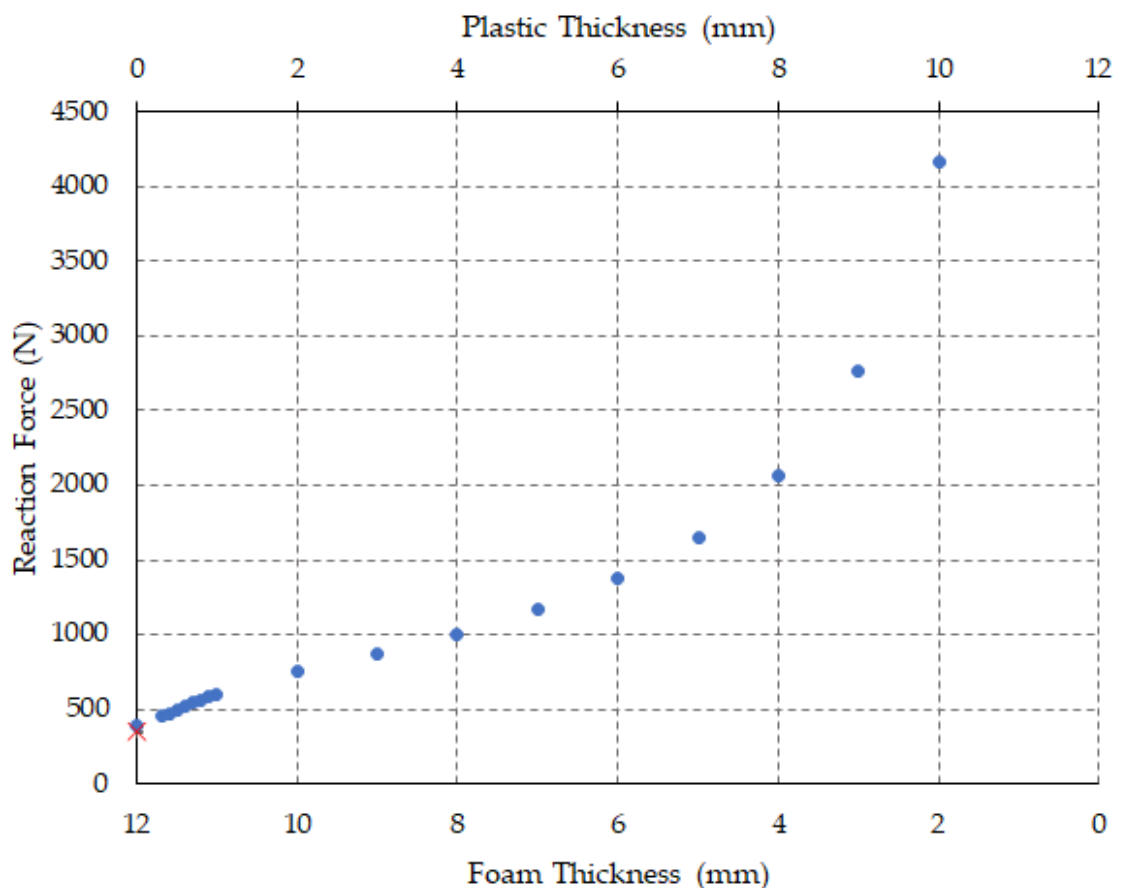
Figure 4-12: Reaction force of FE simulations replicating the hardness test (ISO 2439 Method-C) with varying thickness of foam (non-hard) and plastic (hard) layer. Red marks the force of control material in isolation when tested as per ISO 2439 Method-C.

Adding a 1 mm hard shell on top of a foam padding (11 mm) did not substantially increase in the stresses induced in the foam in comparison to when the foam was in isolation. When the thickness of the shell was increased (6 mm) the stresses induced in the foam were noticeably higher (Figure 4-13-C).
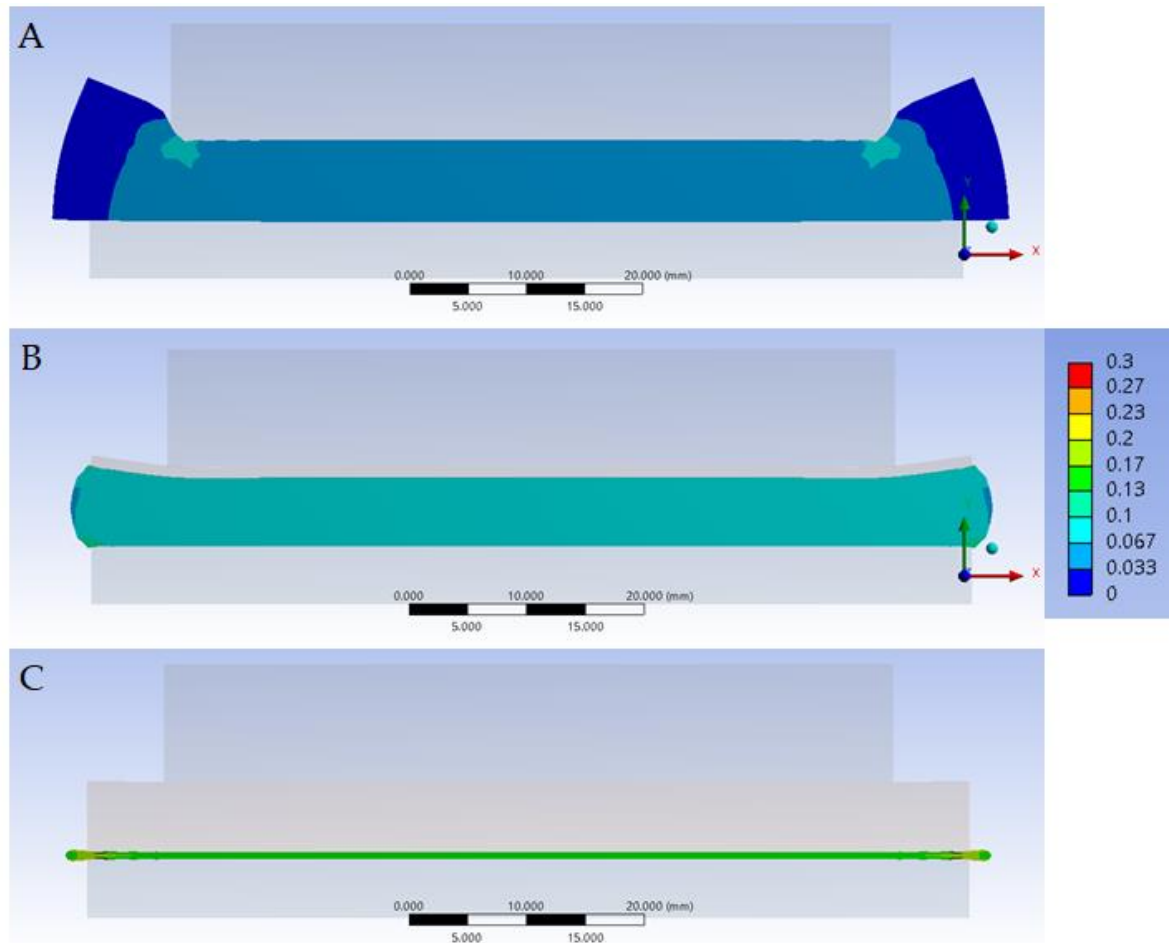
Figure 4-13: Contours of equivalent stress (MPa) induced in the foam material at 40% compression when (A) no hard shell is present (B) thin -1 mm hard shell is present and (C) a thick - 6 mm hard shell is present on top.

4.4   **Discussion**

All hardness test methods provided a statistically significant correlation ($p < 0.05$) to the peak impact acceleration at 4.9 J impact energy only, whereas padding density had no significant correlation at any energy level. Relationships changed between density and impact peak acceleration (positive to negative), thickness or hardness and peak impact acceleration (large negative to low negative / positive) as impact energy increased. At the lowest impact energy (4.9 J), the more compliant padding

gave higher peak acceleration on impact because the material would bottom out (Figure 4-9-A), while harder padding tended to withstand the impact and reduce peak acceleration. In contrast, for higher energy impacts, there was no significant correlation (apart from E at 9.8 J) because the samples were bottoming out (compression > 90%) and providing little to no resistance to impact as seen on the HSV image in Figure 4-9-B&C (noted in all rugby padding at 9.8 J and in all rugby padding and the control material at 14.7 J impact).

Large variances were noticed in hardness and peak impact acceleration values for Sample 10, which may be due to the irregular geometry highlighted in Figure 4-2-C (Sample 10). While measuring density, it was noticed that the extracted cylindrical specimens were often warped. While the E_{PROP} during density calculations accounted for only 0.2% of the error, the E_{INTER} was 17%, indicating that measuring foam density can also be prone to human error. The presence of fabric in certain samples (as it was glued to the padding) added further uncertainty to the measured density values. When comparing the hardness testing methodologies, Methods A, B and D measure force after a period of hold. The often-viscoelastic nature of padding material means that the stress can relax during this period of hold, with reducing force readings compared to the value at the end of the loading ramp. As stated in ISO 2439, the reduction in force values can be noticed when comparing values obtained from Methods A and C, with the instantaneous force values obtained using Method C being higher (or similar) for most samples.

For hardness testing, the accuracy of the force measurement depends mainly on the load cell used in the universal testing machine (<0.5%). Since the operator needs to input the sample thickness, variance in the thickness measurement can lead to variance in the hardness measurement. For hardness measurements, E_{INTRA} and E_{INTER} were calculated as 4% and 7% respectively, indicating that even though there is human error in measuring hardness (from manual measurement of thickness), it appears to be lower than for density measurements. The non-uniform / irregular

geometry of the padding adds further uncertainty to the thickness measurement. The irregular geometry can affect the hardness response during a compression test but can be accounted for by adjusting the compression platen size to ensure sufficient area is being tested.

Based on the FE study of the effect of placing a hard shell over padding material, there was increase in the reaction force values as the thickness of the hard layer increased. When the hard layer is lower than the 40% compression target (<4.8 mm in a 12 mm padding) the compression occurs mostly in the non-hard section of the padding and the hard layer just transfers the force. When the hard layer is thicker than the compression target, the reaction force starts to grow exponentially as the hard layer starts to compress.

The FE simulations show that if a thin layer of hard shell is placed on top of a foam padding the change in the hardness response is not obvious (Figure 4-12). This suggests that a hardness test may not be able to detect the presence of a hard shell on top of a foam padding. Currently, as the Regulation-12 states that the padding construction may be of one material only and no sandwich constructions allowed, use of a hard shell on top of a foam padding is restricted. However, there is potential of low-density high hardness (e.g., Auxetics) materials being used as padding materials in rugby in the future. Since there is no test for hardness defined in the regulation there is a need to define a suitable method to measure the hardness or hardness of padding materials being used.

Apart from compression tests, bend tests were considered to measure the flexural rigidity of the padding. Most paddings were noted to have varied structures as shown in Figure 4-2 to help conform to the shoulder and improve fit (Moroney, 2021). Hence a bend test may not be able to detect hard materials unless it has a uniform and continuous construction. Hardness testing, using the ISO 2439 standards, could be applied in Regulation-12 to measure the hardness of padding, but only if the test ensures that an adequate area of the padding is being

compressed. Hardness testing can be applied to intact samples of padding (as they would be worn by rugby players), unlike density, which requires the extraction of specimens. The benefits of hardness testing along with the limitations faced and human error measured in measuring density, provide some justification for replacing the density criterion in Regulation-12 with a hardness parameter, though there is a need for further work.

To improve understanding of hardness parameters, padding materials with different density and hardness ranges, such those used in sports like boxing, ice hockey and American football, could be explored. The testing could be carried out at different temperatures to analyse the change in hardness response based on temperature as done by Signetti et al. (2019). Also, the range of compression for testing hardness needs to be considered. Densification of foams starts at ~45% strain and the strain at the onset of densification can vary between foams (Sun et al., 2016). Densification of foam leads to an exponential increase in hardness with compression. To ensure the hardness test accounts for the densification of the foam, the method used to test the padding must have higher compression strain, such as adapting the 65% compression used in Method E. Method B has a 65% compression requirement as well, but the force value noted is after a hold, which may reduce the overall hardness of the padding depending on the viscoelasticity of the material.

4.5   Hertzian Contact Modelling

4.5.1   Introduction and Theory

Hertzian (Hertz, 1881) contact modelling predicts the stress and deformation developed when two bodies come into contact. The model can be used to understand and analyse contact between bodies of similar and / or different shapes and sizes. The model considers the properties of the materials (Young's moduli and Poisson's ratio) in contact to determine the change in contact area and deformation. Based on the force applied, the model predicts the maximum contact pressure and the pressure distribution along the thickness of the materials. Using the contact

pressure and the Young's modulus of each material, the strain induced in each material can be estimated. For the purpose of understanding the strain induced in the simulant used in the shoulder surrogate (defined in Section-2.11), contact modelling was used. A cylindrical contact model (Figure 4-14) was used as the shoulder surrogate defined in Section-2.11 had a hemicylindrical construction.
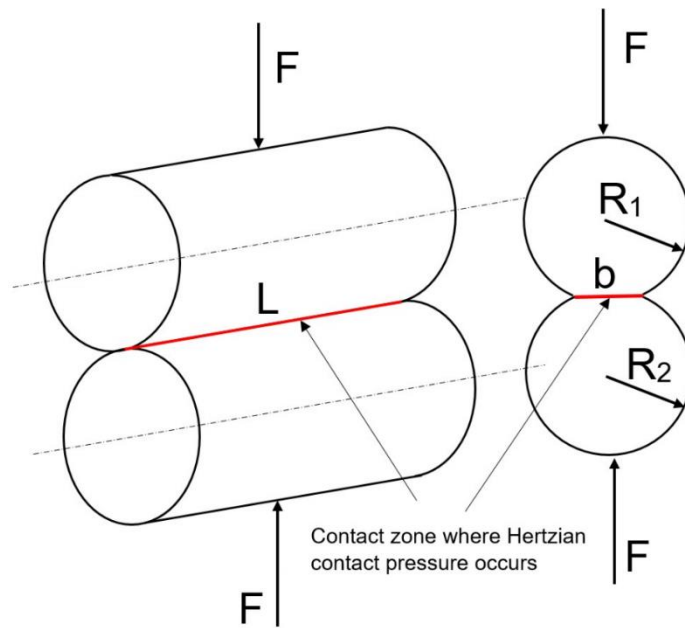
Figure 4-14: Hertzian Contact between two cylinders (Dahl et al., 2017).

4.5.2   Method and Assumptions:

For this study, two cylindrical models were used to generate the contact to mimic the diameter of the shoulder surrogate developed. The model was then adapted to predict contact pressure between the flat contact zone in Figure 4-14.

$$p_0 = \left(\frac{E^* F}{\pi L R}\right)^{\frac{1}{2}}$$

Equation 4-5

Where, p_0 is the maximum contact pressure, E^* is the equivalent Young's modulus calculated using Equation 4-6, F is the force applied on the bodies in contact, L is the length of contact and R is the effective radius calculated using Equation 4-6.

$$E^* = \frac{1 - v_1^2}{E_1} + \frac{1 - v_2^2}{E_2}$$

Equation 4-6

Where E_1 and v_1 are the Young's Moduli and Poisson's ratio of the first cylinder and E_2 and v_2 are the Young's Moduli and Poisson's ratio of the second cylinder.

$$\frac{1}{R} = \frac{1}{R_1} + \frac{1}{R_2}$$

<div align="right">Equation 4-7</div>

Where R_1 and R_2 are the respective radii of the two cylinders in contact.

The two cylinders were defined to have the same diameter and were assigned material properties of the surrogate simulant and the padding respectively. Using the maximum pressure developed and the Young's moduli of the materials in contact, the maximum strain in each cylinder was calculated. Two materials, D3O® ST (harder than the surrogate silicone) (E = 0.47 MPa, 65% Compression: 2930 ± 71 N) and Poron® XRD (softer than the surrogate simulant) (E = 0.103 MPa, 65% Compression: 144 ± 0.6 N) were modelled to be in contact, individually with the surrogate simulant (E = 0.18 MPa, 65% Compression: 144 ± 0.6 N). The strains induced in the padding and the surrogate simulant were plotted over a range of applied forces.

A sample (approx. 10 × 10 mm) of the surrogate simulant was placed under a padding (D3O®-ST and Poron XRD respectively) of similar dimension to mimic contact between padding and surrogate simulant. The simulant and foam combination were then subjected to a compression (of 250 N) using the universal testing machine and compression platens identical to the setup defined in Section 4.3.1. The deformation induced was photographed and visually compared.

4.5.3 Results:

When a padding, harder than the surrogate simulant, comes in contact with the surrogate simulant, strain is higher in the surrogate simulant (Figure 4-15-A & Figure 4-16 A-B). Alternatively, if a padding, softer than the surrogate simulant, comes in contact with the surrogate simulant, the strain is higher in the padding (Figure 4-15-B and Figure 4-16 C-D).
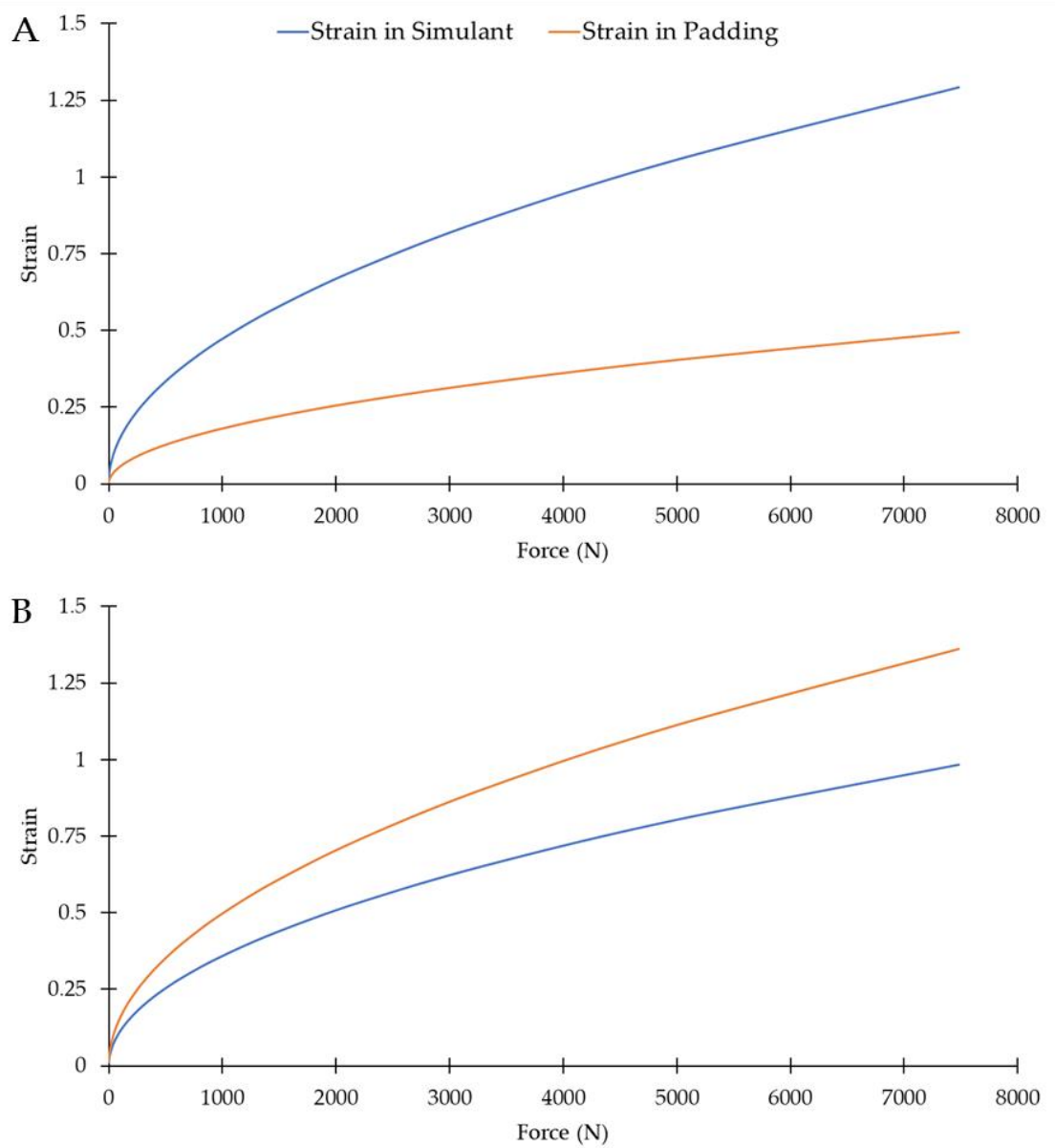
Figure 4-15: Strain comparison between test bed material and padding when (A) padding is harder than the surrogate simulant and (B) padding is softer than surrogate simulant.
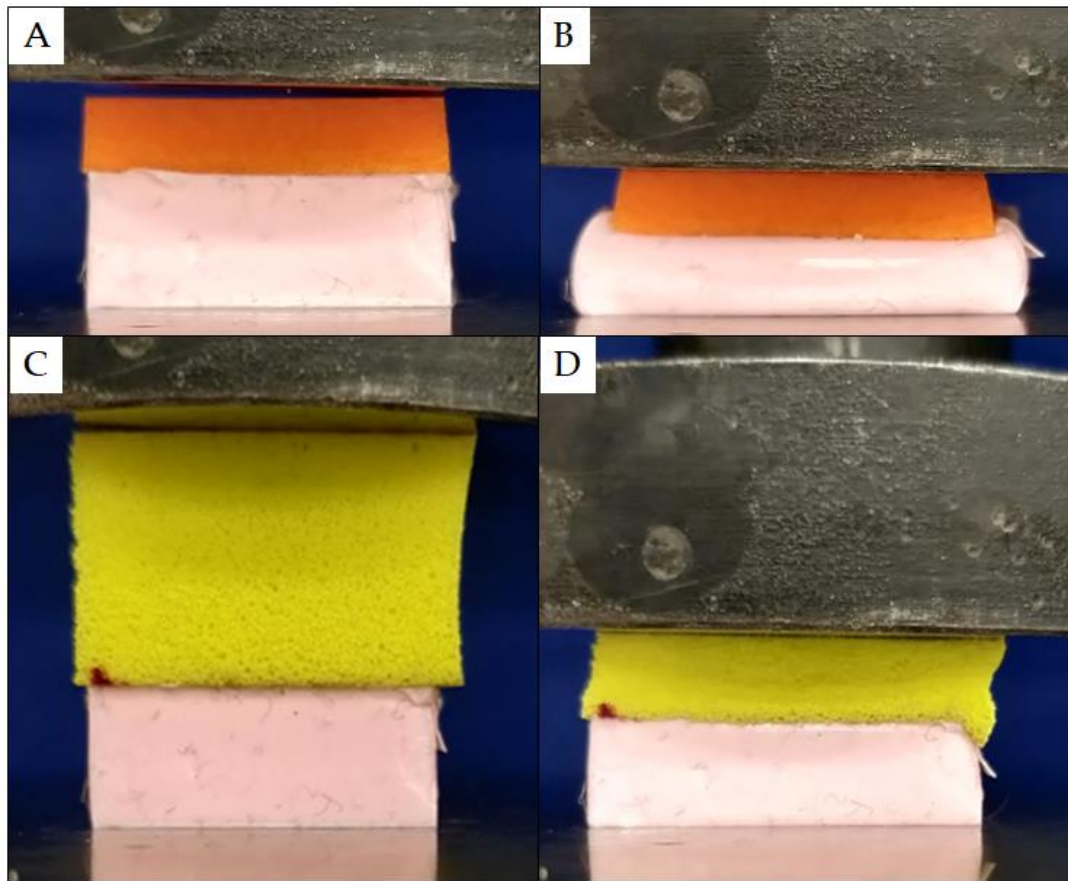
Figure 4-16: Comparison of simulant layer in contact with a harder foam (D3O) under (A) No load and (B) 250 N load- showing higher strain induced in the simulant against (C) a softer foam (Poron XRD) under no load and (D) 250 N load applied showing higher strain induced in the foam.

4.5.4 Discussion:

Padding being harder than the surrogate simulant does not imply the occurrence of a cut or laceration on contact. The results demonstrate that the risk of a cut or laceration occurring would be higher if the padding used is harder than the surrogate simulant. To ensure that any padding used does not increase the risk of injuries (such as cuts and lacerations) to the opponent without padding, allowable hardness values in Regulation-12 should be set lower than the soft tissue hardness value.

4.5.5 Limitations of the model:

The Hertzian model does not consider frictional contact properties and only considers uniform and linear material properties across the material. Since the shoulder surrogate is a combination of different materials, it is important to understand that this model was only used to illustrate the trends.

4.6   **Recommendation for Limitation Setting**

The 65% compression force values were measured using ISO 2439 Method E for manufacturer samples and other raw materials such as PlastaZote-LD-60 (Control material), D3O-ST, Poron-XRD, auxetic foam (Duncan et al., 2021), sporting PPE such as cricket gloves, a boxing head guard and some off the shelf upholstery foams. Six samples of the surrogate simulant were tested as per the same methodology and the range of force values obtained were plotted to compare the hardness in relation to the PPE materials (Figure 4-15).

Based on the results shown in Figure 4-17 and on the Hertzian contact modelling, the limit for hardness of the body padding must be lower than the lowest measured shoulder surrogate simulant hardness (1,282 N using ISO 2439 Method E). Setting the limit at 750 N for 65% compression would allow a margin of safety[4] of 0.7 to 1 (Factor of Safety: 1.7-2.0). The manufacturer samples currently fall below the recommended limit with the highest force value recorded at 631 N.

Setting the limit to be lower than the shoulder surrogate simulant, ensures no increased risk to an athlete without padding. Upon contact between a player wearing padding and another without padding, if the padding compresses much more easily than the skin tissue then the risk of the padding causing a cut or laceration is minimal, i.e., a soft foam is unlikely to cut the skin, whereas a hard plate might.

---

[4] Margin of Safety = Factor of Safety – 1
Factor of Safety = (Failure Load/Design Load)
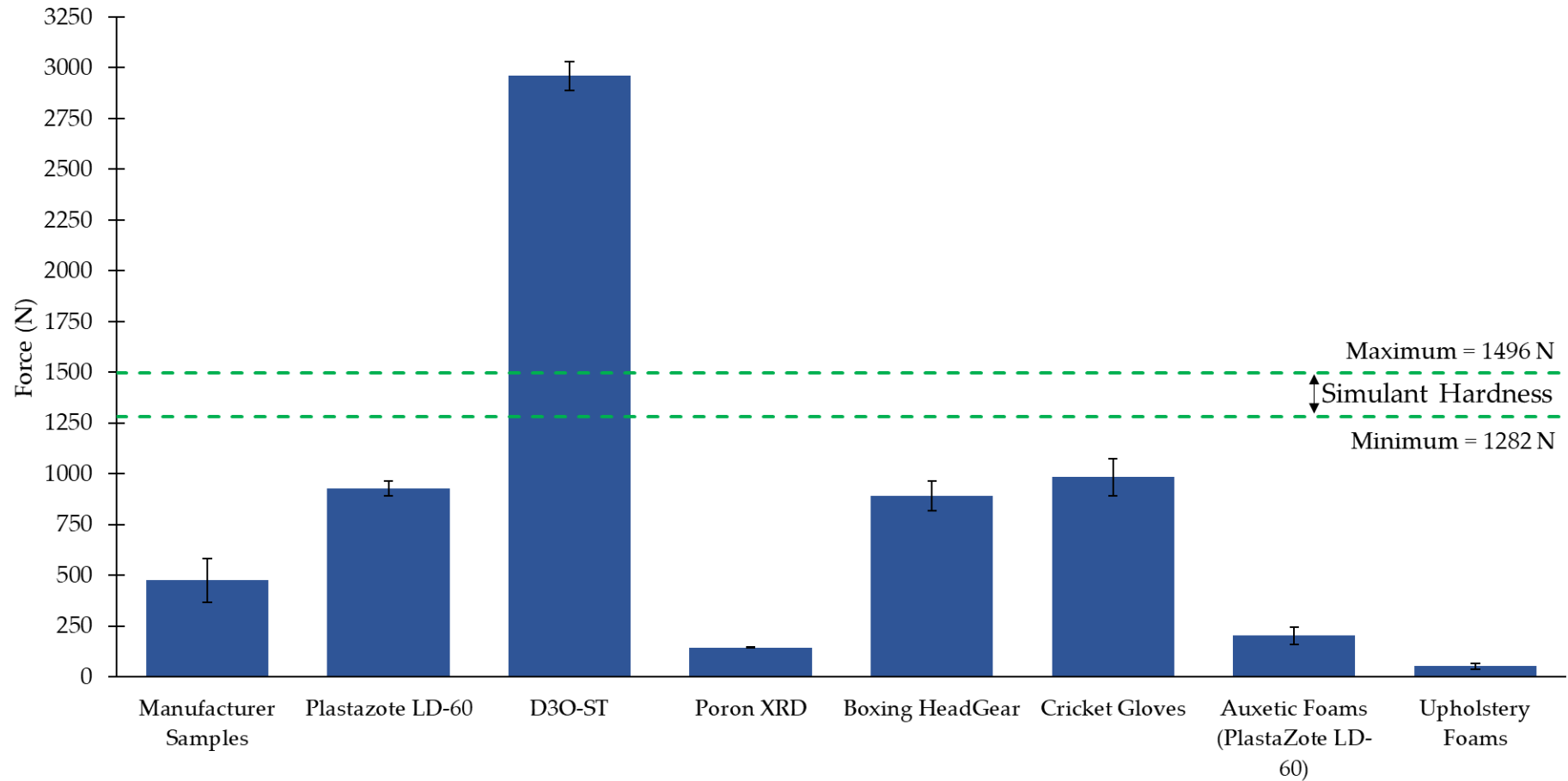
Figure 4-17: Force values at 65% compression (as per testing carried out using ISO 2439 Method E) comparing the surrogate simulant and manufacturer samples to different sporting PPEs and commercial foams.

4.7   Conclusion

The hardness and densities of each of the 11 commercially available padded clothing and one control material were compared against their peak acceleration for an impact test at 4.9, 9.8 and 14.7 J. Hardness parameters and thickness showed a significant negative correlation with peak impact acceleration at 4.9 J, while density showed no significant correlation. Results from impact tests at energies of 9.8 and 14.7 J indicate that the padding materials bottomed out (as seen in Figure 4-9) due to the hard impactor and anvil. Furthermore, quasi-static hardness testing has shown potential to prevent the use of hard materials, such as hard plastic shells, which may increase the risk of injuries such as cuts and lacerations. Findings from this chapter provide evidence that testing density of the padding is erroneous and unreliable. Hardness testing of the padding if carried out to the right method / strain would help eliminate use of hard paddings through a simple non-destructive test methodology. Based on the Hertzian contact modelling, a suitable limit for hardness testing of body padding has been identified as 750 N for 65% compression. The findings of this chapter would help World Rugby™ modify the testing methodology for body padding in Regulation-12 and help them to introduce simpler testing methods to replace the density criterion.

4.8   Chapter Summary

Replacement criterion for the material density requirement in Regulation-12 was investigated and a hardness test using 65% compression adapted using ISO 2439 Method E was identified as a suitable option. FE modelling was carried out to test the effect of introducing a hard material atop the foam padding. Hertzian contact modelling was used to model the contact between soft tissue and padding to be able to define a suitable limitation to the hardness limit. A flow chart is presented in Figure 4-18 highlighting the various stages of the research. The findings of this chapter could help World Rugby to change the material property requirement for padded clothing and its testing procedure in Regulation-12.

Background
- Density criterion is to ensure no stiff material are being used.
- Density of the material can be reduced while increasing hardness as shown in literature.
- Measuring hardness could be used to regulate body padding

Testing
- Hardness measurement using Compression testing as per ISO 2439.
- Density testing of the padding material as per ISO 835.
- Impact Testing at three different impact energies.
- Intra and inter-user error testing.

Results
- Hardness testing is simpler and less error prone than density testing.
- Hardness testing is a non-destructive test, testing the final product rather than material.
- Hardness Complements the impact test.
- FE-Simulation used to see effect of adding stiff padding layer.

Hertzian Contact Model
- Contact between simulant and padding modelled.
- Hardness values of body paddings compared against surrogate simulant and other sporting PPEs.
- Limitation calculation to ensure padding does not cause increased risk to opponent without padding.

Conclusions
- Testing hardness allows for simpler testing of body padding in its final form.
- All current paddings are within recommendation limits and there is room for improvement.

Figure 4-18: Summary of the work done in Chapter-4.

5. Development of a FE Model of a Shoulder Surrogate

5.1 Introduction

In Chapter 2, a surrogate shoulder developed by Hughes et al. (2020) for impact testing rugby padding was presented. This chapter focuses on developing and validating a finite element model of the surrogate shoulder across a range of impact energies. The validated model will be used to simulate impact induced damage to the silicone of the shoulder surrogate, and hence soft tissue injuries such as cuts and lacerations, in Chapter VI (Figure 5-1). This chapter details the steps taken to model the silicone of the surrogate, simulate impact tests on the shoulder surrogate at three energies and to compare the results against experimental tests.
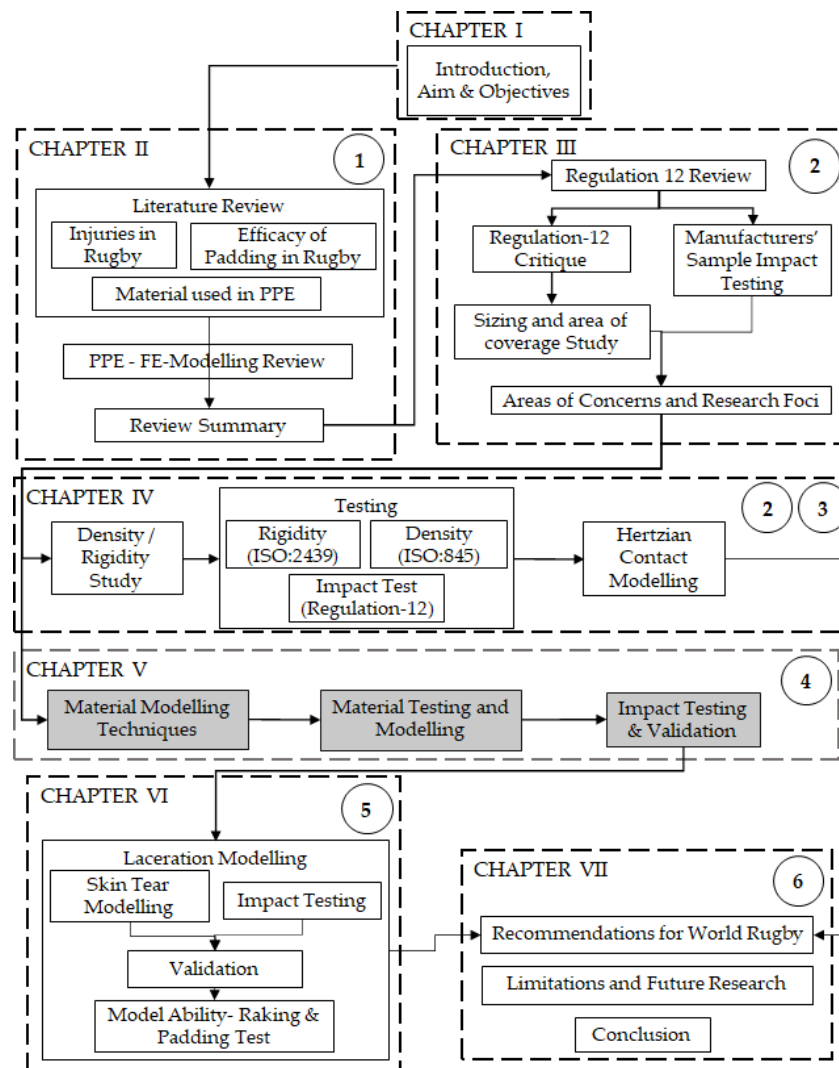
Figure 5-1: Layout of Thesis showing the placement of Chapter V with respect to the overall project. Numbers in circles correspond to objectives listed in Chapter-1.

5.2   Material Modelling Techniques

As outlined in Section 2.9, various material models have been used by researchers to model PPE materials and anatomical structures. A proportion of the literature (Payne et al., 2015b; Marchesseau et al., 2010; Larrabee Jr and Galt, 1986; Lapeer et al., 2010; Hendriks et al., 2003; Evans, 2009; Benítez and Montáns, 2017) suggests that hyperelastic material models (Figure 5-2-A) are well suited to modelling the low strain rate stress vs. strain response of human skin tissue and associated simulants. Further, Ogden and Mooney-Rivlin models have been shown to fit stress vs. strain curves for skin tissue more closely than the Neo-Hookean model. Some researchers (Silver et al., 2001; Shergold et al., 2006; Khatyr et al., 2004; Delalleau et al., 2008; Payne et al., 2015b) suggest using viscoelastic modelling (Figure 5-2-B) in parallel with the hyperelastic models to predict the tissue response under different strain rates. The following section will describe some hyperelastic and viscoelastic modelling techniques that will be used in the subsequent sections.
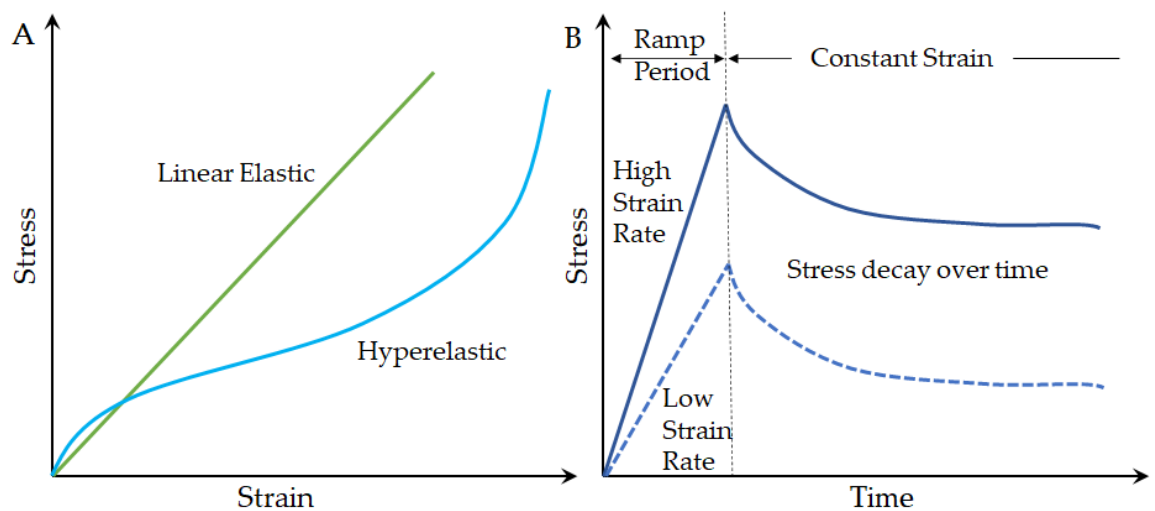
Figure 5-2: Diagrams illustrating typical examples of (A) stress vs. strain curves of linear elastic and hyperelastic materials from quasi-static tensile tests and (B) stress curves over time for a viscoelastic material during stress relaxation tests with different strain rates in the loading ramp.

5.2.1   Hyperelastic Models

When the stress vs. strain curve of a material is nonlinear, information beyond that defined in a linear elastic material model is required to capture this behaviour within an FE model. One way to describe nonlinear behaviour is by using a

hyperelastic material model. The various material models that can be used to describe hyperelastic behaviour are variants of a polynomial form made up of parameters input as material constants (Ansys, 2015). Three hyperelastic models that are often applied to materials typically used for impact protection are Mooney-Rivlin, Ogden and Reduced Polynomial (Yeoh) (Table 2-5 & Table 2-6). The following sections describe the Mooney-Rivlin, Ogden and Yeoh hyperelastic curve-fitting models that are available in Ansys© and have been used by others when modelling soft tissue simulants, as noted in Chapter 2.

Mooney-Rivlin Model

The Mooney-Rivlin model (Mooney, 1940; Rivlin, 1948) has been used to model biological tissues and simulants (Table 2-6). The model works by defining the strain energy function shown in Equation 5-1

$$W = \sum_{i.j=1}^{n} C_{ij}(I_1 - 3)^i(I_2 - 3)^j + \sum_{m=1}^{M} D_m(J - 1)^{2m} \qquad \text{Equation 5-1}$$

where W is strain energy, $C_{i,j}$ are coefficients related to the distortional curve, $I_{1,2}$ are the invariants of the strain energy density functions, D_m is the volumetric curve, and J is the determinant of the deformation gradient. In Ansys©, D_m is assumed to be zero unless volumetric curve data is provided, making the material incompressible (i.e. $v = 0.5$ / constant volume when deformed) and reducing Equation 5-1 to 5-2

$$W = \sum_{i.j=1}^{n} C_{ij}(I_1 - 3)^i(I_2 - 3)^j \qquad \text{Equation 5-2}$$

The Mooney-Rivlin material model formulation in LS-DYNA® (e.g. *MAT_HYPERELASTIC_RUBBER) uses Poisson's ratio instead of D_m to define compressibility. Hence, defining a Poisson's ratio in LS-DYNA®, overcomes the incompressibility limitation during hyperelastic modelling. The Mooney-Rivlin model has been reported to work well for strains up to 200% (Kim et al., 2012), but

it cannot accurately capture an upturned S curvature shaped stress vs. strain curve (Newton-Mann, 2019).

Ogden

The Ogden model uses the strain energy function shown in Equation 5-3 (Ogden, 1972),

$$W = \sum_{i=1}^{n} \frac{2\mu_i}{\alpha_i^2} (\lambda_1^{\alpha_i} + \lambda_2^{\alpha_i} + \lambda_1^{-\alpha_i}\lambda_2^{-\alpha_i} - 3)$$

Equation 5-3

where, λ_i are the principal extension ratios, μ_i are shear moduli and α_i are material constants (curve fitting coefficients). The Ogden model is able to capture an upturn S shaped stress vs. strain curve, it is well suited to modelling rubbers and tends to perform better than other models under large strains (700%) (Shahzad et al., 2015). While the Ogden model has been reported to have better stress prediction at higher strains, it has been reported to underpredict stress at lower strains (Payne et al., 2015b).

Yeoh or Reduced Polynomial

The Yeoh Model uses the generalised version of the model presented by Yeoh (1993) for incompressible materials, and its strain energy function is described in Equation 5-4,

$$W = \sum_{i=1}^{n} C_i(I_1 - 3)^i$$

Equation 5-4

where, C_i are the material constants and I_1 is the invariant of the strain energy density function. When $n = 1$, the model reduces to a neo-Hookean model for incompressible materials.

These hyperelastic material models provide material coefficients based on a fit to an experimentally derived stress vs. strain curve. The number of parameters used in the model (n) account for different turning points within a stress vs. strain curve,

with a general rule being that $n = 1$ gives a linear fit, $n = 2$ gives one turning point (like in a quadratic curve) and $n = 3$ gives two turning points (Ansys©, 2015).

The hyperelastic models in Ansys© have different parameter models inbuilt, such as 2-, 3- 5- and 9-parameter models for Mooney Rivlin and 2-, 3- & 5-parameters for Ogden and Yeoh. Based on the nature of the stress vs. strain curve, varying the number of parameters can influence how well a material model fits the curve. Using the strain energy density function, the stress in the material is calculated by obtaining the derivative of W with respect to strain. The strain energy density function, when used for an isotropic hyperelastic material only considers the strain components and does not consider other factors such strain rate dependency.

5.2.2 Viscoelastic Modelling

As the hyperelastic models do not account for strain rate dependency, the material model for silicone of the surrogate shoulder needs to combine a viscoelastic and a hyperelastic model. Rate dependency (shown in Figure 5-2-B) can be modelled using a non-linear model, such as the Prony series (Equation 5-5),

$$G(t) = \sum_{i=1}^{n} \alpha_i e^{-\beta_i t}$$

Equation 5-5

where: $G(t)$ is shear relaxation moduli, i is the number of Prony series terms, α_i are the shear moduli, β_i are the decay constants and t is time. The Prony series has been used to model rate dependency in tissue simulants (Payne et al. 2015b), sports balls (Ranga and Strangwood, 2010) and PPE (Newton-Mann, 2019).

In the following sections, the three hyperelastic models (Mooney Rivlin, Ogden and Yeoh) presented in Section 5.42.1 along with the Prony series modelling presented in 5.2.2 will be used to model the silicone of the shoulder surrogate. Impact simulations with the shoulder surrogate using the three hyperelastic models, each combined with a Prony series, for the silicone will be compared against

experimental impact data at 14.7, 9.8 and 4.9 J. A flowchart of the methodology is presented in Figure 5-3.
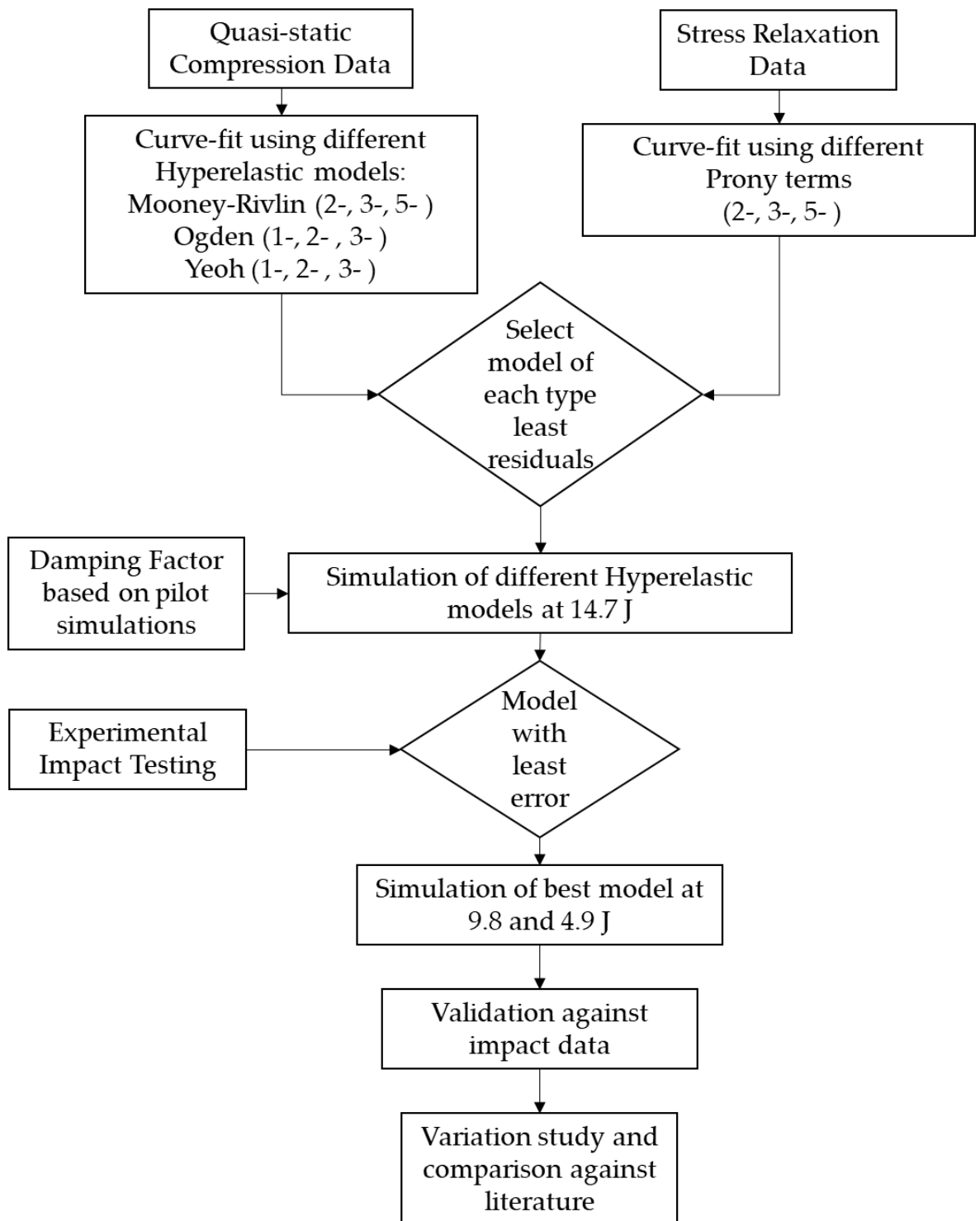
Figure 5-3: Flowchart summarising the methodology used to model and validate the shoulder surrogate.

5.3   **Material Modelling Methodology**

5.3.1   Sample preparation and density measurement

Three cylindrical samples of the silicone presented by Hughes et al. (2020) (using a 29 mm Ø and 12.5 mm height mould as per ASTM D395-*Standard Test Methods for Rubber Property - Compression Set*) were made at The University of Sheffield for compression testing. The silicone samples were weighed using a balance (ABS 220-4N, KERN®, Germany. Accuracy ± 0.1 mg). The diameter and height of the samples was measured using a vernier calliper (Composite Digital Vernier Calliper, Silverline®. Accuracy: ±0.01 mm) and the volume was calculated. Using the measured mass and volume, the density of the silicone was calculated.

5.3.2   Quasi-Static Compression

Compression testing was undertaken using a Hounsfield Universal testing machine (with a 10 kN load cell accuracy ±50 N) at a strain rate of $0.67s^{-1}$ (500 mm/min test speed, which was the machine maximum) until 70% compression. The platens (identical to the ones used in hardness testing in Chapter 4) were greased on both contact faces to limit friction with the sample and reduce any barrelling effect. An approach speed of 1 mm·min^{-1} was applied until a preload of 1 N to ensure the compression platen contacted the sample before testing. The force and displacement data were taken from the test machine to calculate engineering stress and strain from the measured sample dimensions.

Pilot testing showed the first compression of the silicone to be different from the subsequent compressions, indicating stress softening (Mullin and Tobin, 1965). So, during analysis the first compression of each sample was not taken into consideration. Three specimens of the silicone were tested three times each (total of six curves after removal of first compression), with at least a minute between each test. The median stress-strain curve across all three samples was selected (visually) for material modelling.

Tensile data was not used for the modelling as pilot simulations using both tensile and compression data (at equal strain rate of 0.67 s^{-1}) resulted in the simulations showing high error in peak impact forces (under predicted peak force and over predicted deformation) in comparison to the experimental results. The chamois leather (artificial skin simulant) was too thin (1.5 mm) to (accurately) compression test in isolation. Compression test was, therefore, undertaken with a chamois leather layer (1.5 mm) on top of the silicone sample. Such testing gave an assessment of the effect of adding the chamois leather on the stress vs. strain curve of the silicone. Unfortunately, the chamois leather layering on top of the silicone tore above 65% compression. This damage / tear resulted in a drop in the stress vs. strain curve, at 65% compression, which affected the curve fitting function while material modelling. Results for compression testing the chamois leather were, therefore, not used for material modelling, i.e., only the silicone was modelled.

5.3.3 Stress Relaxation Testing

The silicone sample was compressed to 50% strain (as per Payne et al. (2015b) at a strain rate of 6.7 s^{-1} (1,000 mm/min, which was the machine maximum) using a hydraulic compression machine (Instron®, 10kN load cell with accuracy: ± 100 N), and then held at this strain for 60 seconds. The force curve during the 60 second hold was converted to shear modulus (μ), using a Young's modulus calculated in the ramp time (from the gradient of a linear trend line) and an assumed Poisson's ratio of 0.48 (Delalleau et al., 2006).

$$\mu = \frac{E}{2\,(1 + \upsilon)}$$

Equation 5-6

Three samples were tested, and the median shear stress vs. time curve was used for Prony series curve fitting.

5.3.4 Hyperelastic model and Prony series curve fitting

The median stress vs. strain data from the compression test was imported into Ansys© Workbench v19.1 as uniaxial test data. Mooney-Rivlin (2-, 3- and 5-

parameter), Ogden (1-, 2- and 3-parameter) and Yeoh (1-, 2- and 3-parameter) hyperelastic models were individually fitted to the data using the *curve-fit* command. The software provides a residual as a measure of how well a model fits to the data. For each model, the number of terms that gave the lower residual for the curve fit was chosen. The corresponding hyperelastic constants returned by the software were then used to develop an FE model of the silicone. Outputs from the finite element model were subsequently compared against experimental impact test data.

The stress relaxation data was imported into Workbench using the *viscoelastic shear data* function. As the stress in the silicone relaxed quickly (< 3 seconds), both the shear response over the full 60 seconds and also data cropped to just 5 seconds after the loading period were compared. The Prony series relaxation *curve-fit* option was used with different numbers of terms (2-5) to find the one with the lowest residual.

The Ansys© LS-DYNA® manual (Keywords User's Manual, Volume-II Material model, 2018) recommends 3 to 5 terms for a Prony series, but a 2-term fit was also analysed as the 3 to 5 term models did not fit the data well. The effect of applying the factor-of-10 rule (Meissner, 1978, Sorvari and Malinen, 2006), which means removing the initial part of the curve in the relaxation phase that corresponds to ten times the duration of the loading ramp time, was assessed in the FE model. Applying the factor-of-10 rule meant removing data before 0.348 s as the loading ramp time was 0.0348 seconds long. The Prony series relaxation curve-fit (between 2 and 5 terms) providing the best fit to the cropped stress relaxation test data was used to analyse the effect of applying the factor-of-10 rule.

5.4   **Material Modelling Results**

The density of the silicone was calculated as $1,072 \pm 75$ kg·m^{-3} (mean ± S.D.). The gradient of the stress vs. strain curve, and hence the silicone stiffness, increased with the strain rate (Figure 5-4).
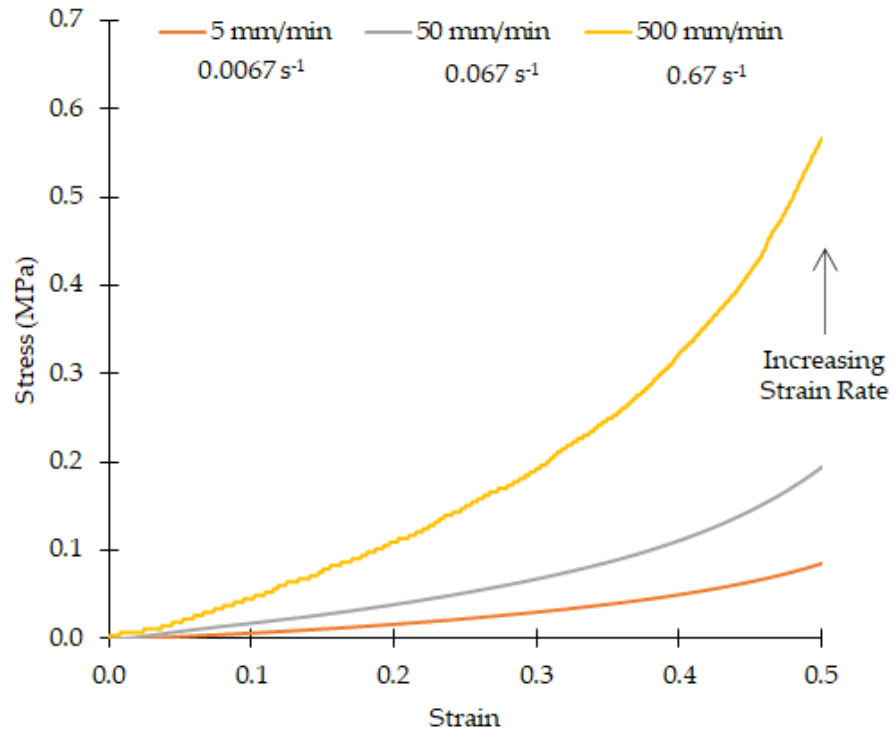
Figure 5-4: Compressive stress vs. strain curve of the silicone at different strain rates up to 50% compression.

Across the six compressions (3 samples – 2 repeats each), the variance in stress vs. strain data was under 0.1% (Figure 5-5).
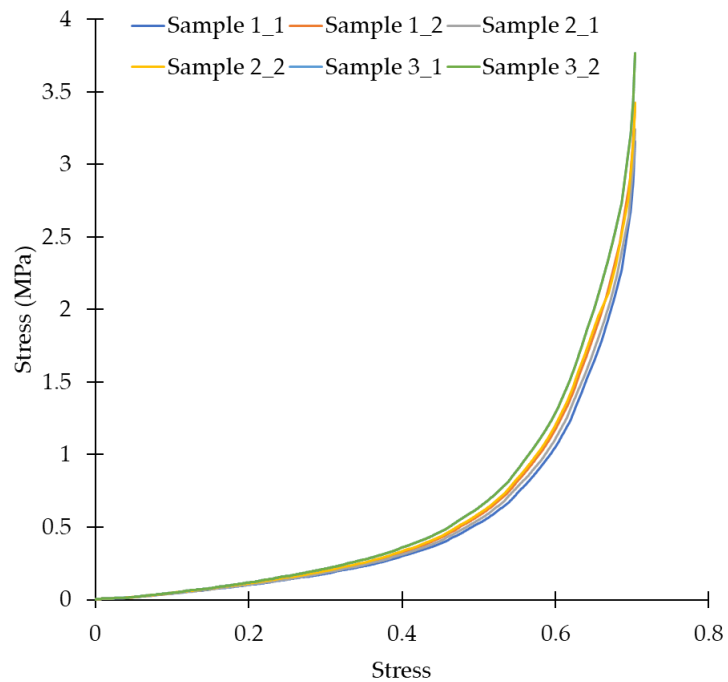
Figure 5-5: Compressive stress vs. strain curve of the silicone samples (3 samples x 2 repeats each) up to 70% compression at 500 mm/min (0.67 s^{-1}).

The stress vs. strain curve of the silicone with the chamois leather on top was similar to that of the silicone in isolation, with a variance under 0.05% (Figure 5-6). The stress vs. strain curve was noted to have a slight change at ~65% strain, due to the chamois leather tearing.
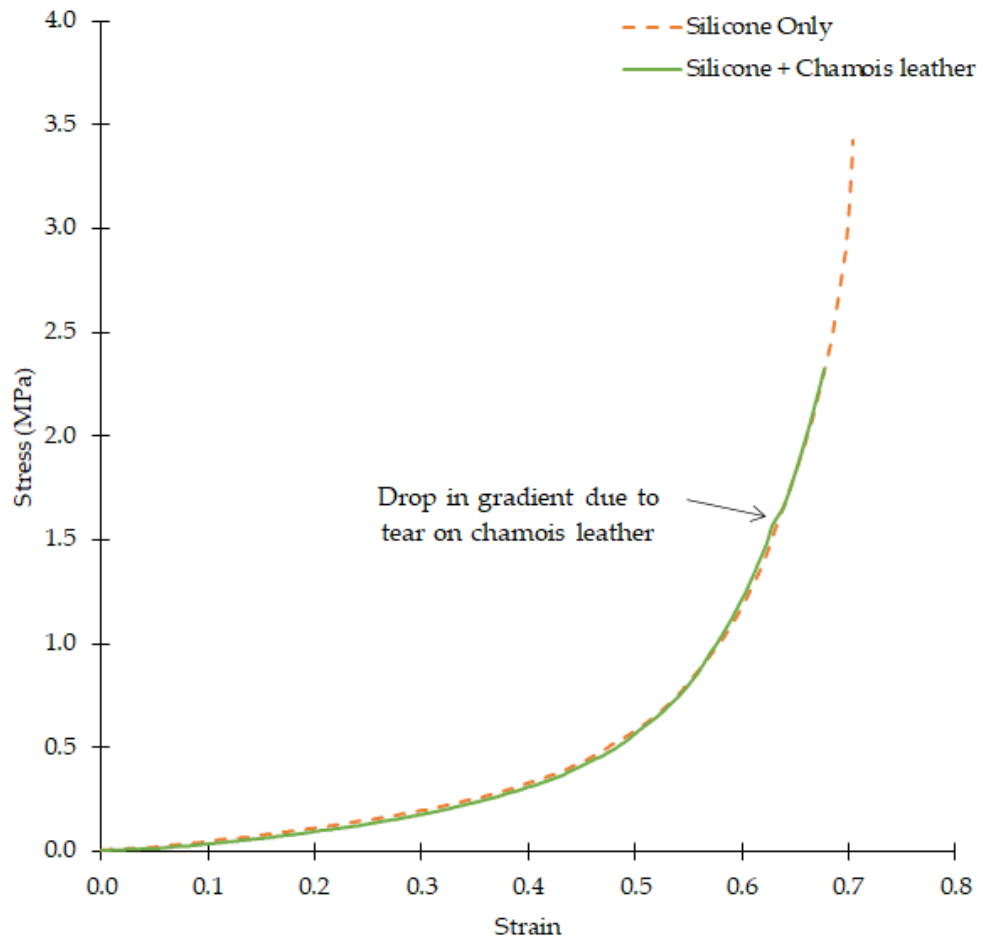
Figure 5-6: Compressive stress vs strain curve comparing the curve of a silicone sample with and without the chamois layer at 500 mm/min (0.67 s-1). Only the median curve is plotted to show the drop in stress value.

For stress relaxation testing, the shear modulus decayed rapidly during the constant strain hold phase after the load application, and then relaxed to a steady value of ~3.3 MPa after about one second (Figure 5-7).
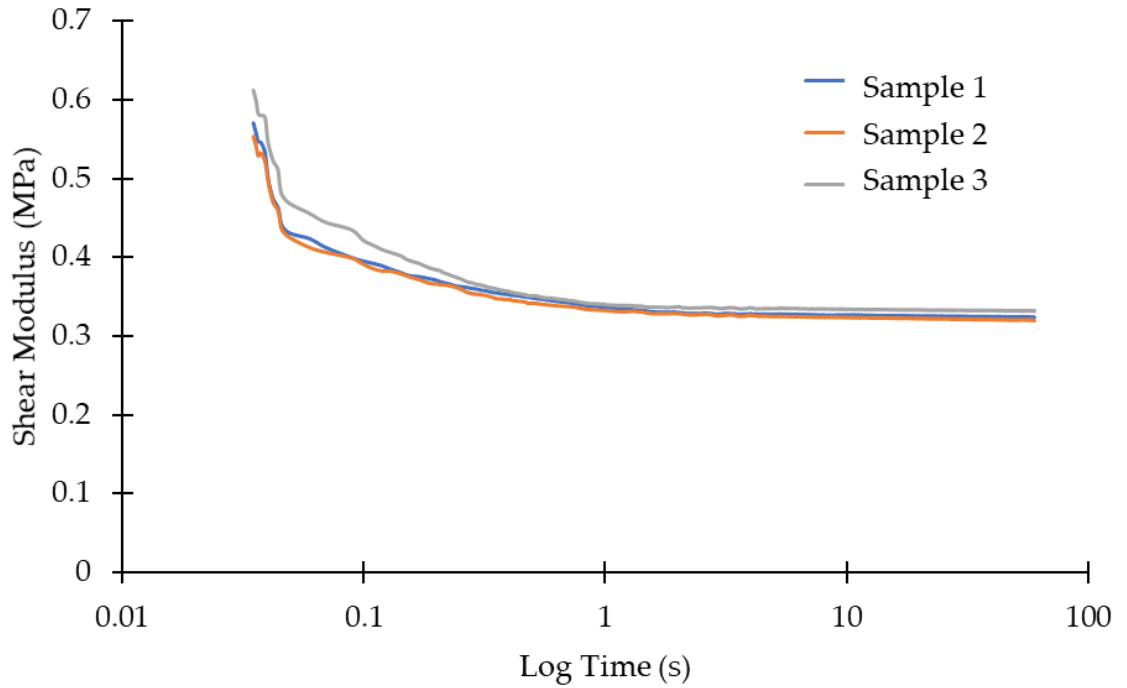
Figure 5-7: Shear Modulus curve of the silicone under stress relaxation testing.

The 5-parameter Mooney-Rivlin curve fit (Table 5-1) gave a lower residual (8) than the 2- and 3-parameters (87 and 37, respectively). The 5-parameter Mooney-Rivlin curve fit followed the experimental data well until a strain of ~0.65, above which it overpredicted stress for a given strain (Figure 5-8).

Table 5-1: Mooney-Rivlin 5-parameter calculated hyperelastic constants and residual.

Coefficient Name	Calculated Value	Calculated Unit
Incompressibility Parameter D_m	0	Pa^{-1}
Material Constant C_{01}	1.01E+06	Pa
Material Constant C_{02}	2.47E+07	Pa
Material Constant C_{10}	-9.30E+05	Pa
Material Constant C_{11}	-3.60E+07	Pa
Material Constant C_{20}	1.37E+07	Pa
Residual	8.09	-
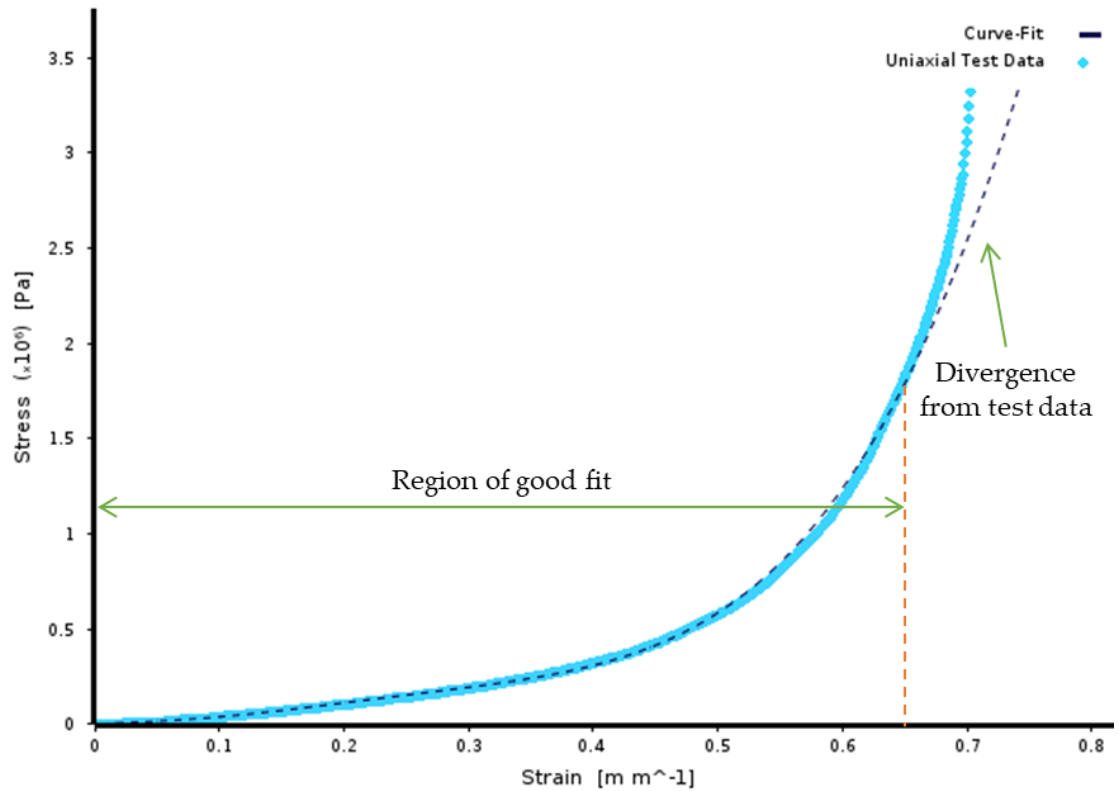
Figure 5-8: Mooney-Rivlin-5 parameter curve fit against uniaxial test –compressive stress vs. strain data.

Amongst the different parameters of the Ogden model, the 3-parameter model (Table 5-2) provided the best fit with the lowest residual (22 vs. 300 and 384 for 1- and 2-parameter, respectively).

Table 5-2: Ogden 3-parameter calculated hyperelastic constants and residual.

Coefficient Name	Calculated Value	Calculated Unit
Incompressibility Parameter D	0	Pa^-1
Material Constant A_1	16.296	
Material Constant A_2	16.376	
Material Constant A_3	16.450	
Material Constant μ_1	316.701	Pa
Material Constant μ_2	316.715	Pa
Material Constant μ_3	316.717	Pa
Residual	21	

The 3-parameter Ogden model underpredicted the measured stress until just over 50% strain, beyond which it overpredicted stress (Figure 5-9).
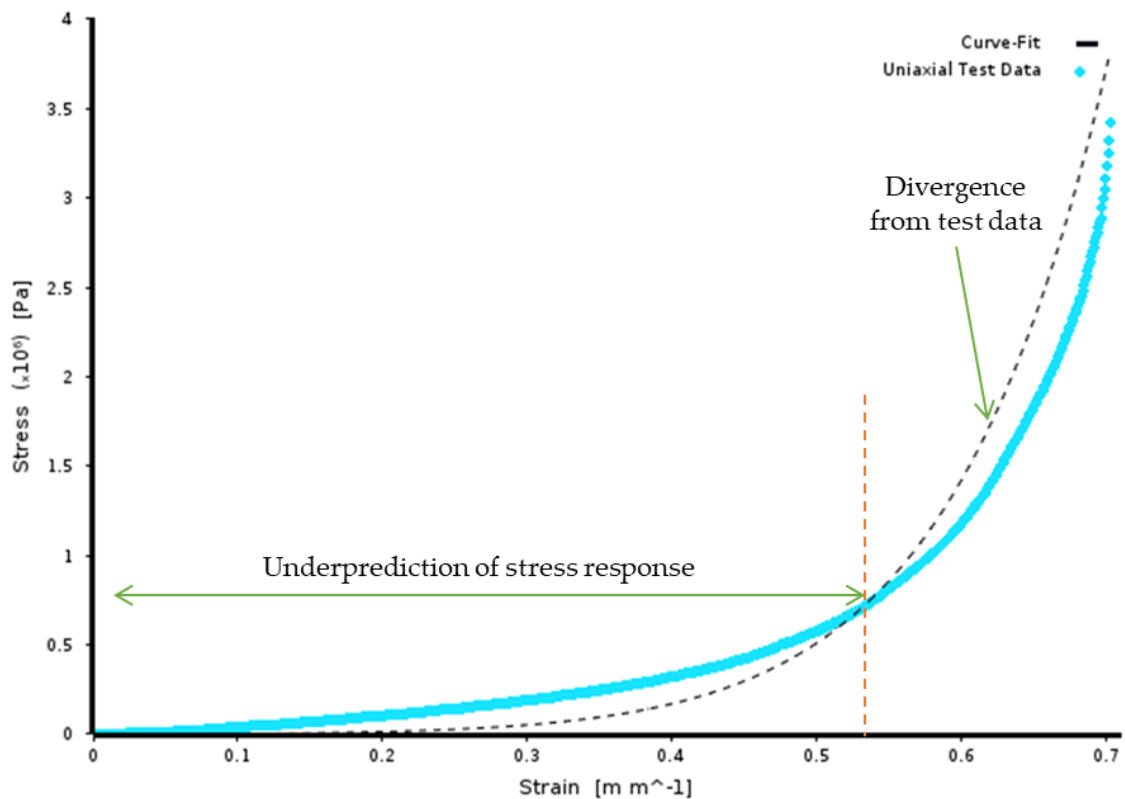
Figure 5-9: Ogden 3-parameter curve fit against uniaxial test –compressive stress vs strain data.

Amongst the Yeoh models the 3-parameter curve fit model (Table 5-3) provided the lowest residual (24 vs. 243 and 36 for 1- and 2-parameter, respectively).

Table 5-3: Yeoh-3 parameter calculated hyperelastic constants and residual.

Coefficient Name	Calculated Value	Calculated Unit
Incompressibility Parameter D	0	Pa^-1
Material Constant C_{10}	68,062.2	Pa
Material Constant C_{20}	8,617.7	Pa
Material Constant C_{30}	192,533.0	Pa
Residual	23.5	

The Yeoh 3-parameter model provided a reasonable fit to the test data until about 60% strain, beyond which it underpredicted stress (Figure 5-10).
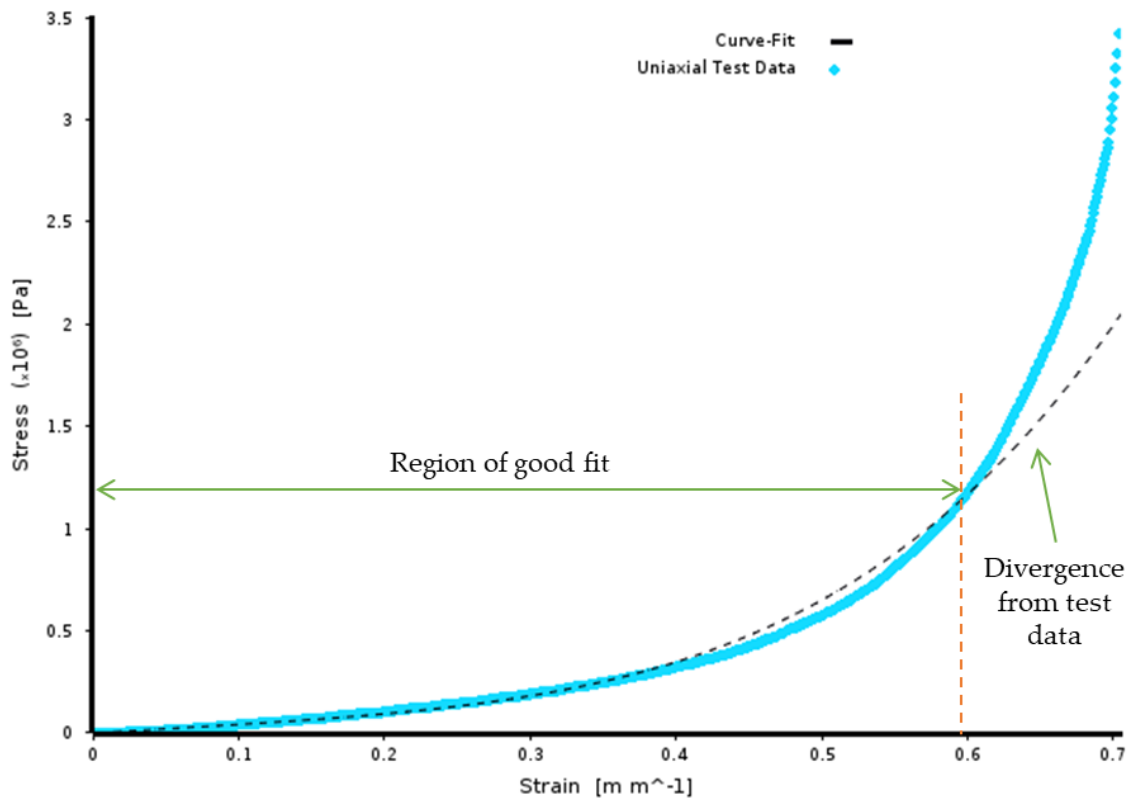
Figure 5-10: Yeoh 3-parameter curve fit against uniaxial test –compressive stress vs. strain data.

For Prony series curve fitting, a 2-term fit followed the data more closely than a 3- or 5-term. In particular, a 2-term fit was able to follow the rapid decay in shear moduli after the loading phase more closely (Figure 5-11). The 2-term curve fit was similar for the 60 and five second curve inputs.
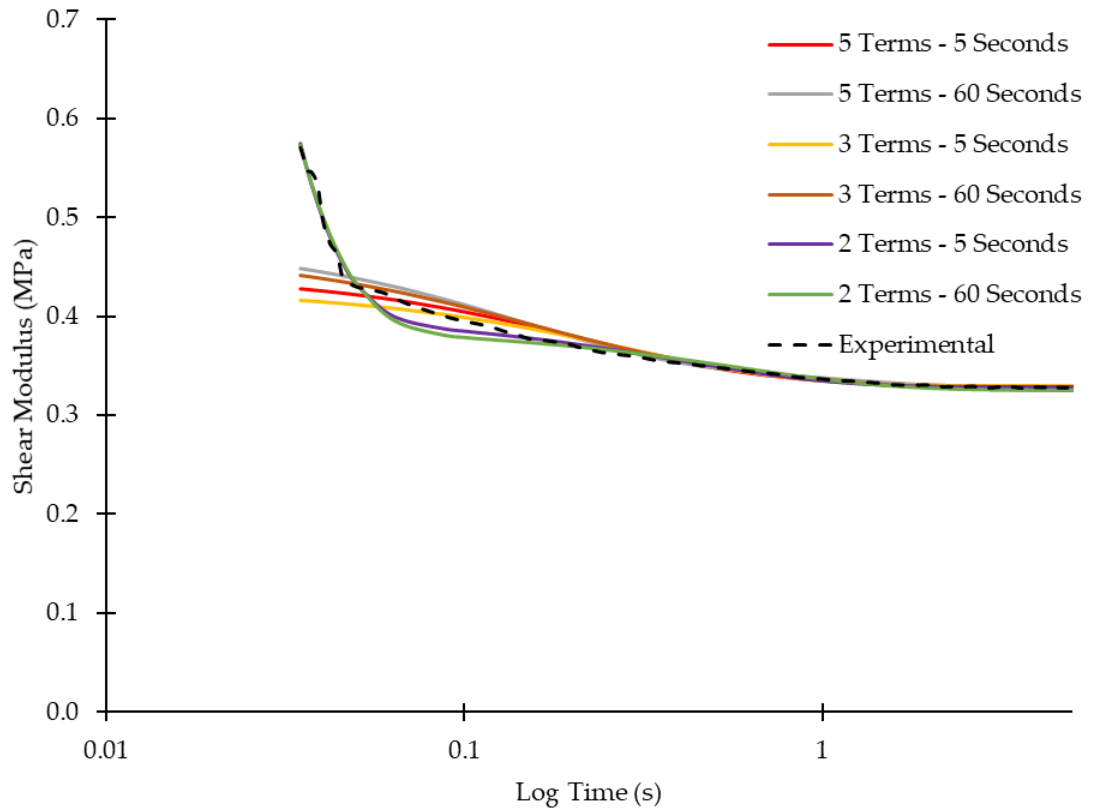
Figure 5-11: Prony series curve fit for 2-,3-, and 5-terms for 5 and 60 second curve data in comparison to the experimental data.

Table 5-4: Prony series 2-term values obtained for 60 seconds and 5 seconds shear response data input.

Data Input and Fit	Index i	Relative Moduli(i)	Relaxation Time(i) (s)
5 seconds - 2-term	1	0.0116	0.40463
	2	0.9347	0.01005
60 seconds - 2-term	1	0.9121	0.01137
	2	0.0141	0.58181

Applying the factor-of-10 rule meant removing data that included the rapid decay in shear modulus at the start of the relaxation phase, and just leaving the comparatively flatter shear response (Figure 5-12). For the cropped data, a 4-term Prony series gave the best fit, so it was combined with the 5-parameter Mooney-Rivlin hyperelastic model in Section 5.2.1 to assess the effect of applying the factor-of-10 rule.
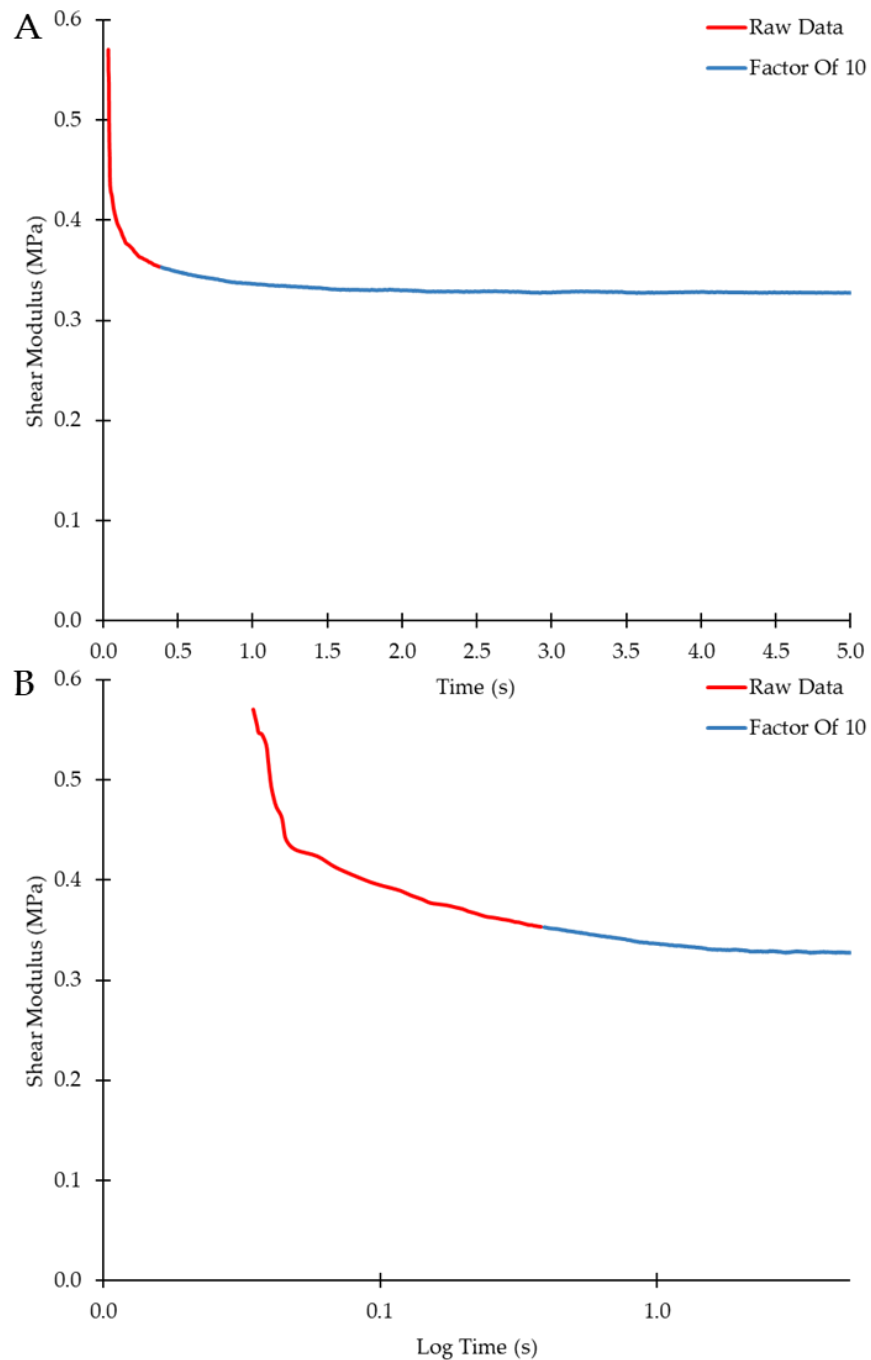
Figure 5-12: Comparison of shear response when the data is cropped as per the factor- of-10 rule shown in both (A) a linear time axis and (B) a logarithmic time axis.

5.5 Experimental Impact Testing and Simulation Methodology

5.5.1 Experimental Impact Testing

The drop mass and impact energies were the same as those used when testing rugby padding on a rigid anvil in Chapter 4. Three shoulder surrogate samples were impacted at energies of 4.9, 9.8 and 14.7 J by dropping a 5 kg mass (flat face, Ø 130

mm) (Figure 5-13) from 0.1, 0.2 and 0.3 m, respectively. The anvil, with the surrogate fixture on top, was fixed on the four load cells with the same data acquisition system and settings as described in Chapter 4. Each impact was also filmed with a HSV Camera with identical equipment, load cell synchronisation and settings as described in Chapter 4.
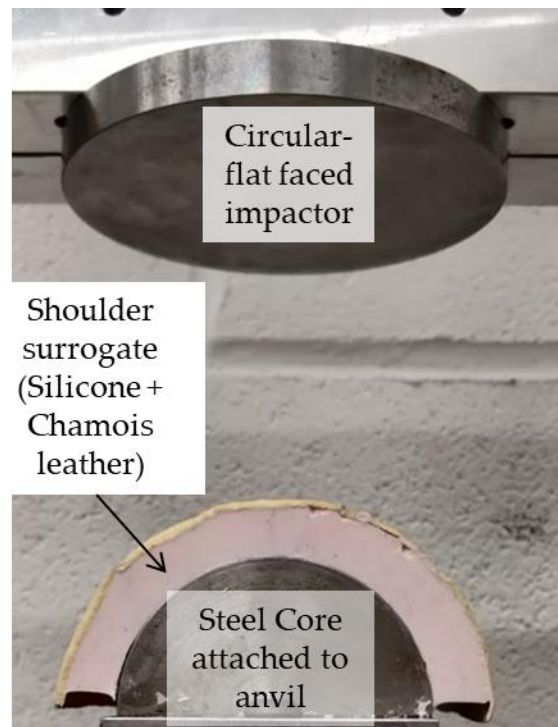
Figure 5-13: Drop test setup used for testing the shoulder surrogate.

Each sample was impacted three times at each energy with at least one minute between impacts. The voltage readings from each load cell were saved in MS Excel® and converted to force as defined in Section 4.2.2. The force vs. time data for each impact was plotted alongside the outputs from the FE simulations, as detailed in the following Section 5.5.3.

5.5.2 Impact Modelling Setup

The geometry (Figure 5-14) of the shoulder surrogate and the flat circular impactor was modelled in SolidWorks© (version 2018, Dassault Systems) and the corresponding .sldprt file was imported into Ansys© workbench Geometry using Design Modeller's import external geometry function. The geometric centre of the

impactor was aligned to that of the surrogate in the widthwise (x-axis) and lengthwise (z-axis) directions, and the impactor was placed 2 mm above (y-axis) the surrogate.
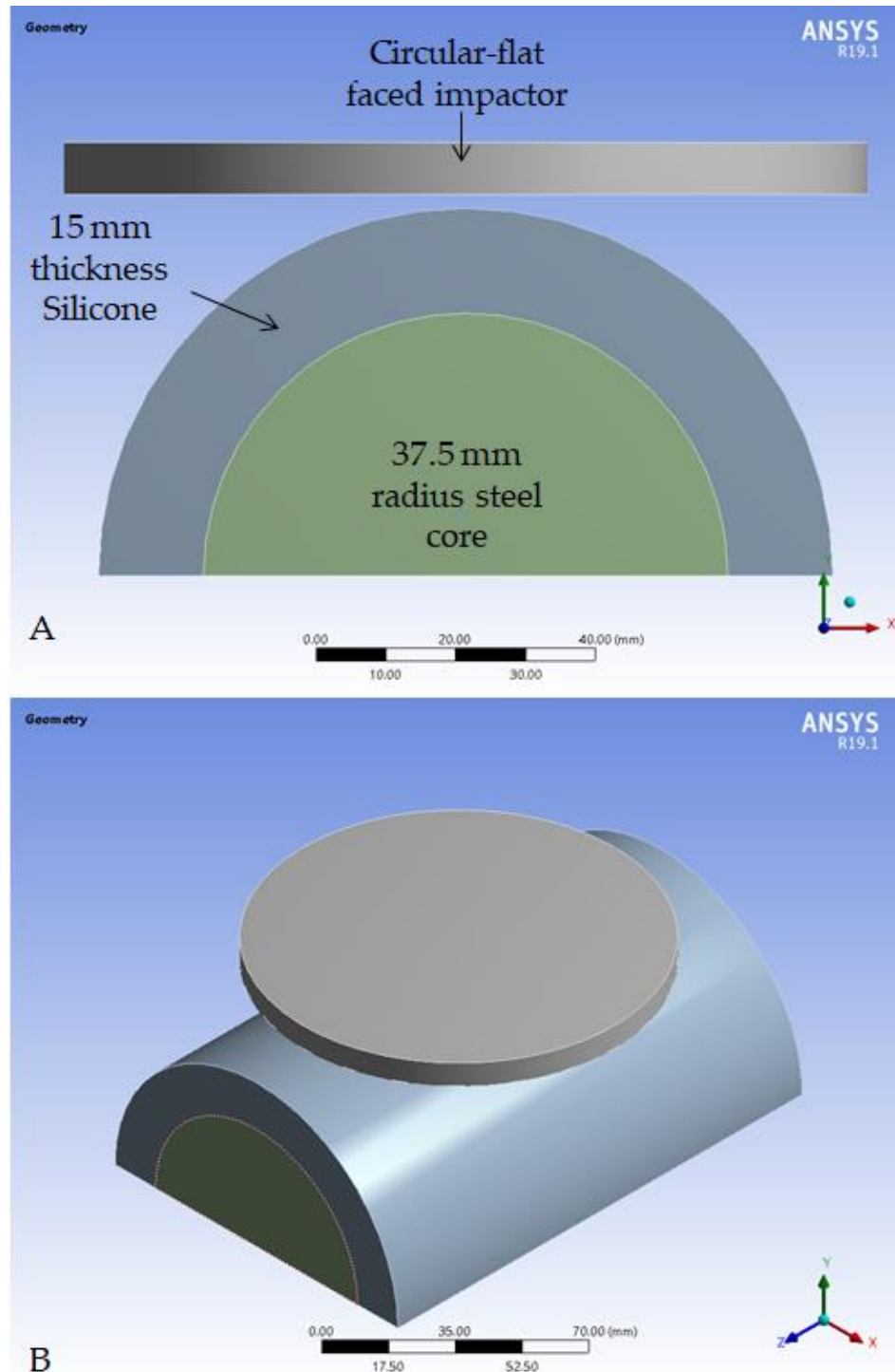
Figure 5-14: (A) Cross-sectional view and (B) isometric view of the geometry setup for the FE-Simulation of the impacts.

The impactor and steel core were assigned rigid material models (*MAT_RIGID). The material properties of the impactor and steel core are in Table 5-5. Due to the lower volume of the impactor in the model compared to the one in the experiment (where the cylindrical impactor was attached to the rails of the drop rig via a horizontal bar as seen in Figure 5-13), the assigned density of the impactor was artificially increased to give the required mass of 5 kg. The material properties of the silicone were taken from the hyperelastic models and the Prony series terms obtained in Section 5.4.

Table 5-5: Material Properties of different geometries modelled for simulation.

Part	Density (kg·m⁻³)	Young's Modulus (E) (GPa)	Poisson's Ratio (ν)	Source
Impactor	64,829	200	0.3	Ansys© library – Structural steel, but with increased density
Steel core	7,850	200	0.3	Ansys© library - Structural Steel

As the impactor and steel core were defined as rigid bodies, the default element type (hexahedral / ELFORM=1) and mesh size of 6 mm was applied. The silicone layer was assigned a tetrahedral mesh (ELFORM=10), to prevent negative volume errors, of size 3 mm (Figure 5-15) based on a mesh convergence study (Appendix B). These settings resulted in a total of 26,148 nodes and 108,980 elements with a mean quality of 0.85 ± 0.09 and a mean skewness of 0.215 ± 0.12 (Table 5-6).

Table 5-6: Mesh properties of different geometries modelled for simulation.

Part	Nodes	Elements*
Impactor	2,217	1,408
Silicone	20,944	105,220
Steel core	2,987	2,352

*All single point integration
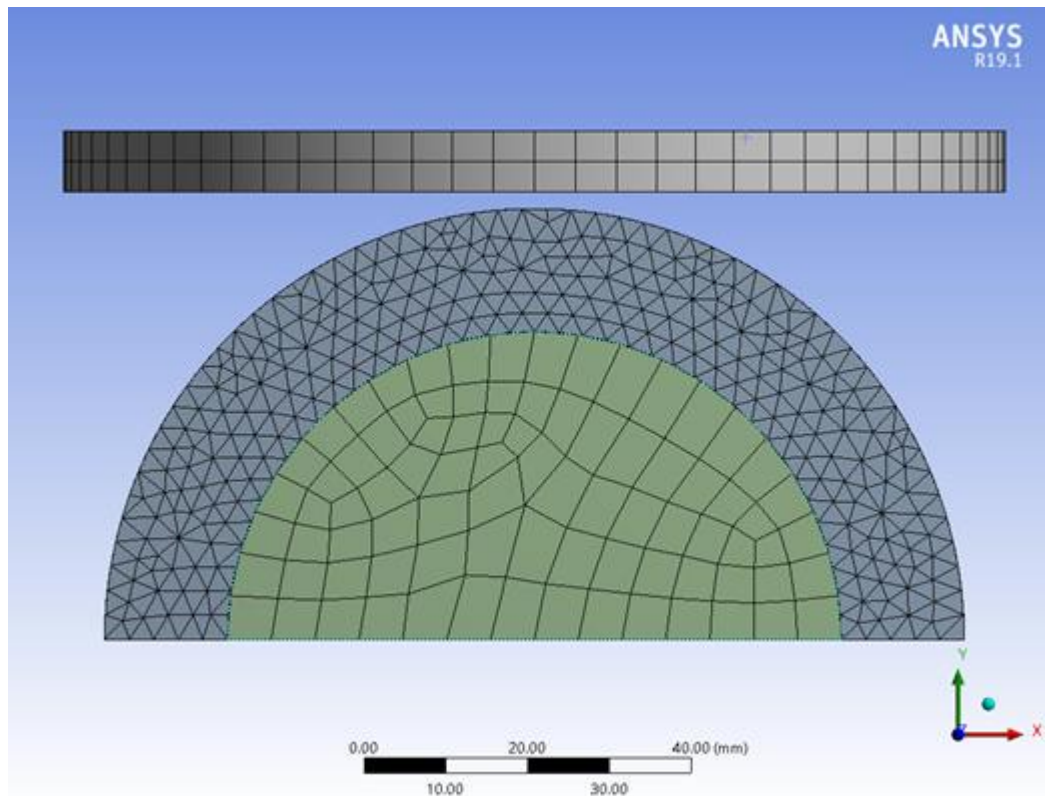
Figure 5-15: Cross sectional view of the mesh in the FE model of the shoulder surrogate.

The model was set up to replicate the impact test (Figure 5-16). Contact (*CONTACT_AUTOMATIC_SURFACE_TO_SURFACE) was defined between the silicone and steel core with a static and dynamic coefficient of friction of 0.3. The steel core was fully constrained, and the impactor was assigned an initial velocity (*INITIAL_VELOCITY_RIGID_BODY) equal to that of the corresponding impact energy (Table 5-7). The simulation was set up with a time step safety factor of 0.4. The time step safety factor was reduced from the default value of 0.9 to prevent the elements passing through each other at the point of first contact.
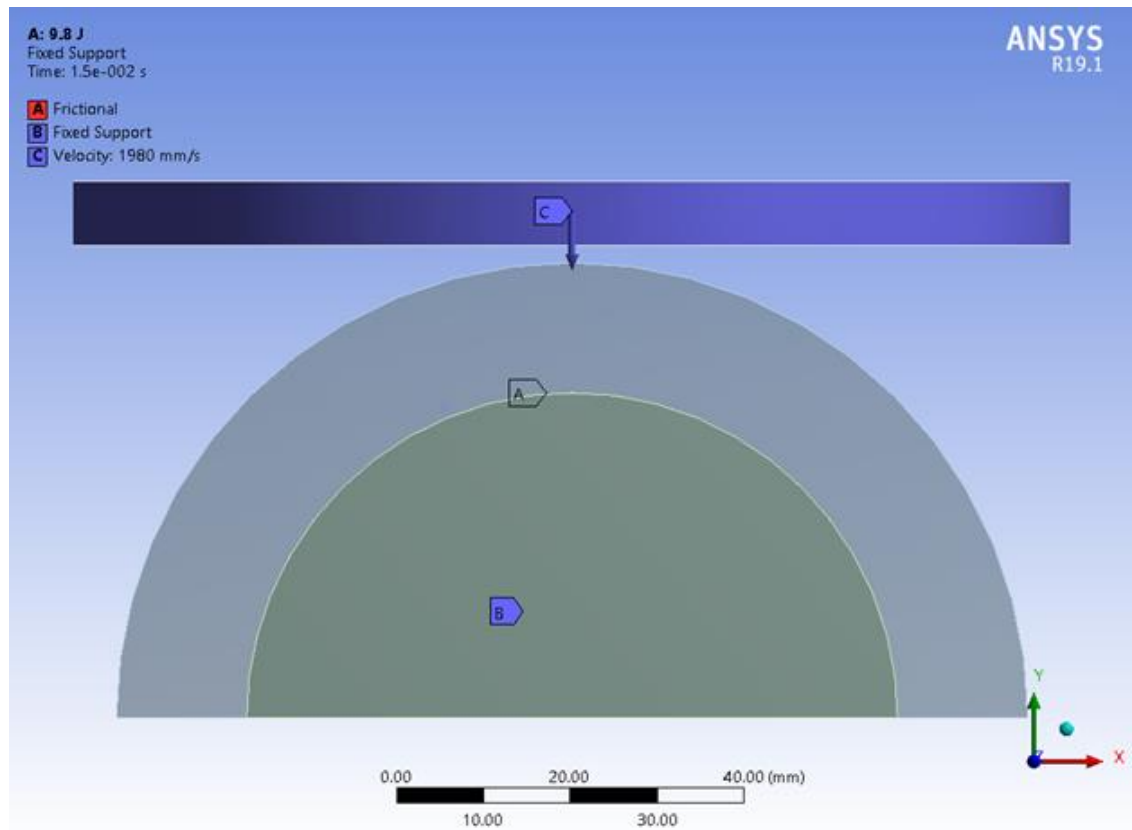
Figure 5-16: Boundary conditions for the FE-simulations showing (a) frictional contact, (b) fixed support for steel core and (c) impact velocity for a 9.8 J impact.

Table 5-7: Initial velocity and simulation end times assigned for simulations at each impact energy.

Impact Energy (J)	Initial velocity (m/s)	Simulation Duration (s)
4.9	2.42	0.01
9.8	1.98	0.015
14.7	1.40	0.0175

Frequency independent damping (input as a shear modulus) was introduced to reduce vibrations of the silicone that were observed in pilot simulations. The frequency independent damping in turn increased the stiffness of the silicone under impact, resulting in higher impact forces. When the shear modulus of the silicone was calculated from the Young's modulus measured during quasi-static compression testing (0.18 MPa), the peak impact forces during pilot simulations at 14.7 J were lower (> 30%) than for the corresponding experiments. The maximum value found for the Young's modulus of human skin tissue under dynamic testing

in the literature was 140 MPa (Kalra et al., 2016, Jacquemoud et al., 2007). Converting the maximum Young's Modulus of 140 MPa to shear modulus using 0.48 as the Poisson's ratio, the value of 47 MPa was obtained and applied to the material model (Equation 5-7).

Simulations using the three hyperelastic material models (i.e. 5-parameter Mooney-Rivlin, 3-parameter Ogden and 3-parameter Yeoh), each combined with a 2-term Prony series, were run at 14.7 J (as per the Regulation-12 test method) to find out which one gave the closest agreement to the experimental data (further explanation in Section 5.6.2). The material model in closest agreement with the experimental data at 14.7 J (5-parameter Mooney-Rivlin with 2-term Prony series) was then also compared to the experimental data obtained at 4.9 and 9.8 J impact energies.

The output results files from the simulations (.d3plots) were loaded into LS-Prepost for post-processing. Using the RCFORCE (contact force data) option through the ASCII data files produced by the simulation, the contact temporal force between the silicone and the steel core was obtained. Using the integration option in LS-Prepost, the area under the curve (impulse) was computed. The force and time data were exported as MS Excel® files, and the data was analysed alongside the experimental data for validation purposes.

5.5.3 FE Model Validation

Validation of the model against the experiment involved comparing peak impact force, impact duration, impulse and maximum deformation, as defined below.

In the experiment, the start of an impact was taken as the time point when the force from the load cells was first observed to start increasing. Any systematic offset of the force from zero before the observed start of impact (taken as the last point before the clear increase and typically under 15 N) was then subtracted from the temporal force data. Experimental impact duration was then calculated as the time from the start of the impact until the temporal force first dropped below 0 N. Simulation

impact duration was the time from the first non-zero force value until the force returned to zero. Maximum deformation of the silicone was measured using the HSV footage, as the distance between the position of the impactor when it struck the silicone to the position where it temporarily stopped moving at the time point of maximum compression of the silicone. To obtain maximum deformation from the simulations, the initial vertical distance (2 mm) between the silicone and impactor was subtracted from the maximum vertical displacement of the impactor.

Though the data for each of the three impacts at each energy was noted and tabulated, the outputs from the FE model were only compared against the first impact, to limit any effect of silicone degradation (as pilot testing at 14.7 J, on a different shoulder surrogate, showed an increase in force values with repeated impacts).

5.5.4 FE Model Sensitivity Study

For the 5-parameter Mooney-Rivlin model, the effect of, (i) adding Prony series terms, (ii) applying the factor-of-10 rule and (iii) varying the frequency independent damping were studied. The effect of adding a Prony series was studied by simulating the 5-parameter Mooney-Rivlin model with and without the 2-term Prony series at impact energies of 4.9, 9.8 and 14.7 J.

The cropped shear relaxation data (i.e. after the factor-of-10 rule was applied) was used to model the Prony series and the resulting coefficients were added to the 5-parameter Mooney-Rivlin model. The resulting simulation force vs. time data was plotted alongside the 5-parameter Mooney-Rivlin model with a 2-term Prony series (without factor-of-10 rule) and without any Prony series.

The effect of using shear modulus, in the range of 20 to 100 MPa, to apply frequency independent damping was studied, along with no damping, at an impact energy of 14.7 J. The force vs. time data obtained for each of the variations of the material model were plotted to understand the differences / variance.

5.5.5 Comparison against Silicone Models from the Literature

The FE model with the material model combining a 5-parameter Mooney-Rivlin and a 2-term Prony series was also compared against the single material silicone models from Payne et al. (2015b). Coefficients of single material simulant models developed by Payne et al. (2015b) (listed in Table 5-8) were used. The material model used was a 2-parameter Mooney-Rivlin with a 3-term Prony series. Payne and colleagues specified software (Abaqus) specific damping in their models for the silicone, so damping was not included when recreating their silicone models here. Results from the silicone material model developed here and those from Payne et al. were compared at 4.9 J as at higher impact energies the simulation returned negative volume errors.

Table 5-8: Mooney-Rivlin Coefficients and Prony series terms used for modelling three silicones.

	Mooney–Rivlin coefficients			Prony series		
	D_{10}	C_{01}	C_{10}	i	g(i)	τ(i)
Silastic 3481	–	61,100	13,500	1	0.0617	0.18
				2	0.0385	5.55
				3	0.033	96.1
Silastic 3483	–	76,500	791	1	0.0502	0.218
				2	0.0287	8.62
				3	0.026	90
Silastic 3487	–	53,100	1,590	1	0.0552	0.232
				2	0.0351	8.8
				3	0.0392	88.1

5.6 Results

5.6.1 Experimental Results

Peak force, maximum deformation and impulse all increased with the impact energy, while impact duration decreased (Table 5-9). At the highest impact energy,

the variance in the peak impact force was highest, suggesting that the sample could have undergone degradation.

Table 5-9: Summary of results from the experimental impacts at impact energies of 14.7, 9.8 and 4.9 J (mean ± SD).

Impact Energy (J)	Peak Force (N)	Impact Duration (ms)	Maximum Deformation (mm)	Impulse (Ns)
14.7	5,648 ± 124	6.9 ± 0.02	5.2 ± 0.08	15.6 ± 0.06
9.8	4,058 ± 24	8.2 ± 0.06	3.4 ± 0.08	13.2 ± 0.07
4.9	2,433 ± 33	10.1 ± 0.05	3.0 ± 0.05	10.9 ± 0.03

5.6.2   FE Simulation Results

Of the three hyperelastic models (Mooney-Rivlin, Ogden and Yeoh) assigned to the silicone at 14.7 J, the 5-parameter Mooney-Rivlin model combined with a 2-term Prony series was in closest agreement with the experiment, with a mean error of ~7% across the four assessment parameters (Table 5-10). The Ogden model returned the same impact duration as the experiment, but larger discrepancies in the other three parameters (>25%) made it unsuitable for modelling the silicone.

The 5-parameter Mooney-Rivlin with a 2-term Prony series model at 9.8 and 4.9 J resulted in mean errors of 10 and 9% across the four assessment parameters, respectively (Table 5-11). Visual comparisons of force vs. time plots and high-speed video footage from the experiment and animations from the FE-simulations for impacts at 14.7 J indicate good agreement (Figure 5-17).

Table 5-10: Comparison of three Hyperelastic models used to model the silicone at 14.7 J.

Model	Peak Force		Maximum Deformation		Impact Duration		Impulse		Mean Error %
	N	Error %	mm	Error %	ms	Error %	Ns	Error %	
Experimental	5,499	-	5.1	-	6.8	-	15.5	-	
5-Parameter Mooney-Rivlin	5,538	+1	4.7	-7	6.3	-7	13.3	-14	7
3-Parameter Ogden	4,040	-27	3.8	-25	6.8	0	11.5	-26	19
3-Parameter Yeoh	3,578	-35	6.9	+35	7.3	+7	11.7	-25	26

Table 5-11: Comparison of 5-parameter Mooney-Rivlin 2-term Prony model against experimental impact data at 14.7, 9.8 and 4.9 J.

Energy J	Model	Peak Force		Deformation		Impact Duration		Impulse		Mean Error %
		N	Error %	mm	Error %	ms	Error %	Ns	Error %	
14.7	Experimental	5,499	-	5.1	-	6.8	-	16	-	7
	FE Model	5,538	+1	4.7	-7	6.3	-7	13	-14	
9.8	Experimental	4,071	-	3.5	-	8.1	-	13	-	10
	FE Model	4,040	-1	3.8	+9	6.8	-16	11	-12	
4.9	Experimental	2,399	-	2.9	-	10.5	-	11	-	9
	FE Model	2,460	+3	3.1	-7	9.0	+11	9	-18	
							Overall Error Mean			8.6
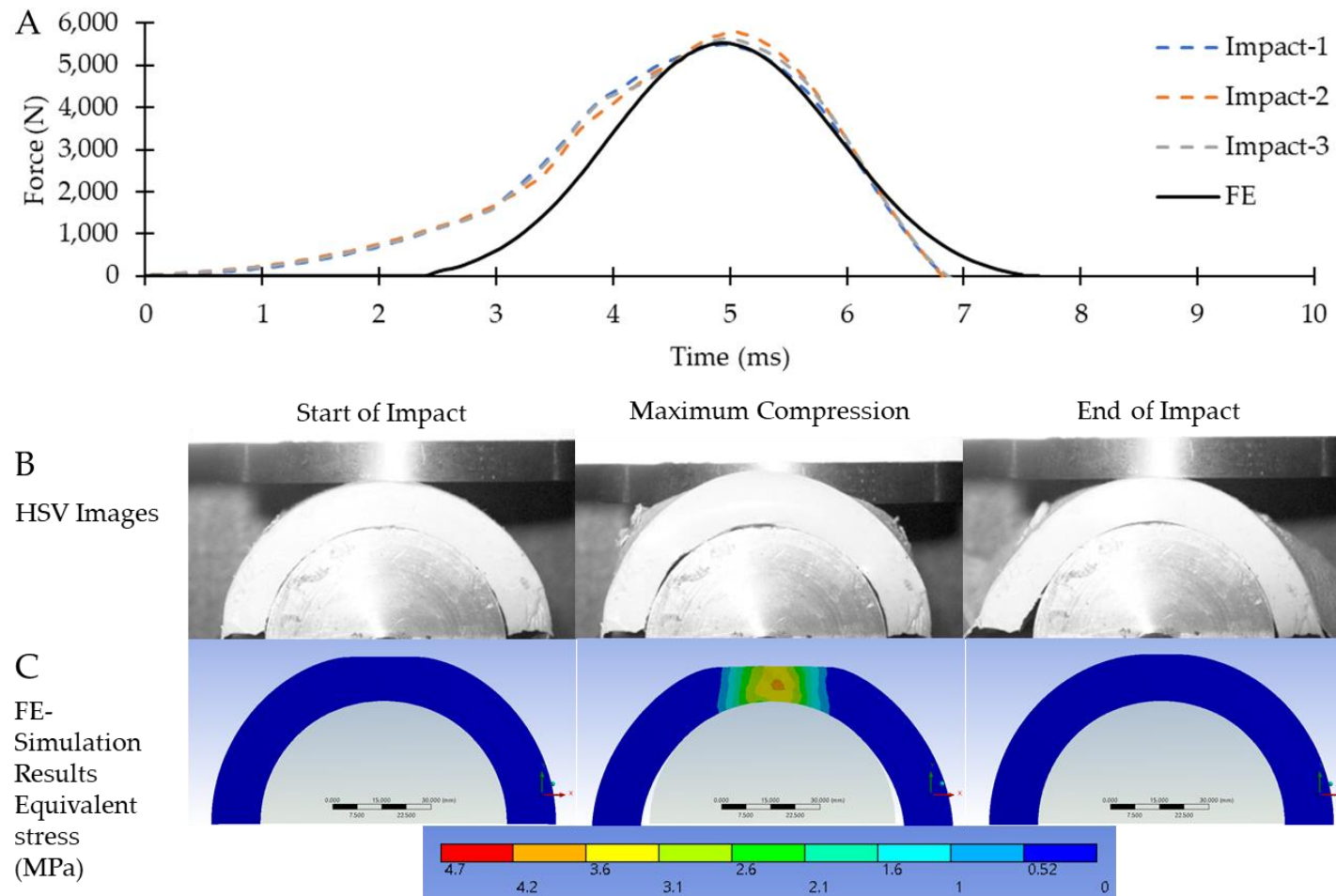
Figure 5-17: (A) Force time plot of 14.7 J impacts in comparison to 5-parameter Mooney-Rivlin 2-term Prony series model along with (B) images from the high-speed camera and (C) FE simulations with contours of equivalent stress (MPa). Simulation impact trace shifted to match peak force timings.

The loading curve of the simulated impacts had a steeper gradient than that of the experimental impacts (Figure 5-18).
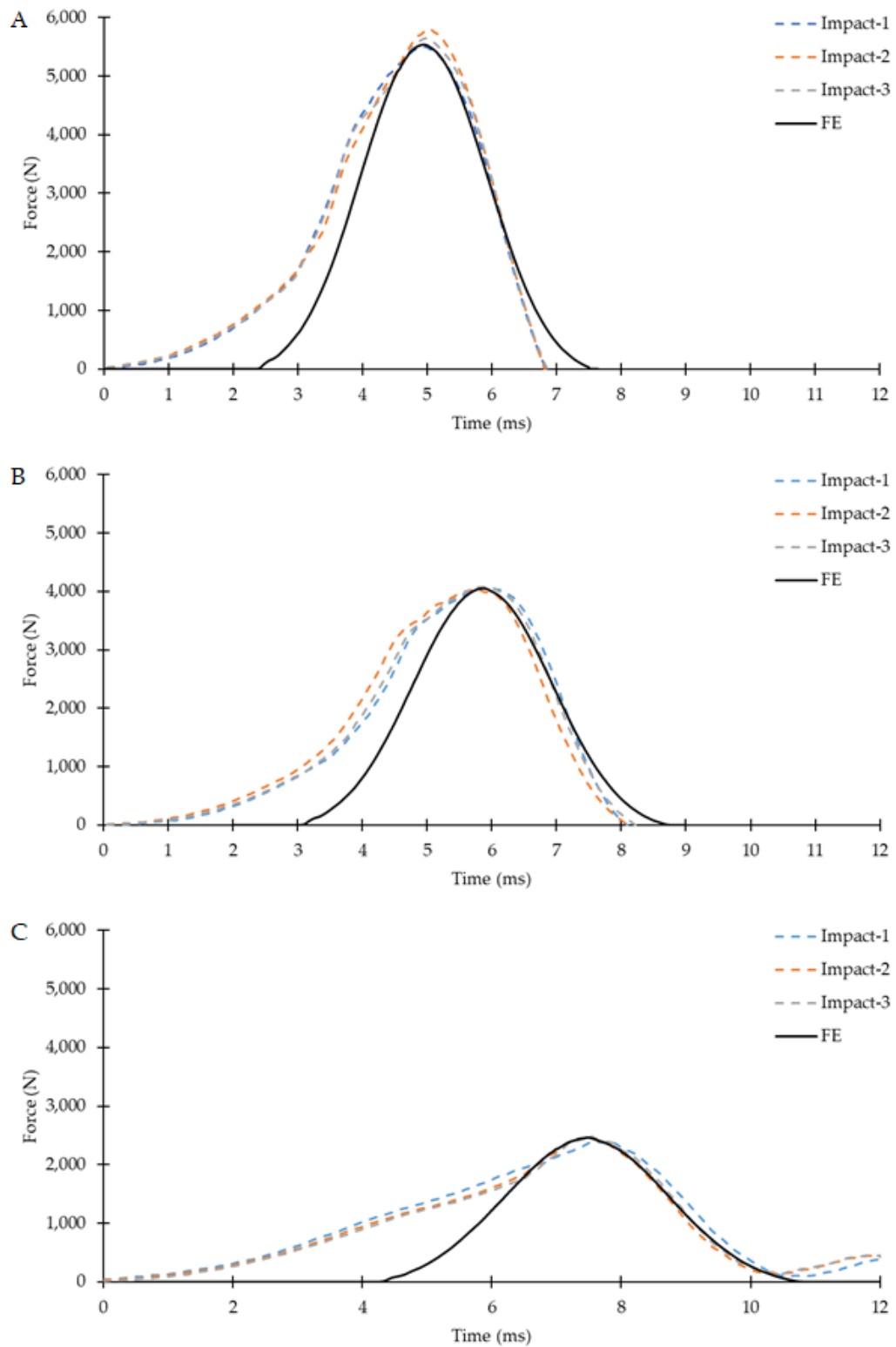
Figure 5-18: Force trace of the impact (experimental and simulated) at (A) 14.7 J (B) 9.8 J and (C) 4.9 J. Simulation impact trace shifted to match peak force timings.

5.6.3   Sensitivity Study Results

Adding the 2-term Prony series to the 5-parameter Mooney-Rivlin material model increased the peak impact force (Figure 5-19, Table 5-12) by up to 20%.
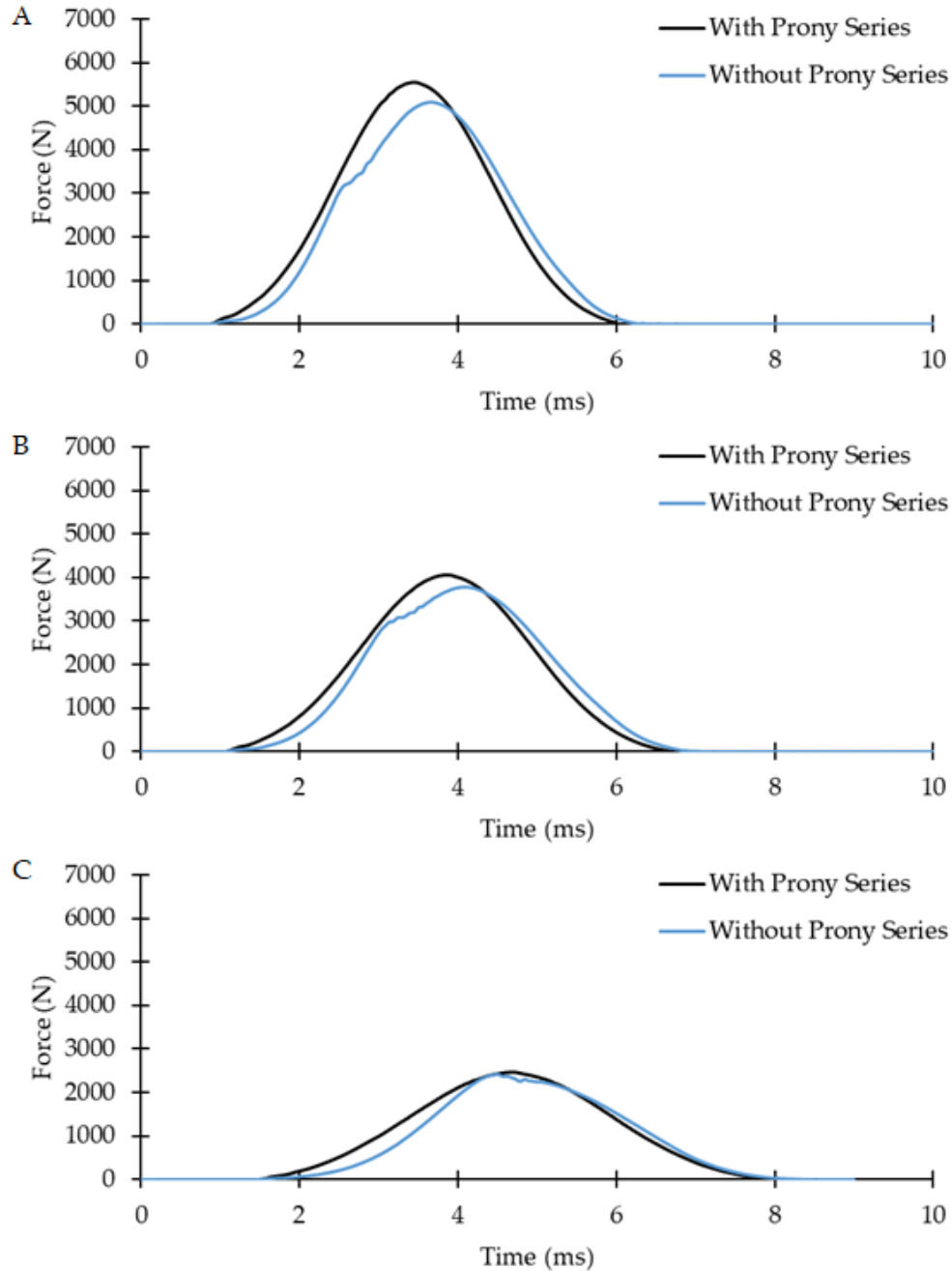
Figure 5-19: Force trace comparing the effect of the Prony series on the impact force at (A) 14.7 (B) 9.8 and (C) 4.9 J.

As well as increasing peak forces, adding a Prony series to the Mooney-Rivlin model decreased impact durations and maximum deformations (Table 5-12).

Table 5-12: Effect of adding Prony series to the 5-parameter Mooney-Rivlin model at 14.7, 9.8 and 4.9 J.

Energy (J)	Change in Peak Force - N (%)	Change in Impact Duration - ms (%)	Change in Deformation mm (%)
4.9	+ 52 (+ 2)	-0.48 (- 5)	-0.52 (- 9)
9.8	+ 282 (+ 7)	-0.53 (- 7)	-0.43 (- 7)
14.7	+ 916 (+ 20)	-0.56 (- 8)	-0.72 (- 9)

When the factor-of-10 rule was applied to the stress relaxation data used in the Prony series fitting, peak force increased (Figure 5-20). Applying the factor-of-10 rule made the simulation behave almost as if no Prony series was included.
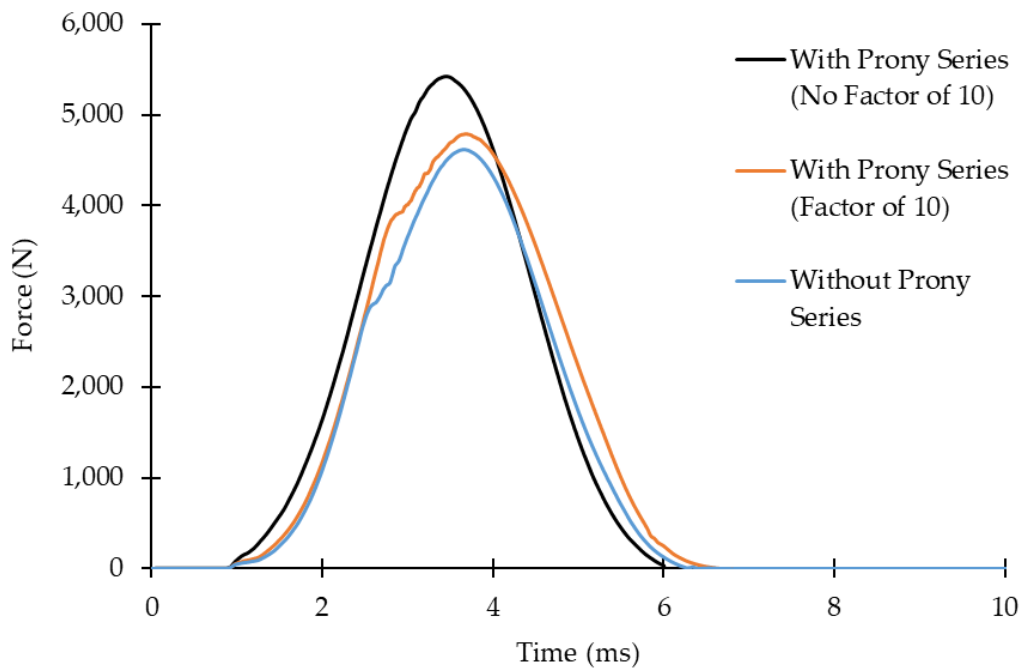
Figure 5-20: Force time trace from the model comparing the effect of factor-of-10 rule on the model at 14.7 J.

Peak impact force increased (Figure 5-21). with the shear modulus that was used to determine the frequency independent damping, while deformation and impact duration decreased (Table 5-13).
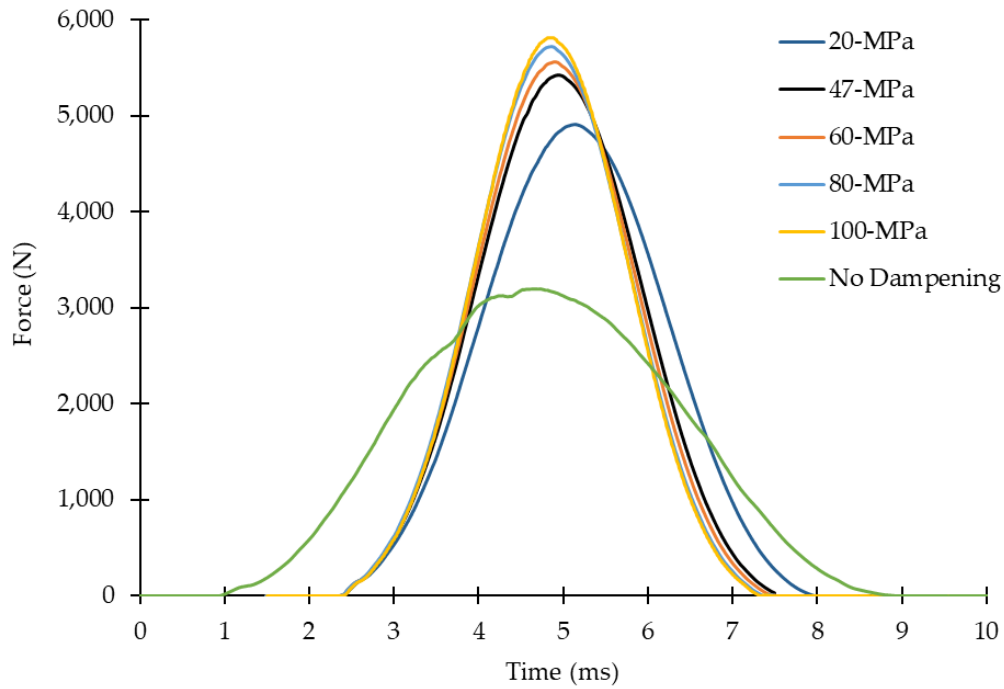
Figure 5-21: Force vs. time plot showing the effect of using different values of shear modulus to define frequency independent damping, as well as a model without damping, at 14.7 J impact.

Table 5-13: Comparison of peak force, impact duration deformation and impulse due to addition of frequency independent damping against no damping.

Shear Modulus (MPa)	Peak Force		Impact Duration		Deformation		Impulse	
	N	Change (%)	ms	Change (%)	mm	Change (%)	Ns	Change (%)
No Damping	3,190	-	9.7	-	6.8	-	12.7	-
20	4,910	+54	6.8	-30	4.9	-28	12.8	0.1
47*	5,430	+70	6.3	-35	4.6	-32	12.7	-0.1
60	5,560	+74	6.2	-36	4.6	-33	12.7	-0.2
80	5,720	+79	6.2	-37	4.5	-34	12.7	-0.2
100	5,776	+81	6.1	-37	4.5	-34	12.7	-0.3

* denotes the damping value used for the final model.

5.6.4 Comparison against Silicone Models from the Literature

Impact simulations at 4.9 J showed that using single material silicone models based on those of Payne et al. (2015b) gave peak forces under half of those for the model developed here (Figure 5-22). The maximum von Mises stress induced in the model developed here was also about four to five times higher than the single material simulants defined by Payne et al. (2015b)(Figure 5-23).
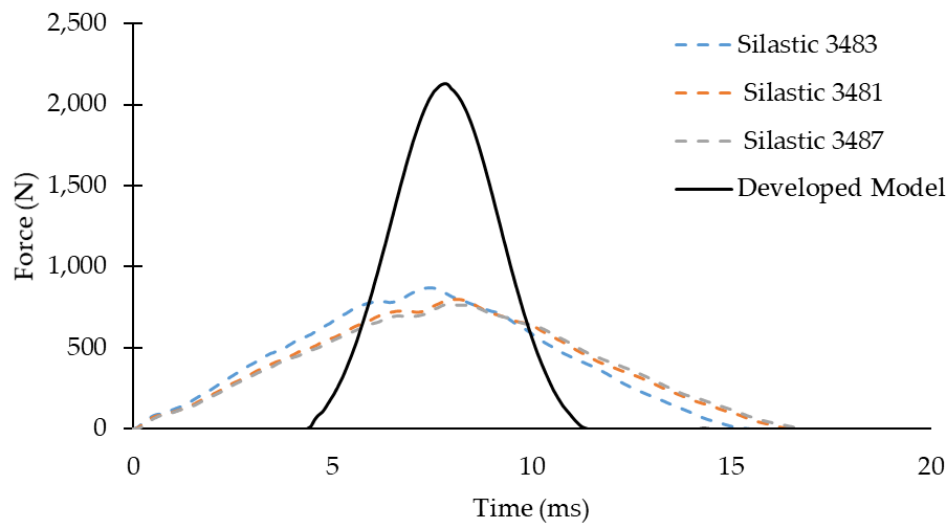
Figure 5-22: Force trace comparing the silicone models defined by Payne et al. (2015b) and model developed in this study.
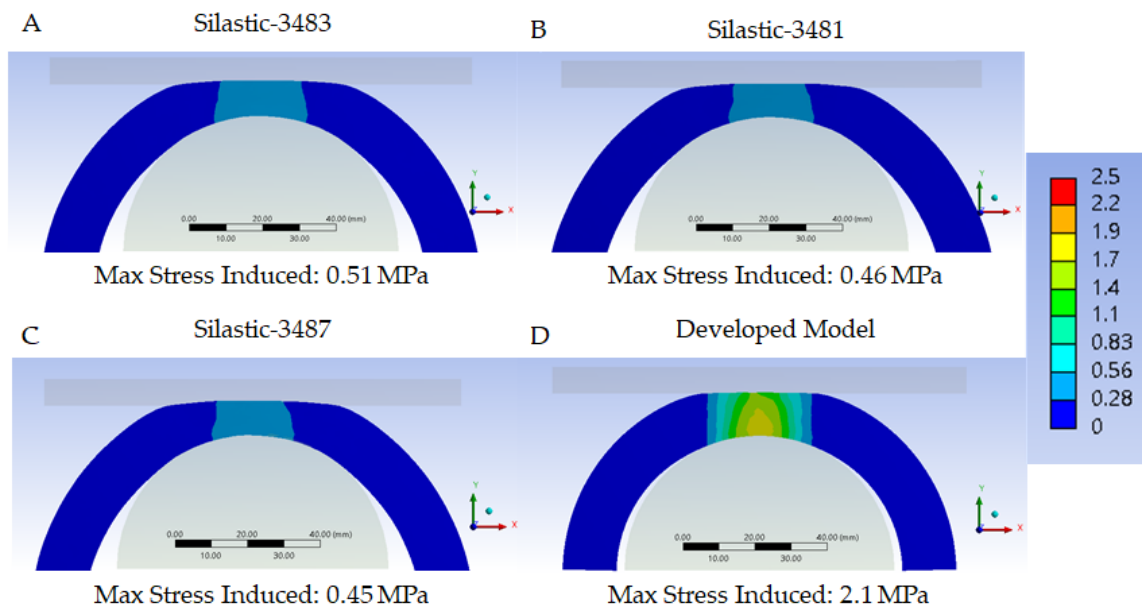
Figure 5-23: Maximum equivalent stress induced at 4.9 J impact for three material simulants (a, b & c) defined by Payne et al (2015b) and the model developed here (d).

5.7 **Discussion**

The methods applied to model the silicone developed by Hughes et al. (2020) have been described. The median quasi-static compressive stress vs. strain curve for the silicone was selected for modelling. Three hyperelastic models (Mooney Rivlin, Ogden & Yeoh) were fitted to the stress vs. strain data, with varying numbers of parameters. A 5-parameter Mooney Rivlin model gave the best fit to the experimental data, followed by a 3-parameter Ogden model and then a 3-parameter Yeoh model. These three hyperelastic material models were used to develop finite element models of the silicone, and corresponding simulations for an impact at 14.7 J were compared to data from an equivalent experiment (first impact).

A knock-on effect of the hyperelastic material models deviating from the quasi-static stress vs. strain curve (Figures 5-8, 5-9 and 5-10) was observed when comparing peak impact forces from the experiment and simulations (Table 5-10). Even with frequency independent damping and a Prony series included in the material model, the simulations with the Ogden and Yeoh models unpredicted peak force by 27 and 35%, respectively (Table 5-10). The contact duration predicted by the simulation with the Ogden material model agreed with the experiment, but peak force, maximum deformation and impulse were underpredicted by at least 25% (Table 5-10). As expected from the superior fit to the stress vs. strain curve, a simulation with a 5-parameter Mooney-Rivlin hyperelastic material model combined with a 2-term Prony series provided better agreement with the experiment than those with the Ogden and Yeoh models. This Mooney-Rivlin model showed under 10% discrepancy with the experimental values across all four assessment parameters for all three impact energies of 4.9, 9.8 and 14.7 J (Table 5-11). Across the three energies, the Mooney-Rivlin model predicted peak force to

within 3% of the experiment, and the largest error at each energy was for impulse (>10%).

Stress relaxation testing showed the silicone to be viscoelastic (i.e., decreasing force under constant strain), so Prony series shear relaxation data was combined with the hyperelastic material model to simulate strain rate dependency. Adding a Prony series to the 5-parameter Mooney-Rivlin material model increased peak force, and reduced impact duration and maximum deformation across the three impact energies (Table 5-12). The extent to which the Prony series increased peak impact force (2 to 20%) increased with the impact energy, while the changes in impact duration and maximum deformation remained almost constant (5-8 and 7-9%, respectively) (Table 5-12). When applying the factor-of-10 rule to the stress relaxation data, the rapid initial decay in shear modulus of ~0.2 MPa (~40%) in under 0.5 ms was removed (Figure 5-12). The shear modulus data with the factor-of-ten rule applied, even though still decaying, was much flatter than the data when the rule was not applied. Hence when the Prony series was modelled using the Factor-of-10 rule, the resulting simulation underpredicted peak impact force. While the Prony series has been shown to account for strain rate dependency (Payne et al. (2015), Newton-Mann et al. (2017)) the material model in the simulations is also reliant on a quasi-static stress vs. strain curve. Hence the highest strain rate available was used to test the silicone during quasi-static compression.

The simulations showed that introducing frequency independent damping to the material model affected the response of the silicone under impact (Figure 5-21). Inputting 47 MPa as the shear modulus for the frequency independent damping gave a 70% increase in peak force, a 35% decrease in impact duration and a 32% reduction in maximum deformation, in comparison to a model without damping (Table 5-13). When the shear modulus was varied (20 to 100

MPa) to determine the effect of varying the amount of damping, peak impact forces were most influenced (change of 54 to 81%), followed by contact durations (30 to 37%) and then maximum deformation (28 to 34%) (Table 5-13).

Both Ogden and Mooney-Rivlin material models have been shown in the literature to be good predictors of the stress vs. strain curve for skin and soft tissue simulants. Shergold et al. (2006) state that for skin, the Ogden model provided the best fit to the high strain rate (4,000 s^{-1}) uniaxial compression data in comparison to Mooney-Rivlin model. Flynn et al. (2011) carried out cyclic micro-loading (1.5 mm compressing) using a force sensitive robot and claimed that the Ogden model provided the best curve fit to the experimental data in comparison to other hyperelastic models. Joodaki and Panzer (2018) also reviewed hyperelastic models used to model skin and claim that the Ogden model provides best fit to uniaxial tensile test data. Almost all models reviewed were based on the testing of skin in isolation and did not consider the underlying soft tissue nor muscle. Most of the material models that have been fitted to data for skin have not been implemented into finite element models for simulating impact.

Payne et al. (2014) showed that silicones used for modelling human soft tissue in thigh surrogates were better characterised with Mooney-Rivlin material models in comparison to Ogden material model. Payne et al. (2015b) further developed the surrogate silicone models and validated them against experimental impact testing. The quasi-static stress vs. strain data of the surrogate developed by Payne et al. (2015b) is comparable to the silicone model developed for this research (Figure 5-24), as expected because the base silicone used is similar.
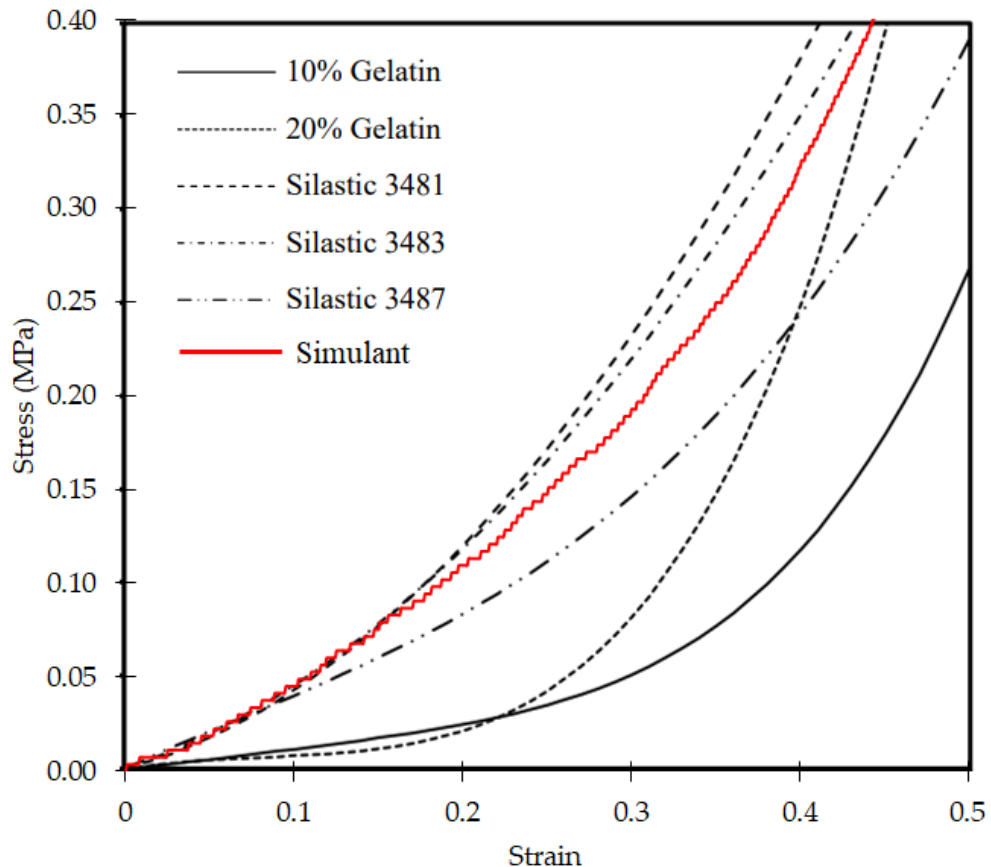
Figure 5-24: Quasi-static compressive stress vs. strain data of the silicone developed against the responses of materials used to model the thigh surrogate by Payne et al. (2015b).

When compared against the material model developed here in a simulated impact with an energy of 4.9 J, the silicone models of Payne et al. (2015b) showed a lower peak force (by ~2.5 times) and a longer impact duration (by ~2 times) (Figure 5-23). The silicone models of Payne and colleagues also had a lower von Mises stress at maximum compression (Figure 5-23). These results suggest that the silicone used in the shoulder surrogate was stiffer than those of Payne et al. (2015).

The difference in the silicones modelled by Payne et al. (2015b) and the one here could be related to the anatomy being studied (thigh vs. shoulder). The soft tissue layers in the thigh surrogate developed by Payne et al. (2015b) had a total thickness (skin exterior to bone exterior) over three times that of the silicone in the shoulder surrogate (50 vs. 15 mm). This difference in thickness could explain why the silicone models developed by Payne et al. (2015b) did

not work well when applied to the shoulder surrogate, and gave negative volume errors for simulations with impact energies of 9.8 and 14.7 J. The difference may also be the damping and element distortion setting options between the software used by Payne (Abaqus) and in this study. This difference has been investigated by recreating the simulations of Payne et al. (2015b) (Appendix C) and seeing the effect of adding similar damping settings to those used here to the models developed by Payne et al. (2015b) (Appendix D).

A limitation of this study was that the silicone samples tested under quasi-static compression and stress relaxation were made from the same batch of silicone. Testing samples from different batches of silicone would provide a better understanding of manufacturing variability. Also, the compression samples consisted of only the silicone and the chamois leather (skin simulant) was placed on top and the median (three repeats) stress vs. strain curve was plotted for comparison (Figure 5-6). When moulding silicone for the shoulder surrogate, the chamois leather was placed in the mould, so the two materials bonded. Compression samples could be cut out from a sheet of silicone that was moulded, and hence bonded, with chamois leather.

For impacts at 14.7 J on the finite element model of the shoulder surrogate, the material model developed for the silicone was shown to be dependent on the value of frequency independent damping (Figure 5-21). Only the uniaxial compression test data was used to model the hyperelastic response of the silicone. For modelling a hyperelastic material in Ansys©, volumetric response data, along with biaxial test data can also be used. Using volumetric response data (from volumetric compression tests) to model the silicone would remove the need to assume or test for Poisson's ratio. The Poisson's ratio used in the material model for the silicone was taken from the literature (Delalleau et al., 2006). Another option would be to measure the Poisson's

ratio of the silicone, such as by filming tensile tests and measuring the position of discrete markers placed on the sample or by applying a speckle pattern to the sample and using digital image correlation. The compression rate during the loading ramp for stress relaxation testing was limited by the maximum strain rate (6.7 s^{-1}) of the test equipment. Also shear data obtained for the Prony series curve fit was obtained from a compression test. Compressing the silicone faster during the loading phase of a stress relaxation test may provide data for modelling the Prony series that better accounts for strain rate dependency under impact.

The 5-parameter Mooney-Rivlin material model combined with a 2-term Prony series developed here is summarised in Table 5-14. The model can be used to study force propagation through the shoulder surrogate and could be developed to analyse PPE for sports and other scenarios where the shoulder anatomy is concerned. The silicone and chamois leather material were modelled as a single material and hence could be adapted to mimic different soft tissue anatomies of the human body by altering the thickness to match the anatomy under study.

Table 5-14: Summary of all material data/settings used for modelling the silicone used in the shoulder surrogate.

Material Property / Setting	Value	Units	Source
Density	1,072	kg·m^{-3}	Test Data
Poisson's Ratio	0.48	-	Delalleau et al. (2006)
Shear Modulus (for frequency independent damping)	47	MPa	Jacquemoud et al., 2007
SIGF – limit setting for damping	0.01		LS-DYNA® Model Volume-II
Mooney-Rivlin Hyperelastic Coefficients			Curve fit in
Incompressibility Parameter D_1	0	Pa^{-1}	Ansys©
Material Constant C_{01}	1.01E+06	Pa	Workbench
Material Constant C_{02}	2.47E+07	Pa	using Uniaxial
Material Constant C_{10}	-9.30E+05	Pa	Test data
Material Constant C_{11}	-3.60E+07	Pa	
Material Constant C_{20}	1.37E+07	Pa	
Prony Series Terms			Curve fit in
Relative Moduli (1)	0.0116		Ansys©
Relative Moduli (2)	0.9347		Workbench
Relaxation Time (1)	0.40463	s	using stress
Relaxation Time (2)	0.01005	s	relaxation data

5.8   **Chapter Summary**

The silicone developed by Hughes et al. (2020) to mimic soft tissue in a shoulder (muscle, fat and skin) surrogate was modelled in Ansys© LS-DYNA®. The material properties were obtained using quasi-static compression testing (curve fit using hyperelastic models) and compressive stress relaxation testing (curve fit using a Prony series shear response). The resulting finite models were compared against experimental data from impact tests at energies of 4.9, 9.8 and 14.7 J. The accuracy of the finite element models was assessed using four parameters, peak impact force, maximum deformation, impact duration and impulse. Of the candidates tested, the 5-parameter Mooney-Rivlin material model along with a 2-term Prony series was identified as the one with the best agreement with the experiment, with under 10% mean difference in the assessment parameters across the three impact energies. A summary of the chapter is presented in Figure 5-25. The finite element model of the shoulder surrogate can now be used to simulate different impacts and can be used to understand different stresses or other parameters of the surrogate simulant. The next chapter will focus on further developing the FE-Model to simulate damage to the silicone.

Background/ Literature
- Most literature focus only on skin and not the underlaying muscle and fat layer.
- Simulant developed by Payne et al. is similar, but is focused on thigh anatomy and of force propagation, not injury to the human skin
- Biofidelic shoulder surrogate developed at Sheffield was replicated in CAD & modelled.

Modelling Techniques
- Modelling of skin/ skin simulants have been carried out in literature with most models being mathematical and have not been validated against impact testing.
- Most models use different hyperelastic modelling techniques such Mooney-Rivlin, Ogden, Yeoh & viscoelastic properties modelled using Prony Series.

Testing & Validation
- Shoulder surrogate silicone impacted at 4.7, 9.8 and 14.7 J impact energy-Regulation-12 setup
- For material modelling, stress vs strain data obtained from silicone compression testing and viscoelastic data obtained from stress relaxation testing.
- Different hyperelastic models compared against impact test data for validation

Results
- 5-parameter Mooney-Rivlin model with 2 term Prony series provided lowest errors against experimental impact data.
- The model was found to be dependent on the shear independent damping factor and the Prony series terms.

Conclusions
- A finite element model mimicking the shoulder surrogate was developed and validated against impact testing.
- The model will be used to predict damages to the silicone in Chapter-6

Figure 5-25: Summary of work presented in Chapter-5.

6. Laceration Model Development and Validation

6.1 Chapter Introduction

Chapter 5 presented a material model for modelling the silicone of the shoulder surrogate designed by Hughes et al. (2020). In this chapter, the steps taken to develop a finite element model that can simulate impact induced damage to the silicone are presented (Figure 6-1). Such a FE model has potential to be used as a tool for predicting the risk of soft tissue injuries during rugby impact scenarios, and for assessing the efficacy of padding in reducing the risk of such injuries.
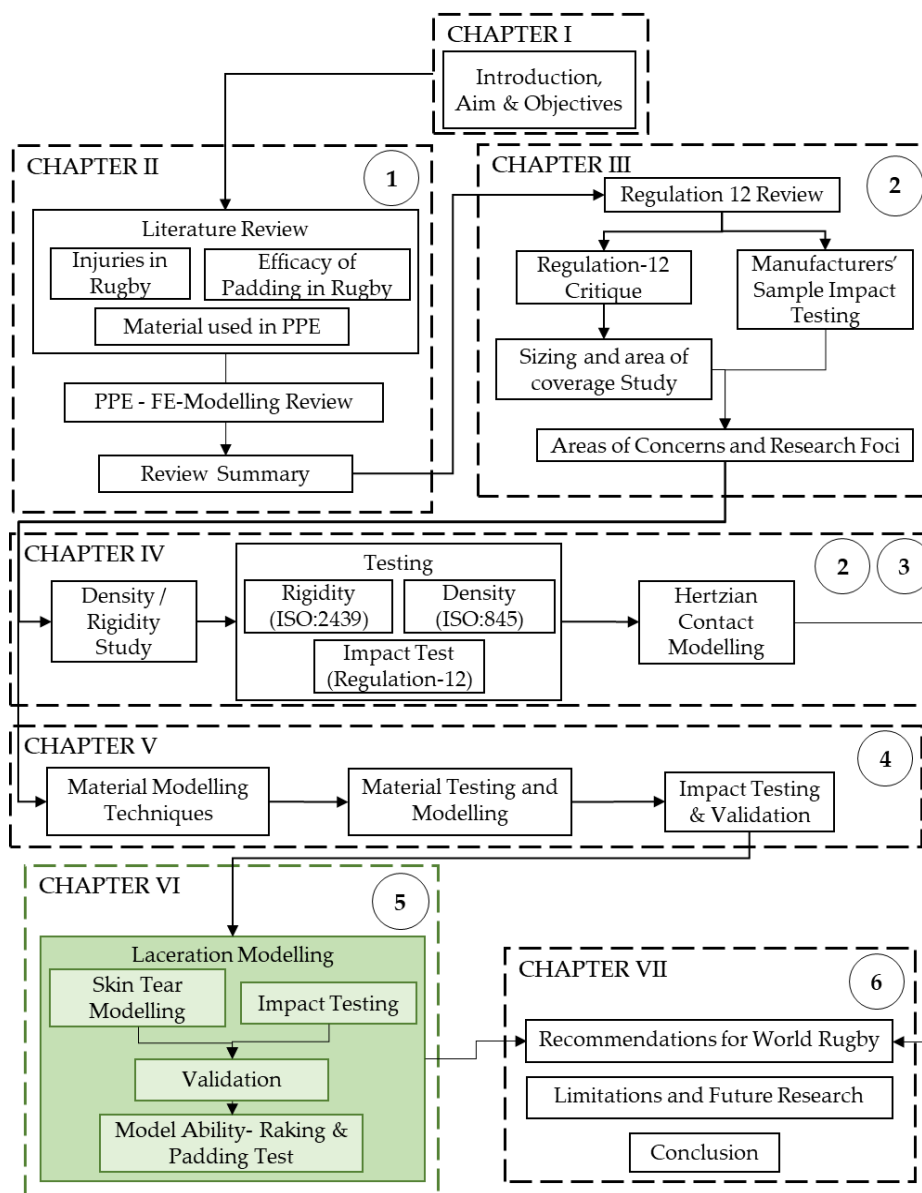
Figure 6-1: Layout of thesis showing the placement of Chapter 6 with respect to the overall project. Numbers in circles correspond to objectives listed in Chapter 1.

6.2 Introduction to Laceration Modelling Techniques

Previous sections have discussed the various material models for skin and muscle tissue that have been used in the literature. Much of the literature discussed in the previous chapters show that FE modelling techniques have been applied to study various parameters, such as force and pressure distribution of soft tissue under different loading conditions, heat transfer through the surface of skin and vibrational analysis of skin. Most research on predicting damage of protective materials occurs in studies focused on ballistic impacts (Silva et al., 2005; Bürger et al., 2012), armour development (Choudhary et al., 2020; Banerjee et al., 2017) and impact scenarios in the automobile industry (Kurtaran et al., 2003).

With the objective of developing an FE model capable of predicting soft tissue injuries, such as cuts and lacerations, it is important to understand the options available to predict injury and its extent. Injury prediction in an FE model is possible by applying damage detection (permanent change in element shape) or element deletion (removal of element once predefined criteria is met) criterion. Ansys© and LS-DYNA® have a library of material models with built-in failure criteria, which can be used for predicting material damage under different loading scenarios (Table 6-1).

Table 6-1: LS-DYNA material models with failure criterion options.

Material Number	Material Title	Material Applicable
3	Plastic Kinematic / Isotropic	Ceramics, Plastics & Metals
11	Steinberg: Temp. Dependent Elastoplastic	Metals
13	Isotropic Elastic Plastic with Failure	Metals
15	Johnson / Cook Plasticity Model	Metals
16	Pseudo TENSOR Geological Model	Soil
17	Oriented Crack (Elastoplastic with Fracture)	Metal & Plastic
22	Composite Damage	Composites
26	Honeycomb	Ceramic & Foam
32	Laminated Glass (Composite)	Composite & Glass
40	Nonlinear Orthotropic	Ceramic
52	Bamman Damage	Metal
54	Composite Damage with Change Failure	Ceramic
55	Composite Damage with Tsai-Wu Failure	Ceramic
73	Low Density Viscous Foam	Foams
83	Fu Change Foam	Foams
96	Brittle Damage	Bricks
183	Simplified Rubber with Damage	Rubbers

The issue with adapting a material model with existing damage prediction capability (i.e., one of those in Table 6-1) is that the properties are not easily changeable to mimic a silicone. Most of the material models with fracture prediction capabilities are either ductile (metallic), having a defined plastic phase before fracture, or brittle (such as wood or ceramic), where the fracture may occur at low strain. Skin tissue simulants are usually elastomeric, with comparatively smaller plastic regions and large strains before fracture.

In LS-DYNA® version 950 (LS-DYNA® Keyword User's Manual- Nonlinear Dynamic Analysis of Structures Version 950, 1999), a general failure criteria card for solid elements, termed *MAT_ADD_EROSION, was introduced that is independent of the material model. This failure criterion card allows the user to add different element deletion criteria to any material model. These element deletion criteria cause the solver to "erode" or delete an element once the element deletion criterion is met. According to the LS-DYNA user manual (LS-DYNA® Keyword User's Manual R10-Volume II-Material Models, 2018a), several element deletion criteria are available. Each element deletion criterion can be applied independently, and if any one or more of them (depending on the user setting) are satisfied, the element is removed from the calculation. Some of the criteria for failure are:

1. $P \geq P_{min}$ where, P is the pressure (positive in compression) in the element, and P_{min} is the pressure at failure (limit).

2. $\sigma_1 \geq \sigma_{max}$, where σ_1 is the maximum principal stress, and σ_{max} is the principal stress at failure.

3. $\varepsilon_1 \geq \varepsilon_{max}$, where ε_1 is the maximum principal strain, and ε_{max} is the principal strain at failure.

4. $\gamma_1 \geq \gamma_{max}$, where γ_1 is the shear strain, and γ_{max} is the shear strain at failure.

In relation to sporting equipment, Fortin-Smith et al. (2019) simulated a ball impacting on baseball bats to predict the nature of breaks that may occur. Using material properties for wood and adding element deletion criterion based on a

principal strain threshold, they were able to mimic cracks occurring in the wooden bat following impact with the baseball (Figure 6-2). The failure strain of the wood was obtained in a Charpy impact test on rectangular samples, and then applied to the wood material model using the *MAT_ADD_EROSION card. The models were used to determine relationships between the properties of the wood (e.g., slope of grain and density) and the nature of damage occurring in the baseball bat.
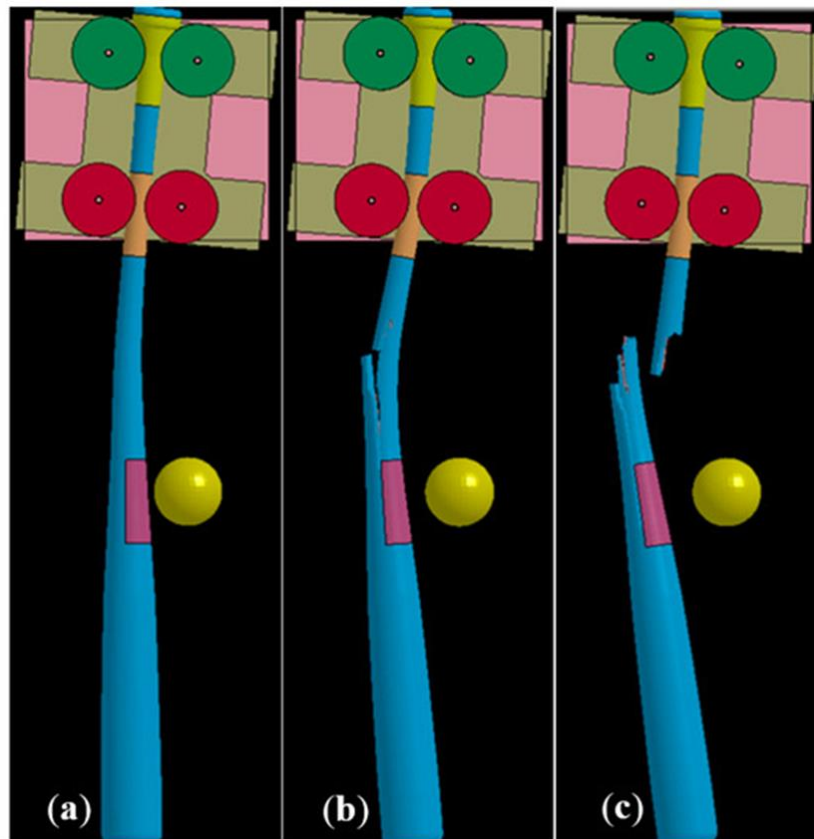
Figure 6-2: Simulation images from Fortin-Smith et al. (2019) showing different failure modes (a) no crack (b) cracking but no breaking - single piece failure and (c) cracking and separation – multi-piece failure.

The *MAT_ADD_EROSION criterion is defined in the K-word Manual (LS-DYNA® Keyword User's Manual R10-Volume II-Material Models, 2018) as a set of two cards (Table 6-2). The settings within these cards allow damage prediction capabilities to be added to material models, such as the one developed for silicone in Chapter 5 and will be used in Section 6.7- Stud Impact FE Modelling methodology.

Table 6-2: *MAT_ADD_EROSION cards with variable definitions. Only variables with non-zero values are applied.

Card 1	1	2	3	4	5	6	7	8
Variable	MID	EXCL	MXPRES	MNEPS	EFFEPS	VOLEPS	NUMFIP	NCS
Default	None	None	0.0	0.0	0.0	0.0	1.0	1

Card 2	1	2	3	4	5	6	7	8
Variable	MNPRES	SIGP1	SIGVM	MXEPS	EPSSH	SIGTH	IMPULSE	FAILTM
Default	None	None	None	None	None	None	None	None

Where,

MID: Material-ID for which this erosion definition applies.

EXCL: Exclusion of any optional failure cards (if any)

MXPRES: Maximum pressure at failure

MNEPS: Minimum principal strain at failure

EFFEPS: Maximum effective strain at failure

VOLEPS: Volumetric strain at failure

NUMFIP: Number of failed integration points before element deletion

NCS: Number of failure criterions to be met before element deletion

MNPRES: Minimum pressure at failure

SIGP1: Principal stress at failure

SIGVM: Equivalent stress at failure

MXEPS: Maximum principal strain at failure

EPSSH: Tensorial shear strain at failure

SIGTH: Threshold stress

IMPULSE: Stress impulse for failure

FAILTM: Failure time

Details of the impact testing and FE modelling methodologies (Figure 6-3) will be outlined in the following sections.
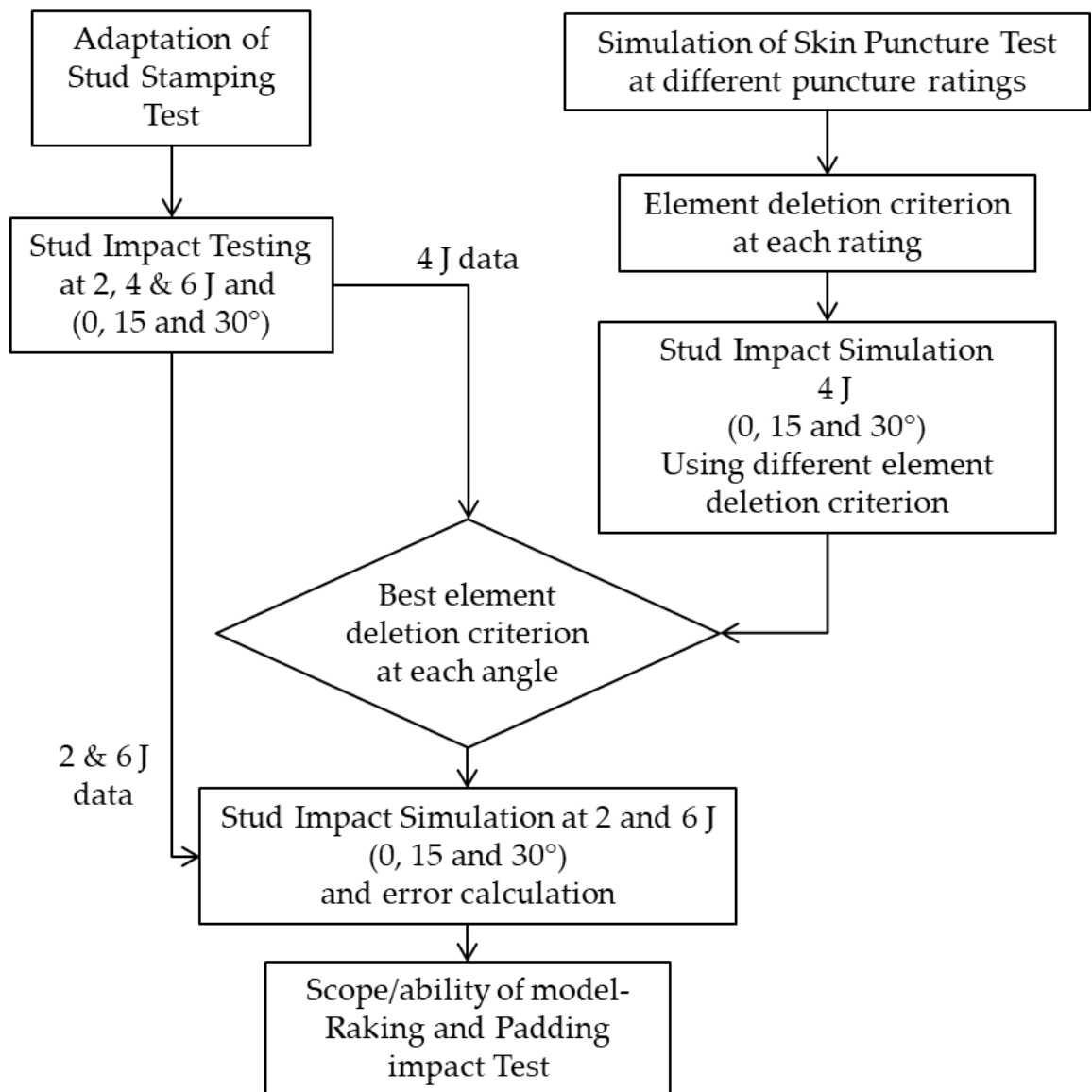
Figure 6-3: Flowchart representing the methodology used to model the stud impact FE simulations.

6.3 Impact Test Adaptation

To support the development of a model of a stud impact on the shoulder surrogate, in terms of gaining experimental data for validation purposes, the skin stamping test was adapted from Regulation-12 Schedule-2 (BS 6366-'*Specification for studs for rugby football boots*' - presented in Chapter-2, Section 2.7). The skin stamping test method was chosen as it provides a scenario (contact between stud and skin) that is similar to an event that may occur during a game of rugby. The skin stamping test

recommends an impact with an energy of 4.17 J, achieved by dropping an 8.5 kg mass from 50 mm (impact speed of 1 m·s⁻¹). The skin stamping test parameters, as shown in Chapter 2-Section 2.7, do not have any justification for the test parameters. Oudshoorn et al. (2018) state that the skin stamping test uses an impact mass that is too heavy and an impact speed and energy that are too low, in comparison to actual stud stamping events during rugby. As such, a test with a lower mass that is dropped from higher would be more representative of actual stud stamping events during rugby than the skin stamping test in Regulation-12. Oudshoorn and colleagues also note that the skin stamping test in Regulation-12 does not account for angular impacts.

Recent work by Baines et al. (2018) calculated the work done, during a foot strike, from the measured ground reaction force, at 3.8 J. Studies have reported the effective total mechanical energy of a foot strike during walking or running as between 0.24 to 6 J (Cavanagh et al., 1984; Aerts and De Clercq, 1993; De Clercq et al., 1994; Chi and Schmitt, 2005). The impact test setup from Chapter 5-Section 5.5.2 was modified by replacing the flat impactor with an aluminium stud (18 mm Stud Set-Carta Sport) (matching the stud requirements in Appendix E). Following this modification to the impact test setup, the mass of the impactor was 3.65 kg, which is closer to the effective mass values (0.5-2.9 kg) reported by Oushoorn et al. (2018) for a foot strike than the 8.5 kg mass stated in Regulation-12 Schedule-2 Test B. Pilot testing with a fresh shoulder surrogate showed the silicone to tear at impact energies over 2.5 J when struck with the 3.65 kg stud impactor.

Four joules impact energy was chosen to support the development of the FE model, i.e., to identify appropriate element deletion criterion settings in the *MAT_ADD_EROSION card. Four joules is similar to the energy at foot impact reported elsewhere (Chi and Schmitt, 2005; Baines et al., 2018), and when a 3.65 kg drop mass is used it gives a vertical impact speed of 1.5 m·s⁻¹ (comparable to 1.6 to 1.7 m.s⁻¹ vertical foot speed at ground contact (Weyand et al., 2000; Weyand et al.,

2010; Clark et al., 2014). Impacts at 4 J also resulted in a clearly noticeable tear to the chamois leather. Impact testing was also carried out at 2 and 6 J (to account for the 0.2-6 J range of total foot energy reported in literature) to check the robustness of the FE model. At each energy level, impacts were carried out at angles (between the horizontal axis and the angle plate) of 15° and 30° along with perpendicular impacts (0° between vertical axis and impactor). These test angles covered the range of roll and pitch reported by Oudshoorn et al. (2018) during a stamp on a crash test dummy (Figure 6-4). The 4 J impact energy chosen represents an accidently stamping which my occur during a collision during a gameplay scenario. Even though the paddings are not designed to protect against a stud impact, stud contacts are the most likely scenario under which a player might obtain a cut or a laceration.
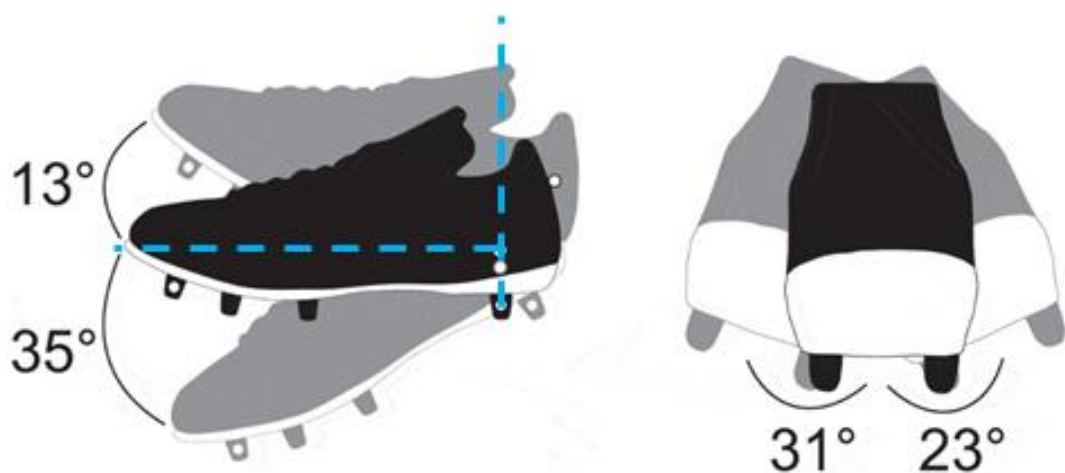
Figure 6-4: Roll and Pitch angles on impact as reported by Oudshoorn et al. (2018) during stamping.

6.4   Impact Testing Methodology

Six samples of the shoulder surrogate silicone moulded with chamois leather were made (by the PhD student working on the project at the University of Sheffield) for impact testing (identical to the one shown in Figure 2-20). Each silicone sample was placed atop the steel core and subject to quasi-static compression testing before and after impact testing. The role of the compression testing was to, i) measure the stiffness of each sample, ii) quantify inter-sample variance and iii) quantify any degradation from impact testing.

6.4.1 Compression testing

Before impact testing, each surrogate sample was compression tested using a uniaxial testing machine (Hounsfield HK10S) with a 1 kN load cell (0.5% or 5 N accuracy) and a 62 mm diameter flat indenter. Three different areas of the surrogate silicone sample (surrogate moved horizontally along the direction of its long axis to change the lengthwise position) were compressed to 20% strain (at a rate of 20 mm.min^{-1}) to quantify the stiffness. The compression test was adapted from ISO2439-Method D (20% compression at a rate of 20 mm·min^{-1} and 30 s hold), but the hold after compression was not maintained as the intention of the test was to measure the instantaneous stiffness of the surrogate silicone and not the viscoelasticity. Of all the compression methods in ISO 2439 (Methods A-E presented in Chapter 4), the one with the lowest value of maximum compression (ISO2439-Method D, 20% compression) was used to ensure the silicone did not tear nor otherwise degrade or sustain damage during testing. The compression tests after impact testing for quantifying any degradation of the sample were at approximately the same locations as those from before impact testing. The three compression values before impact testing were compared across the samples using Welch's ANOVA (95% confidence level). The compression values before and after impact testing were compared using Welch's 2-Sample t-Test (95% confidence level).

6.4.2 Stud Impact Testing

Table 6-3 summarises the conditions under which the six silicone samples were impact tested. Out of the six surrogate samples, one (Sample 5) was used for testing of manufacturer padding. The other five samples were assigned randomly to test at different impact energies and angular orientations without padding. Pilot testing showed only superficial damage (no tear) to the chamois leather for 2 J impacts, so only one surrogate (Sample 1) was tested at this energy. Two samples were tested at each energy (for all three angular orientations).

Table 6-3: Summary of impact energies and orientation of impact test carried out on each sample of silicone.

Sample number	2 J			4 J			6 J		
	0°	15°	30°	0°	15°	30°	0°	15°	30°
1	×	×	×						
2							×	×	×
3				×	×	×			
4				×	×	×			
5	Used for manufacturer sample testing								
6							×	×	×

The angle plate was positioned horizontally under the stud impactor (Figure 6-5) for 0° impacts. For angular impacts the angle plate was rotated 90° around the vertical axis and then inclined to angles of 15° and 30° (Figure 6-6-D & E) to ensure impacts were along the central axis. The angle of the plate was measured using a digital inclinometer (SPI ®-Digital Inclinometers, UK; accuracy ± 0.1°).
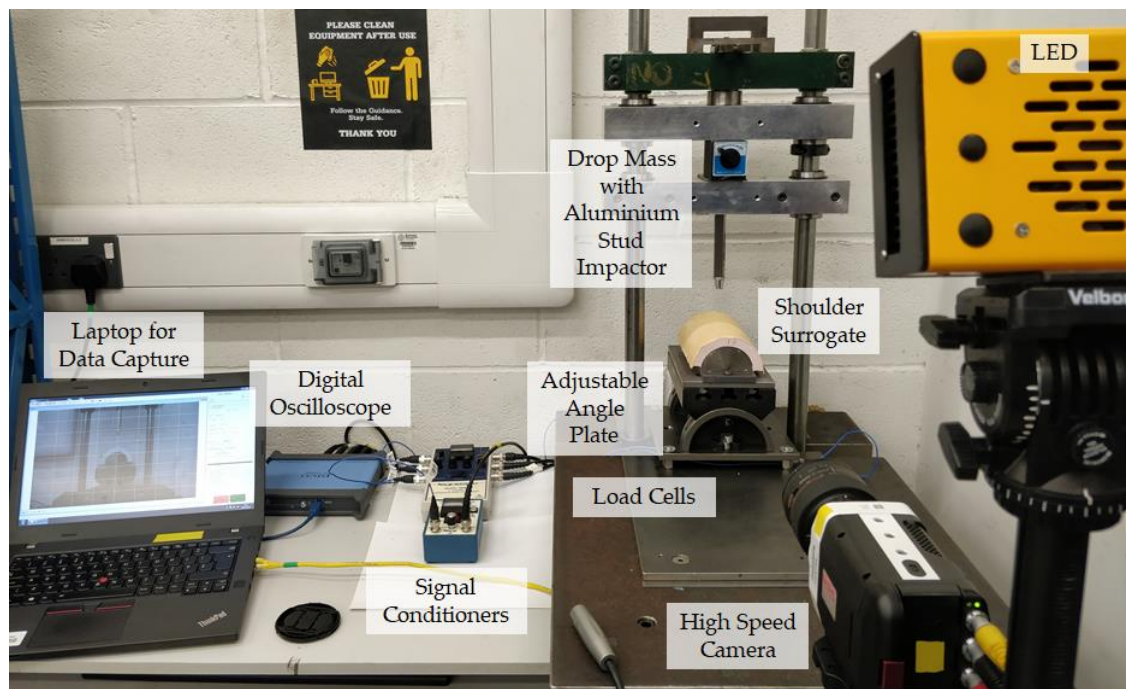
Figure 6-5: Stud impact testing showing the silicone surrogate mounted for perpendicular impact.
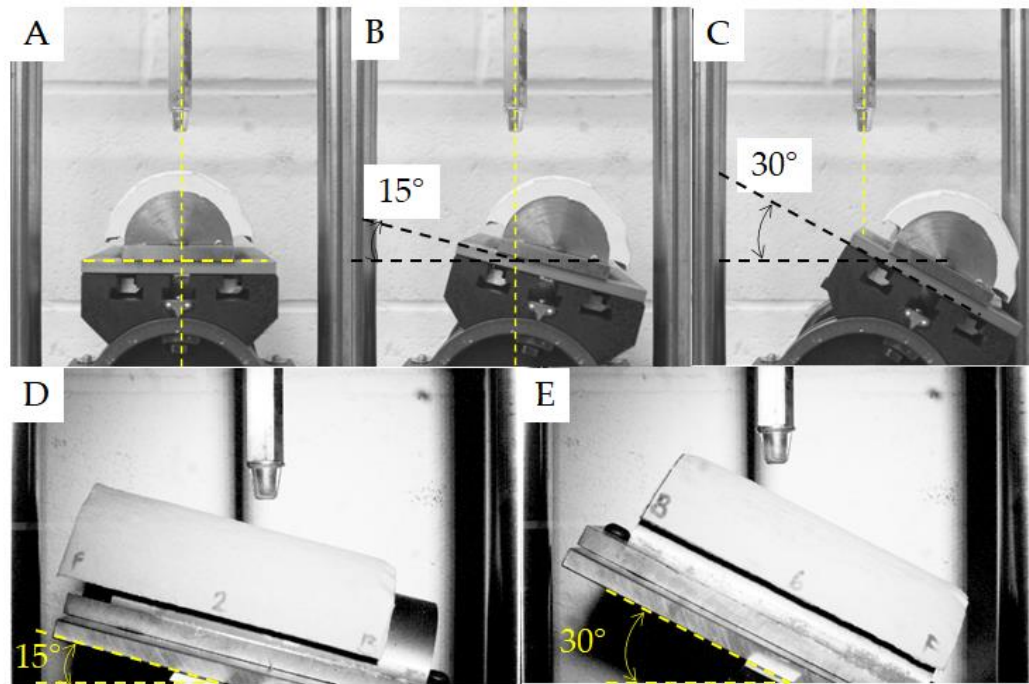
Figure 6-6: Impact test setup for (A) 0° orientation (central impact), (B) 15° without rotation (non-central impact), (C) 30° without rotation (non-central impact) (D) 15° after rotation and (E) 30° after rotation. Orientation B and C are illustrated to show the issue with angle and were not used to carry out impact testing

Each silicone sample was impacted three times at the assigned energy and at each angle setting (total of nine impacts), with at least one minute between impacts. Pilot testing highlighted the importance of changing the impact location for each repeat (due to the damage caused) (Appendix F). Therefore, the silicone was moved on the steel core between impacts to change the impact location by at least 1 cm. The data acquisition system, and settings, were the same as used for impact testing in Chapter 5-Section 5.5.2.

After three impacts at a specific energy and angular orientation, the dimensions of any damage caused to the silicone (i.e. indent, hole, tear) by the stud were measured with a vernier calliper and photographed with a camera (Nikon D3200 with zoom lens: AF-Micro Nikkor 60 mm F 1:2.8 D, Nikon Corporation®, Japan). The camera was placed on a tripod and activated with a remote trigger. The force and time values corresponding to a tear in the silicone (explained in Section 6.3-C) for each test orientation were compared using Welch's ANOVA Tests with Games-Howell post hoc for pairwise comparison (confidence level of 95%).

6.5 Impact Testing Results

6.5.1 Compression

No significant difference was found for force values at 20% compression taken before impact testing across the six silicone samples (p = 0.108). Comparison of compression results before and after impact testing indicated that the silicone samples degraded after impact testing, as the force values at 20% compression increased after impact testing. However, the force values at 20% compression taken before and after impact testing were not significantly different (p > 0.05: range 0.078-0.476) (Figure 6-7). (Minitab® analysis output in Appendix J). Although not significant there is a noted increase in the stiffness of the surrogate post impact showing degradation of the surrogate.
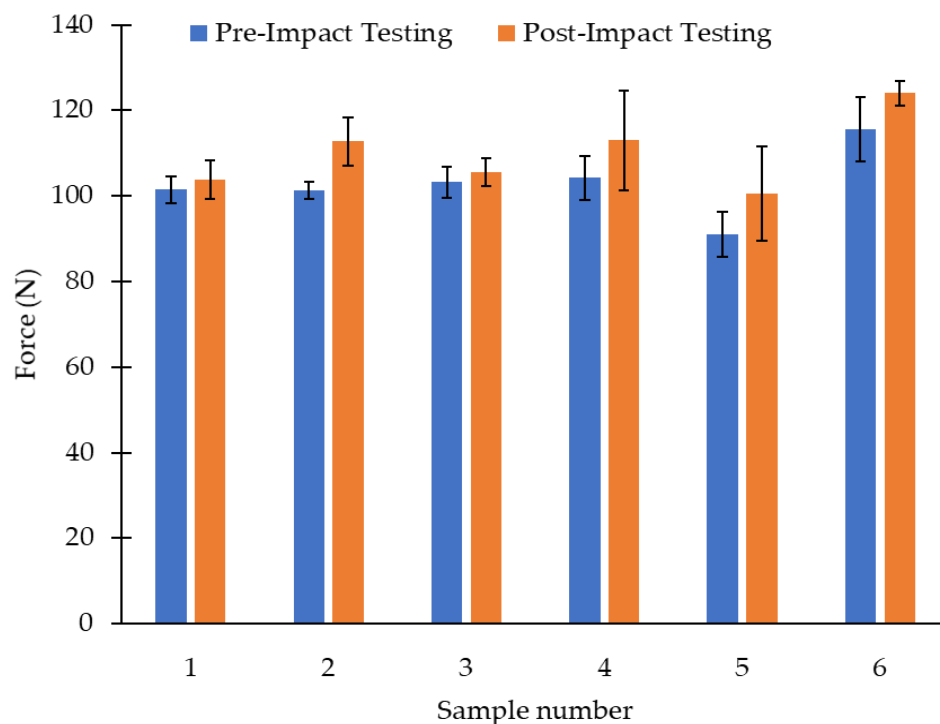
Figure 6-7: Mean compression force values (error bars show SD) for 20% compression pre- and post- impact testing.

6.5.2 Stud Impact Test – Experimental Data

Peak force increased with the impact energy, while impact duration decreased (Figure 6-8). Impact duration increased with the impact angle (0 to 30°), while peak force decreased (Figure 6-8 15° & 30°). The key values for each impact are tabulated in Section 6.5-C following the detailed explanation of the force traces in Section C.
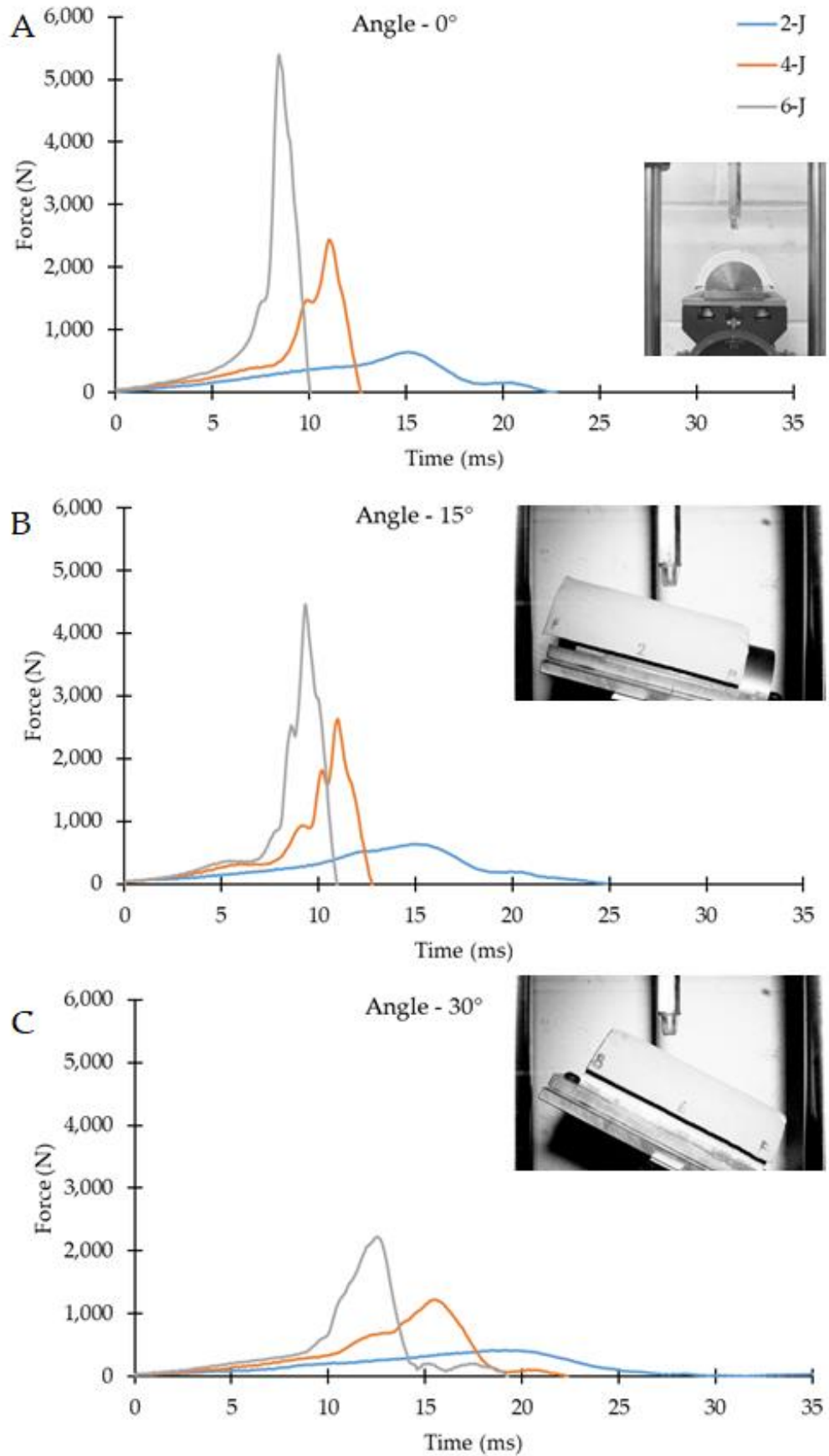
Figure 6-8: Force time trace for stud impact at (A) 0° (B) 15° and (C) 30° impact at 2, 4 and 6 J.

6.5.3 Stud Impact Force Trace Breakdown and Results

During the impact the stud can pierce through the silicone and strike the steel core of the shoulder surrogate, causing a sharp spike in force. For these impacts, peak force does not coincide with the time at which the stud pierces the silicone. As such, simply comparing peak impact force values between the experiment and simulation is not a suitable method for determining whether the model can accurately predict the scenarios that cause the silicone to tear or otherwise sustain damage.

The general shape of the force traces for each orientation for impact energies of 4 and 6 J were similar (Figure 6-8). Therefore, only one force trace for the impact energy of 4 J at each orientation is presented, along with the corresponding HSV images, in Figures 6-9 to 6-11. For a 4 J impact at 0°, the force increased gradually (at ~60 N/ms) from when the stud struck until the chamois leather tore (Point B on Figures 6-9-11), which then resulted in a slight reduction in the loading rate. The change in the force vs. time relationship after the silicone tore was less pronounced for the 0° orientation but can be clearly seen at 15° (Figure 6-10-Point B) and 30° (Figure 6-11-Point B) orientations. Following the tear, the impact force increased (between points B and C) as the silicone compressed until it split (Point C), with a corresponding drop in force. After the silicone split, the force increased rapidly to its peak value for the impact, suggesting that the stud struck the steel core of the shoulder surrogate (as can be noted in the HSV images). During impacts at 15° and 30°, the force trace had two local maxima after the silicone split.

During angular impacts, when the stud struck the steel core of the shoulder surrogate it deflected sideways, deviating from the vertical axis. As the impactor straightened it regained contact with the steel core, causing an increase in vertical force. For the 15° orientation the second contact on the steel core gave the peak force for the impact (Figure 6-10), while for the 30° orientation, the peak force came from the first contact (Figure 6-11). For the 30° orientation, the thickness of silicone acting between the stud and steel core of the shoulder surrogate was higher, which

explains the longer time to reach peak force (at ~16 ms). So, by the time the second contact on the steel core occurred, the force response was low as more impact energy had been transferred. Conversely, for the 15° impact, the sideways deviation of the stud impactor from the vertical was visually less pronounced and hence the second contact on the steel core gave a higher force.

The graphs in Figures 6-9 to 6-11 indicated that while assessing injuries such as cuts and lacerations, using a peak impact force value will not be a useful parameter. The peak impact values occur due to rigid-on-rigid impact causing a sharp peak. It is essential to understand the loading mechanics of the injury and the graphs help us identify some simple trends. With increase in angle, the loading rates have been noted to reduce, from ~60 N/ms to 30 N/ms. The force at tear is higher at a higher loading rate but the time to tear is shorter. In terms of gameplay, it may suggest that short-duration impact contact (such as a tackle) might result in a cut or a laceration quicker than a low force tackle which may be longer in duration (scrum contact).
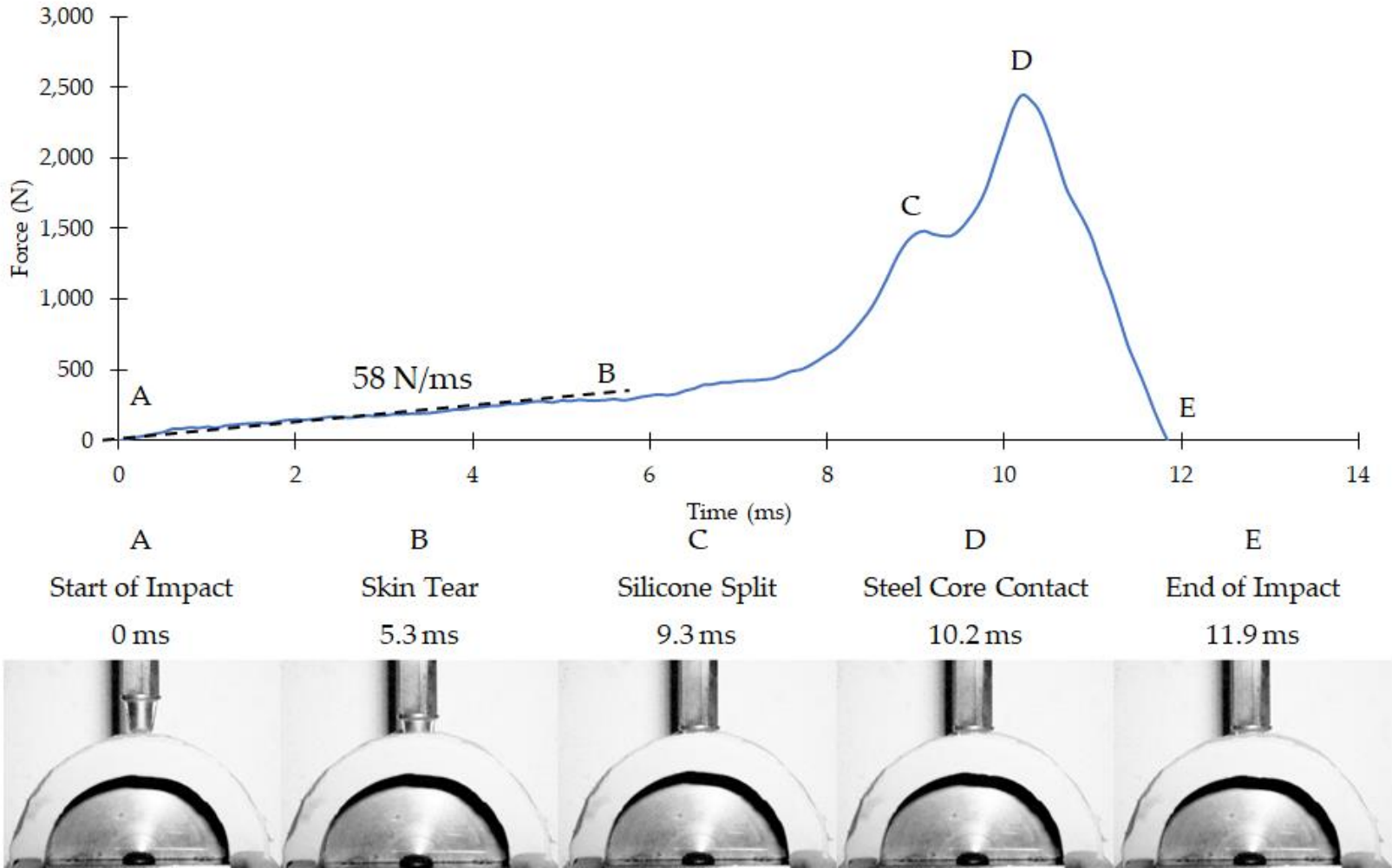
Figure 6-9: Breakdown of force trace of a 4 J impact at 0° along with the corresponding HSV images. Dashed line represents the loading trendline between A and B.
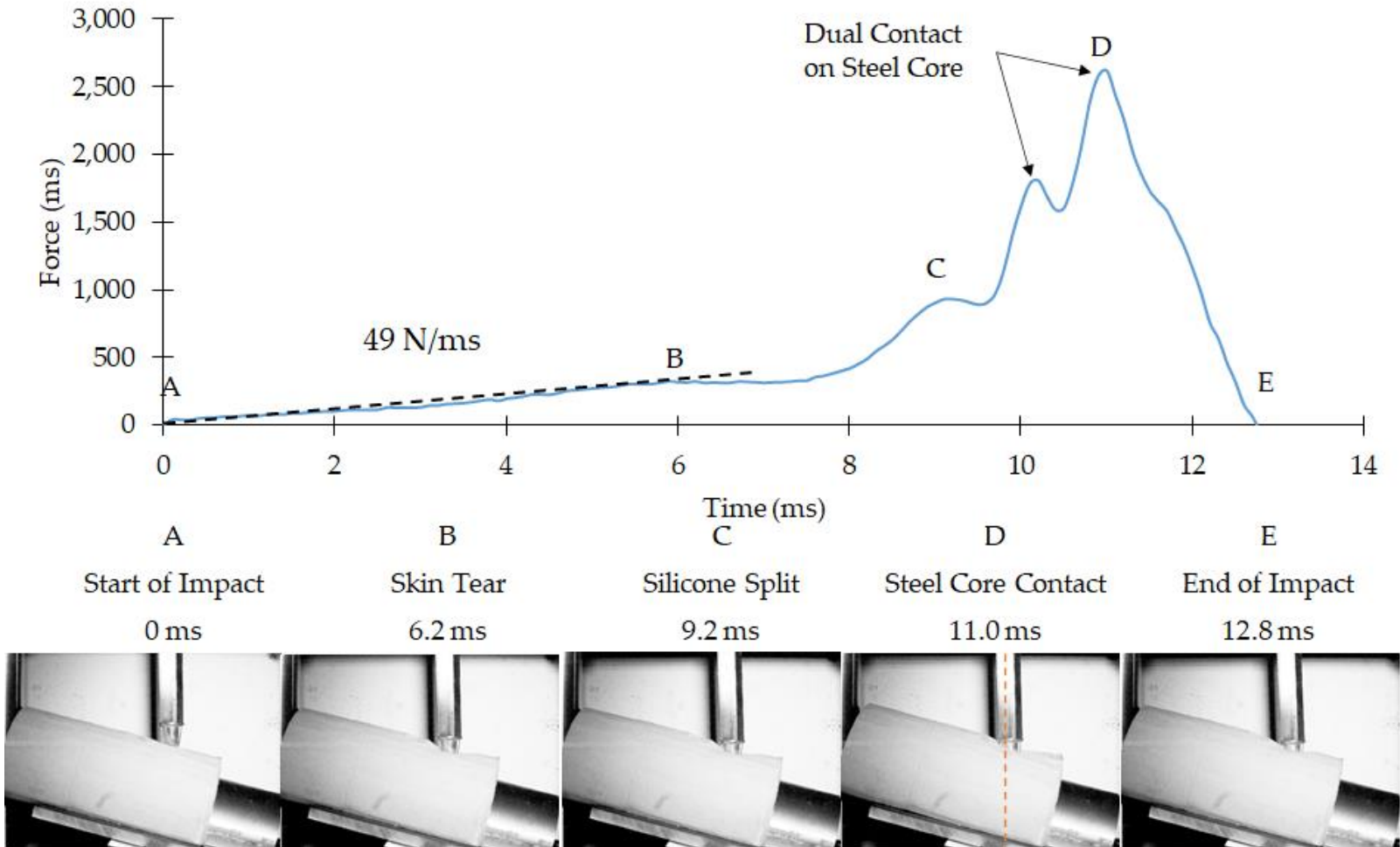
Figure 6-10: Breakdown of force vs. time trace of a 4 J impact at 15° along with the corresponding HSV images. Dashed line represents the loading trendline between A and B.
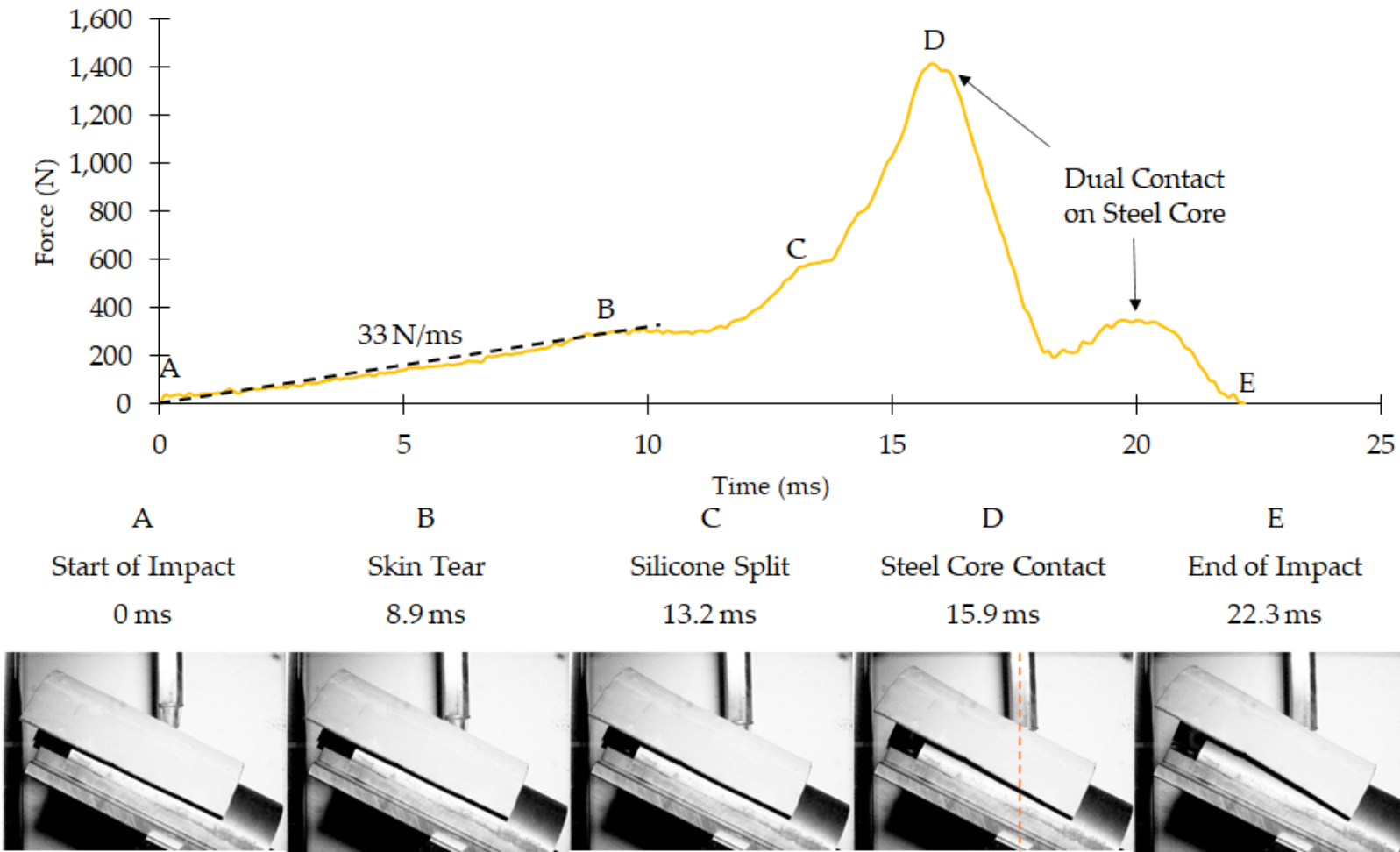
Figure 6-11: Breakdown of force vs. time trace of a 4 J impact at 30° along with the corresponding HSV images. Dashed line represents the loading trendline between A and B.

For comparison against the FE model, the force that caused the chamois leather to tear (Point B in Figures 6-9, 10 & 11) was used along with the time to reach this tear (time taken from A to B). At 2 J impact energy, as there was no noticeable cut / tear in the silicone the peak force and time to reach this peak were noted. The time to reach the peak force increased with the angle of impact, while the peak force decreased.

Table 6-4: Peak force and time to peak for a 2 J stud impact.

Orientation (°)	Peak Force (N)		Time to Peak (ms)	
	Mean	SD	Mean	SD
0	692	57	13.7	0.6
15	634	11	14.7	0.4
30	433	23	18.1	1.2

At 4 and 6 J energy impacts, the time from initial contact until the silicone tore increased with the impact angle, while the peak force decreased (Table 6-5).

Table 6-5: Force and Time to tear for 4 J and 6 J impact at each orientation and significant difference.

Serial	Energy (J)	Angle (°)	Force at tear (N)		Time to tear (ms)	
			Mean ± SD	Different to*	Mean ± SD	Different to*
1	4	0	365 ± 34	3,6	5.2 ± 0.3	2,3,5,6
2	4	15	304 ± 27	3,4	6.6 ± 0.1	1,3,4,5,6
3	4	30	232 ± 21	1,2,4,5	9.1 ± 0.3	1,2,4,5,6
4	6	0	414 ± 36	2,3,5,6	4.9 ± 0.1	2,3,5,6
5	6	15	338 ± 24	3,4	6.0 ± 0.1	1,2,3,4,6
6	6	30	261 ± 28	1,4	7.5 ± 0.2	1,2,3,4,5

* Difference is significant with $p < 0.05$.

6.5.4   Chamois Leather Damage Results

A visual summary (photographs) of damage to the chamois leather from stud impacts is summarised in Figure 6-12. The damaged region was usually the area under contact with the stud and was about the size of the face of the stud. The nature of the damage was dependent on the orientation of the impact. For 0° impacts, the damage was circular with the tear in the chamois leather resembling a round hole. For angular impacts the damage was more elliptical, with the tear more pronounced on the side where the stud first struck the chamois leather.

Scale: Image Edge is 2 cm x 2 cm
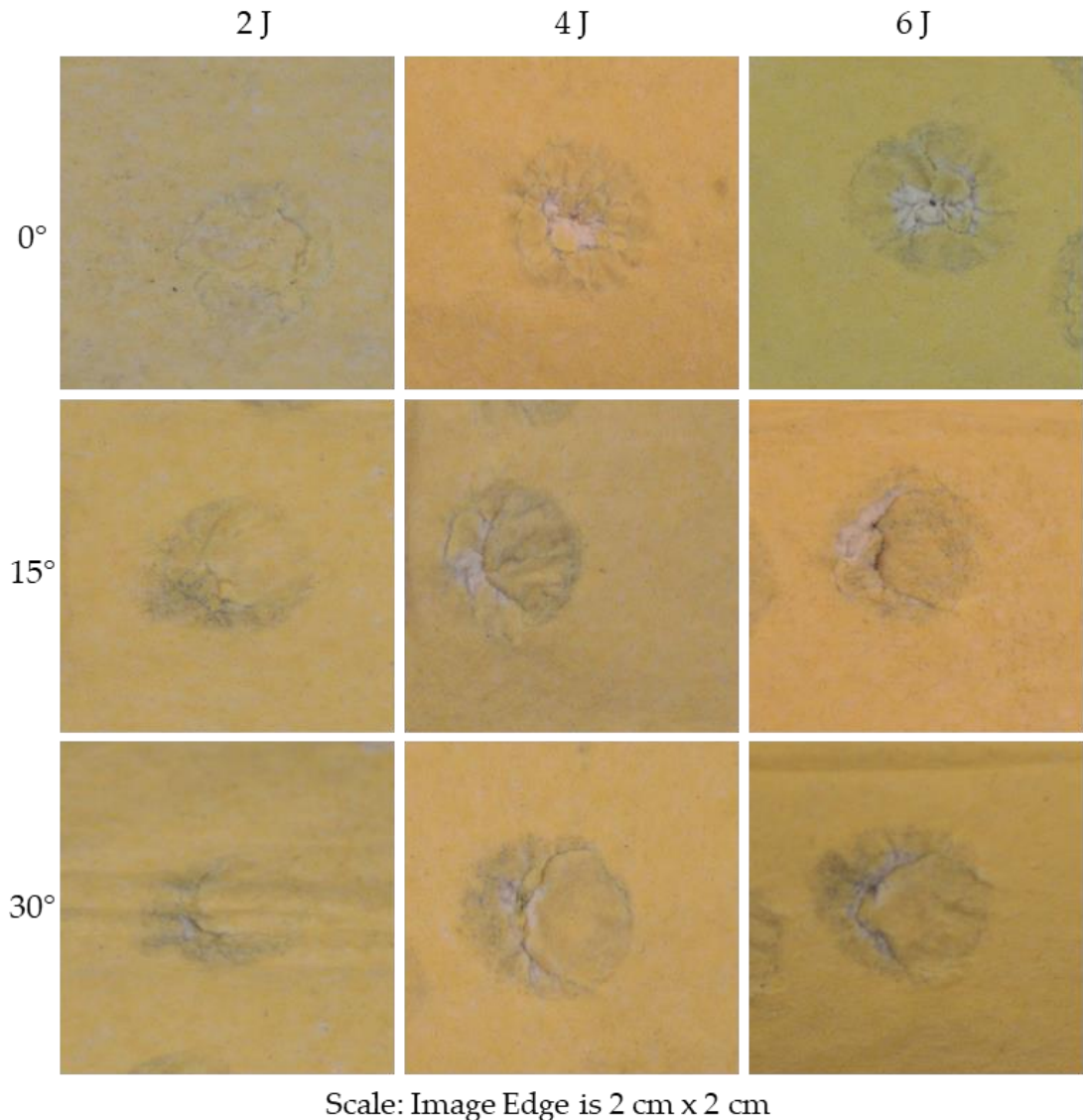
Figure 6-12: Nature of tear / damage occurring on the chamois leather following the impact at each energy and orientation, the columns represent the energy and the rows represent the angle of impact.

6.6 Simulant Tear Modelling Setting

To create the FE model capable of predicting impact induced damage to the skin simulant, an appropriate element deletion criterion was needed. As the chamois leather used in the surrogate was intended to mimic human skin, failure criteria for both skin and chamois leather were studied. The failure criterion of skin is varied and dependent on factors such as age, gender, environmental conditions, and orientation to Langer lines (Joodaki and Panzer, 2018; Annaidh et al., 2010). Quantifying the force that causes injury to human skin is challenging due to

variability in impactors (blunt or sharp) and the varied nature of contact (Parmar et al., 2012).

Literature suggests that the tensile stress to break chamois leather (7.5 - 21.3 MPa) is comparable to that of skin (1.0-45 MPa) but also variable (large range of values) (Shergold et al., 2006; Kalra et al., 2016; Annaidh et al., 2014; Agache et al., 1980). Ankersen et al. (1999) carried out tensile and stab resistance testing on synthetic chamois leather and pigskin. They concluded that the stab resistance of these materials is not dependent on their tensile strength. Puncture tests on skin or skin simulants, such as chamois leather, have been carried out using sharp objects, such as blades and knives (Ankersen et al., 1999; Gilchrist et al., 2008; Ni-Annaidh et al., 2013). The construction of a soft tissue surrogate (i.e., skin and underlying tissue) has been shown to affect the puncture rating of the skin layer (Ni-Annaidh et al., 2013).

As presented in Chapter 2-Section 2.11, the initial skin tissue simulant used for the shoulder surrogate was manufactured by SynDaver™ (Florida, USA) and consisted of synthetic skin and fat tissue layers. SynDaver™ state (Data Sheet in Appendix G) that their skin simulants have a puncture / toughness rating of either two, four, six or ten newtons (detailed in Section 6.6). SynDaver™ skin tissue simulant with a puncture rating of 2 N was used initially by the research team at the University of Sheffield and was later replaced by silicone and synthetic chamois leather (due to the lower cost). Since only a small amount (20 x 20 cm) of the SynDaver™ simulant originally used remained available, repeated impact testing was not possible to compare its performance against synthetic chamois leather. Hence, the initial design of the shoulder surrogate with the SynDaver™ skin simulant was only impacted with the stud during pilot tests to visually compare any damage against that of the chamois leather.

During pilot testing with the stud at 4 J impact energy, damage to the chamois leather was visually observed to be lower than that to the SynDaver™ skin simulant.

The observed difference in damage could be because the SynDaver™ simulant used was of the lowest puncture rating (2 N), although the puncture rating of the chamois leather was unknown.

Since the required equipment defined by SynDaver™ to carry out the puncture testing on the chamois leather was unavailable at the university, the test was simulated using the FE model developed in Chapter 5. The FE model of the silicone developed in Chapter 5 combined the silicone and chamois into one material model. Using this single material model for simulated puncture testing allowed the setup to include the response of the whole surrogate (like the SynDaver™ simulant) and not just the skin layer in isolation.

Since there was a difference in the observed level of damage between the SynDaver™ skin simulant and the chamois leather for an equivalent stud impact, the puncture simulations were carried out for the complete range of puncture ratings from 2 to 10 N, in steps of 2 N. This range of puncture ratings helped to determine the most suitable element deletion criterion for the chamois leather in the FE model. As presented in Section 6.2, parameters such as pressure, stress, strain, and shear can be used to define element deletion in the *MAT_ADD_EROSION card in Ansys© LS-DYNA®. For this research, principal stress was used as the criterion for failure of the chamois leather, as it can be used to define different material failure criteria (Meyer and Labuz, 2013). For the stud impact FE simulations (detailed in Section 6.7), the maximum principal stress predicted during puncture test simulations was used as the element deletion criteria.

6.6.1 Puncture Test FE-Model

SynDaver™ defines the puncture test as a compression test with a 1 mm blunt Tungsten rod moving at 15 mm/sec (Data Sheet in Appendix G). Geometry representing the puncture test, consisting of the rod (1 mm diameter with 0.5 mm filleted edges) and a cylindrical structure (10 mm diameter and 3 mm thickness) for the silicone, was modelled (Figure 6-13) using SolidWorks© (v2018, Dassault

Systems). The corresponding .sldprt file was imported into Ansys© workbench geometry using Design Modeller.
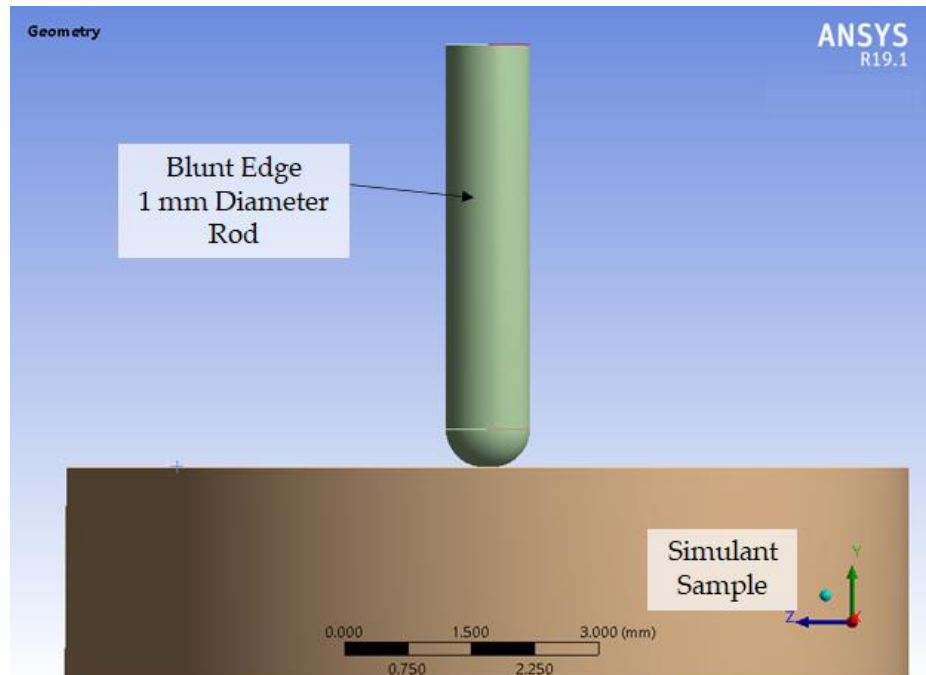
Figure 6-13: CAD model of the puncture test geometry.

The rod was assigned a rigid material model (*MAT_RIGID) (identical to the steel core properties presented in Chapter 5), which was constrained to only allow for linear motion along the y-axis (i.e. vertical loading). The material model assigned to the silicone was the same as in Chapter 5 - Table 5-14). The silicone layer was assigned a tetrahedral mesh of size 0.5 mm. A mesh refinement (of size 0.075 mm) was applied at the centre of the upper face of the silicone sample, surrounding the area of contact with the rod, using a sphere of influence (0.6 mm diameter) (Figure 6-14). The rod was assigned default mesh settings resulting in an average edge length of 0.3 mm (Table 6-6).

Table 6-6: Mesh details for the simulant puncture test setup.

Part	Mesh Type	Elements	Nodes
Rod	Hexahedral (ELFORM=1)	574	840
Silicone*	Tetrahedral (ELFORM=10)	12,050	66,603

*As in Chapter 5, the silicone and chamois leather were modelled as one material with uniform properties.
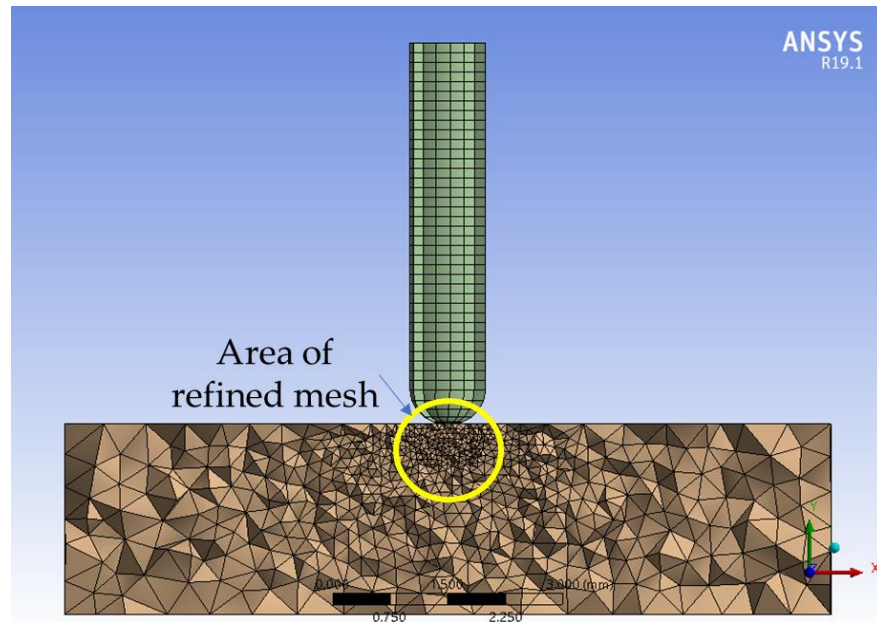
Figure 6-14: Cross sectional view of the puncture test mesh with refinement.

The underside and the circular edge of the silicone geometry was fixed. Contact (*CONTACT_AUTOMATIC_SURFACE_TO_SURFACE) was defined between the silicone and steel rod with a static and dynamic coefficient of friction of 0.3. A constant force, ranging from 2 to 10 N (in steps of 2 N), was applied to the rod in the negative y-axis direction to compress it into the silicone (Figure 6-15). Upon application of force, the maximum principal stress occurring on the surface of the silicone was noted (Figure 6-16). The maximum principal stress values for the silicone increased with the force applied to the rod (Table 6-7).
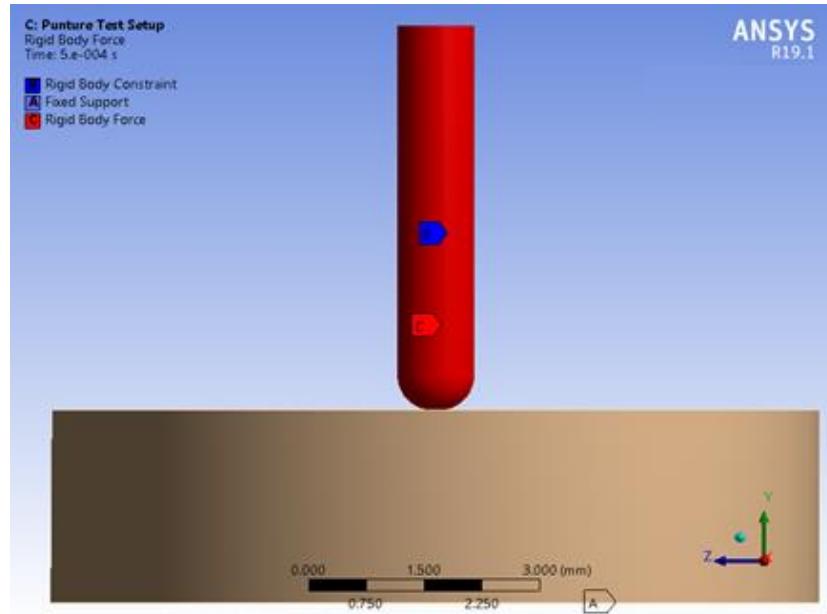
Figure 6-15: Boundary conditions applied on the geometries in silicone puncture test simulation.
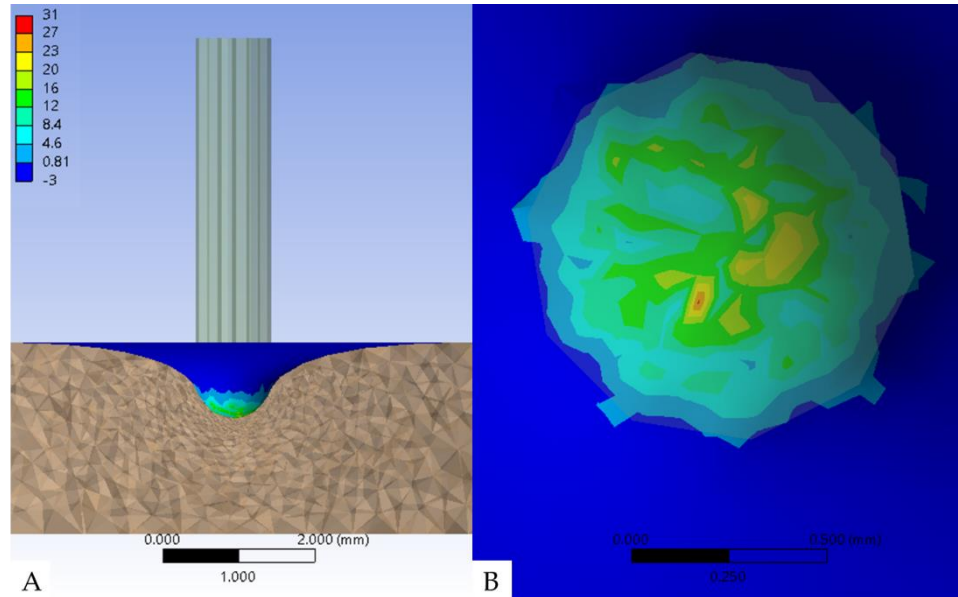
Figure 6-16: (A) Cross-sectional and (B) top-down view of contours of principal stress (MPa) measured on the surface of the silicone layer under 6 N applied force during puncture test simulation.

Table 6-7: Maximum principal stresses measured off the surface of the silicone during puncture test simulation.

Applied Force (N)	Maximum Principal Stress (MPa)
2	3.1
4	15.9
6	31.0
8	41.3
10	57.8

6.7 Stud Impact FE Modelling Methodology

The geometry of the surrogate and the stud impactor (identical to the stud used in the impact test and meeting the stud design requirements mentioned in Regulation-12 Schedule-2-Appendix E) were modelled in SolidWorks© (version 2018, Dassault Systems). The corresponding .sldprt file was imported into Ansys© workbench Geometry using Design Modeller. The geometric centre of the stud impactor was aligned to that of the surrogate in the widthwise (x-axis) and lengthwise (z-axis) directions, and the impactor was placed 1 mm above (y-axis) the surrogate. For the 15° and 30° impact orientations, the silicone and rigid core were rotated about the x-axis in Design Modeller to mimic the experimental setup (Figure 6-17).
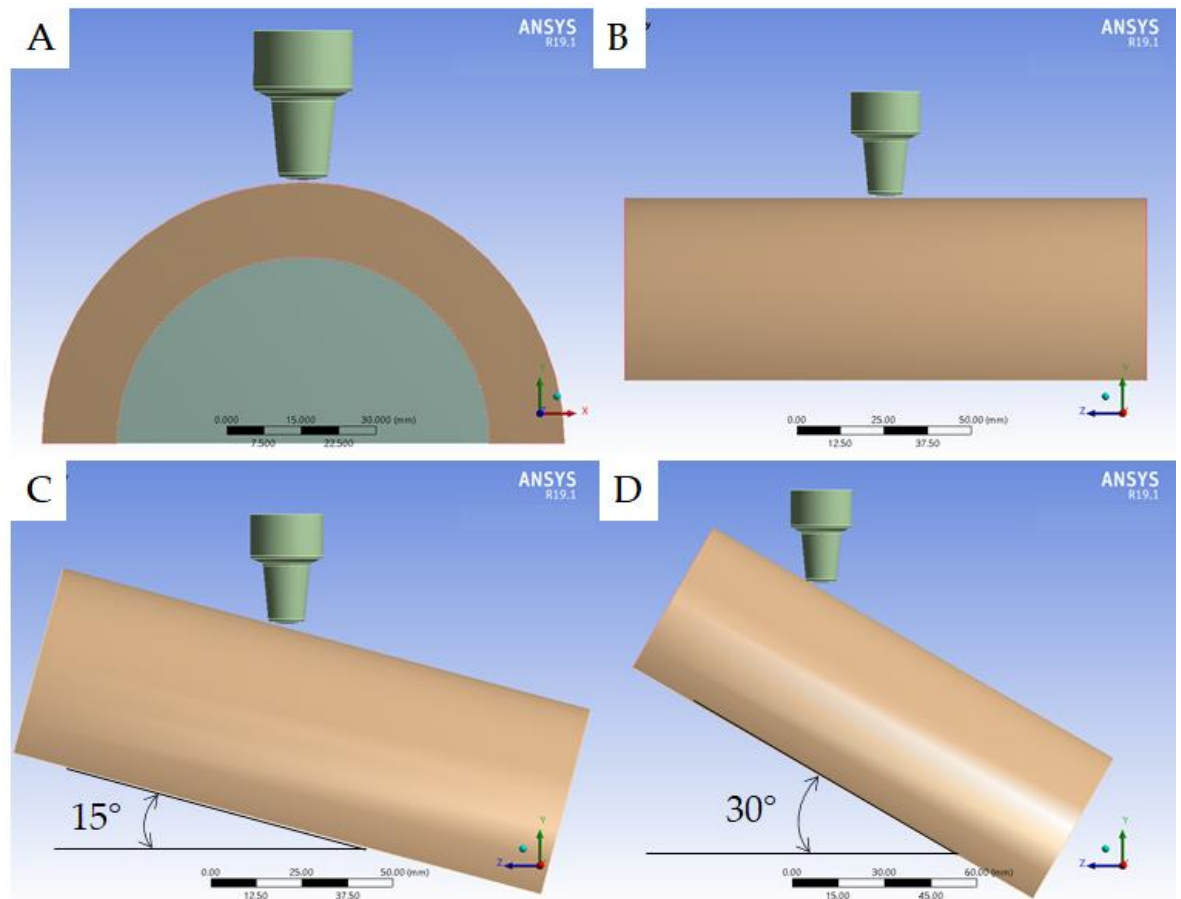
Figure 6-17: Geometrical setup for the stud impact test showing (A) cross sectional layout and (B) side view of 0° orientation before the silicone and rigid core were rotated for (C) 15° and (D) 30° orientation.

The stud impactor and steel core were both defined as rigid materials (*MAT_RIGID) (Table 6-8). As with the flat faced impactor in Chapter 5, the assigned density of the stud impactor was increased to obtain the required mass of 3.65 kg (mass of the impactor used for experimental testing). The material model assigned to the silicone was the same as in Chapter 5 (Table 5-14).

Table 6-8: Material properties of stud impactor and steel core used during the stud impact modelling.

Part	Density (kg·m⁻³)	Young's Modulus (GPa)	Poisson's Ratio	Source
Stud Impactor	6.7E05	0.2	0.33	Ansys© library – Aluminium with modified Density
Steel Core	7,850	200	0.30	Ansys© library- Structural Steel

The stud impactor and steel core were assigned the default hexahedral mesh (ELFORM=1), giving an average sizing of 6 mm. The silicone layer was assigned a tetrahedral mesh (ELFORM=10) of size 3 mm (identical to settings used in Chapter 5). The mesh surrounding the area of contact with the stud was further refined to 0.8 mm (mesh size setting) using a sphere of influence of diameter 20 mm (Figure 6-18), to improve the prediction of damage to the silicone (as determined from pilot simulations). A refined mesh was not applied to the entire silicone layer, as this was not needed for accurate damage prediction, meaning it would have unnecessarily increased the simulation time. These settings resulted in a mesh (detailed in Table 6-9) with a mean quality of 0.85 ± 0.09 and a mean skewness of 0.218 ± 0.12.
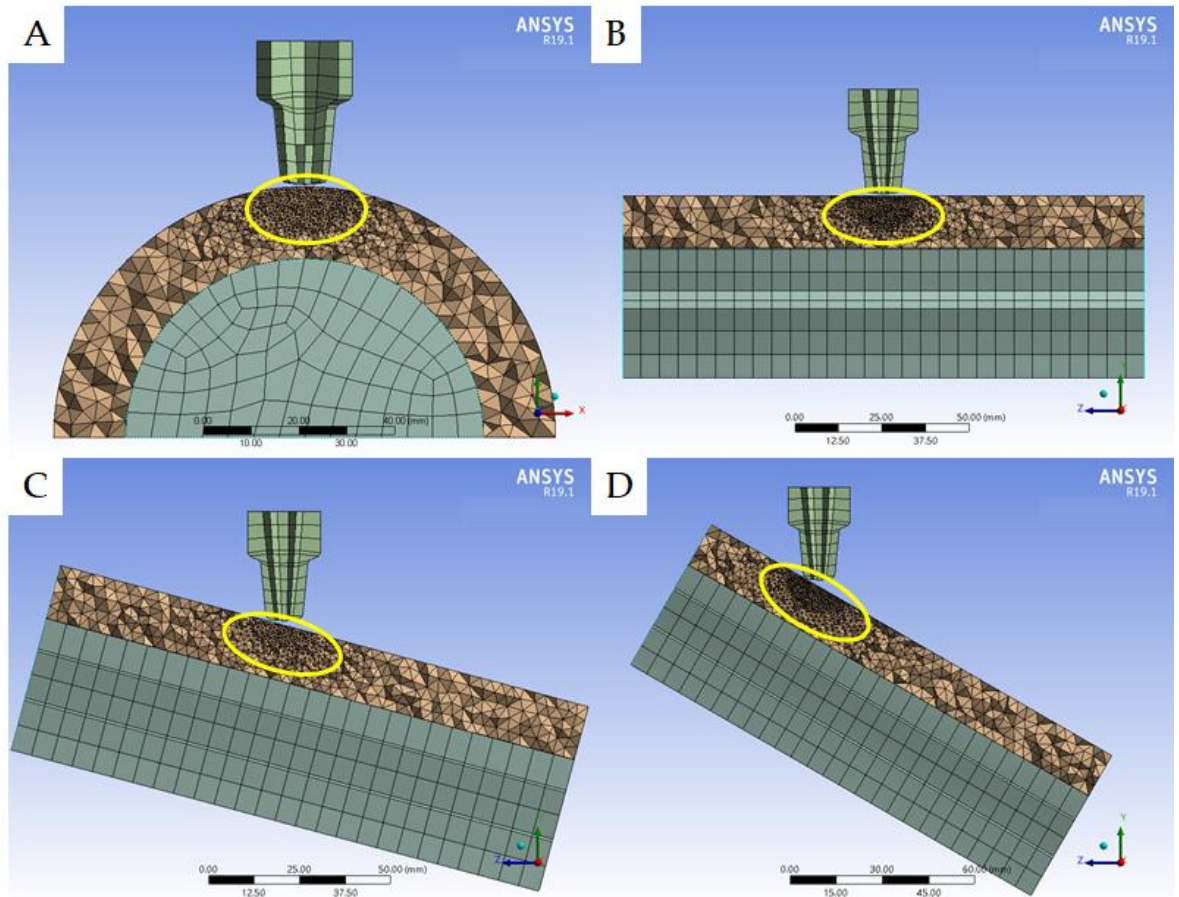
Figure 6-18: Mesh refinement carried out closer to the impactor geometry shown in (A) cross sectional layout and side view of (B) 0° (C) 15° and (D) 30° orientation. Yellow ellipse highlights region of refined mesh.

Table 6-9: Mesh details for different parts in the stud impact setup.

Part	Elements	Nodes
Stud Impactor	154	216
Silicone - 0°	158,562	30,198
Silicone - 15°	155,164	29,660
Silicone - 30°	159,288	30,369
Steel Core	1,898	2,430

*The number of elements and nodes for the silicone change with the angular orientation as the position and area under the sphere of influence change with orientation.

The boundary conditions in the model were set to replicate the experimental impact test setup. The steel core of the shoulder surrogate was fully constrained. The stud impactor was assigned an initial velocity (*INITIAL_VELOCITY_RIGID_BODY) in

the direction of the negative y-axis and constrained to only allow motion in the y-axis (Figure 6-19).
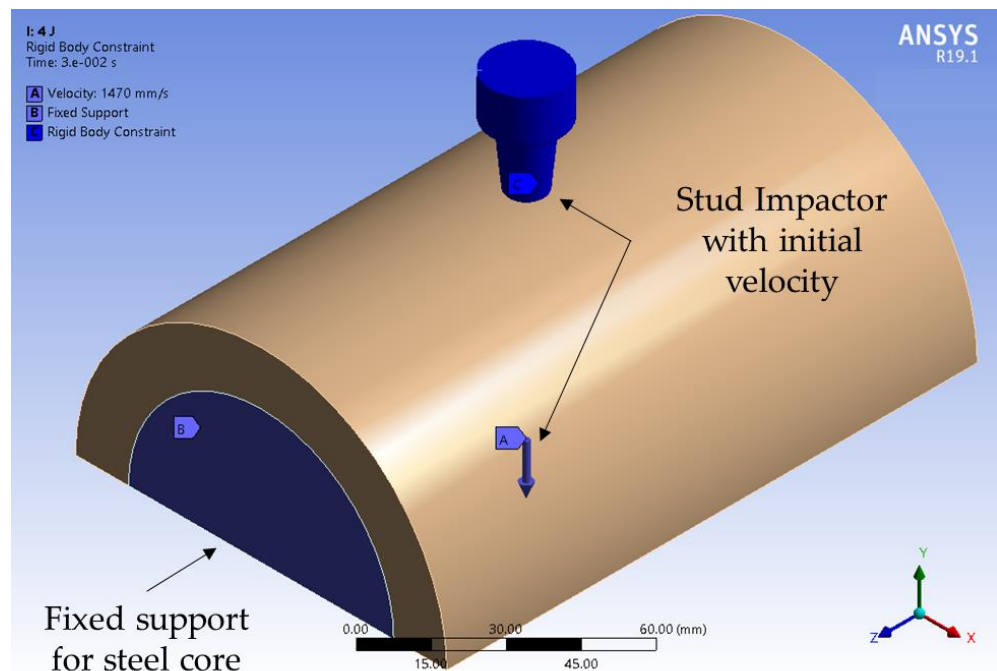
Figure 6-19: Boundary conditions applied for the stud impactor testing setup.

Pilot simulations using contact between the stud and silicone parts led to a drop in force once the elements in contact were deleted. Due to the compliant nature of the silicone, once an element was deleted, a shockwave propagation caused the silicone elements to pass through the stud impactor. Simulations with element deletion criteria for predicting damage are typically carried out between materials with high stiffness, such as metal-to-metal or metal-to-ceramic, which do not have high vibration amplitude. Hence contact between the stud and silicone was limited to the top surface of the silicone.

Contact between the stud outer surfaces and the top surface of the silicone layer (*AUTOMATIC_SURFACE_TO_SURFACE) was defined with a static and dynamic coefficient of friction of 0.3 (Figure 6-20). The contact force calculated between these surfaces were used to quantify the force when the first element was deleted (i.e. force at silicone tear). Element deletion was identified through solution information text output at every timestep in WorkBench. Only the top surface of the silicone was

used to define contact with the stud (rather than the entire part), as the silicone modelled in the Chapter 5 was of one material (combining the chamois leather and the silicone layer) and only damage caused to the top layer was being analysed.
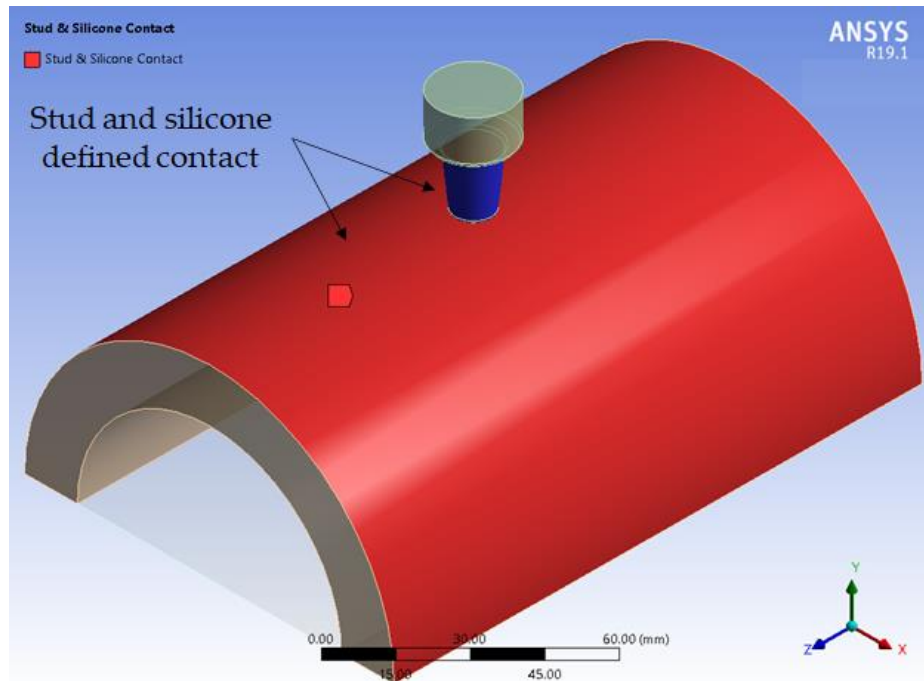
Figure 6-20: Contact region defined between the stud impactor (blue) and the silicone top surface (red) to track force at tear.

The *MAT_ADD_EROSION card (defined in Section 6.2) (Snippet shown in Appendix I) was included in the FE model, with principal stress defined as the element deletion criterion. Pilot simulations indicated that using the same principal stress value for the element deletion criteria across the three impact orientations (0, 15 & 30 degrees) did not provide good agreement with the experimental results, in terms of the force required to tear the silicone. The principal stress values in Table 6-7 were each independently assigned as the element deletion criteria, and corresponding simulations were run at an impact energy of 4 J at each of the three orientations to find the most appropriate element deletion criterion for each orientation. The principal stress for element deletion criteria for each orientation identified at 4 J was then used in corresponding simulations at 2 and 6 J, and compared against the experimental data as a further, and more independent, check of the model.

The impact velocities and corresponding durations of the simulations are in Table 6-10. The simulations were assigned a time step safety factor of 0.4 (identical to the setting used in Chapter 5- Section 5.5.2). The maximum vertical force (force in y-axis) before the silicone tore and the time to reach the tear was compared against the experimental results.

Table 6-10: Initial velocity of the stud impactor for the stud impact simulation.

Impact Energy (J)	Initial velocity (m/s)	End Time (ms)
2	1.0	2.5
4	1.5	1.0
6	1.8	0.75

6.8   **Validation Results**

At 4 J impact energy, the force to cause a tear in the silicone increased with the principal stress used to define the element deletion criterion (Figure 6-21). The force to tear the silicone decreased as the orientation angle increased. At 0° impact, the 16 MPa element deletion criterion gave the closest tear force to the experimental data (8% difference). For 15° and 30° impact angles, the 31 MPa element deletion criterion gave the closest tear force to the experimental data (1 and 13% respectively).
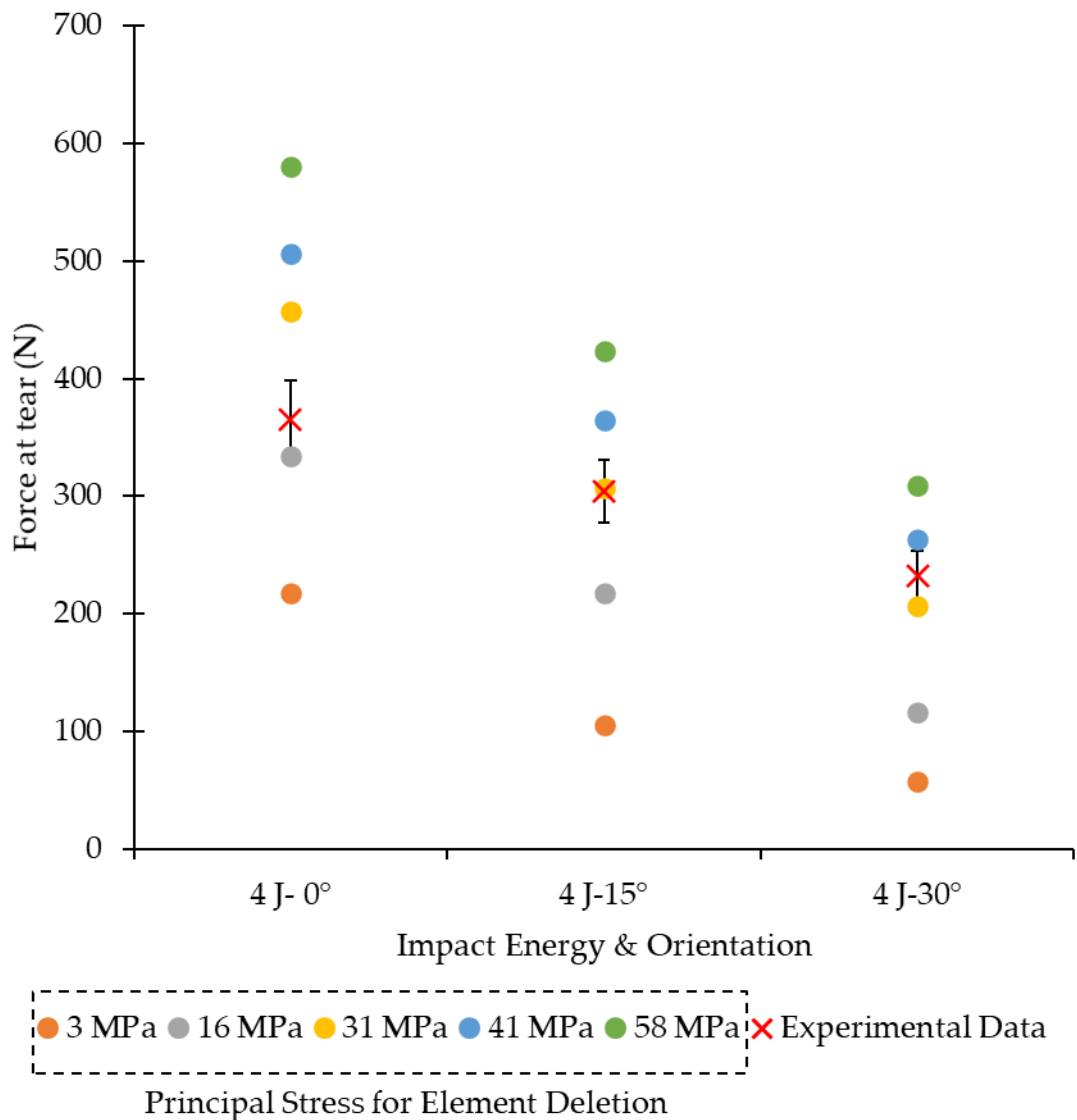
Figure 6-21: Peak force at tear values during a 4 J impact, at three orientations, using different principal stress values compared against experimental data.

Peak force values predicted by the simulations with an impact energy of 2 J were lower than those from the corresponding experiment, as were the times to reach the peak force (Table 6-11).

Table 6-11: Peak Force and time to peak values for a 2 J stud impact simulation.

Angle (°)	Peak Force (N)			Time to Peak (ms)		
	Experiment	FE	Difference %	Experiment	FE	Difference %
0	692	493	-29	13.7	8.6	-37
15	604	440	-27	14.7	10.9	-26
30	433	351	-19	18.1	11.7	-35

For 4 and 6 J impact energy, the force at which the silicone tore decreased with both the angle of impact and the impact energy. The time from when the stud struck the silicone until it tore increased with the impact angle. The simulations consistently underpredicted the time to tear the silicone in comparison to the experimental data (Table 6-12).

Table 6-12: Simulation force and time to tear values with percentage difference in comparison to experimental data.

Energy & Angle	Experimental		Simulation Results			
	Force at tear N	Time to tear ms	Force at Tear N	Difference %	Time to Tear ms	Difference %
4J-0°	365	5.2	334	-8	3.9	-25
4J-15°	304	6.6	307	+1	5.4	-17
4J-30°	232	9.1	263	+13	6.9	-22
6J-0°	414	4.9	372	-10	3.9	-20
6J-15°	338	6.0	313	-8	5.0	-18
6J-30	261	7.5	253	-3	6.1	-19

6.9   **Validation Discussion**

The methods applied to model damage to the silicone used in the shoulder surrogate following a stud impact have been defined. A principal stress of 16 MPa for the element deletion criteria (4 N puncture rating) provided the best agreement with the experiment stud impact test at 4 J-0° orientation, in terms of the force required to tear the silicone. At the 15° and 30° orientations, the simulation showed the best agreement with the experimental impact data when a principal stress of 31 MPa was used for the element deletion criteria.

For the 2 J impact simulation, peak force was underestimated in comparison to the experimental impact test. During experimental impact testing at 2 J, plastic deformation (i.e., permanent) of the chamois leather was noticed with no tear (Figure 6-12). The simulation at 2 J did not predict a tear, nor did it show any plastic deformation as a setting for plastic deformation was not included in the model. The lower peak force for the simulation in comparison to the experiment at 2 J impact energy may have been due to the plastic deformation of the silicone during experimental testing. To overcome this issue, adding the ability to predict plastic damage (using cards like *MAT_ADD_GENERALIZED_DAMAGE) along with element deletion may improve force prediction under concentrated impacts where the silicone might deform permanently but not tear (i.e. those with low impact energy and / or less concentrated loads).

At 4 and 6 J impact energy, tear force decreased with an increase in angular orientation, potentially because the thickness of the silicone acting between the stud and steel core increased. During the 0° orientation impact simulations, when the stud struck the silicone the stress induced was symmetrical over the contact region cross section (Figure 6-22-A). During the angled impact simulations, the stress induced in the silicone was asymmetrical and localised under the side of the stud struck (Figure 6-22-B & C).
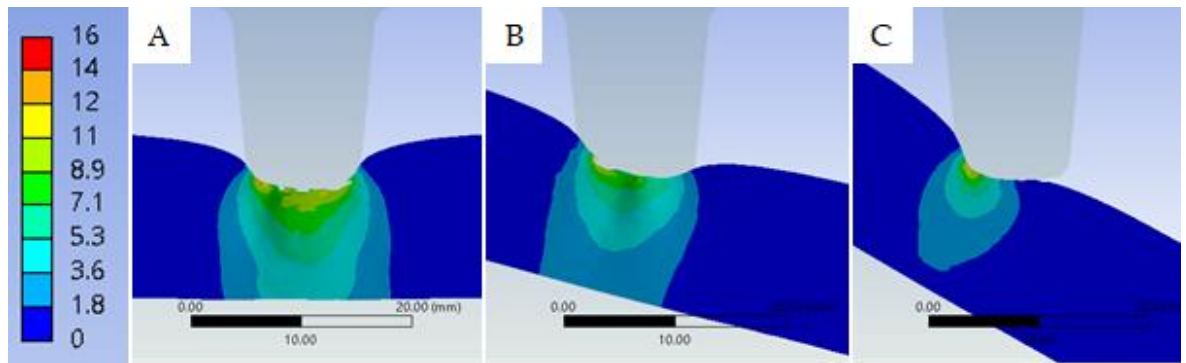
Figure 6-22: Sectional view of the stress induced in the silicone at time step just before element deletion during 4J impact at different orientations: (A) 0° at 3.4 ms (B) 15° at 3.5 ms and (C) 30° at 3.4 ms.

As contact was only defined between the top surface of the silicone and the stud, once elements on the surface of the silicone were deleted the corresponding contact force dropped to zero (Figure 6-23). For the 0° orientation, the force values dropped off the peak almost instantaneously following deletion of elements on the surface of the silicone that were in contact with the stud. For impacts at 15 and 30° angular orientations, the force values tended to drop off in a stepped fashion, as the surface of the stud was still in contact with the top surface of the silicone even after the elements that first met the principal stress criterion were deleted (Figure 6-23).
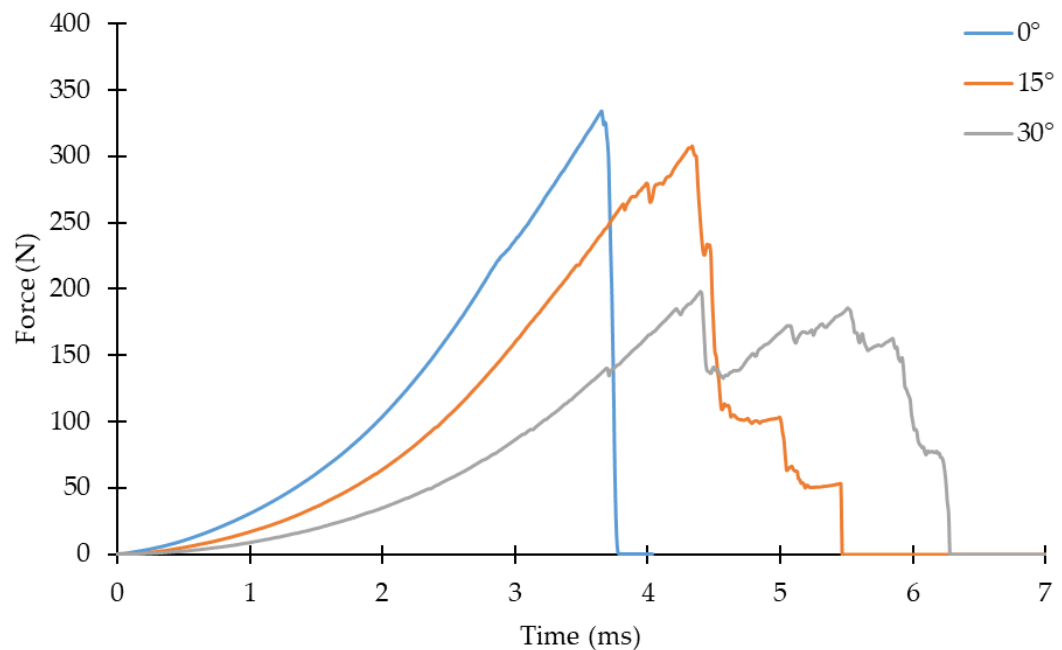
Figure 6-23: Simulation force time trace shown for the contact between the stud and top surface of the silicone layer at 4 J impact at different impact angles.

The reason for the sudden drop in contact force during the simulations can be understood better with the stress plots shown in Figure 6-24-26. For the 0° orientation, the elements in the top surface of the silicone were deleted between 3.7 and 4.1 ms, and it took a bit longer for the first element to be deleted at 15° and 30°. During the 0° impact, the element deletion occurred across the circular contact area acting between the silicone and the stud. For angular impacts, the element deletion started on the side where the stud first struck the silicone, before propagating across the surface of the silicone. In Figure 6-24 at 4.1 ms, the elements on the top surface of the silicone that were contacting the stud are deleted, which explains the force drop off noted in Figure 6-23. While in simulations at 15° and 30° orientations since the first element deletion was localised to the region where the stud first struck, the entire contact region acting between the top surface of the silicone and the stud was not deleted. As such, stress was still being induced on the surface of the silicone even after element deletion for the angled impacts (4.5 ms in Figure 6-25 or 5 ms in Figure 6-26). (Figures showing the maximum principal stress on the surface of the silicone are presented in Appendix H).

Equivalent Stress (MPa)
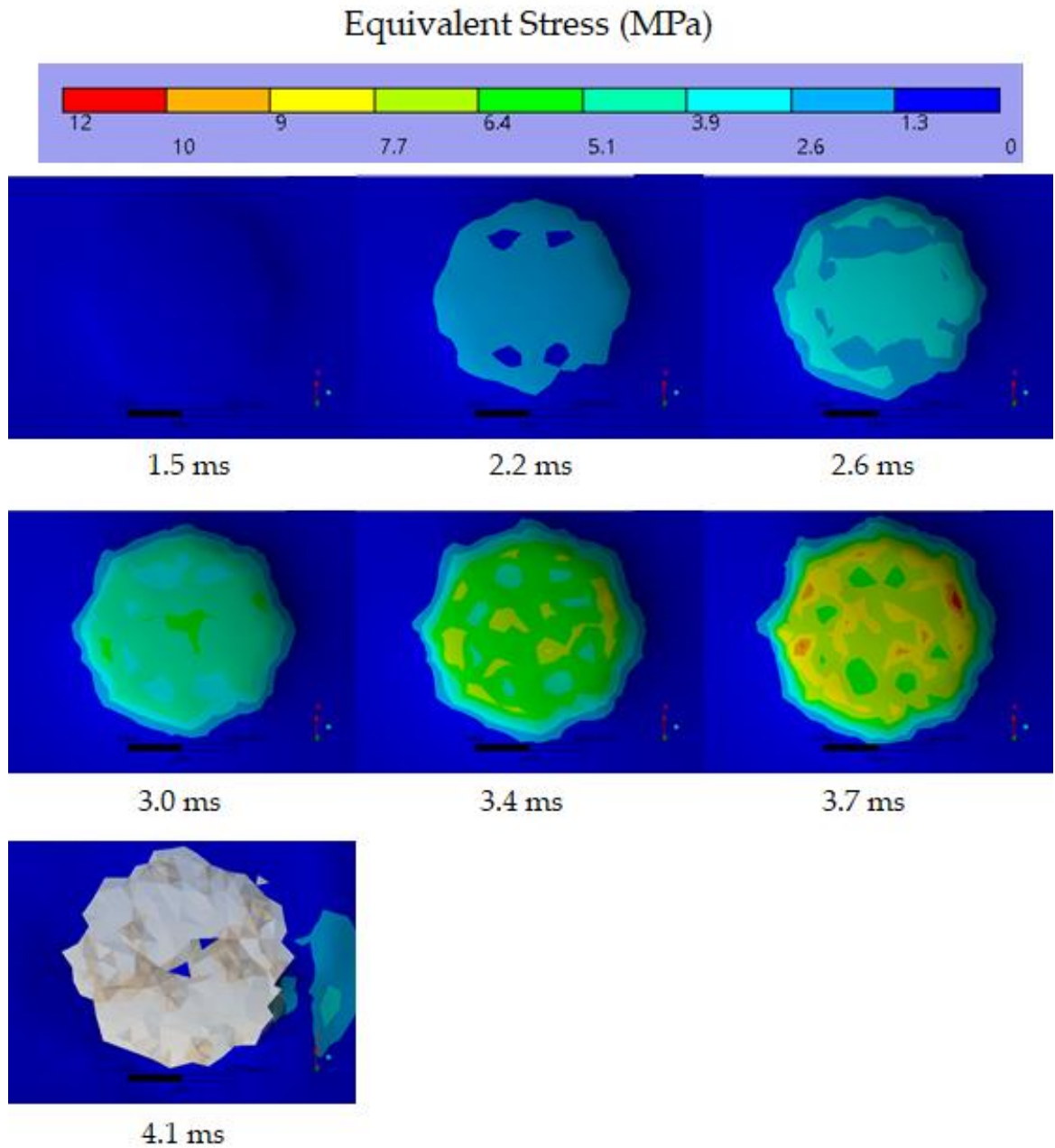
Figure 6-24: Equivalent stress contours occurring on the silicone top surface at 0° orientation at different time steps during the simulation. (Stud geometry has been hidden to get a clear view of the silicone top surface). Element deletion criterion: maximum principal stress value of 16 MPa.
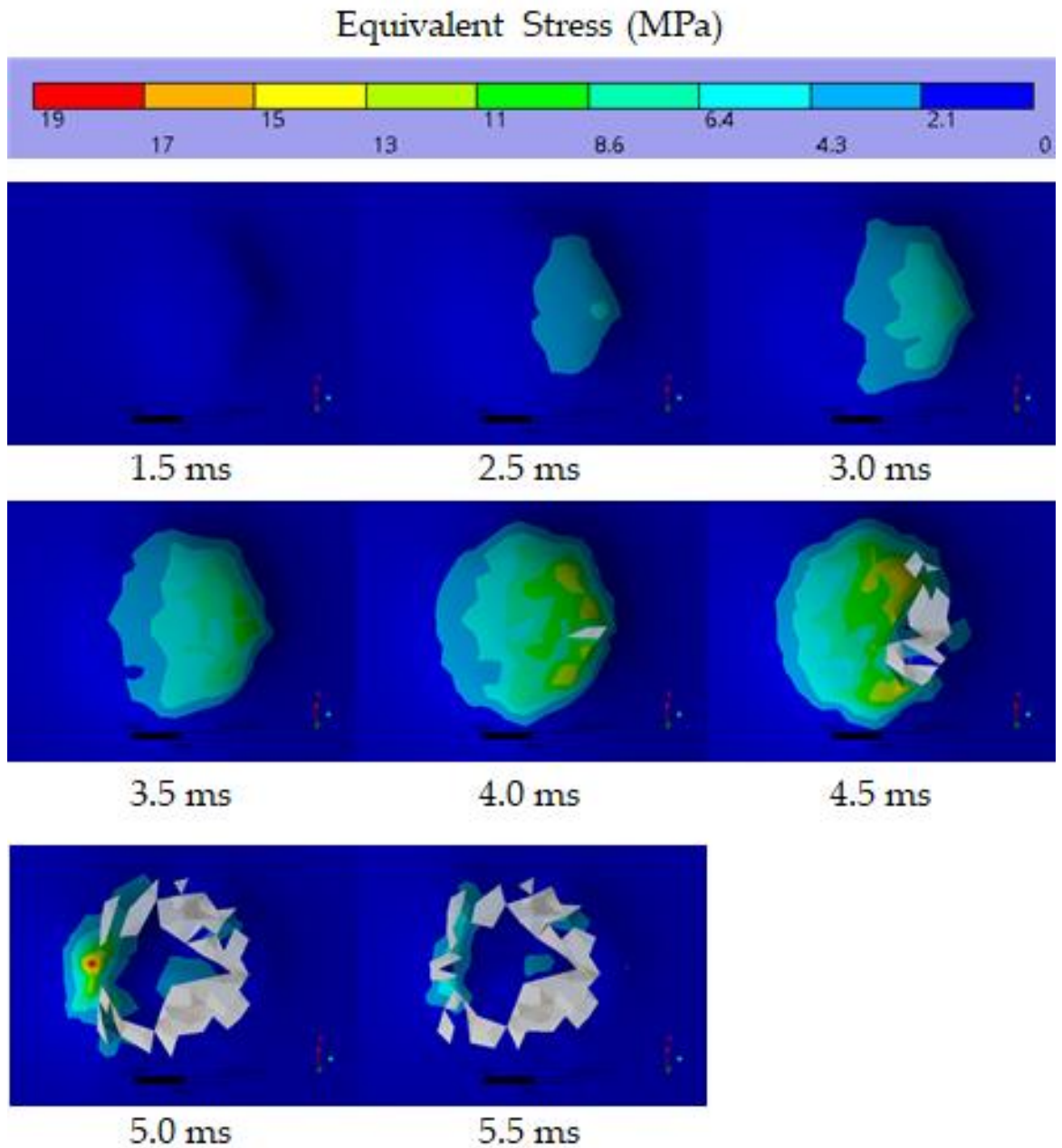
Figure 6-25: Equivalent stress contours occurring on the silicone top surface at 15° orientation at different time steps during the simulation. (Stud geometry has been hidden to get a clear view of the silicone top surface). Element deletion criterion: maximum principal stress value of 31 MPa.
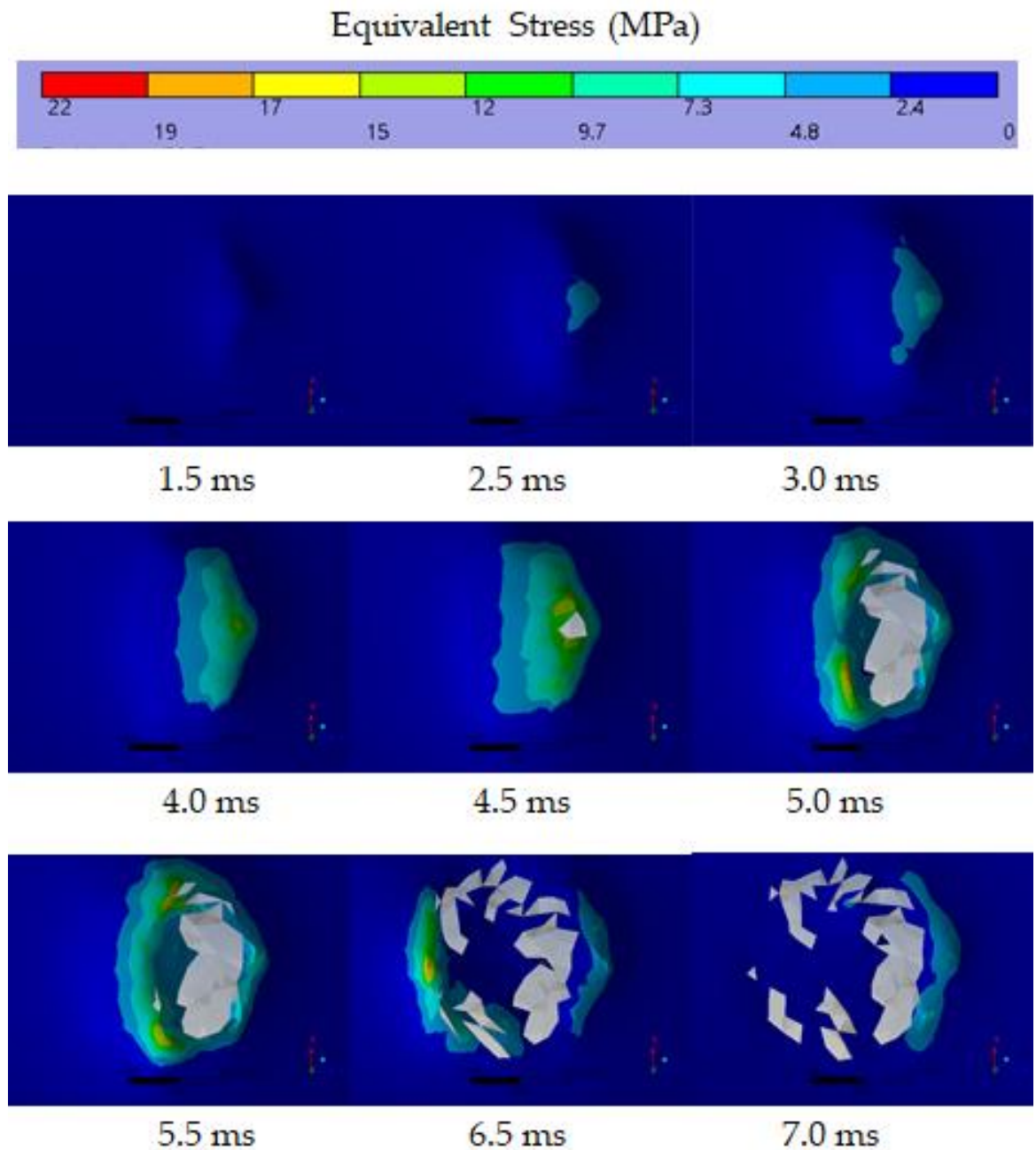
Figure 6-26: Equivalent stress contours occurring on the silicone top surface at 30° orientation at different time steps during the simulation. (Stud geometry has been hidden to get a clear view of the silicone top surface). Element deletion criterion: maximum principal stress value of 31 MPa.

The shape of the predicted damage to the silicone in the simulations was similar to that observed in photographs from the experiments presented in Figure 6-12. The area of element deletion on the surface of the silicone was approximately circular, corresponding to where the stud contacted the silicone. Similar to the damage observed in the chamois leather in the experimental impact testing, for the 0° impact

the damage predicted was more circular (Figure 6-27-A). On angular impacts, although the damage area was circular, the first elements to be deleted were those in the region where the stud first struck the silicone, and there were some elements in the centre which remained intact (Figure 6-27-B&C).
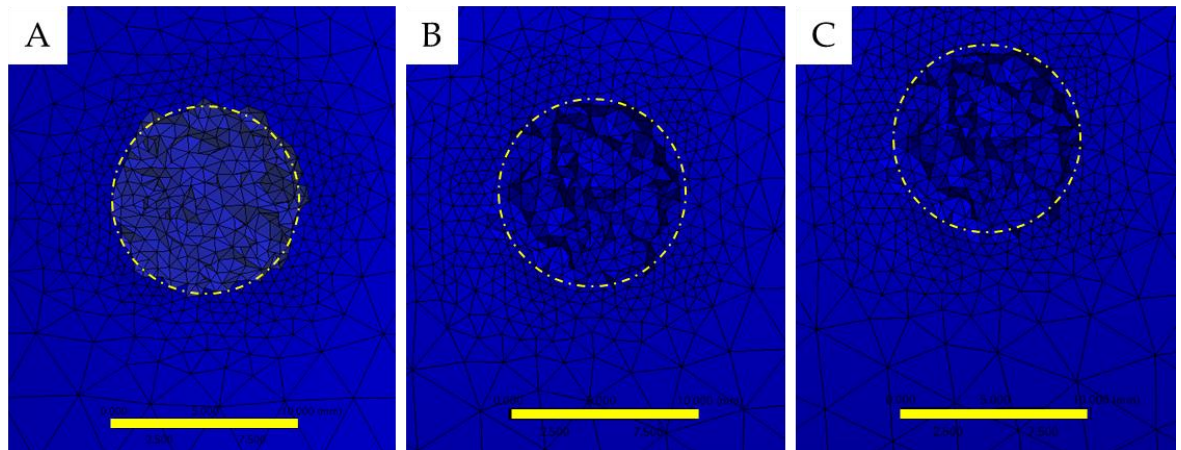
Figure 6-27: Silicone damage during simulation of 4 J impact at (A) 0° (B) 15° and (C) 30°. 10 cm reference line and 10 mm diameter circle provided. (The differences in colouring is due to lighting orientations in Ansys©).

A different maximum principal stress limit for element deletion criterion for each stud impact testing orientation was identified. The element deletion criteria applied for angular impacts (31 MPa principal stress) was higher than for 0° impacts (16 MPa principal stress). Ankersen et al. (1999) showed the tear rating of synthetic chamois leather to depend on the loading orientation, which they claimed was due to the orientation of the fibres in the synthetic chamois leather.

Based on the data presented in Section 6.5.1, there was variance (although not significant) between the quasi-static compressive response of the silicone samples used in the shoulder surrogates. Due to the nature of the silicone fabrication, each sample was moulded individually, and a fresh batch of silicone was required for each new sample. Differences between batches of silicone used could account for some of the observed variations in the quasi-static compression response (Figure 6-7) and impact test results across the silicone samples (Table 6-4 & 5).

For all of the stud impact simulations, the time to peak force and the time to tear the silicone values had high discrepancies with those from the experiment (ranging from 15 to 35%). All the time to peak and time to tear values were under predicted by the simulation in comparison to the experiment. This underprediction was likely because of differences in the shape of the force vs. time curves between the experiment and simulations for tests with a flat impactor noticed in Chapter 5-Section 5.6.2. As noted in these flat impact tests, the loading curve during an experimental impact had a lower gradient than that of the simulation, and hence took longer to reach the peak force. During the stud impact testing, the model therefore reaches higher stress values earlier, which triggers the element deletion and results in an earlier time to tear. Ensuring the impact response of the silicone in the model better matches that of the experiment should therefore help to reduce discrepancies when predicting when damage occurs.

The tear criterion for the chamois leather was simulated over a range of puncture values used to define commercially available skin and soft tissue simulants (SynDaver™ Tissue simulant). Puncture testing on the chamois leather in combination with the underlying silicone would help to identify and define the most appropriate tear criterion for use in the model. Also, the puncture test that was simulated to determine the tear criterion for the model was a quasi-static compression test (15 mm/sec). A limitation of this study is that the puncture test simulation carried out was not validated against experimental data. Building a replicative puncture test rig and validating the puncture test would help define the element deletion criterion with more accuracy. Determining the principal stress to tear the chamois leather under dynamic loading may provide better element deletion prediction during impact. Testing the shoulder surrogate using standard cut or puncture resistance tests (such as cut resistance testing in BS EN ISO 13997) may also provide more accurate values for element deletion criterion, which in turn could improve the accuracy of the model.

The FE model used principal stress as the defining element deletion criterion. As outlined in Section 6.2, the *MAT_ADD_EROSION card allows other parameters for element deletion. With a view to improving element deletion prediction in the model, different / multiple parameters could be included in the element deletion criterion. By defining more element deletion criterions and by increasing the number of failure criterions to be met before element deletion (NCS option, Table 6-2), the solver would only delete elements if all the defined element deletion criterions were met. To improve the prediction of damage caused to the silicone during simulation, other properties such as strain (effective, principal or volumetric), pressure or shear stress (preferably obtained from different test methods) could be used in combination with principal stress.

For impact energies of 4 and 6 J, the model was within 15% of the peak force at tear values from the experiment. During simulated impacts, the contact force acting between both the stud and surface and the steel core and silicone were measured. Once the stud strikes the silicone, the corresponding contact force increases as expected (compared against experimental data) until element deletion occurs. If some of the elements, and hence part of the contacting surface, do remain, then a reduced contact force is detected (as noticed in angular impacts). Therefore, the stud-silicone contact force was only meaningful up until the point when the silicone tore. Techniques such as re-meshing the body at every time step, or defining contact using *AUTOMATIC_NODE_TO_SURFACE (which defines the contact between a node and surface) or *ERODING_SURFACE_TO_SURFACE (which redefines the contact surface at every time step) could help improve the stud-silicone contact force prediction capability of the model throughout the entire impact. Using these techniques can substantially increase the simulation duration, especially with single core computational capabilities. Using clusters with the possibility of SMP (Symmetric Multi-Processing) MPP (Massively Parallel Processing) could help with reducing runtime.

6.10 Scope of the FE Model

The model presented in Sections 6.7 and 6.8 predicted the damage caused to chamois leather during stud impact. Two other tests, (i) manufacturer sample stud impact and (ii) raking were carried out, as detailed in the following sections. The manufacturer sample test was carried out to assess the efficacy of the paddings in reducing the risk of soft tissue injuries, such as cuts and lacerations. The raking test was carried out to simulate an injury when a stud is moved along the surface of the skin. These tests were simulated using the FE model to showcase some of its possible uses.

6.10.1 Manufacturer Sample Testing & Padding Simulation

To check the efficacy of manufacturers' paddings, each of the samples was placed on top of the shoulder surrogate and impacted using the stud impactor at 4 J- 0° orientation. Peak impact force was noted, and any damage to the chamois leather was photographed using the setup defined in Section 6.4.1. Peak impact forces across the manufacturer sample paddings ranged between 840 and 1,260 N. In comparison to the damage caused to the chamois leather from a stud impact on the surrogate in isolation (without padding) presented in Section 6.5.4-Figure 6-12, the paddings reduced the extent of damage to the chamois leather. Indeed, the chamois leather tore for only two out of the eleven padding samples (Figure 6-28). For the nine other samples, only superficial damage (no tear) to the chamois leather was noted.
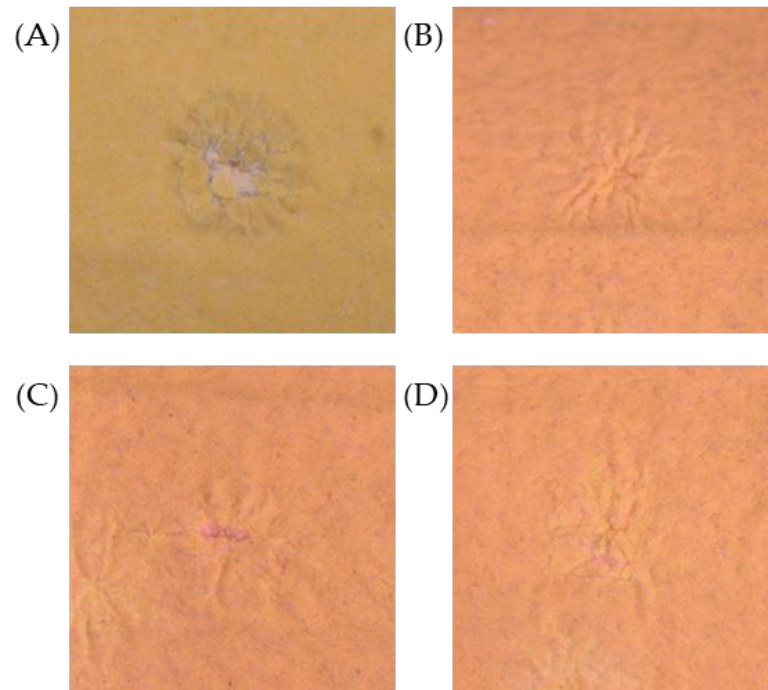
Figure 6-28: Damage caused to the chamois leather during (A) stud impact test with no padding, in comparison to damages caused during manufacturer sample testing with different extent of damages: (B) shows superficial damage to the chamois leather but not a cut / tear, while (C) and (D) show signs of a tear which are smaller in comparison to (A).

To study the effect of placing padding on the shoulder surrogate, a stud impact simulation was run using the setup defined in Section 6.7. The setup was run in three different scenarios, shoulder surrogate with, (i) no padding, (ii) 10 mm EVA foam padding (Figure 6-29-A) and (iii) 5 mm hard plastic covering (Figure 6-29-B).
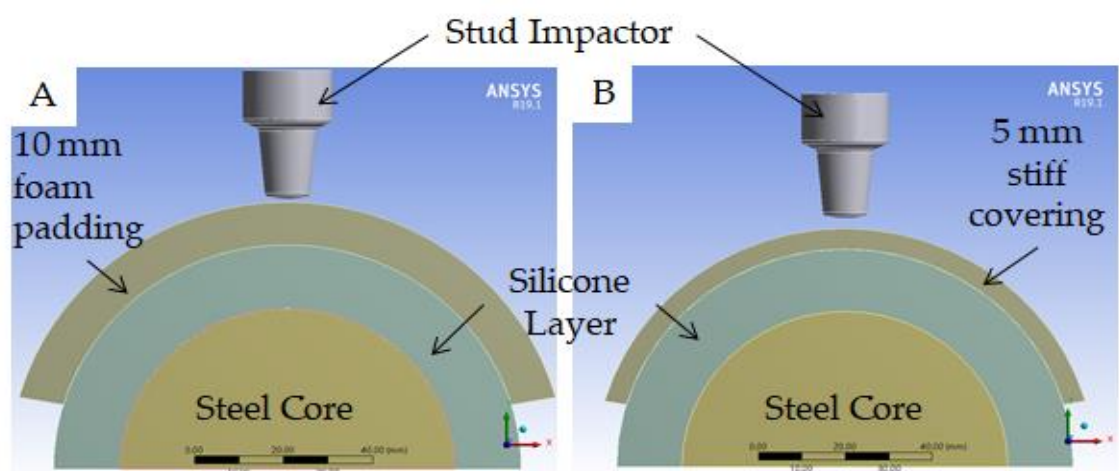
Figure 6-29: Geometry setup for comparison of simulation of padding efficacy using a (A) foam or (B) hard covering on the shoulder surrogate.

For the 10 mm foam padding, the material model used was EVA foam and the stiff plastic covering was High Density Polyethylene-HDPE (both from the Ansys© library and identical to the materials used in hardness test simulations in Section 4.2.5). Both the foam padding and hard covering were meshed using hexahedral meshes with a body sizing of 2 mm. The other parts were meshed as in Section 6.7 and resulting mesh for the model is detailed in Table 6-13.

Table 6-13: Mesh details for different parts in the stud impact padding simulation.

Part	Elements	Nodes
Stud Impactor	154	216
Silicone	158,562	30,198
*10 mm - Foam Padding	35,112	29,250
*5 mm - Hard Covering	19,272	14,040
Steel Core	1,898	2,430

*The foam padding and hard covering were used in separate simulations.

Contact between the, i) foam padding and silicone, ii) hard covering and silicone, and iii) stud impactor outer surface and silicone surface, was defined as frictional (*AUTOMATIC_SURFACE_TO_SURFACE) with a static and dynamic coefficient of friction of 0.3. The element deletion criterion was set as a principal stress of 31 MPa, as used for 0° impacts in Section 6.8. Element deletion criterion was not applied to the foam padding nor the hard covering.

The peak force for the foam padding simulation was 638 N, with 2,137 N for the hard covering. When comparing the simulations with and without foam padding, more elements were deleted, and hence there was more damage to the silicone, without padding (Figure 6-30).
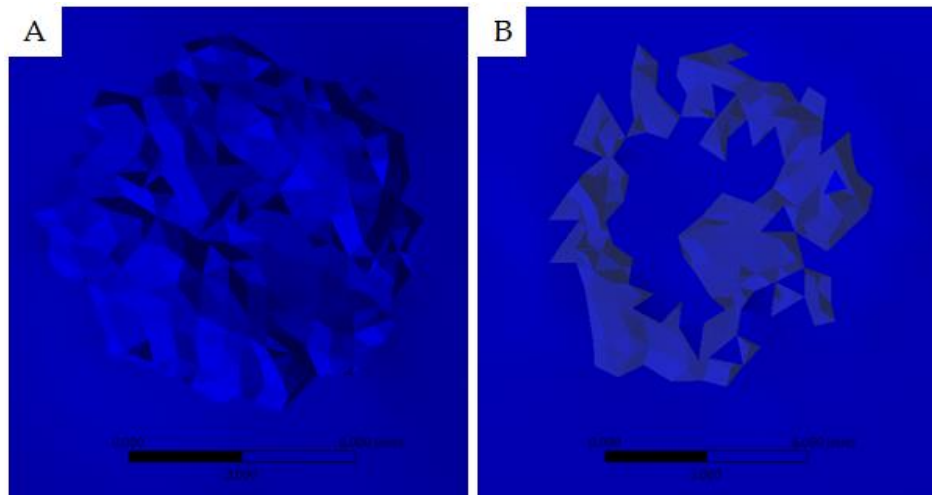
Figure 6-30: Visual comparison of damage area when the surrogate is impacted with (A) no padding and (B) 10 mm foam padding.

With a refined mesh, calculating the number of elements deleted using the solution information sheet can be time consuming. Future work may look at using text analysis macros or MATLAB scripts to analyse the number of elements being deleted using the solution information sheet. For a simpler understanding of the efficacy of padding at reducing damage to the silicone, the simulations were also run without any mesh refinement. Using no mesh refinement allowed easier calculation of the elements deleted (by looking at solution information and counting the deleted elements-Snippet in Appendix I-Figure 8-9). Results showed that more (~50%) elements were deleted from the simulant when no padding was present (Figure 6-31). Reducing the mesh decreased the simulation run time from 327 to 43 minutes but also resulted in loss of quality of the shape of damage detected.

No Padding
21 Elements Deleted

10 mm Foam Padding
14 Elements Deleted
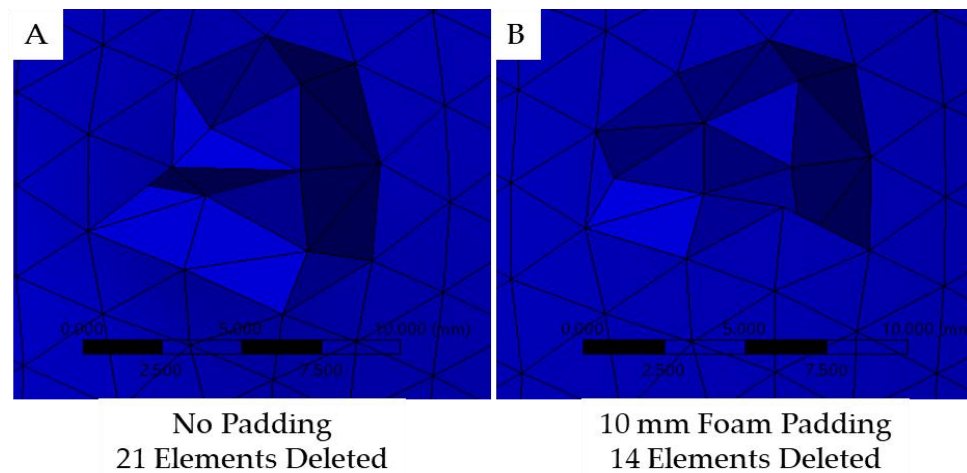
Figure 6-31: Comparison of damage area (with no mesh refinement) when the surrogate is impacted with (A) no padding and (B) 10 mm foam padding.

Simulation with a hard covering showed no damage to the silicone. The hard covering spread the impact force over an area that was larger than the face of the stud (Figure 6-32) reducing the principal stress in the elements so none of them were deleted.
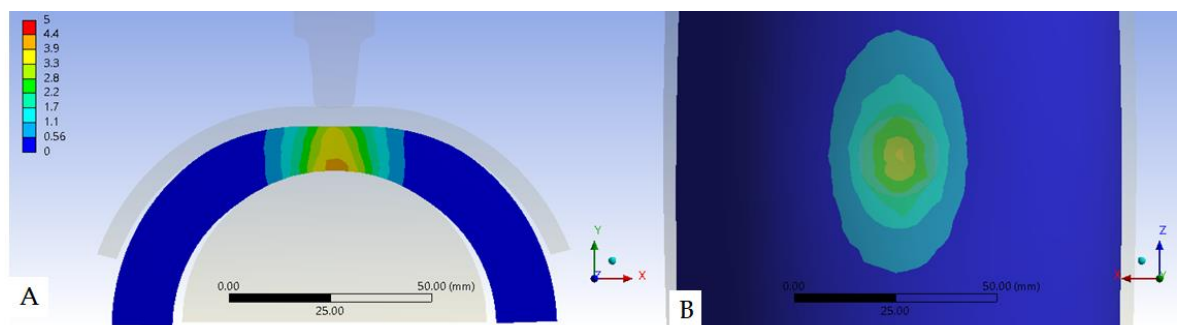
Figure 6-32: Contours of equivalent stress (MPa) across the cross section of the geometry during a 4 J impact on a shoulder surrogate with 5 mm HDPE padding on top. The increase in area of stress induced compared to the stud impactor face is visible in (A) cross sectional and (B) top view.

The peak force from the simulation with the EVA foam padding covering the shoulder surrogate (638 N) was lower than the experimental values for the manufacturer samples (840 – 2137 N). The discrepancy in peak forces between the experiment and simulation may be due to differences in the material properties of the manufacturer samples, as well as the geometry, and the EVA used in the model. Most of the samples used by the manufacturers had layers of fabric on either side

of the padding material. These fabrics which are fused, or vacuum moulded together may have influenced the impact response of the padding.

During foam impact simulations, it was noted that the foam elements were deleted upon impact, hence it can be assumed that the solver applied the same element deletion criterion to the foam and the silicone to avoid negative volume elements. To improve the model, analysing the padding and the fabric (if any) to determine their failure characteristics would help define the element deletion criterion for the padding material in the software. Applying material specific settings, would help improve the element deletion prediction and improve the accuracy of the force values predicted.

Stud impact simulations along with raking and padding material simulations show that the model developed has the potential to detect damage to the skin simulant. The model can predict damage shape during different impacts, but the specific shape of the damage is dependent on the size of the mesh. While the model can predict force until the silicone tears, once elements start getting deleted, the contact between the surfaces is removed leading to a drop in force.

6.10.2 Raking simulation

A bespoke test rig developed by, and located at, the University of Sheffield was used to simulate raking impact. The setup consisted of a set of four studs mounted on a plate and a cuboidal (200 × 150 × 8 mm) simulant (skin and silicone layer) that was moulded specifically for this test (Figure 6-33-A). The test conditions were based on the description of raking by Oudshoorn et al. (2018). The test rig was set to operate in a two-stage process, first, a vertical load compressed the studs into the soft tissue simulant and then a horizontal load created a raking action with the vertical load maintained, causing the studs to rake along the length of the simulant.
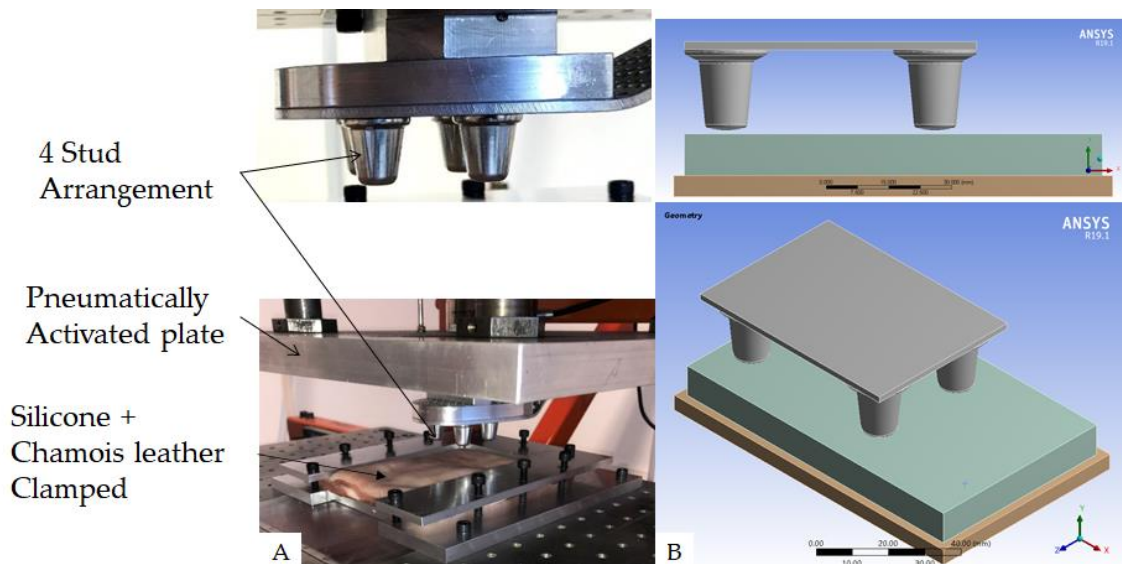
Figure 6-33: (A) Pneumatically driven raking test setup with its (B) CAD representation used for FE simulation.

To reduce simulation time, the width and length of the simulant in the model were reduced to 100 and 60 mm, respectively (Figure 6-33-B). The geometric centre of the stud arrangement was aligned to that of the simulant in the widthwise (z-axis), one end of the stud arrangement was aligned with edge on the simulant (x-axis) and was placed 1 mm above (y-axis) the simulant. The stud arrangement and base were each assigned a rigid material model (*MAT_RIGID). The simulant was assigned the material model developed in Chapter 5 (Table 5-14). The simulant was assigned a mesh refinement of 1.5 mm body size setting, while the other parts were assigned default mesh sizings. The resulting mesh is detailed in Table 6-14.

Table 6-14: Mesh details for different parts in the raking simulation.

Part	Type	Elements	Nodes
Stud Arrangement	Tetrahedral (ELFORM=10)	31,917	6,870
Simulant	Tetrahedral	157,671	30,098
Base	Hexahedral (ELFORM=1)	1,566	952

The vertical faces of the simulant were fully constrained with fixed supports. A vertical pressure of 7 MPa was applied to the upper face of the part with the studs, and then after a half second delay, a horizontal displacement of 60 mm along the x-axis was applied (Figure 6-34). Contact between the stud outer surfaces and the

simulant was defined (*AUTOMATIC_SURFACE_TO_SURFACE) using a static and dynamic coefficient of friction of 0.3. The element deletion criterion used was 31 MPa maximum principal stress value. The pressure applied was identical to the experimental value, but the horizontal displacement was scaled to reduce simulation time (12 hours and 53 minutes after scaled geometry and boundary conditions).
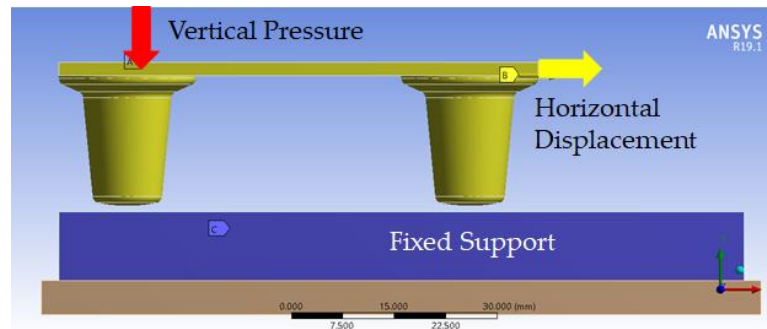
Figure 6-34: Boundary conditions for the raking test simulation.

Damage to the chamois leather during the experimental raking test and to the silicone in the simulation were compared visually. The damage caused to the silicone in the simulation was visible along the line of contact between the stud and simulant (Figure 6-35).
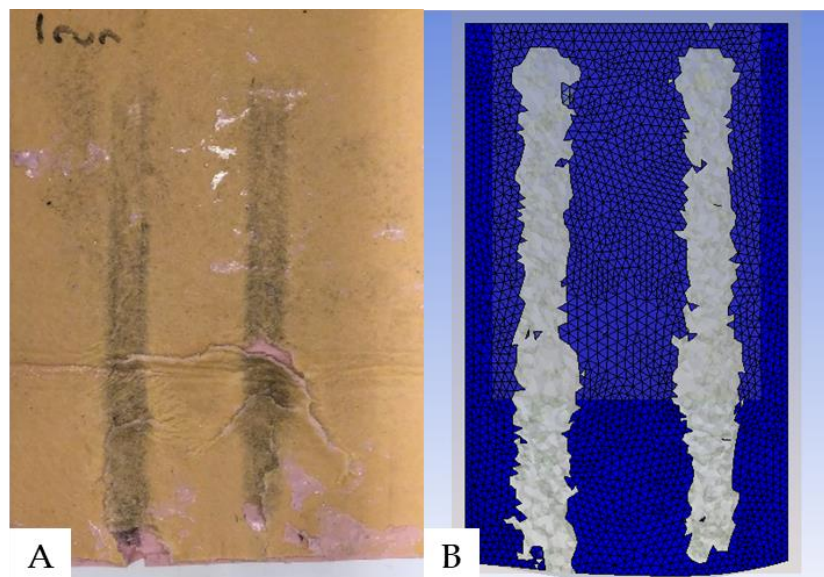
Figure 6-35: Damage caused to the (A) chamois leather during raking test and (B) damage caused to the simulant during FE simulation.

The FE model was capable of predicting the shape of the damage induced to the silicone during a raking test and can be used to study the stresses induced throughout the test, as shown in Figure 6-36.
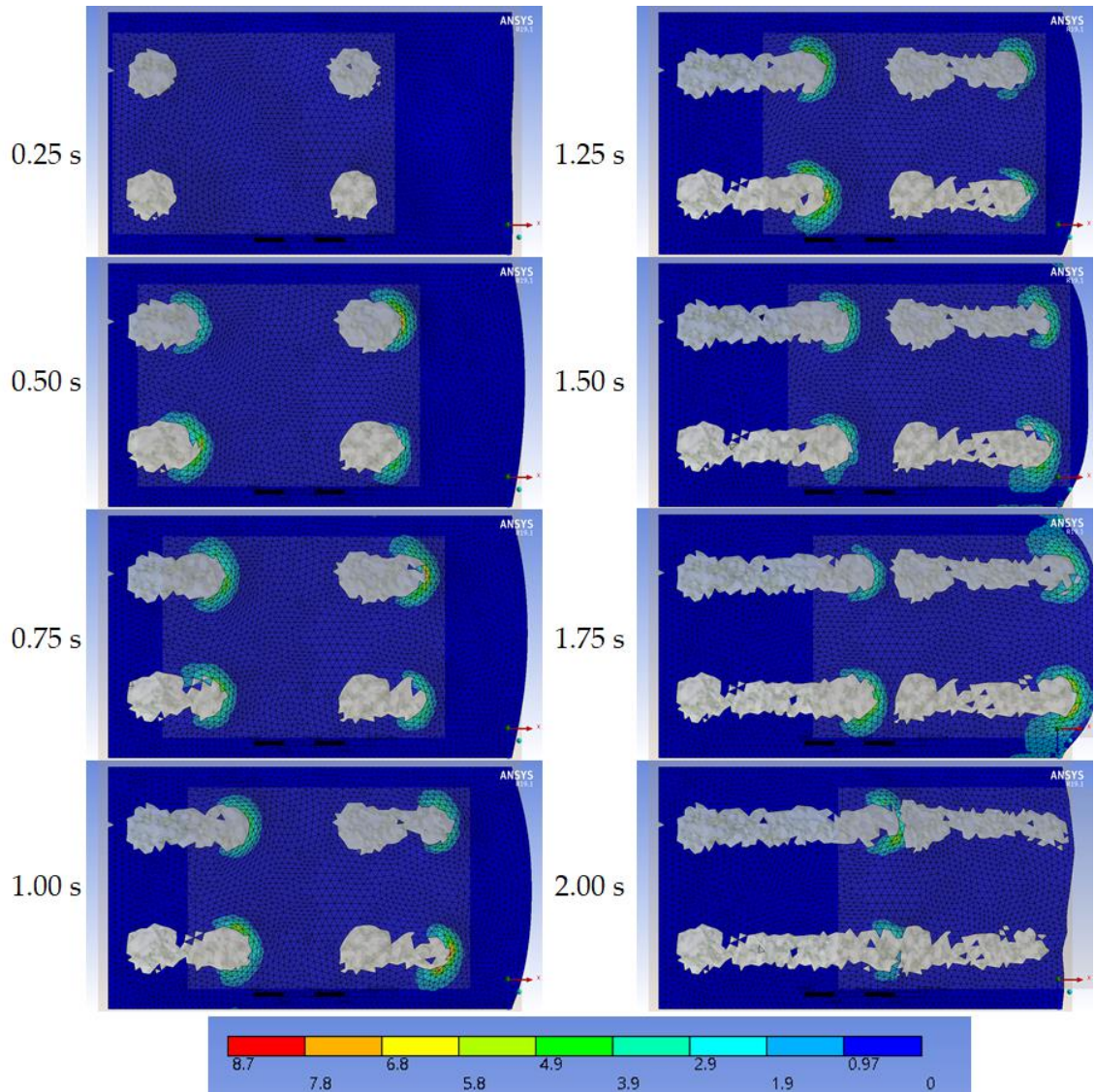
Figure 6-36: Contours of equivalent stress (MPa) induced in the simulant during a raking test simulation. Element deletion criterion: maximum principal stress value of 16 MPa.

6.11 Applications of the model

The model can detect damage to the skin simulant when struck by a stud under different impact or raking scenarios. The model could help in analysing the efficacy of a padding (current or futuristic) and help World Rugby™ to set regulations for padding material. Using such a model, manufacturers may be able to improve padding performance in terms of the ability to prevent soft tissue injuries, by testing

candidate materials and designs virtually before prototyping. Regulatory authorities can use these modelling techniques to predict the effect of new and emerging material technologies (e.g., mechanical metamaterials), provided they have an accurate material model for said material. Libraries of materials, such as MatWeb or Ansys© Granta Material property database, could provide the material models for use in simulations for materials being used or have the potential to be used in PPE.

Aside from stud impacts, the model could potentially be used to test the extent of damage to the skin simulant using impactors that represent anatomical structures, e.g., elbow, knee, or head. Shoulder-to-shoulder, elbow-to-shoulder, or knee-to-shoulder impacts could be simulated to understand the force propagation and the risk of soft tissue injury. The literature review identified that the increased use of artificial turf pitches has led to more injuries to the skin tissue, e.g., abrasions. A model for artificial turf, such as the one developed by Cole (2020), could be developed to simulate contact between turf and skin, and help understand the types of skin injuries that may occur.

6.12   Chapter Summary

Stud impact testing on the shoulder surrogate was carried out at energies of 2, 4 and 6 J at 0°, 15° and 30° orientations. Using the shoulder surrogate material model developed in Chapter 5, puncture tests mimicking the procedure used by SynDaver™ were simulated. The maximum principal stresses for the simulated puncture tests with applied loads between 2 and 10 N were obtained. The different principal stress values obtained from the puncture test simulations were then trialled in simulations at 4 J impact energy with a stud, to determine those that gave the best agreement with the experimental data for each angular orientation. Using the principal stress setting for each orientation, stud impact simulations were then run at 2 and 6 J and the results were compared against experimental data. Following the comparison of the FE simulation against experimental data for stud impact on

the surrogate, the model was used to simulate a raking test and a test with padding on the shoulder surrogate as a demonstration of the scope and potential of the developed modelling techniques.

Laceration Modelling
- Available models to simulate erosion/injury/crack are designed for metals and ceramics.
- *MAT_ADD_EROSION allows to add element deletion criterion in any material model

Injury Definition Criterion
- Injury to the skin tissue have been defined and modelled using tensile test data.
- Literature suggests the force at tear is not related to tensile performance.
- Literature and standard market simulant state skin tear ratings to be under 10 N.
- Simulation carried out to calculate maximum principle stress between 2-10 N.

Testing & Validation
- Stud impact testing of test bed carried out at 2,4 and 6 J at 0,15 and 30° orientation.
- Replicative simulations run with different maximum principle stress values for each skin rating.
- Different skin deletion criteria were compared against experimental data for each orientation.

Results
- Element deletion criterion for perpendicular impacts was noted as 4 N (31 MPa) the while 6 N(31 MPa) was better for predicting forces at tear for angular impacts
- Errors were higher when measuring time to tear, as the FE model stiffened up quicker than the experimental data

FE-Model Scope
- The FE model was subjected to different testing such as raking and was shown to be able to predict the shape of injury well.
- The FE-model was capable to predicting the reduction in injury when a padding was placed atop the skin simulant.

Figure 6-37: Summary of the work presented in Chapter-6.

7. Conclusion, Limitations and Future Research

7.1 Introduction

The aim of this thesis, as specified in Chapter 1, was to assess the regulations on padded clothing for protection specifically against cuts and lacerations in rugby. Relevant literature and the Regulation-12 documentation were critiqued, and areas of improvement were identified. Methods for testing material properties were assessed and a new test methodology was defined with a recommended limitation limit. Based on the synthetic shoulder surrogate developed by the PhD student at the University of Sheffield, finite element models were developed and validated by comparison against experimental impact data. The developed model was then impact tested using a stud to mimic injuries to the skin simulant. The model was then used to explore the different test methodologies that can be simulated to test the efficacy of padding used in rugby.

This chapter summarises the work carried out during this PhD thesis and presents how the objectives of the study have been met (Figure 7-1). The research questions raised by World Rugby™, before the PhD project started, will be answered along with recommendations for improving Regulation-12. The strengths and limitations of the work will be presented alongside recommendations for future work. The work within this PhD is two-fold; (i) to increase the knowledge of PPE and injury within research and (ii) to make recommendations to World Rugby™ to help them develop their regulations for padding clothing, thus increasing the research at both an industrial / societal perspective and academia.
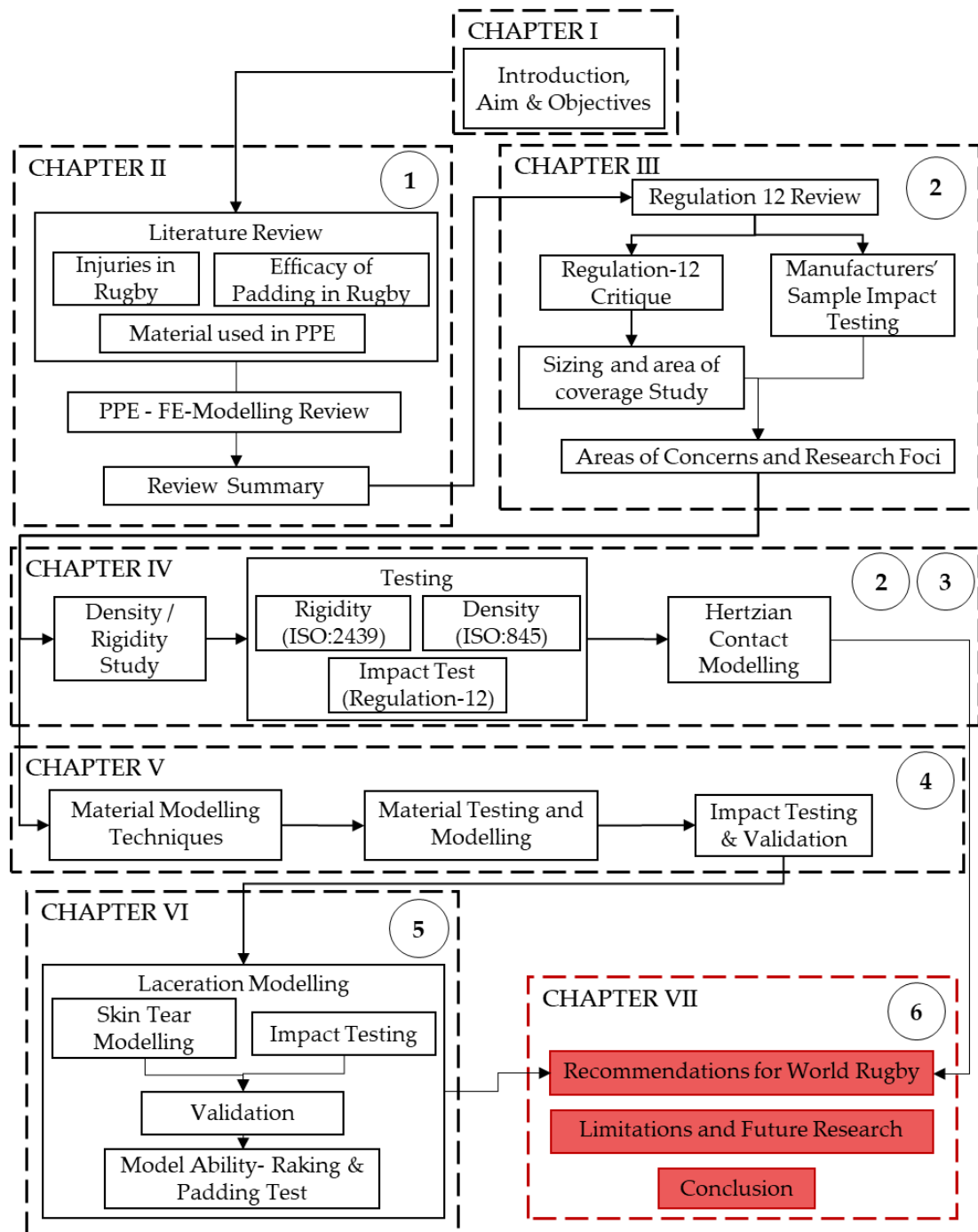
Figure 7-1: Layout of Thesis showing the placement of Chapter 7 with respect to the overall project. Numbers in circles correspond to objectives listed in Chapter 1.

7.2   **Summary of Research**

7.2.1   Objective 1

Objective 1 was to undertake a comprehensive review of literature relating to injury mechanisms in rugby, protective sports clothing, FE modelling of PPE and skin tissue, and advances in apparel and material technologies. It was found that skin

injuries are often under-reported, with differences in injury definition between studies. In addition, the main cause for skin injuries reported was stud contact (Oudshoorn et al., 2016). Studies involving impact testing of rugby shoulder paddings have focussed on force attenuation properties (which is not the intended purpose stated by World Rugby™) (Usman et al., 2011; Harris and Spears, 2010).

To the best of the author's knowledge, no studies have assessed the ability of rugby paddings to protect against skin injuries. Modern materials, such as auxetics, dilatants and bio-inspired materials, were shown to have potential to improve rugby padding, in terms of the ability to offer protection against soft tissue injuries. Auxetics and dilatants can also offer better indentation resistance and impact force attenuation than the foams (e.g., EVA) traditionally used in PPE. Stab resistant materials were also reviewed, and they were shown to reduce risk of soft tissue injuries. However, the modern and stab resistant materials reviewed tend to have a higher density (>100 kg·m^{-3}) than the limit (60 kg·m^{-3}) specified in the current World Rugby™ Regulation-12.

The review of testing methodologies showed that most tests for assessing the ability of PPE to protect against skin injuries involve a sharp object, such as a blade or knife, which does not represent scenarios during a game of rugby. The skin stamping test in the World Rugby™ Handbook that is designed to check the effect of changing the stud design, on a soft tissue simulant. The skin stamping test was identified as the most appropriate test methodology for the testing risk of skin injuries. However, whilst being replicative of a realistic impact scenario (stud to skin) during a game of rugby, this test does not have reasoning behind the experimental parameters, such as the impact mass (8.5 kg) and drop height (50 mm, resulting in an impact energy of 4.17 J).

The literature review showed that FE modelling is a well-established technique for predicting the performance of sporting PPE. The material properties of skin have been reported to be varied (affected by age, location of skin sample and other

biological factors) with studies tending to focus on the skin structure in isolation, without considering the underlying muscle and fat layer. Simulants such as silicones have been used by researchers to mimic the human skin and its underlying tissue (Payne et al., 2015; Petrone et al., 2019). Payne et al. (2015b) fabricated a silicone-based surrogate for impact testing of PPE. The focus of the FE model was to understand impact force propagation rather than damage to the skin layer.

The literature review identified a gap in knowledge in testing for efficacy of PPE for risks against cuts and lacerations. The review also helped in critiquing the Regulation-12 documentation and in understanding areas of improvement.

7.2.2 Objective 2

Objective 2 was to critically review current regulations for rugby padded clothing and to identify any potential gaps and areas for improvement. Regulation-12 documentation was textually critiqued followed by testing of manufacturers' samples using Regulation-12 instructions and areas of ambiguity were identified. The areas of focus identified were as follows:

i. **Density as the defining material property**: density regulation was intended to limit the use of hard materials for padding in rugby. While the current limitation of density to a maximum of 60 $kg \cdot m^{-3}$ restricts the padding materials to foams, the literature review showed that the hardness of a material can be varied without changing the density. Hence, density may not be a useful material limiting parameter in the future.

ii. **Impact testing methodology**: Currently, the impact test is defined as a rigid impactor on a rigid anvil, which is not representative of an impact during the game of rugby. Moreover, the intention of the padding is to reduce risk of cuts and lacerations (which is also not tested), hence a biofidelic anvil is required to assess injury to the skin.

iii.   **Location of the padding**: Wordings in the regulation allow manufacturers to place padding outside the shoulder region without needing to meet the impact attenuation test limitations.

The findings of the critique were presented at the World Rugby™ Manufactures meeting in 2018. Following discussions with the manufacturers and World Rugby™, an updated regulation: *Performance Specification for Body Padding* (updated to include all padding on a jersey) was introduced in 2019, based on the findings in Chapter 3.

7.2.3   Objective 3

Objective 3 was to identify materials that could be used to prevent cuts and lacerations in rugby, and to identify any contradictions of using these materials. PPE are often focused on indentation resistance and force attenuation; they are typically constructed using a hard outer shell (such as HDPE) and a soft underlying foam e.g. shin pads and American football shoulder pads. The hard outer layer prevents indentation whilst the soft foam layer improves energy absorption. Allowing the use of hard materials for indentation resistance can increase risk of injury to an opponent with no PPE. While the current density limitation of 60 kg·m^{-3} limits the materials to foam, with advances in technology there might be a possibility that future materials may be fabricated with low density and high hardness.

Chapter 4 demonstrated that testing for density did not provide any information about the hardness of the material and was erroneous. While hardness measurements were straightforward, they also tested the final product rather than just the material in isolation. Using the Hertzian contact model, a value of 750 N for a 65% compression was calculated to be the recommended hardness limit. This limit ensures that if two athletes (one with padding and one without padding) do come in contact, the strain induced in the padding is higher than the strain induced in the skin tissue. Hence the theoretical risk of injury to the player with no PPE is reduced.

7.2.4   Objective 4

Objective 4 was to develop and validate an FE model to predict the performance of a biofidelic impact surrogate model representing the human skin, fat, and muscle layer. A synthetic shoulder surrogate mimicking the shoulder muscle and fat anatomy was fabricated by the PhD student on the project at The University of Sheffield with a layer of chamois leather as skin simulant. This shoulder surrogate was developed specifically for the purpose of testing efficacy of shoulder paddings in rugby. Based on the literature, hyperelastic material models with a Prony series were identified as suitable methods to computationally model the shoulder surrogate material. In Chapter-5, quasi-static compression and stress relaxation data was used and different material models were generated.

Simulations were compared against experimental impact testing at 4.9, 9.8 and 14.7 J impact energy using peak force, impact duration, maximum deformation, and impulse. The 5-parameter Mooney-Rivlin model with a 2-term Prony series was identified as the model that gave the best agreement with the experimental data (< 10% mean error across the four parameters). Following the initial comparison to the experimental data, the effects of adding a Prony series, applying the factor-of-10 rule to stress relaxation data and varying damping values were presented.

7.2.5   Objective 5

Objective 5 was to apply the developed model to predict injury to human skin tissue which could then be used to analyse current and future materials in their ability to prevent injuries such as cuts and lacerations. In Chapter 6, the silicone model developed from Chapter 5 was used to simulate the skin puncture test by SynDaver™ over an applied force range of 2 to 10 N. The maximum principal stress calculated at each applied load was used to define the element deletion criterion using a *MAT_ADD_EROSION card. Experimental testing was carried out at 2, 4 and 6 J at 0, 15 and 30° by adapting the skin stamping test from Regulation-12. The element deletion criterion for simulations at each angular impact at 4 J were

identified, and then compared against 2 and 6 J impact energy. The model was also shown to be able to mimic different scenarios in rugby such as raking and testing of manufacturers' padding. The model was shown to predict the force to tear the silicone (< 10 % difference to experimental data) and the shape of the damage caused to the skin simulant, but underpredicted the time to tear (> 20% difference to experimental data).

This bespoke material model also has potential to be applied to predict damage on other surrogates that utilise silicones, such as a thigh surrogate (Payne et al. 2015b) or a head surrogate (Petrone et al. 2019).

7.2.6   Objective 6

Objective 6 was to recommend methods for testing padded clothing designed to reduce cuts and lacerations in rugby. Based on the simulations carried out in Chapter 6, the stud stamping test can be used as a reference test to measure the efficacy of padded clothing in rugby. The FE models defined in Chapter 6 (stud impact and raking) along with the FE compression test for hardness defined in Chapter 4, would allow manufacturers and World Rugby™ to assess current and futuristic materials. Using the FE model to simulate an impact with no padding, and then comparing it with a padding in place would help understand the efficacy of the padding in reducing the injury risks. Also, the model could be applied to other tests, such as raking with and without padding, to allow the effect of padding on soft tissue injury risk to be predicted.

7.3 Research Questions by World Rugby™

In Chapter 1, the four research questions raised by World Rugby™ were listed. Based on the findings of this thesis, the answers to the questions raised are explained below.

RQ1) Is the current requirement for padded clothing appropriate for the modern game of rugby, how and why?

The regulation does not state the intended reasoning of allowing shoulder / body padding which can lead to misunderstanding. For many users such as amateur / recreational players and coaches, it is essential that they understand that the padding is only designed to reduce risk of injuries to the skin and not meant to provide excessive impact attenuation. The regulation needs to state clearly that the intended purpose of padded clothing is to reduce the risk of cuts and lacerations and not to reduce impact force. The test methodologies do not provide enough details and defining properties such as density are erroneous to measure while not providing any useful information regarding material hardness. Parts of the regulations are appropriate for testing the performance of padded clothing, but areas of improvement, such as density regulation, impact testing and location of padding have been identified and presented in Chapter 3 and in Section 7.3.2. Overall, Regulation-12 needs to be improved to keep up with advances in technology and be future proof.

Recommendations for World Rugby**:** The regulations for shoulder paddings / body paddings need to undergo a change and updated based on the findings of this research. The test methodologies need to reflect actual loading mechanisms occurring during a gameplay scenario. As shown in Chapter 3, the ambiguity in the wordings allow misinterpretation of intended limits and use, any confusion should be eliminated to provide a clear understanding of the regulation to meet its intended purpose.

RQ2) Is the current requirement for padded clothing appropriate in permitting the use of modern technology, how and why?

Based on the details of Objective 1 and 2 presented in sections 7.2.1 and 7.2.2 most modern materials currently do not meet the Regulation-12 density requirements. These modern materials have shown capabilities in improving the indentation resistance and impact force attenuation and could potentially in the future fall within the density limit of the current regulation.

If the density requirement is replaced by hardness criterion as suggested in Chapter 4, more materials have the potential of being used as rugby padding. The impact attenuation testing could ensure the materials do not provide excessive impact protection while hardness testing could ensure the padding is not hard enough to pose a risk of soft tissue injuries.

<u>Recommendations for World Rugby</u>**:** Current regulations limit the materials that could be used by the manufacturers. Using the testing methodologies and recommendations provided in this research will allow manufacturers more room to play with and innovate. Along with improving the regulation, World Rugby must keep monitoring the use of modern technology to ensure that any innovation applied to PPE in rugby does not alter that nature of the game

RQ3) Considering that the intention for padded clothing is to continue to protect against cuts and lacerations only, devise an updated regulation with testing procedures that permits the latest technology.

The current test methodology of impacting with a rigid flat striker with a rigid anvil does not provide information on the efficacy of padding in reducing cuts and lacerations. Testing for cuts and laceration could be done by introducing an impact test with a biofidelic anvil, and the development process of such a test could be informed using the FE models developed in this thesis. To be able to assess the extent of injury a biofidelic anvil mimicking the human skin tissue and

the underlying anatomy must be defined. Then, the usability of a padding could be tested using three tests: (i) quasi-static hardness test (adapted from ISO 2439) presented in Chapter 4 to ensure the material is not too hard, (ii) impact attenuation testing to ensure excessive impact protection is not provided, and (iii) an impact test using a biofidelic anvil to gauge the ability to reduce the risk of cuts and lacerations. While devising the new regulation, care must be taken to ensure the intention and wordings are clearly defined. World Rugby™ intends to reduce the risk of cuts and lacerations, but padding does not eliminate the risk of such injuries. Any material or fabric could potentially reduce the risk of cuts and lacerations, but the extent of protection offered must be studied and a limitation must be defined. Defining a minimal threshold of protection offered against cuts and lacerations would help eliminate materials which may not offer enough protection from being defined as padding.

Recommendations for World Rugby: To protect against cuts and lacerations, the test methods must be replicative of a scenario that could result in such an injury. Using a rigid anvil would not provide any information of the ability of a padding in reducing the risk of cuts and lacerations. As shown in Chapters 5 & 6 using a biofidelic anvil or a surrogate to test for soft tissue injuries will provide more realistic information. While testing with surrogates may not be durable as it degrades during impact, using a validated FE model could provide an insight about the performance capability of the product.

RQ4) If no restriction were placed on the performance of padded clothing by World Rugby™, what would the development of such clothing look like?

If no restrictions were placed on the performance requirement of padded clothing, all PPE used in other sports could have potential uses in rugby. If the single material construction limitation is removed, PPE used in American football, such as hard-shell shoulder paddings could be adopted for better impact force attenuation and penetration resistance. Testing of manufacturer samples showed

that the current foam padding materials bottom out on impact at 14.7 J, which is likely due to the requirement in Regulation-12 for the peak acceleration to exceed 150 g. Removal of restrictions may result in harder and / or thicker paddings to help increase impact force attenuation. Currently, due to the regulation restrictions, padding outside the shoulder areas is thinner than in the shoulder area padding, and removal of restrictions may result in thicker paddings being placed in different areas of the jersey.

Removal of restrictions would likely result in thicker paddings, maybe even with hard shells, to improve impact protection capabilities along with reduced risk of cuts and lacerations. While such padding could reduce the risk of soft tissue injuries, the improved impact protection would also go against the current intended purpose of padding. Use of hard-shell PPE may lead to reduction in soft tissue injuries but may also lead to change in playing mechanism which in turn may lead to different types injuries.

Recommendations for World Rugby: Removing all restrictions / regulation on padded clothing performance could potentially change the way the game is played. Paddings in rugby would start resembling hard shell PPE used in other sports such as American football or ice hockey. While the current regulations need to be updated, they must also be monitored continually to monitor the epidemiology and impact of PPE in reducing their risks.

7.4   Original Contribution to Knowledge & Limitations

This section will highlight the contribution to research knowledge and limitations of the current PhD thesis. It will examine the experimental work and findings from Chapters 4-6 which would help improve Regulation-12 and contribute to research knowledge.

Chapter 4:

Contribution to knowledge: The chapter reported that testing for density of rugby padding is erroneous and does not provide any useful information about the material hardness. Compression testing using ISO:2439 methods showed the potential of testing for hardness of the padding. Using the hardness testing allows testing of the padding in its final form (usually fused with fabric) and is a non-destructive test. Hertzian contact modelling helped understand the different strains induced during contact between the padding material and shoulder surrogate. By ensuring no increased risk to an athlete without any PPE, the maximum hardness value was defined.

Limitations: The Hertzian contact model assumed constant material properties across the surrogate rather than including separate layers for the steel core, silicone and chamois leather.

Future Work: To improve the Hertzian contact model, the different layers of the surrogate may be modelled individually using FE softwares and the contact between each layer can be studied. Also, different PPE materials being tested can be compiled and stored in a database to understand the trends of materials being used, and also so they can be compared against new materials as they are developed.

Chapter 5:

Contribution to knowledge: An FE model capable of modelling impacts onto the shoulder surrogate was developed and compared against experimental data. This model can be used to study impacts on the shoulder anatomy and can be modified

to mimic different anatomical structures. The FE model developed was based on the novel shoulder surrogate designed by the PhD Student at The University of Sheffield as a tangential part of the World Rugby™ research project.

Limitations: Only uniaxial compression data from the surrogate silicone was used to model the hyperelastic response as the response was similar to when the silicone and chamois leather were compressed in combination. The strain rate for stress relaxation testing was limited by the speed of the testing machine. The FE model was created as a single material model (combining the silicone and skin layer into one structure). Also, the FE model was dependent on the damping values introduced.

Future Work: To improve the material model, testing the silicone using bi-axial, volumetric compression tests or Dynamic Mechanical Analysis (DMA) would allow more data for the software to better predict the material properties. Poisson's ratio for the surrogate silicone was taken from the literature. Measuring the Poisson's ratio of the silicone, such as by combining DIC with material testing, or using volumetric compression data would remove the need to rely on a value of Poisson's ratio from the literature. Stress relaxation testing can also be carried out at higher strain rates using faster testing machines or by reducing the sample thickness.

Chapter 6:

Contribution to knowledge: Using the *MAT_ADD_EROSION card, a novel FE model capable of predicting injuries such as cuts and lacerations, was developed and compared against experimental data. The ability of the model to test different scenarios such as raking and testing for padding efficacy were presented. The model can be used to predict efficacy of current and futuristic padding materials and can be used to study the extent of skin injuries during impact.

Limitations: As the FE model developed has a single material construction only the top layer of the material was analysed for element deletion as the focus was on skin

injuries. The element deletion criterion for defining the injury criterion was obtained from the FE simulation of the skin puncture test defined by SynDaver™ and was not validated experimentally.

Future Work: A puncture test on the synthetic chamois leather (across a range of loading rates and indenter shapes and sizes) could be used to define the element deletion criterion more accurately. A principal stress value was used to define the element deletion criterion, with more testing, other parameters such as strain and pressure could be used alongside principal stress. The model could be improved by splitting the geometry (as published by Payne et al. 2015b) into different structures for skin, fat and muscle layer with individual element deletion criteria. Element deletion leads to gaps between contacting surfaces or removal of a contact surface altogether, which hinders contact force prediction. Using options such as remeshing at every timestep or resurfacing after deletion of an element could overcome this issue. These options are computationally expensive, which could be addressed by improving computational power or by reducing the size and complexity of the model, such as by applying planes of symmetry or by developing a 2D model. For future work, standard cut tests such as BS EN ISO 13997 could be used to test the cut resistance of the padding material. The extent of agreement between results from the cut resistance test and extent of skin injury during a stud impact could be studied to check if a test method from a current standard could be implemented within Regulation-12.

7.5 Scope of Research

With further development, the model could be used for understanding skin injuries within the sport of rugby, as well as other sports and other industries too. The literature review showed skin injuries on the rise due to the use of artificial turfs. Modelling the turf surface alongside the model developed in this thesis could help analyse the contact between skin and turf and hence understanding the risks of injuries in these scenarios. The interaction with turf can be applied to different

sports such as football and hockey, where there is increasing use of artificial surfaces. Interaction between medical especially surgical equipment and human skin can be simulated to analyse the equipment design.

7.6   **Overall Conclusion**

This PhD thesis presented the development of a novel FE model for predicting the extent of skin damage on a synthetic shoulder surrogate. The model was validated against experimental data. The developed model has been used to show different test scenarios that could be employed to analyse efficacy of padding. The novelty of this research is that the FE modelling techniques developed can be applied to different silicones or other materials where damage or injury detection is required. It is also applicable for other pieces of sporting equipment, PPE or areas where objects come into contact with the human skin surface. Overall, the findings from this research can provide the scientific evidence for improvement of Regulation-12.

References

Allen, T., Haake, S. and Goodwill, S. (2009) 'Comparison of a finite element model of a tennis racket to experimental data.' *Sports engineering*, 12(2) pp. 87-98.

Allen, T., Shepherd, J., Hewage, T., Senior, T., Foster, L. and Alderson, A. (2015) 'Low-kinetic energy impact response of auxetic and conventional open-cell polyurethane foams.' *physica status solidi (b)*, 252(7) pp. 1631-1639.

Ankersen, J., Birkbeck, A. E., Thomson, R. D. and Vanezis, P. (1999) 'Puncture resistance and tensile strength of skin simulants.' *Proceedings of the Institution of Mechanical Engineers, Part H: Journal of Engineering in Medicine*, 213(6) pp. 493-501.

Ankrah, S. and Mills, N. (2003) 'Performance of football shin guards for direct stud impacts.' *Sports Engineering*, 6(4) p. 207.

Ankrah, S. and Mills, N. (2004) 'Analysis of ankle protection in Association football.' *Sports Engineering*, 7(1) pp. 41-52.

Annaidh, A., Ottenio, M., Bruyère, K., Destrade, M. and Gilchrist, M. D. (2010) *Mechanical properties of excised human skin.* Springer.

Annaidh, A. N., Destrade, M., Ottenio, M., Bruyere, K. and Gilchrist, M. D. (2014) *Strain rate effects on the failure characteristics of excised human skin.*

Ansys. (2015) *ANSYS Mechanical Advanced Nonlinear Materials, Appendix 4A: Hyperelasticity.*: [Online] [Accessed on 10th January 2018]

Bahr, R. and Krosshaug, T. (2005) 'Understanding injury mechanisms: a key component of preventing injuries in sport.' *British journal of sports medicine*, 39(6) pp. 324-329.

Banerjee, A., Dhar, S., Acharyya, S., Datta, D. and Nayak, N. (2017) 'Numerical simulation of ballistic impact of armour steel plate by typical armour piercing projectile.' *Procedia engineering*, 173 pp. 347-354.

Banwell, G., Mohr, S., Rothberg, S. and Roberts, J. (2012) 'Using experimental modal analysis to validate a finite element model of a tennis racket.' *Procedia Engineering*, 34 pp. 688-693.

Bathgate, A., Best, J. P., Craig, G. and Jamieson, M. (2002) 'A prospective study of injuries to elite Australian rugby union players.' *British journal of sports medicine*, 36(4) pp. 265-269.

Benítez, J. M. and Montáns, F. J. (2017) 'The mechanical behavior of skin: Structures and models for the finite element analysis.' *Computers & Structures*, 190 pp. 75-107.

Best, J. P., McIntosh, A. S. and Savage, T. N. (2005) 'Rugby World Cup 2003 injury surveillance project.' *British journal of sports medicine*, 39(11) pp. 812-817.

Biesen, E. and Smith, L. (2007) 'Describing the plastic deformation of aluminium softball bats.' *Sports Engineering*, 10(4) pp. 185-193.

Brewer, J. and Davis, J. (1995) 'Applied physiology of rugby league.' *Sports Medicine*, 20(3) pp. 129-135.

British Standards Institution (BSI). (2011) BS 6366:2011 Specification for studs for rugby football boots.

Brooks, J. H. and Kemp, S. P. (2008) 'Recent trends in rugby union injuries.' *Clinics in sports medicine*, 27(1) pp. 51-73.

Brooks, J. H., Fuller, C., Kemp, S. and Reddin, D. B. (2005a) 'Epidemiology of injuries in English professional rugby union: part 2 training Injuries.' *British journal of sports medicine*, 39(10) pp. 767-775.

Brooks, J. H., Fuller, C., Kemp, S. and Reddin, D. B. (2005b) 'A prospective study of injuries and training amongst the England 2003 Rugby World Cup squad.' *British journal of sports medicine*, 39(5) pp. 288-293.

Brooks, J. H., Fuller, C., Kemp, S. and Reddin, D. B. (2005c) 'Epidemiology of injuries in English professional rugby union: part 1 match injuries.' *British journal of sports medicine*, 39(10) pp. 757-766.

Cauvin, S., Liles, D., Robson, S. and Stammer, A. (2011) Emulsions Of Dilatant Organopolysiloxanes. Google Patents.

Chadwick, S., Semens, A. and Arthur, D. (2011) 'Economic impact report on global rugby/Part IV: Rugby World Cup 2011.' *Coventry: Coventry University/MasterCard Worldwide,*

Chan, N. and Evans, K. (1998) 'Indentation resilience of conventional and auxetic foams.' *Journal of cellular plastics*, 34(3) pp. 231-260.

Choudhary, S., Singh, P. K., Khare, S., Kumar, K., Mahajan, P. and Verma, R. K. (2020) 'Ballistic impact behaviour of newly developed armour grade steel: An experimental and numerical study.' *International Journal of Impact Engineering*, p. 103557.

Coto, N. P., Meira, J. B. C., e Dias, R. B., Driemeier, L., de Oliveira Roveri, G. and Noritomi, P. Y. (2012) 'Assessment of nose protector for sport activities: finite element analysis.' *Dental traumatology*, 28(2) pp. 108-113.

Crichton, J., Jones, D. R. and Funk, L. (2012) 'Mechanisms of traumatic shoulder injury in elite rugby players.' *Br J Sports Med*, 46(7) pp. 538-542.

Dąbrowska, A., Rotaru, G. M., Derler, S., Spano, F., Camenzind, M., Annaheim, S., Stämpfli, R., Schmid, M., et al. (2016) 'Materials used to simulate physical properties of human skin.' *Skin Research and Technology*, 22(1) pp. 3-14.

Dahl, M., Wettergren, H. and Tidefelt, H. (2017) *Modelica Spur Gears with Hertzian Contact Forces.* Linköping University Electronic Press.

Delalleau, A., Josse, G., Lagarde, J.-M., Zahouani, H. and Bergheau, J.-M. (2006) 'Characterization of the mechanical properties of skin by inverse analysis combined with the indentation test.' *Journal of biomechanics*, 39(9) pp. 1603-1610.

Delalleau, A., Josse, G., Lagarde, J. M., Zahouani, H. and Bergheau, J. M. (2008) 'A nonlinear elastic behavior to identify the mechanical parameters of human skin in vivo.' *Skin research and Technology*, 14(2) pp. 152-164.

Diani, J., Fayolle, B. and Gilormini, P. (2009) 'A review on the Mullins effect.' *European Polymer Journal*, 45(3) pp. 601-612.

Diridollou, S., Berson, M., Vabre, V., Black, D., Karlsson, B., Auriol, F., Gregoire, J., Yvon, C., et al. (1998) 'An in vivo method for measuring the mechanical properties of the skin using ultrasound.' *Ultrasound in medicine & biology*, 24(2) pp. 215-224.

Duncan, O., Foster, L., Senior, T., Allen, T. and Alderson, A. (2016) 'A comparison of novel and conventional fabrication methods for auxetic foams for sports safety applications.' *Procedia engineering*, 147 pp. 384-389.

Duncan, O., Shepherd, T., Moroney, C., Foster, L., Venkatraman, P. D., Winwood, K., Allen, T. and Alderson, A. (2018) 'Review of auxetic materials for sports applications: Expanding options in comfort and protection.' *Applied Sciences*, 8(6) p. 941.

Evans, S. L. (2009) 'On the implementation of a wrinkling, hyperelastic membrane model for skin and other materials.' *Computer methods in biomechanics and biomedical engineering*, 12(3) pp. 319-332.

Evans, S. L. and Holt, C. A. (2009) 'Measuring the mechanical properties of human skin in vivo using digital image correlation and finite element modelling.' *The Journal of Strain Analysis for Engineering Design*, 44(5) pp. 337-345.

Flynn, C., Taberner, A. and Nielsen, P. (2011) 'Mechanical characterisation of in vivo human skin using a 3D force-sensitive micro-robot and finite element analysis.' *Biomechanics and modeling in mechanobiology*, 10(1) pp. 27-38.

Fortin-Smith, J., Sherwood, J., Drane, P., Ruggiero, E., Campshure, B. and Kretschmann, D. (2019) 'A Finite Element Investigation into the Effect of Slope of Grain on Wood Baseball Bat Durability.' *Applied Sciences*, 9(18) p. 3733.

Freitag, A., Kirkwood, G., Scharer, S., Ofori-Asenso, R. and Pollock, A. M. (2015) 'Systematic review of rugby injuries in children and adolescents under 21 years.' *British journal of sports medicine*, 49(8) pp. 511-519.

Fuller, C. (2016) 'Epidemiology of rugby injuries.' *In Science and Football VIII*. Routledge, pp. 107-111.

Fuller, C. and Molloy, M. G. (2011) 'Epidemiological study of injuries in men's international under-20 rugby union tournaments.' *Clinical journal of sport medicine*, 21(4) pp. 356-358.

Fuller, C., Taylor, A. and Molloy, M. G. (2010a) 'Epidemiological study of injuries in international rugby sevens.' *Clinical Journal of Sport Medicine*, 20(3) pp. 179-184.

Fuller, C., Sheerin, K. and Targett, S. (2013) 'Rugby world cup 2011: international rugby board injury surveillance study.' *British journal of sports medicine*, 47(18) pp. 1184-1191.

Fuller, C., Laborde, F., Leather, R. and Molloy, M. G. (2008) 'International rugby board rugby world cup 2007 injury surveillance study.' *British journal of sports medicine*, 42(6) pp. 452-459.

Fuller, C., Taylor, A., Douglas, M. and Raftery, M. (2020) 'Rugby World Cup 2019 injury surveillance study.' *South African Journal of Sports Medicine*, 32(1)

Fuller, C. W., Clarke, L. and Molloy, M. G. (2010b) 'Risk of injury associated with rugby union played on artificial turf.' *Journal of sports sciences*, 28(5) pp. 563-570.

Fuller, C. W., Sheerin, K. and Targett, S. (2012) 'Rugby World Cup 2011: International Rugby Board Injury Surveillance.'

Fuller, C. W., Taylor, A. and Raftery, M. (2015) 'Epidemiology of concussion in men's elite rugby-7s (sevens world series) and rugby-15s (rugby world cup, junior world championship and rugby trophy, Pacific nations cup and English premiership).' *British journal of sports medicine*, 49(7) pp. 478-483.

Fuller, C. W., Taylor, A. and Raftery, M. (2018) 'Eight-season epidemiological study of injuries in men's international Under-20 rugby tournaments.' *Journal of sports sciences*, 36(15) pp. 1776-1783.

Fuller, C. W., Taylor, A., Kemp, S. P. and Raftery, M. (2017) 'Rugby world cup 2015: World Rugby™ injury surveillance study.' *Br J Sports Med*, 51(1) pp. 51-57.

Fuller, C. W., Brooks, J. H., Cancea, R. J., Hall, J. and Kemp, S. P. (2007a) 'Contact events in rugby union and their propensity to cause injury.' *British journal of sports medicine*, 41(12) pp. 862-867.

Fuller, C. W., Raftery, M., Readhead, C., Targett, S. G. and Molloy, M. G. (2009a) 'Impact of the International Rugby Board's experimental law variations on the incidence and nature of match injuries in southern hemisphere professional rugby union.' *South African medical journal*, 99(4)

Fuller, C. W., Raftery, M., Readhead, C., Targett, S. G. and Molloy, M. G. (2009b) 'Match injuries in Southern Hemisphere professional rugby union: Impact of the International Rugby Board's Experimental Law Variations.' *South African Medical Journal*, 99(4) p. 232.

Fuller, C. W., Ashton, T., Brooks, J. H., Cancea, R. J., Hall, J. and Kemp, S. P. (2010c) 'Injury risks associated with tackling in rugby union.' *British journal of sports medicine*, 44(3) pp. 159-167.

Fuller, C. W., Ekstrand, J., Junge, A., Andersen, T. E., Bahr, R., Dvorak, J., Hägglund, M., McCrory, P., et al. (2006) 'Consensus statement on injury definitions and data collection procedures in studies of football (soccer) injuries.' *Scandinavian journal of medicine & science in sports*, 16(2) pp. 83-92.

Fuller, C. W., Molloy, M. G., Bagate, C., Bahr, R., Brooks, J. H., Donson, H., Kemp, S. P., McCrory, P., et al. (2007b) 'Consensus statement on injury definitions and data collection procedures for studies of injuries in rugby union.' *British journal of sports medicine*, 41(5) pp. 328-331.

Gerrard, D. F. (1998) 'The use of padding in rugby union.' *Sports Medicine*, 25(5) pp. 329-332.

Gilchrist, M. D., Keenan, S., Curtis, M., Cassidy, M., Byrne, G. and Destrade, M. (2008) 'Measuring knife stab penetration into skin simulant using a novel biaxial tension device.' *Forensic science international*, 177(1) pp. 52-65.

Goodwill, S., Kirk, R. and Haake, S. (2005) 'Experimental and finite element analysis of a tennis ball impact on a rigid surface.' *Sports engineering*, 8(3) pp. 145-158.

Greenhalgh, E., Bloodworth, V., Iannucci, L. and Pope, D. (2013) 'Fractographic observations on Dyneema® composites under ballistic impact.' *Composites part A: Applied science and manufacturing*, 44 pp. 51-62.

Groves, R. B., Coulman, S., Birchall, J. C. and Evans, S. L. (2012) 'Quantifying the mechanical properties of human skin to optimise future microneedle device design.' *Computer methods in biomechanics and biomedical engineering*, 15(1) pp. 73-82.

Harris, D. and Spears, I. (2010) 'The effect of rugby shoulder padding on peak impact force attenuation.' *British journal of sports medicine*, 44(3) pp. 200-203.

Headey, J., Brooks, J. H. and Kemp, S. P. (2007) 'The epidemiology of shoulder injuries in English professional rugby union.' *The American journal of sports medicine*, 35(9) pp. 1537-1543.

Hendriks, F., Brokken, D. v., Van Eemeren, J., Oomens, C., Baaijens, F. and Horsten, J. (2003) 'A numerical-experimental method to characterize the non-linear mechanical behaviour of human skin.' *Skin research and technology*, 9(3) pp. 274-283.

Hertz, H. (1881) 'On the contact of elastic solids.' *Z. Reine Angew. Mathematik*, 92 pp. 156-171.

Hodgson, L., Gissane, C., Gabbett, T. J. and King, D. A. (2007) 'For debate: consensus injury definitions in team sports should focus on encompassing all injuries.' *Clinical Journal of Sport Medicine*, 17(3) pp. 188-191.

Hrysomallis, C. (2009) 'Surrogate thigh model for assessing impact force attenuation of protective pads.' *Journal of science and medicine in sport*, 12(1) pp. 35-41.

Hughes, A., Driscoll, H. and Carré, M., 2020. Development of Silicone Elastomer for Use in the Assessment of Padded Clothing in Rugby Union. In *Multidisciplinary Digital Publishing Institute Proceedings* (Vol. 49, No. 1, p. 77).

Hurtado, M.M., Peppelman, M., Zeng, X., Van Erp, P.E.J. and Van Der Heide, E., 2016. Tribological behaviour of skin equivalents and ex-vivo human skin against the material components of artificial turf in sliding contact. *Tribology International*, *102*, pp.103-113.

International Organisation for Standardization (ISO). (2008) ISO 2439: Flexible cellular polymeric materials - Determination of hardness (indentation technique).

International Organization for Standardization (ISO). (1999) ISO 13997:1999 Protective clothing - Mechanical properties - Determination of resistance to cutting by sharp objects.

International Organization for Standardization (ISO). (2005) ISO 22958:2005 Textiles. Water resistance. Rain tests: exposure to horizontal water spray.

International Organization for Standardization (ISO). (2006) 'ISO 845: Cellular plastics and rubbers - Determination of apparent density.'

International Organization for Standardization (ISO). (2015) BS EN 13594:2015 Protective gloves for motorcycle riders.

International Organization for Standardization (ISO). (2016a) BS EN 388:2016 Protective gloves against mechanical risks.

International Organization for Standardization (ISO). (2016b) BS EN ISO 12947:2016 Textiles. Determination of the abrasion resistance of fabrics by the Martindale method.

International Organization for Standardization (ISO). (2018) BS EN ISO 15487:2018 Textiles. Method for assessing appearance of apparel and other textile end products after domestic washing and drying.

Jachowicz, J., McMullen, R. and Prettypaul, D. (2007) 'Indentometric analysis of in vivo skin and comparison with artificial skin models.' *Skin Research and Technology*, 13(3) pp. 299-309.

Jakoet, I. and Noakes, T. D. (1998) 'A high rate of injury during the 1995 Rugby World Cup.' *South African Medical Journal*, 88(1) pp. 45-47.

Jang, W.-H., Kim, K.-O., Beom, H.-K. and Kwon, S.-E. (2008) 'Effect of Sensitivity Variation for Mounting Methods of Accelerometer in Crash Test.' *Transactions of the Korean Society of Automotive Engineers*, 16(6) pp. 115-120.

Johnson, A., Bingham, G. A. and Wimpenny, D. I. (2013) 'Additive manufactured textiles for high-performance stab resistant applications.' *Rapid Prototyping Journal*,

Joodaki, H. and Panzer, M. B. (2018) 'Skin mechanical properties and modeling: A review.' *Proceedings of the Institution of Mechanical Engineers, Part H: Journal of Engineering in Medicine*, 232(4) pp. 323-343.

Junge, A., Cheung, K., Edwards, T. and Dvorak, J. (2004) 'Injuries in youth amateur soccer and rugby players—comparison of incidence and characteristics.' *British journal of sports medicine*, 38(2) pp. 168-172.

Kajtaz, M. and Subic, A. (2015) *Experimental investigation into suitability of smart polymers as an impact-absorbing material for an improved rugby headgear.*

Kalra, A., Lowe, A. and Al-Jumaily, A. (2016) 'Mechanical behaviour of skin: a review.' *J. Mater. Sci. Eng*, 5(4) p. 1000254.

Kelkar, P. U., Kim, H. S., Cho, K.-H., Kwak, J. Y., Kang, C.-Y. and Song, H.-C. (2020) 'Cellular auxetic structures for mechanical metamaterials: A review.' *Sensors*, 20(11) p. 3132.

Kerr, H. A., Curtis, C., Micheli, L. J., Kocher, M. S., Zurakowski, D., Kemp, S. and Brooks, J. (2008) 'Collegiate rugby union injury patterns in New England: a prospective cohort study.' *British journal of sports medicine*, 42(7) pp. 595-603.

Kurtaran, H., Buyuk, M. and Eskandarian, A. (2003) 'Ballistic impact simulation of GT model vehicle door using finite element method.' *Theoretical and Applied Fracture Mechanics*, 40(2) pp. 113-121.

Lapeer, R., Gasson, P. and Karri, V. (2010) 'Simulating plastic surgery: from human skin tensile tests, through hyperelastic finite element models to real-time haptics.' *Progress in biophysics and molecular biology*, 103(2-3) pp. 208-216.

Larrabee Jr, W. F. (1986) 'A finite element model of skin deformation. I. Biomechanics of skin and soft tissue: a review.' *The Laryngoscope*, 96(4) pp. 399-405.

Larrabee Jr, W. F. and Galt, J. (1986) 'A finite element model of skin deformation. III. The finite element model.' *The Laryngoscope*, 96(4) pp. 413-419.

Larrabee Jr, W. F. and Sutton, D. (1986) 'A finite element model of skin deformation. II. An experimental model of skin deformation.' *The Laryngoscope*, 96(4) pp. 406-412.

Lawrence, P. R. (1992) 'The challenge of problem-oriented research.' *Journal of Management Inquiry*, 1(2) pp. 139-142.

Leveque, J., De Rigal, J., Agache, P. and Monneur, C. (1980) 'Influence of ageing on the in vivo extensibility of human skin at a low stress.' *Archives of Dermatological Research*, 269(2) pp. 127-135.

Levi, A., Theilen, T.-M. and Rolle, U. (2020) 'Injury surveillance in elite field hockey: a pilot study of three different recording techniques.' *BMJ Open Sport & Exercise Medicine*, 6(1) p. e000908.

LSTC. (2018a) *LS-DYNA Keyword User's Manual Volume I.*

LSTC. (2018b) *LS-DYNA Keyword User's Manual-Volume-II Material Models.*

Mahmud, J., Holt, C. A. and Evans, S. L. (2010) 'An innovative application of a small-scale motion analysis technique to quantify human skin deformation in vivo.' *Journal of biomechanics*, 43(5) pp. 1002-1006.

Marchesseau, S., Heimann, T., Chatelin, S., Willinger, R. and Delingette, H. (2010) 'Fast porous visco-hyperelastic soft tissue model for surgery simulation: application to liver surgery.' *Progress in biophysics and molecular biology*, 103(2-3) pp. 185-196.

Marshall, S. W., Waller, A. E., Dick, R. W., Pugh, C. B., Loomis, D. P. and Chalmers, D. J. (2002) 'An ecologic study of protective equipment and injury in two contact sports.' *International journal of epidemiology*, 31(3) pp. 587-592.

Marshall, S. W., Waller, A. E., LOOMIS, D. P., Feehan, M., CHALMERS, D. J., BIRD, Y. N. and QUARRIE, K. L. (2001) 'Use of protective equipment in a cohort of rugby players.' *Medicine & Science in Sports & Exercise*, 33(12) pp. 2131-2138.

Marshall, S. W., Loomis, D. P., Waller, A. E., Chalmers, D. J., Bird, Y. N., Quarrie, K. L. and Feehan, M. (2005) 'Evaluation of protective equipment for prevention of injuries in rugby union.' *International journal of epidemiology*, 34(1) pp. 113-118.

McIntosh, A. S., McCrory, P., Finch, C. F. and Wolfe, R. (2010a) 'Head, face and neck injury in youth rugby: incidence and risk factors.' *British journal of sports medicine*, 44(3) pp. 188-193.

McIntosh, A. S., McCrory, P., Finch, C. F., Chalmers, D. and Best, J. P. (2003) 'Rugby headgear study.' *Journal of science and medicine in sport*, 6(3) pp. 355-358.

McIntosh, A. S., Savage, T. N., McCrory, P., Frechede, B. O. and Wolfe, R. (2010b) 'Tackle characteristics and injury in a cross section of rugby union football.' *Medicine & Science in Sports & Exercise*, 42(5) pp. 977-984.

Meir, R., Brooks, L. and Shield, T. (2003) 'Body weight and tympanic temperature change in professional rugby league players during night and day games: a study in the field.' *Journal of Strength and Conditioning Research*, 17(3) pp. 566-572.

Meissner, J. (1978) 'Combined constant strain rate and stress relaxation test for linear viscoelastic studies.' *Journal of Polymer Science: Polymer Physics Edition*, 16(5) pp. 915-919.

Mills, N. and Rodriguez-Perez, M. (2001) 'Modelling the gas-loss creep mechanism in EVA foam from running shoes.' *Cellular Polymers*, 20(2) pp. 79-100.

Mills, N. and Gilchrist, A. (2008a) 'Oblique impact testing of bicycle helmets.' *International Journal of Impact Engineering*, 35(9) pp. 1075-1086.

Mills, N. and Gilchrist, A. (2008b) 'Finite-element analysis of bicycle helmet oblique impacts.' *International Journal of Impact Engineering*, 35(9) pp. 1087-1101.

Mills, N., Fitzgerald, C., Gilchrist, A. and Verdejo, R. (2003) 'Polymer foams for personal protection: cushions, shoes and helmets.' *Composites science and technology*, 63(16) pp. 2389-2400.

Mills, N. J. and Masso-Moreu, Y. (2005) 'Finite element analysis (FEA) applied to polyethylene foam cushions in package drop tests.' *Packaging Technology and Science: An International Journal*, 18(1) pp. 29-38.

Mills, N. J., Wilkes, S., Derler, S. and Flisch, A. (2009) 'FEA of oblique impact tests on a motorcycle helmet.' *International Journal of Impact Engineering*, 36(7) pp. 913-925.

Mooney, M. (1940) 'A theory of large elastic deformation.' *Journal of applied physics*, 11(9) pp. 582-592.

Moore, I. S., Ranson, C. and Mathema, P. (2015) 'Injury risk in international rugby union: three-year injury surveillance of the welsh national team.' *Orthopaedic journal of sports medicine*, 3(7) p. 2325967115596194.

Moroney, C. (2021) *The Application of Auxetic Structures for Rugby Shoulder Padding.* Manchester Metropolitan University.

Mullin, L. and Tobin, N. (1965) 'Stress softing in rubber vulcanizates I. Use of stain-amplification factor to describe the elastic behavior of filler-reinforced vulcanized rubber.' *J. Appl. Polym. Sci*, 9 p. 2993.

Newton-Mann, C., Winwood, K., Driscoll, H., Hamilton, N. and Allen, T. (2018) *Finite element model of an impact on a palmar pad from a snowboard wrist protector.* Vol. 2:

Newton-Mann, C. R. (2019) *Finite Element Modelling of Snowboard Wrist Protectors.* Manchester Metropolitan University.

Ni-Annaidh, A., Cassidy, M., Curtis, M., Destrade, M. and Gilchrist, M. D. (2013) 'A combined experimental and numerical study of stab-penetration forces.' *Forensic science international*, 233(1-3) pp. 7-13.

Nicholl, J., Coleman, P. and Williams, B. (1995) 'The epidemiology of sports and exercise related injury in the United Kingdom.' *British journal of sports medicine*, 29(4) pp. 232-238.

Ogden, R. W. (1972) 'Large deformation isotropic elasticity–on the correlation of theory and experiment for incompressible rubberlike solids.' *Proceedings of the Royal Society of London. A. Mathematical and Physical Sciences*, 326(1567) pp. 565-584.

Orr, R. and Cheng, H. L. (2016) 'Incidence and characteristics of injuries in elite Australian junior rugby league players.' *Journal of science and medicine in sport*, 19(3) pp. 212-217.

Ottenio, M., Tran, D., Annaidh, A. N., Gilchrist, M. D. and Bruyère, K. (2015) 'Strain rate and anisotropy effects on the tensile failure characteristics of human skin.' *Journal of the mechanical behavior of biomedical materials*, 41 pp. 241-250.

Oudshoorn, B., Driscoll, H. F., Dunn, M. and James, D. (2016a) 'Causation events of stud laceration injuries in rugby union.' *Procedia engineering*, 147 pp. 496-500.

Oudshoorn, B., Driscoll, H., Dunn, M., Senior, T. and James, D. (2018a) 'Development of a test method for assessing laceration injury risk of individual cleats during game-relevant loading conditions.' *Footwear Science*, 10(1) pp. 1-10.

Oudshoorn, B. Y., Driscoll, H. F., Dunn, M. and James, D. (2016b) 'Pressure sensor calibration for measuring stud-player impacts.' *Procedia engineering*, 147 pp. 688-693.

Oudshoorn, B. Y., Driscoll, H. F., Dunn, M. and James, D. (2018b) 'Kinetic and kinematic analysis of stamping impacts during simulated rucking in rugby union.' *Journal of sports sciences*, 36(8) pp. 914-919.

Oudshoorn, B. Y., Driscoll, H., Kilner, K., Dunn, M. and James, D. (2017) 'Prevalence of laceration injuries in professional and amateur rugby union: a systematic review and meta-analysis.' *BMJ open sport & exercise medicine*, 3(1) p. e000239.

Pain, M. T., Tsui, F. and Cove, S. (2008) 'In vivo determination of the effect of shoulder pads on tackling forces in rugby.' *Journal of sports sciences*, 26(8) pp. 855-862.

Palmer-Green, D. S., Stokes, K. A., Fuller, C. W., England, M., Kemp, S. P. and Trewartha, G. (2013) 'Match injuries in English youth academy and schools rugby union: an epidemiological study.' *The American journal of sports medicine*, 41(4) pp. 749-755.

Palmer, R. M. and Green, P. C. (2010) Energy absorbing material. Google Patents.

Panchal, R., Horton, L., Poozesh, P., Baqersad, J. and Nasiriavanaki, M. (2019) 'Vibration analysis of healthy skin: toward a noninvasive skin diagnosis methodology.' *Journal of biomedical optics*, 24(1) p. 015001.

Payne, T., Mitchell, S. and Bibb, R. (2013) 'Design of human surrogates for the study of biomechanical injury: a review.' *Critical Reviews™ in Biomedical Engineering*, 41(1)

Payne, T., O'Rourke, S. and Malbon, C. (2017) 'Body armour standard (2017).' *Home Office*,

Payne, T., Mitchell, S. R., Bibb, R. J. and Waters, M. (2014) 'Initial validation of a relaxed human soft tissue simulant for sports impact surrogates.'

Payne, T., Mitchell, S., Bibb, R. and Waters, M. (2015a) 'The evaluation of new multi-material human soft tissue simulants for sports impact surrogates.' *Journal of the mechanical behavior of biomedical materials*, 41 pp. 336-356.

Payne, T., Mitchell, S., Bibb, R. and Waters, M. (2015b) 'Development of novel synthetic muscle tissues for sports impact surrogates.' *Journal of the mechanical behavior of biomedical materials*, 41 pp. 357-374.

Payne, T., Mitchell, S., Halkon, B., Bibb, R. and Waters, M. (2016) 'Development of a synthetic human thigh impact surrogate for sports personal protective equipment testing.' *Proceedings of the Institution of Mechanical Engineers, Part P: Journal of Sports Engineering and Technology*, 230(1) pp. 5-16.

Phillips, L. H. (2000) 'Sports injury incidence.' *British Journal of Sports Medicine*, 34(2) pp. 133-136.

Plant, D. J. (2016) Energy absorbing system. Google Patents.

Quarrie, K., Gianotti, S. and Murphy, I. (2020) 'Injury risk in New Zealand rugby union: a nationwide study of injury insurance claims from 2005 to 2017.' *Sports medicine*, 50(2) pp. 415-428.

Quarrie, K., Alsop, J., Waller, A. E., Bird, Y., Marshall, S. W. and Chalmers, D. (2001) 'The New Zealand rugby injury and performance project. VI. A prospective cohort study of risk factors for injury in rugby union football.' *British journal of sports medicine*, 35(3) pp. 157-166.

Quarrie, K. L. and Hopkins, W. G. (2008) 'Tackle injuries in professional rugby union.' *The American journal of sports medicine*, 36(9) pp. 1705-1716.

Quarrie, K. L., Cantu, R. C. and Chalmers, D. J. (2002) 'Rugby union injuries to the cervical spine and spinal cord.' *Sports Medicine*, 32(10) pp. 633-653.

Rahman, M. A. and Babu, D. P. 'Simulation of Car Frontal Fascia During Crash using LS-DYNA.'

Ranga, D. and Strangwood, M. (2010) 'Finite element modelling of the quasi-static and dynamic behaviour of a solid sports ball based on component material properties.' *Procedia Engineering*, 2(2) pp. 3287-3292.

Rivlin, R. (1948) 'Large elastic deformations of isotropic materials IV. Further developments of the general theory.' *Philosophical Transactions of the Royal Society of London. Series A, Mathematical and Physical Sciences*, 241(835) pp. 379-397.

Ruan, F. and Bao, L. (2014) 'Mechanical enhancement of UHMWPE fibers by coating with carbon nanoparticles.' *Fibers and Polymers*, 15(4) pp. 723-728.

Ruznan, W. S., Laing, R. M., Lowe, B. J. and Wilson, C. A. (2018) 'Impact attenuation provided by shin guards for field hockey.' *Sports Engineering*, 21(3) pp. 161-175.

Sabesan, V., Steffes, Z., Lombardo, D. J., Petersen-Fitts, G. R. and Jildeh, T. R. (2016) 'Epidemiology and location of rugby injuries treated in US emergency departments from 2004 to 2013.' *Open access journal of sports medicine*, 7 p. 135.

Scott, R. A. (2005) *Textiles for protection.* Elsevier.

Sehaqui, H., Salajková, M., Zhou, Q. and Berglund, L. A. (2010) 'Mechanical performance tailoring of tough ultra-high porosity foams prepared from cellulose I nanofiber suspensions.' *Soft Matter*, 6(8) pp. 1824-1832.

Seimetz, C., Tan, D., Katayama, R. and Lockhart, T. (2012) 'A comparison between methods of measuring postrual stability: force plates versus accelerometers.' *Biomedical sciences instrumentation*, 48 p. 386.

Seminati, E., Cazzola, D., Trewartha, G., Williams, S. and Preatoni, E. (2017) 'Biomechanical loads in rugby union tackling are affected by tackle direction and impact shoulder.' *ISBS Proceedings Archive*, 35(1), 2017, p. 81.

Shanmugam, L., Feng, X. and Yang, J. (2019) 'Enhanced interphase between thermoplastic matrix and UHMWPE fiber sized with CNT-modified polydopamine coating.' *Composites Science and Technology*, 174 pp. 212-220.

Silva, M. A., Cismaşiu, C. and Chiorean, C. (2005) 'Numerical simulation of ballistic impact on composite laminates.' *International Journal of Impact Engineering*, 31(3) pp. 289-306.

Silver, F. H., Freeman, J. W. and DeVore, D. (2001) 'Viscoelastic properties of human skin and processed dermis.' *Skin research and technology*, 7(1) pp. 18-23.

Sinclair, M. (2009) 'Protective Equipment In Rugby – Literature Review '

Song, J., Ortiz, C. and Boyce, M. C. (2011) 'Threat-protection mechanics of an armored fish.' *Journal of the mechanical behavior of biomedical materials*, 4(5) pp. 699-712.

Sorvari, J. and Malinen, M. (2006) 'Determination of the relaxation modulus of a linearly viscoelastic material.' *Mechanics of Time-Dependent Materials*, 10(2) pp. 125-133.

Soykeabkaew, N., Supaphol, P. and Rujiravanit, R. (2004) 'Preparation and characterization of jute-and flax-reinforced starch-based composite foams.' *Carbohydrate Polymers*, 58(1) pp. 53-63.

Svagan, A. J., Samir, M. A. A. and Berglund, L. A. (2008) 'Biomimetic foams of high mechanical performance based on nanostructured cell walls reinforced by native cellulose nanofibrils.' *Advanced Materials*, 20(7) pp. 1263-1269.

The Engineering ToolBox. (2021) *Friction and Friction Coefficients*. [Online] [Accessed on 30th June 2021] https://www.engineeringtoolbox.com/friction-coefficients-d_778.html

Thomson, A. (2014) *Injury in elite rugby players during the Super 15 Rugby tournament.* University of Cape Town.

Toma, M., Njilie, F., Ghajari, M. and Galvanetto, U. (2010) 'Assessing motorcycle crash-related head injuries using finite element simulations.' *International journal of simulation modelling*, 9(3) pp. 143-151.

Tsui, F. (2011) *Determining impact intensities in contact sports.* Doctorate. Loughborough University.

Usman, J., McIntosh, A. S. and Fréchède, B. (2011) 'An investigation of shoulder forces in active shoulder tackles in rugby union football.' *Journal of Science and Medicine in Sport*, 14(6) pp. 547-552.

Usman, J., McIntosh, A. S., Quarrie, K. and Targett, S. (2015) 'Shoulder injuries in elite rugby union football matches: epidemiology and mechanisms.' *Journal of science and medicine in sport*, 18(5) pp. 529-533.

van den Eijnde, W.A.J., 2017. *Skin injury due to artificial turf. The skin as a readout system* (Doctoral dissertation, [Sl: sn]).

Van Dingenen, J. (1989) 'High performance dyneema fibres in composites.' *Materials & Design*, 10(2) pp. 101-104.

Van Mechelen, W., Hlobil, H. and Kemper, H. C. (1992) 'Incidence, severity, aetiology and prevention of sports injuries.' *Sports medicine*, 14(2) pp. 82-99.

Verdejo, R. and Mills, N. (2004) 'Heel–shoe interactions and the durability of EVA foam running-shoe midsoles.' *Journal of biomechanics*, 37(9) pp. 1379-1386.

Wang, X., Gong, R., Dong, Z. and Porat, I. (2007) 'Abrasion resistance of thermally bonded 3D nonwoven fabrics.' *Wear*, 262(3-4) pp. 424-431.

West, D. J., Cook, C. J., Beaven, M. C. and Kilduff, L. P. (2014) 'The influence of the time of day on core temperature and lower body power output in elite rugby union sevens players.' *The Journal of Strength & Conditioning Research*, 28(6) pp. 1524-1528.

West, S. W., Williams, S., Kemp, S. P., Cross, M. J., McKay, C., Fuller, C. W., Taylor, A., Brooks, J. H., et al. (2020) 'Patterns of training volume and injury risk in elite rugby union: An analysis of 1.5 million hours of training exposure over eleven seasons.' *Journal of sports sciences*, 38(3) pp. 238-247.

Westerman, B., Stringfellow, P. and Eccleston, J. (1995) 'Forces transmitted through EVA mouthguard materials of different types and thickness.' *Australian dental journal*, 40(6) pp. 389-391.

Westerman, B., Stringfellow, P., Eccleston, J. and Harbrow, D. (2002) 'Effect of ethylene vinyl acetate (EVA) closed cell foam on transmitted forces in mouthguard material.' *British journal of sports medicine*, 36(3) pp. 205-208.

Whitmarsh, S. K., Amin, D. B., Costi, J. J., Dennis, J. D. and Huveneers, C. (2019) 'Effectiveness of novel fabrics to resist punctures and lacerations from white shark (Carcharodon carcharias): Implications to reduce injuries from shark bites.' *PloS one*, 14(11) p. e0224432.

Williams, S. (2015) *Risk factors for injury in elite rugby union: A series of longitudinal analyses.* University of Bath.

Williams, S., Trewartha, G., Kemp, S. and Stokes, K. (2013) 'A meta-analysis of injuries in senior men's professional Rugby Union.' *Sports Medicine*, 43(10) pp. 1043-1055.

World Rugby™ Regulation 12: Provisions Relating to Players Dress, World Rugby™ Handbook. p. 32.

World Rugby™. (2015b) *World Rugby™ Handbook.*

World Rugby™. (2019) *Body Padding Performance Specification*. [Online] [Accessed https://www.world.rugby/the-game/player-welfare/equipment/specifications/body-padding

World Rugby™. (2021) *Strategic Plan | World Rugby™*. WorldRugby. [Online] [Accessed on 30th June] https://www.world.rugby/organisation/strategic-plan

Xu, F., Lu, T. and Seffen, K. (2008) 'Biothermomechanics of skin tissues.' *Journal of the Mechanics and Physics of Solids*, 56(5) pp. 1852-1884.

Yeoh, O. H. (1993) 'Some forms of the strain energy function for rubber.' *Rubber Chemistry and technology*, 66(5) pp. 754-771.

Yeomans, C., Kenny, I. C., Cahalan, R., Warrington, G. D., Harrison, A. J., Hayes, K., Lyons, M., Campbell, M. J., et al. (2018) 'The incidence of injury in amateur male rugby union: a systematic review and meta-analysis.' *Sports medicine*, 48(4) pp. 837-848.

Zeng, C., Han, X., Lee, L. J., Koelling, K. W. and Tomasko, D. L. (2003) 'Polymer–clay nanocomposite foams prepared using carbon dioxide.' *Advanced Materials*, 15(20) pp. 1743-1747.

Zhou, W., Reddy, N., Yang, Y. and Scott, R. (2005) 'Overview of protective clothing.' *Textiles for protection*, pp. 3-30.

8.   Appendices

8.1   Appendix A - Sample request letter to manufacturers

November 14, 2017

To Rugby Clothing Brand Representative,

RE: Request of padded clothing samples for research and testing

We are a team of researchers from Manchester Metropolitan University (MMU) and The University of Sheffield (UoS) working on a four year project alongside World Rugby to review and update World Rugby Regulation 12 (padded clothing). We aim to ensure Regulation 12 remains for the best interest of the players and for the good of the game. The research team will provide an overview of the project at the upcoming World Rugby Manufacturers meeting on 23rd November 2017, and you will have opportunity to ask questions, and engage in discussions.

The team at MMU, supported by a full-time PhD student, will review the state-of-the-art in padded clothing, investigating how manufacturers may look to apply the latest and emerging materials and technologies. We aim to identify any consequences of introducing new materials and make suggestions for updating Regulation 12 based on our findings.

For this initial phase of the research, the team requires a range of samples of padded clothing, representing different design approaches, to test against the regulation as it currently stands. Ideally, we would like these samples to be provided by the manufacturers. The next phase of the research will involve going beyond the test protocols outlined in the regulation by testing the samples to assess their protection potential against cuts, lacerations and abrasions.

We require at least two samples of each design of padded clothing for each phase of the research study and hence request at least four samples of your best and most innovative products. Test results will be reported back to World Rugby, who will then make the report/s available to the respective manufacturers. We will implement measures to ensure fair play, maintain transparency and avoid conflict of interest, such as: i) results will be anonymized to ensure it is not possible to link products to manufacturers; ii) reports with all test results will only be circulated if samples are provided from at least five manufacturers; and iii) all communications between manufacturers and the research team will be through an open online forum (details TBC). Manufacturers will be provided with the necessary information to link test results to their products.

The findings from this research will shape the way the regulation updates and improves over the next few years. We urge manufacturers to engage with this research program and help us improve the safety of the players while maintaining the nature of the sport.

We look forward to meeting you on 23rd November, where we will welcome any feedback and suggestions. Following the meeting, based on your feedback, we will circulate our requirements via World Rugby along with details of when and where to send samples.

Yours Faithfully,

Regulation 12 Research Team

Drs. Tom Allen, Heather Driscoll, Matt Carré and Mr. Adil Imam

8.2 Appendix B - Mesh Convergence Study

The shoulder surrogate geometry described in Section 5.5.2 was meshed incrementally using different body sizing settings from 12 mm element size to 3 mm in steps of 1 mm and then in steps of 0.5 mm till 2 mm. The resulting mesh generated was used to run an impact simulation at 14.7 J as defined in section 5.5.2. The maximum deformation and the maximum equivalent stress induced were plotted at every iteration. For element size of 3 mm the maximum deformation and the maximum equivalent stress were noted to converge (~120,000 elements). Further refinements only resulted in increased simulation time.
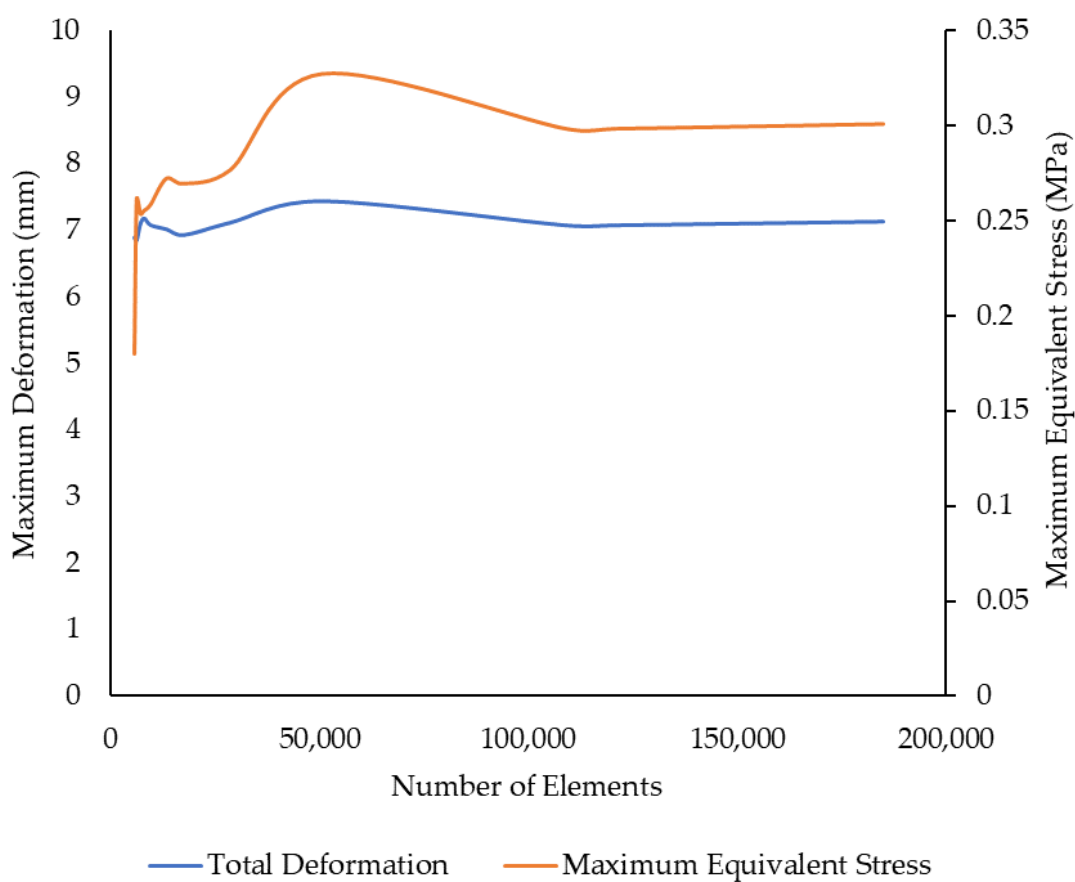
Figure 8-1: Mesh convergence study showing the number of elements and the maximum deformation and maximum equivalent stress induced in the silicone under impact at 14.7 J.

8.3 Appendix C - Simulation of FE Model defined by Payne et al. (2015b)

The single material silicone models generated by Payne et al. (2105b) were studied by recreating the impact scenario they simulated. The impactor setup was defined as a 72 mm diameter, 3 kg hemisphere with an initial velocity of 3 ms⁻¹ (impact energy of 13.5 J). The silicone was formed in the shape of a cylindrical puck of diameter 130 mm and height 50 mm. Here, the impactor was modelled as a sphere and the shape of the puck was maintained as mentioned by Payne et al. (2105b) (Figure Appendix 5-A.1).
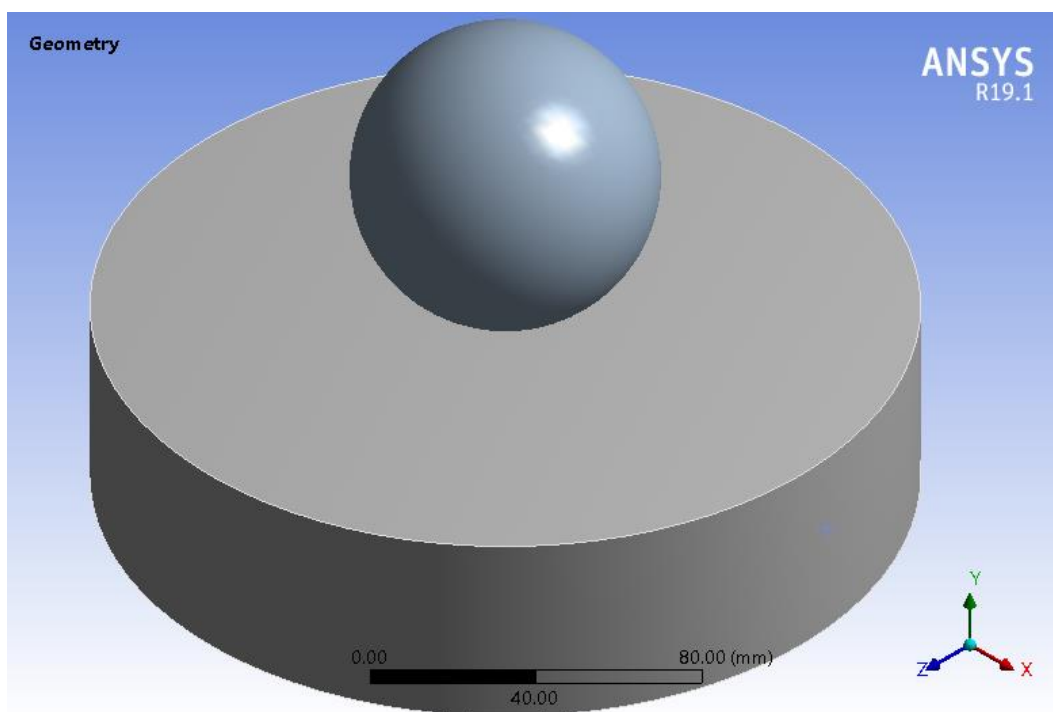
Figure 8-2: Geometry of single material simulation impacts used by Payne et al. (2015b) showing spherical impactor and silicone.

The impactor was assigned a rigid material model (*MAT_RIGID) and the silicone was assigned the different silicone models defined by Payne et al. (2015b). The impactor and silicone were assigned a tetrahedral mesh (ELFORM=10). The impactor was assigned a default mesh sizing (10 mm average sizing) and the silicone mesh was refined using a body sizing of size 3 mm, resulting in the mesh detailed in Table 8-1.

Table 8-1: Mesh details for the geometry setup for simulation impact defined by Payne et al. (2015b).

Part	Nodes	Elements
Silicone	20,646	110,625
Spherical Impactor	4,393	22,536

The bottom face of the silicone was fixed, and the spherical impactor was given an initial velocity of 3 ms^{-1}. The contact was defined between the outer surface of the impactor and the silicone (*AUTOMATIC_SURFACE_TO_SURFACE) with both a static and dynamic coefficient of friction as 0.3.
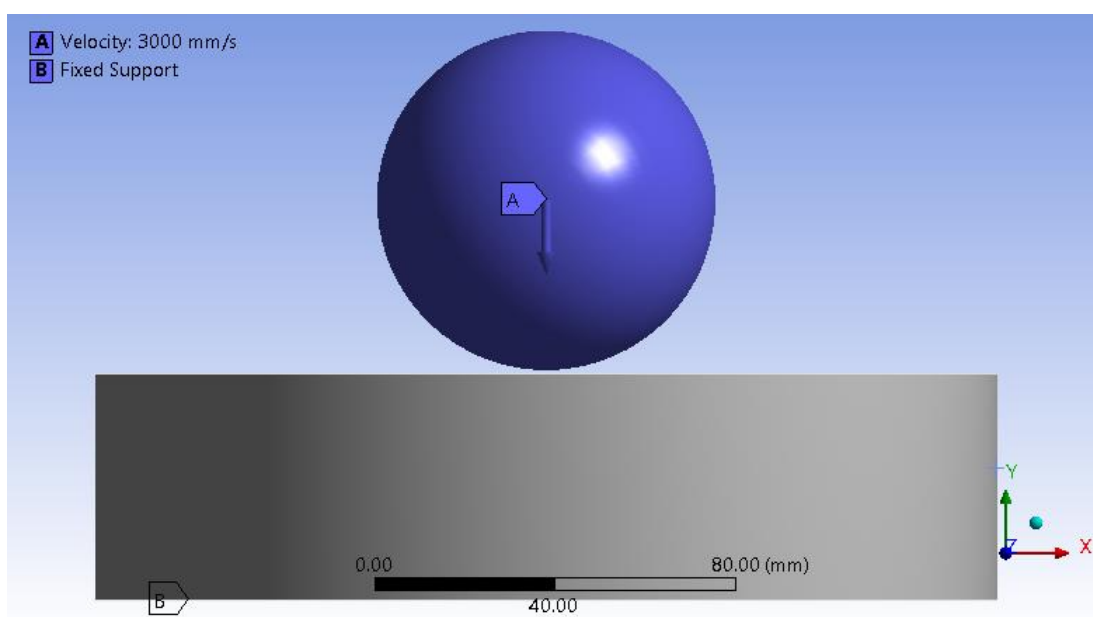
Figure 8-3: Boundary conditions for spherical impactor setup defined by Payne et al. (2015b) .

The simulations were run for a duration of 15 ms and the peak force values were noted. The simulations were run using the three single material silicone models defined by Payne et al. (2015b) (Table 5-8). Payne et al. (2015b) defined a critical damping fraction of 0.1 applied in both the normal and tangential directions. Element distortion limits were also applied by Payne et al. (2015b) to limit the maximum element deformation to a nominal strain of 0.9. These damping and element distortion limits could not be directly replicated in Ansys© Workbench.

The peak impact force values obtained from recreating the simulations in Ansys © were lower than those reported by Payne et al. (2015b) (Table 8-2). This

underprediction of peak impact force may be due to the models omitting the damping and element distortion criterion set by Payne and colleagues. The silicone model developed in Chapter 5 was reliant on the frequency independent damping setting to align closely with the experimental values. The effect of applying the damping settings used for the silicone model developed here to the silicone models developed by Payne et al. (2015b) is investigated in Appendix B.

Table 8-2: Differences between the FE model values reported by Payne et al. (2015b) and recreated simulations in Ansys©.

Model	Simulation Peak Force (N)		Difference (%)
	Reported Value-Abaqus	Recreated in Ansys	
Silicone 3481	1,754	1,003	-43
Silicone 3483	1,335	1,065	-20
Silicone 3487	1,160	980	-16

8.4 Appendix D - Effect of Damping of FE Model defined by Payne et al. (2015b)

Comparison of the single material silicones modelled by Payne et al. (2015b) against the silicone model developed in this study showed discrepancies in peak impact force. For the model developed in Chapter 5, it was noted that adding frequency independent damping substantially increased the peak force values and the dynamic hardness (reduced deformation) of the silicone. Hence, the damping settings (shear modulus of 47 MPa for frequency independent damping) used in Chapter 5 were applied to the single material silicone simulations (4.9 J impact energy) presented in Section 5.5.5). The force traces from the simulations were plotted against those without damping and force traces were compared. Adding damping had more effect on the peak impact force of the silicone modelled here (~700 N increase) than those modelled by Payne et al. (2015b) (~100 N increase) (Figure 8-4). One simulation was performed with a shear stress of 100 MPa (maximum damping applied in the sensitivity study) and the peak force was shown to increase by ~150 N in comparison to when no damping was applied.
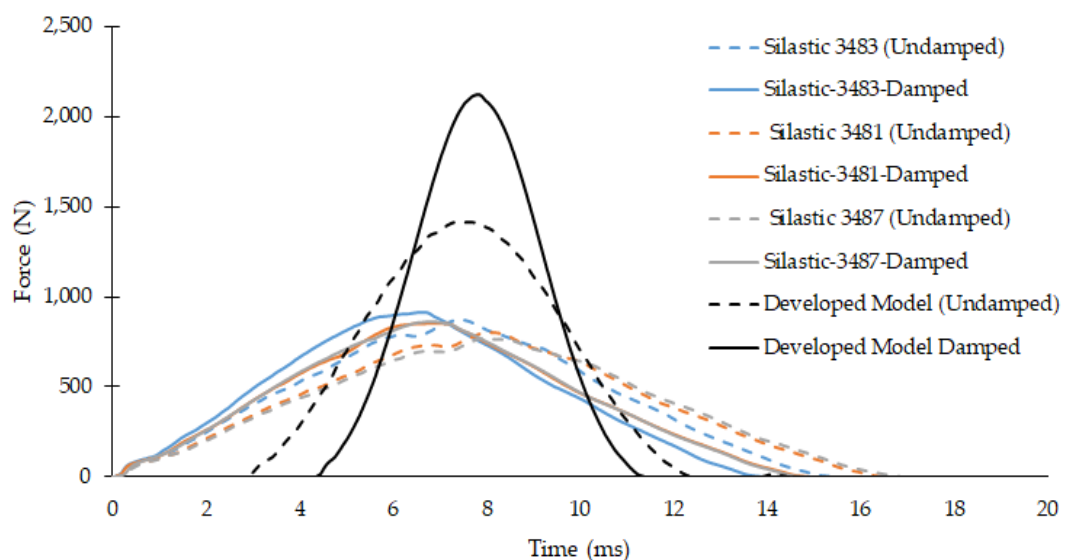
Figure 8-4: Effect of adding frequency independent damping to the model developed by Payne et al. (2015b). Shear modulus value of 47 MPa for frequency independent damping used.

8.5   **Appendix E - Acceptable stud dimensions**

Snippet of the acceptable stud dimensions as defined by World Rugby™ in Regulation-12 Schedule 2

Acceptable dimensions for conical or cylindrical studs/cleats
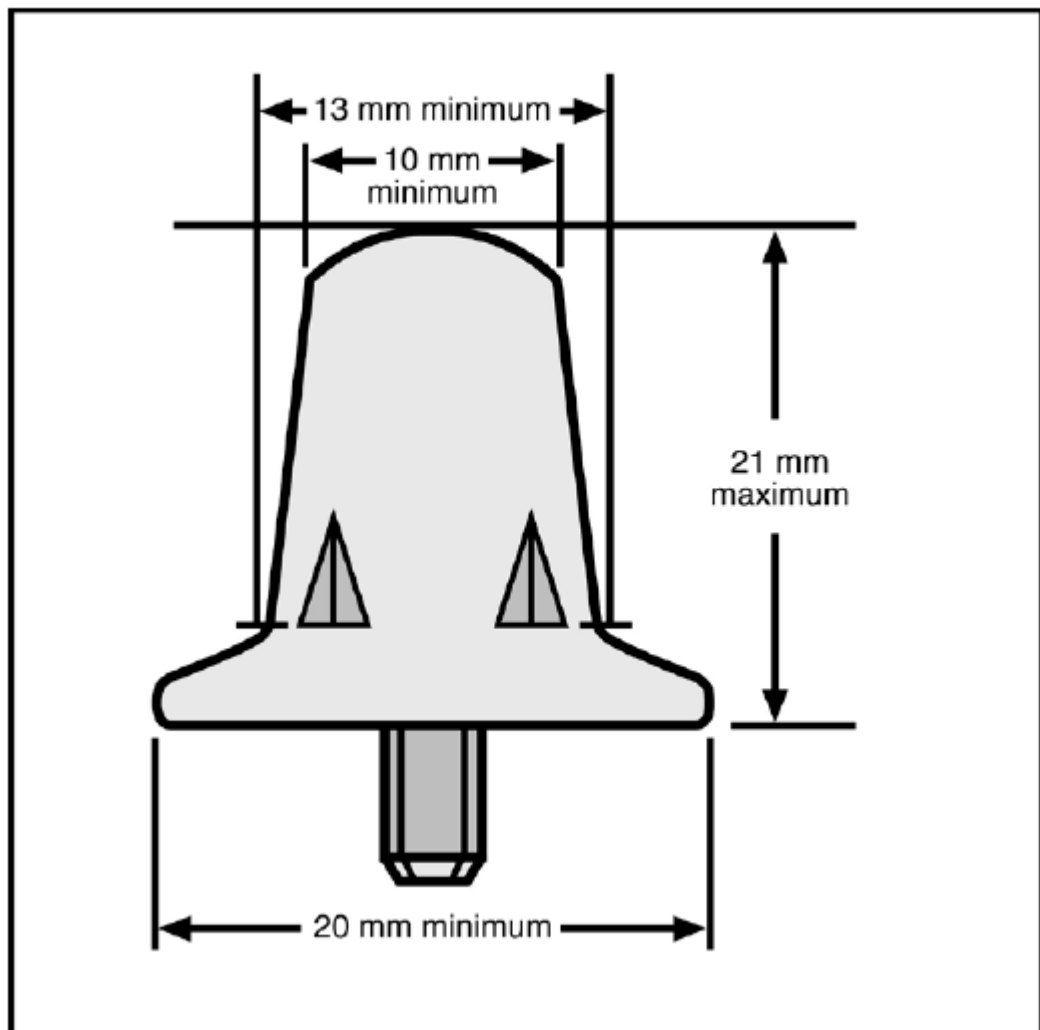
8.6 Appendix F - Effect of stud impact location on impact force

The force trace showed little variance when the silicone was rotated or moved along the length of the steel core to change the impact location. Notable difference can be seen in the force trace when the impact is carried out on the location where a tear already exists (Figure 8-5)
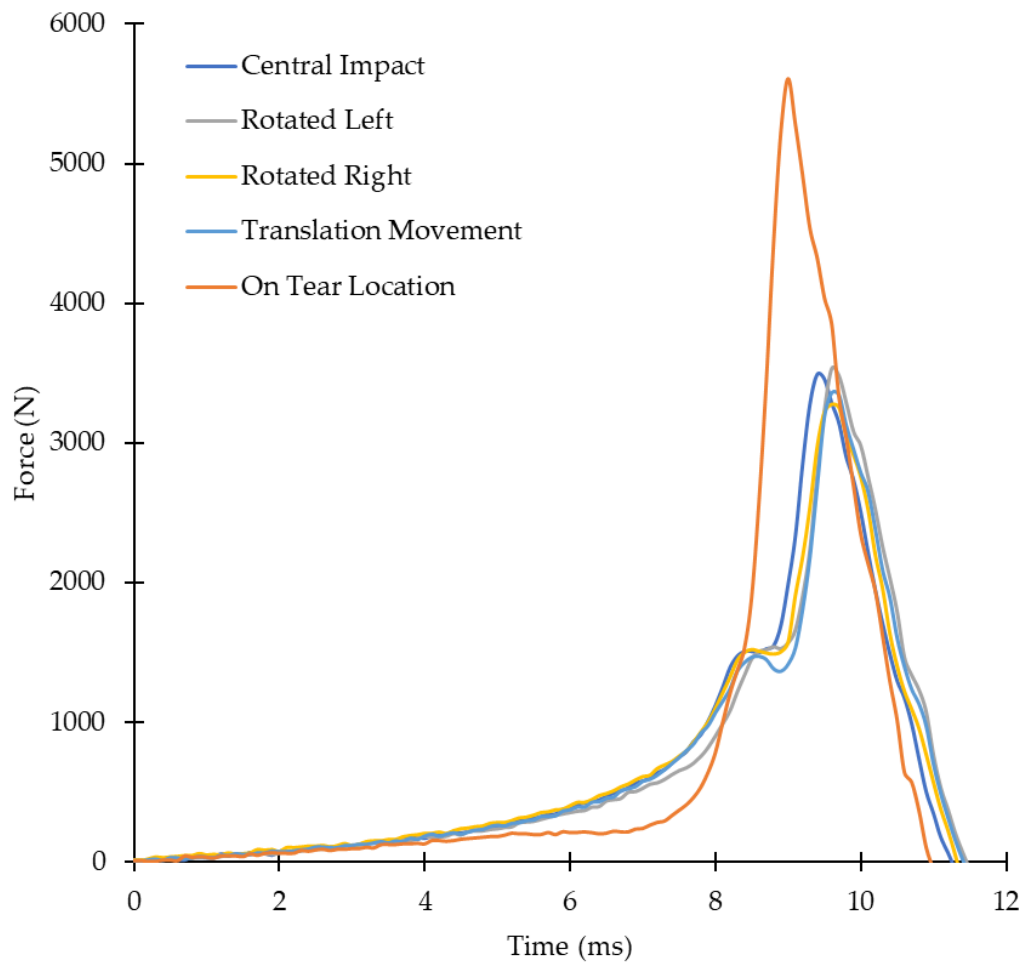
Figure 8-5: Force trace of different impact locations and one impact on existing tear location.

8.7   Appendix G - SynDaver ™ Lab Specification Sheet

SynDaver™ Labs

8506 Benjamin Road, Suite C, Tampa, Florida 33634   •   Main: 813-600-5530   •   Fax: 813-600-3235

Specification Sheet
SynDaver™ Abdominal Tissue Plate
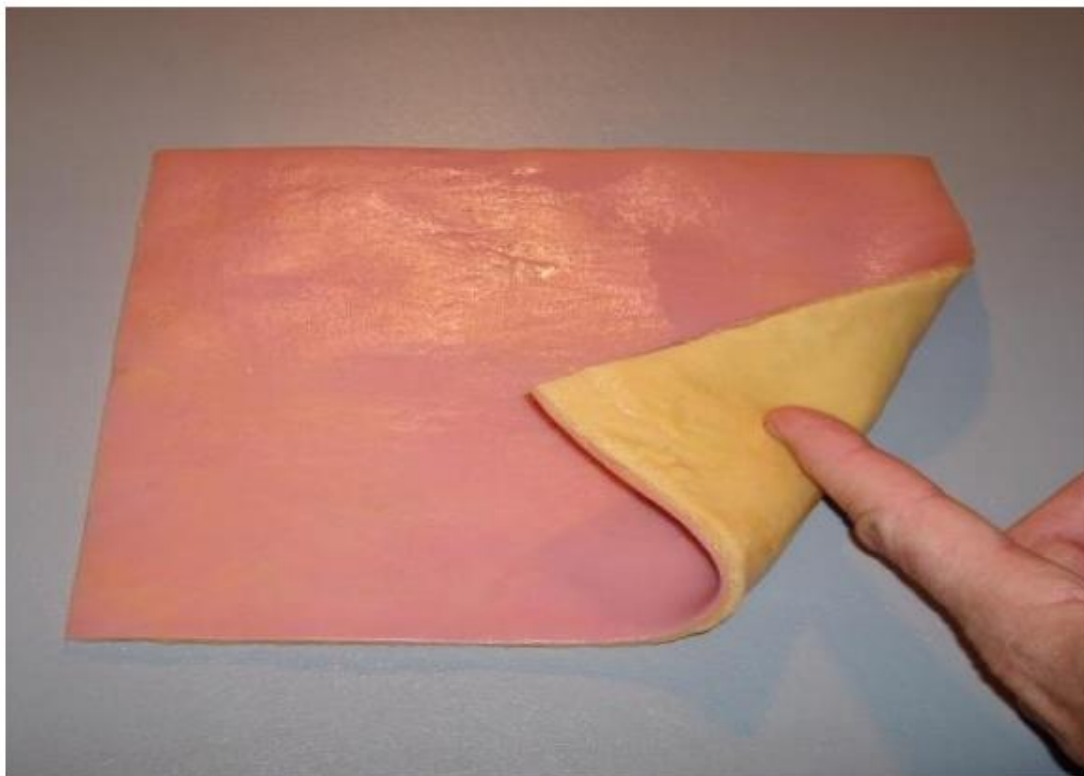
Standard Ethnicities: Caucasian, African, Asian, Albino

Available Pathologies: freckles, moles, skin tags, warts, abcess, fibroids, and scar tissue.

Included Layers: Skin, Bulk Fat, Scarpas Fascia, Bulk Fat, Mucosal Fascia, Skeletal Muscle, Fascia Latae

Skin: 2N Caucasian / 1.0mm Standard

Fat Layers: Bulk Construction / 10.0mm Standard

Fascia Planes: 1.0mm Standard

Skeletal Muscle: Fatty Construction / 10.0mm Standard

Puncture Grades: 2N, 4N, 6N, 10N (all ± 0.2N)
1mm blunt tungsten rod at 15mm / sec

Tensile Modulus (x): 21 ± 1.5 kPa
5mm / sec strain rate with 5% biaxial loading

Tensile Modulus (y): 29 ± 1.7 kPa
5mm / sec strain rate with 5% biaxial loading

SYNDAVER LABS

8.8 Appendix H - Principal Stress Plots

Equivalent stress contours on the surface were plotted in Section 6.9 Figure 6-24-26. Equivalent stress was used as it provided a better visual representation of the stress induced on the surface of the skin. Since principal stress was used for element deletion criterion, plots showing the principle stress occurring on the surface of the silicone are included here (Figures 8-6 to 8).
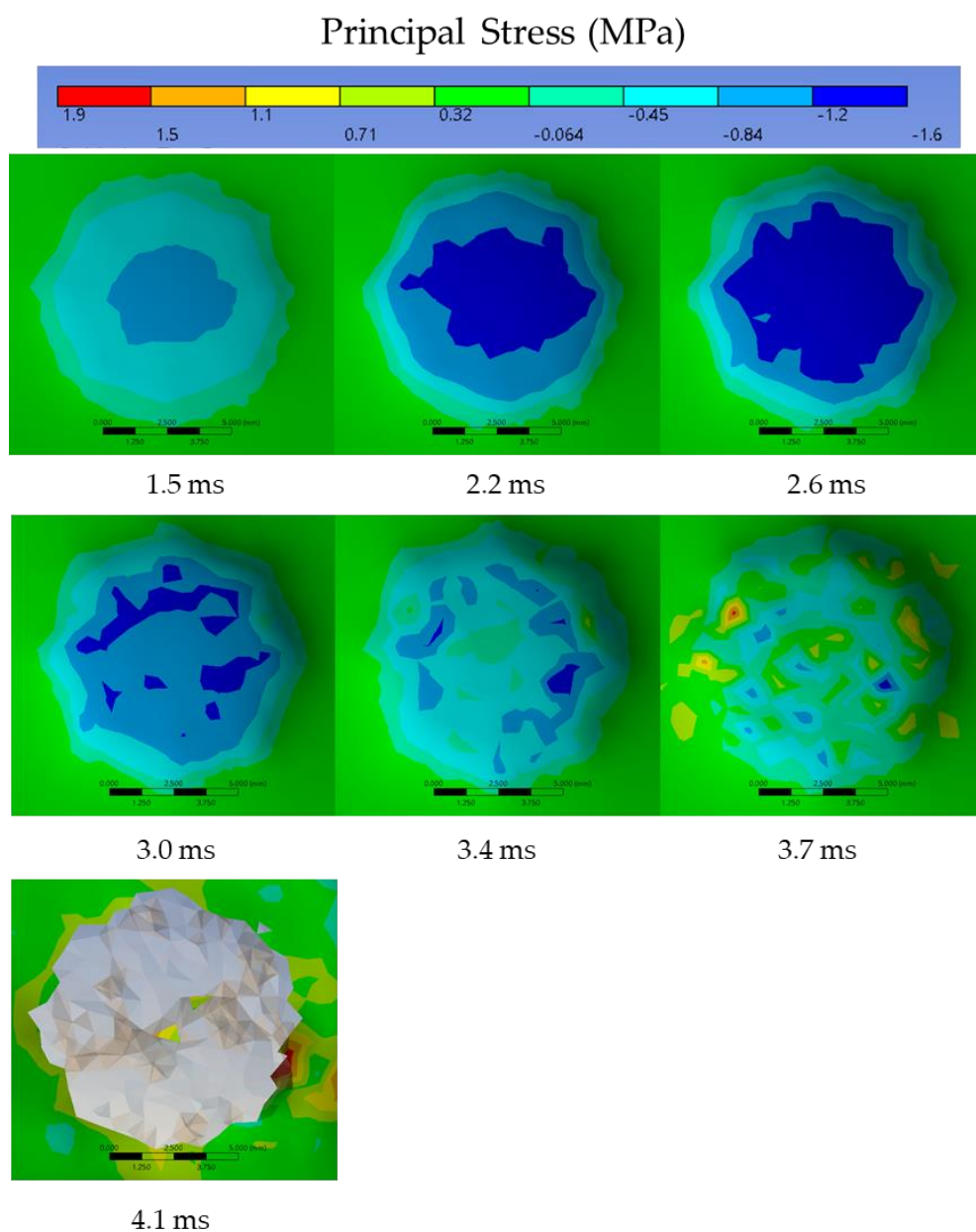
Figure 8-6: Principal stress contours occurring on the silicone top surface at 0° orientation at different time steps during the simulation. (Stud geometry has been hidden to get a clear view of the silicone top surface). Element deletion criterion: maximum principal stress value of 16 MPa.
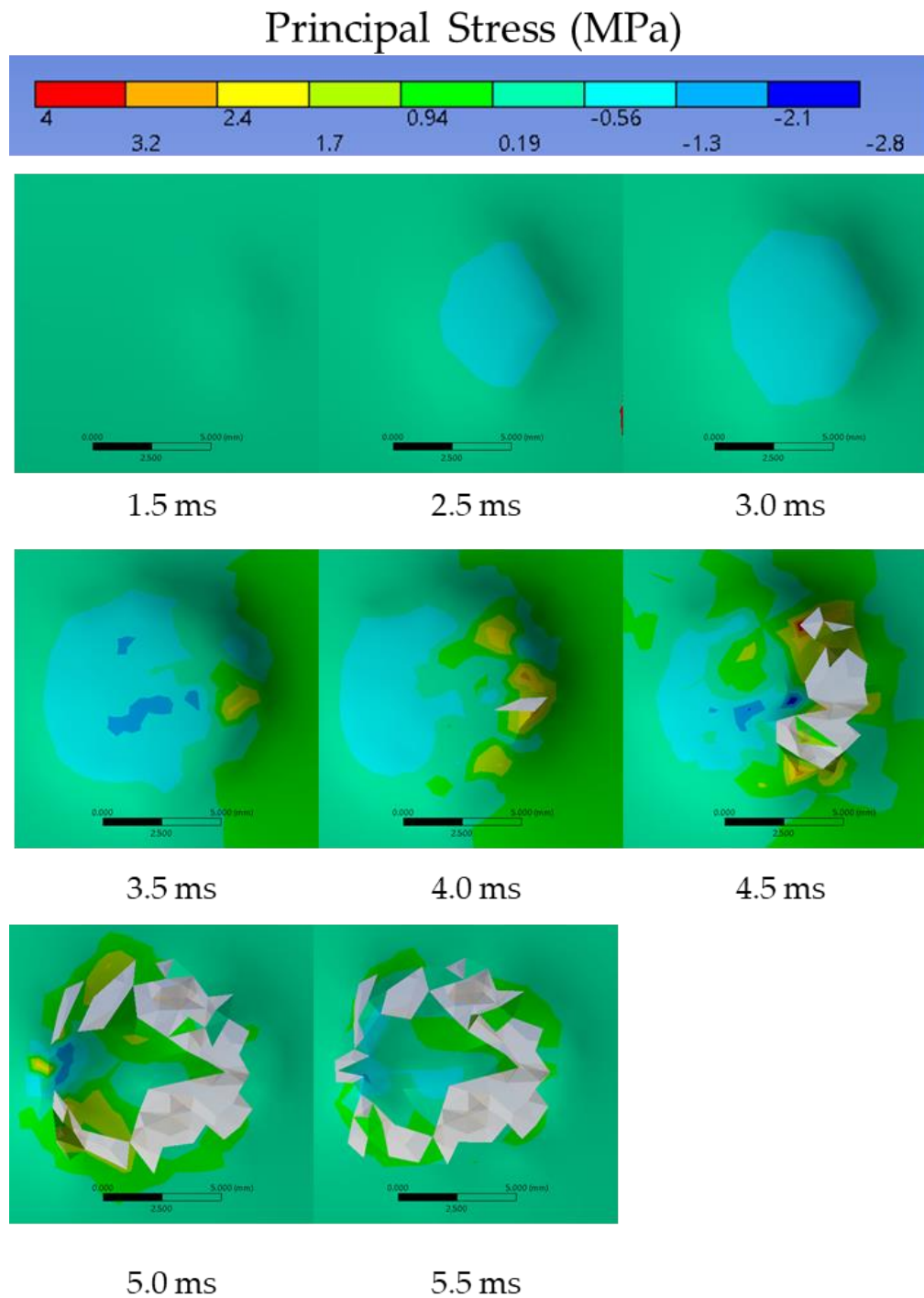
Figure 8-7: Principal stress contours occurring on the silicone top surface at 15° orientation at different time steps during the simulation. (Stud geometry has been hidden to get a clear view of the silicone top surface). Element deletion criterion: maximum principal stress value of 31 MPa.

Principal Stress (MPa)

1.5 ms	2.5 ms	3.0 ms
4.0 ms	4.5 ms	5.0 ms
5.5 ms	6.5 ms	7.0 ms
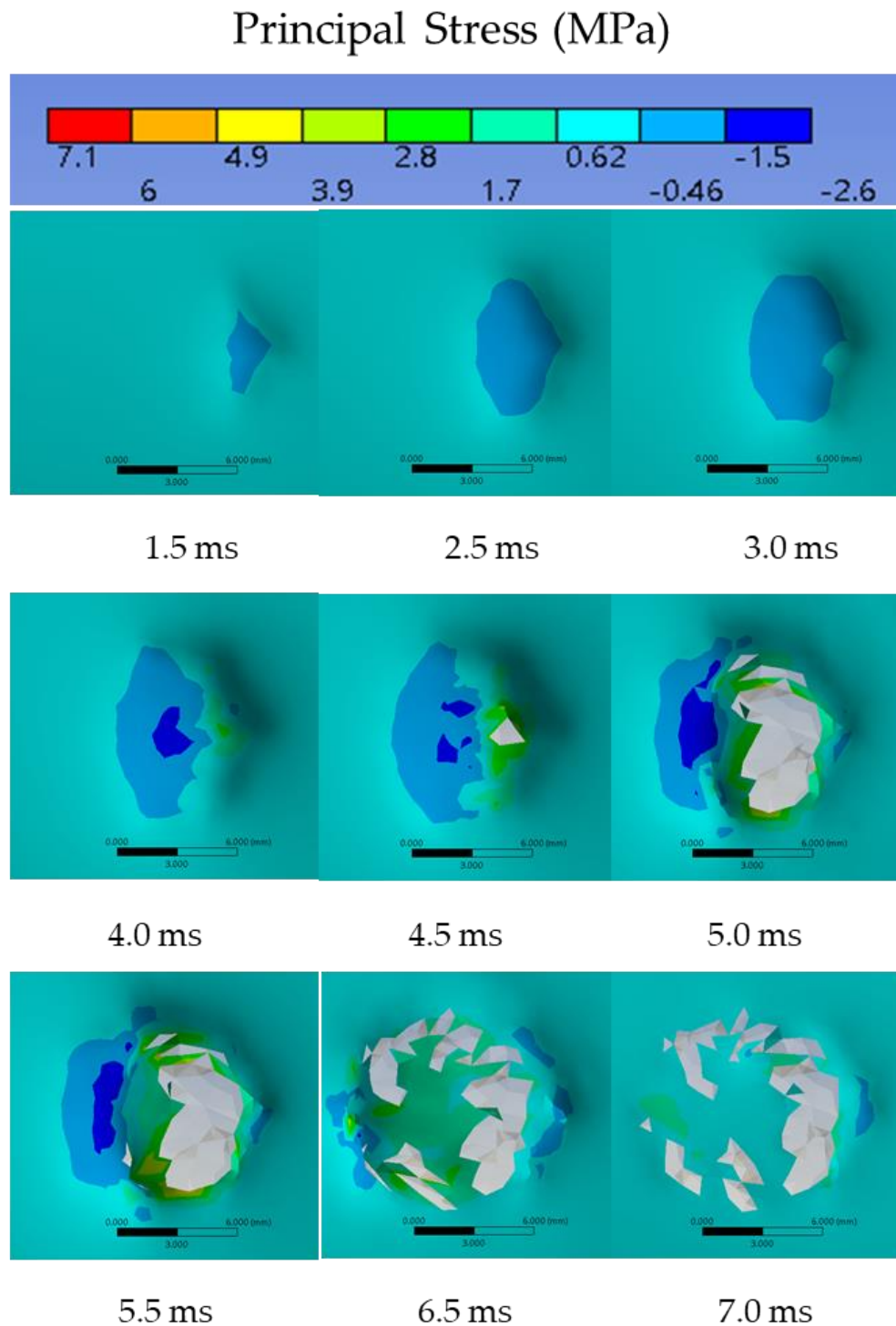
Figure 8-8: Principal stress contours occurring on the silicone top surface at 30° orientation at different time steps during the simulation. (Stud geometry has been hidden to get a clear view of the silicone top surface). Element deletion criterion: maximum principal stress value of 31 MPa.

8.9 Appendix I - K File information and Snippets

A snippet of the K file manual for *MAT_HYPERELASTIC_RUBBER is shown with the corresponding keyword file from the simulation. More information can be found in the LS-DYNA® Keywords User's Manual-Volume II Material Models, available online.

*MAT_HYPERELASTIC_RUBBER

This is Material Type 77. This material model provides a general hyperelastic rubber model combined optionally with linear viscoelasticity as outlined by Christensen [1980].

Card 1	1	2	3	4	5	6	7	8
Variable	MID	RO	PR	N	NV	G	SIGF	REF
Type	A8	F	F	I	I	F	F	F

Card 3 for N = 0. Set the hyperelastic material parameters directly.

Card 3	1	2	3	4	5	6	7	8
Variable	C10	C01	C11	C20	C02	C30	THERML	
Type	F	F	F	F	F	F	F	

Optional Viscoelastic Constants & Frictional Damping Constant Cards. Up to 12 cards may be input. A keyword card (with a "*" in column 1) terminates this input if less than 12 cards are used.

Card 4	1	2	3	4	5	6	7	8
Variable	Gi	BETAi	Gj	SIGFj				
Type	F	F	F	F				

Variable	Description
MID	Material ID
RO	Mass Density
PR	Poisson's Ratio
N	Number of constants to solve for:

	EQ.1: Solve for C10 and C01; EQ.2: Solve for C10, C01, C11, C20, and C02; EQ.3: Solve for C10, C01, C11, C20, C02, and C30
NV	Number of Prony Series term in fit (if raw data is input)
G	Shear Modulus for frequency independent damping
SIGF	Limit Stress for frequency independent frictional damping
REF	Use reference geometry to initialize the stress tensor
C10	
C01	
C11	Material Constants
C20	
C02	
C30	
THERML	Flag for thermal option
Gi	Optional shear relaxation Modulus for the i^{it} term
BETAi	Optional decay constant for the i^{it} term

Based on the snippets from LS-DYNA Manual, the hyperelastic card for the model developed in this study is as below.

```
*MAT_HYPERELASTIC_RUBBER
         1       1E-9      0.48          0          0       46.9       0.01          0
   -0.9302      1.009     -36.07      13.67      24.66          0
  0.011687    0.40463
  0.934729   0.010058
```

The snippet for the element deletion criterion is as below.

```
*MAT_ADD_EROSION
$       ID       excl     mxpres      mneps     effeps     voleps     numfip        ncs
         1          0          0          0          0          0          0          1
$   mnpres      sigp1      sigvm      mxeps      epssh      sigth    impulse     failtm
         0         31          0          0          0          0          0          0
```

Snippet of the Solution information output for a stud impact without refined mesh showing the element deletion at a given time step.

```
1148 t 9.9972E-04 dt 8.84E-07 write d3plot file
1149 t 1.0006E-03 dt 8.84E-07 write intfor file
2306 t 1.9997E-03 dt 8.37E-07 write d3plot file
2307 t 2.0006E-03 dt 8.37E-07 write intfor file
3479 t 2.9993E-03 dt 8.84E-07 write d3plot file
3480 t 3.0002E-03 dt 8.84E-07 write intfor file
4661 t 3.9992E-03 dt 8.32E-07 write d3plot file
4662 t 4.0000E-03 dt 8.32E-07 write intfor file
5000 t 4.2816E-03 dt 8.32E-07 flush i/o buffers
5854 t 4.9994E-03 dt 8.32E-07 write d3plot file
5855 t 5.0002E-03 dt 8.32E-07 write intfor file
7097 t 5.9998E-03 dt 7.61E-07 write d3plot file
7098 t 6.0005E-03 dt 7.61E-07 write intfor file
 solid element        34055  failed at time  6.2086E-03
 solid element        10986  failed at time  6.2108E-03
 solid element        11820  failed at time  6.2116E-03
 solid element        43560  failed at time  6.2131E-03
 solid element        23113  failed at time  6.2138E-03
 solid element        11148  failed at time  6.2161E-03
 solid element        11710  failed at time  6.2161E-03
 solid element        44022  failed at time  6.2460E-03
 solid element        11957  failed at time  6.2505E-03
 node  number          6653 deleted at time  6.2698E-03
 solid element        33162  failed at time  6.2698E-03
 solid element        33346  failed at time  6.3436E-03
 solid element       100151  failed at time  6.3453E-03
 solid element        11940  failed at time  6.3461E-03
 solid element        53472  failed at time  6.3478E-03
 solid element        11852  failed at time  6.3494E-03
 solid element        22709  failed at time  6.3494E-03
 solid element        67212  failed at time  6.3494E-03
 solid element        11848  failed at time  6.3510E-03
 solid element        11541  failed at time  6.3544E-03
 node  number          6654 deleted at time  6.3669E-03
 solid element        53471  failed at time  6.3669E-03
8320 t 6.9997E-03 dt 8.32E-07 write d3plot file
8321 t 7.0006E-03 dt 8.32E-07 write intfor file
9507 t 7.9999E-03 dt 8.35E-07 write d3plot file
9508 t 8.0007E-03 dt 8.35E-07 write intfor file
```

Figure 8-9: Snippet of the solution information sheet showing element deletion.

8.10   Appendix J- Statistics

One-way ANOVA: Comparing Degradation Pre and Post Impact test

Method

Null hypothesis	All means are equal
Alternative hypothesis	Not all means are equal
Significance level	$\alpha = 0.05$

Equal variances were not assumed for the analysis.

Means

Factor	N	Mean	95% CI
1	3	101.50	(93.56, 109.44)
2	3	101.30	(96.56, 106.04)
3	3	103.20	(93.93, 112.47)
4	3	104.20	(91.66, 116.74)
5	3	91.03	(77.91, 104.16)
6	3	115.57	(96.67, 134.46)

Games-Howell Pairwise Comparisons

Grouping Information Using the Games-Howell Method and 95% Confidence

Factor	N	Mean	Grouping
6	3	115.57	A
4	3	104.20	A
3	3	103.20	A
1	3	101.50	A
2	3	101.30	A
5	3	91.03	A

Means that do not share a letter are significantly different.

Games-Howell Simultaneous Tests for Differences of Means

Difference of Levels	Difference of Means	SE of Difference	95% CI	T-Value	Adjusted P-Value
2 - 1	-0.20	2.15	(-11.70, 11.30)	-0.09	1.000
3 - 1	1.70	2.84	(-11.92, 15.32)	0.60	0.985
4 - 1	2.70	3.45	(-15.35, 20.75)	0.78	0.955
5 - 1	-10.47	3.57	(-29.45, 8.52)	-2.94	0.234
6 - 1	14.07	4.76	(-15.47, 43.60)	2.95	0.263
3 - 2	1.90	2.42	(-11.93, 15.73)	0.79	0.953
4 - 2	2.90	3.12	(-17.21, 23.01)	0.93	0.912
5 - 2	-10.27	3.24	(-31.57, 11.04)	-3.17	0.241
6 - 2	14.27	4.53	(-18.77, 47.30)	3.15	0.263
4 - 3	1.00	3.62	(-16.99, 18.99)	0.28	1.000
5 - 3	-12.17	3.74	(-30.97, 6.64)	-3.26	0.172
6 - 3	12.37	4.89	(-16.06, 40.80)	2.53	0.337
5 - 4	-13.17	4.22	(-33.19, 6.85)	-3.12	0.177
6 - 4	11.37	5.27	(-15.73, 38.46)	2.16	0.421
6 - 5	24.53	5.35	(-2.54, 51.60)	4.59	0.067

One-way ANOVA: Force at tear versus Energy-Orientation

Method

Null hypothesis	All means are equal
Alternative hypothesis	Not all means are equal
Significance level	$\alpha = 0.05$

Equal variances were not assumed for the analysis.

Means

Energy-Orientation	N	Mean	95% CI
4_0	6	365.2	(326.0, 404.4)
4_15	6	303.5	(272.2, 334.8)
4_30	6	231.95	(207.55, 256.35)
6_0	6	414.4	(372.8, 455.9)
6_15	6	338.4	(311.2, 365.7)
6_30	6	284.7	(251.9, 317.4)

Games-Howell Pairwise Comparisons

Grouping Information Using the Games-Howell Method and 95% Confidence

Energy-Orientation	N	Mean	Grouping			
6_0	6	414.4	A			
4_0	6	365.2	A	B		
6_15	6	338.4		B	C	
4_15	6	303.5		B	C	
6_30	6	284.7			C	D
4_30	6	231.95				D

Means that do not share a letter are significantly different.

Games-Howell Simultaneous Tests for Differences of Means

Difference of Levels	Difference of Means	SE of Difference	95% CI	T-Value	Adjusted P-Value
4_15 - 4_0	-61.7	19.5	(-130.2, 6.8)	-3.16	0.084
4_30 - 4_0	-133.2	18.0	(-198.2, -68.3)	-7.42	0.001
6_0 - 4_0	49.2	22.2	(-28.1, 126.5)	2.21	0.311
6_15 - 4_0	-26.8	18.6	(-92.8, 39.3)	-1.44	0.706
6_30 - 4_0	-80.5	19.9	(-149.9, -11.1)	-4.05	0.022
4_30 - 4_15	-71.5	15.4	(-125.8, -17.2)	-4.63	0.010
6_0 - 4_15	110.9	20.2	(39.5, 182.3)	5.48	0.003
6_15 - 4_15	35.0	16.2	(-21.4, 91.3)	2.16	0.332
6_30 - 4_15	-18.8	17.6	(-80.0, 42.4)	-1.07	0.884
6_0 - 4_30	182.4	18.7	(114.2, 250.7)	9.73	0.000
6_15 - 4_30	106.5	14.2	(57.0, 156.0)	7.48	0.000
6_30 - 4_30	52.7	15.9	(-3.3, 108.8)	3.32	0.068
6_15 - 6_0	-75.9	19.3	(-145.2, -6.6)	-3.93	0.031
6_30 - 6_0	-129.7	20.6	(-202.0, -57.4)	-6.30	0.001
6_30 - 6_15	-53.8	16.6	(-111.6, 4.1)	-3.24	0.073

One-way ANOVA: Time to Tear versus Energy-Orientation

Method

Null hypothesis	All means are equal
Alternative hypothesis	Not all means are equal
Significance level	$\alpha = 0.05$

Equal variances were not assumed for the analysis.

Means

Energy-Orientation	N	Mean	95% CI
4_0	6	5.2333	(4.9791, 5.4875)
4_15	6	6.6167	(6.5377, 6.6957)
4_30	6	9.117	(8.769, 9.464)
6_0	6	4.8667	(4.6953, 5.0380)
6_15	6	6.0167	(5.8622, 6.1711)
6_30	6	7.5000	(7.2517, 7.7483)

Games-Howell Pairwise Comparisons

Grouping Information Using the Games-Howell Method and 95% Confidence

Energy-Orientation	N	Mean	Grouping				
4_30	6	9.117	A				
6_30	6	7.5000		B			
4_15	6	6.6167			C		
6_15	6	6.0167				D	
4_0	6	5.2333					E
6_0	6	4.8667					E

Means that do not share a letter are significantly different.

Games-Howell Simultaneous Tests for Differences of Means

Difference of Levels	Difference of Means	SE of Difference	95% CI	T-Value	Adjusted P-Value
4_15 - 4_0	1.383	0.104	(0.970, 1.796)	13.36	0.000
4_30 - 4_0	3.883	0.167	(3.291, 4.476)	23.18	0.000
6_0 - 4_0	-0.367	0.119	(-0.793, 0.059)	-3.07	0.101
6_15 - 4_0	0.783	0.116	(0.364, 1.203)	6.77	0.001
6_30 - 4_0	2.267	0.138	(1.787, 2.747)	16.40	0.000
4_30 - 4_15	2.500	0.139	(1.931, 3.069)	18.03	0.000
6_0 - 4_15	-1.7500	0.0734	(-2.0277, -1.4723)	-23.84	0.000
6_15 - 4_15	-0.6000	0.0675	(-0.8515, -0.3485)	-8.89	0.000
6_30 - 4_15	0.883	0.101	(0.480, 1.287)	8.71	0.001
6_0 - 4_30	-4.250	0.151	(-4.815, -3.685)	-28.19	0.000
6_15 - 4_30	-3.100	0.148	(-3.663, -2.537)	-20.95	0.000
6_30 - 4_30	-1.617	0.166	(-2.207, -1.027)	-9.73	0.000
6_15 - 6_0	1.1500	0.0898	(0.8378, 1.4622)	12.81	0.000
6_30 - 6_0	2.633	0.117	(2.215, 3.052)	22.43	0.000
6_30 - 6_15	1.483	0.114	(1.072, 1.894)	13.04	0.000

Descriptive statistics of the different hardness variables measured in Chapter 4, the peak impact acceleration values and measured density are presented below.

Variable	Sample	Total Count	Mean	SD	CV	Minimum	Median	Maximum	Range
A	1	3	220	3	1	218	220	223	5
	2	3	178	2	1	176	177	180	4
	3	3	154	10	7	145	153	165	20
	4	3	204	2	1	202	203	206	4
	5	3	97	19	20	82	90	118	36
	6	3	145	8	5	137	146	152	15
	7	3	169	12	7	158	168	181	23
	8	3	97	9	9	89	97	106	17
	9	3	128	4	3	124	128	132	8
	10	3	196	41	21	152	205	232	80
	11	3	46	1	1	45	46	46	1
	12	3	274	14	5	261	273	289	28

Variable	Sample	Total Count	Mean	SD	CV	Minimum	Median	Maximum	Range
B-25	1	3	129	2	2	127	129	131	4
	2	3	97	4	4	93	98	101	8
	3	3	90	4	5	86	89	94	8
	4	3	111	6	6	104	113	116	12
	5	3	46	7	15	40	44	53	13
	6	3	76	7	9	69	77	83	14
	7	3	102	12	12	89	105	113	24
	8	3	44	9	19	35	46	52	17
	9	3	61	4	6	58	59	65	7
	10	3	96	10	11	90	91	108	18
	11	3	33	2	5	31	34	34	3
	12	3	202	17	8	185	201	219	34

Variable	Sample	Total Count	Mean	SD	CV	Minimum	Median	Maximum	Range

B-40	1	3	234	1	0	233	234	234	1
	2	3	187	8	4	178	188	194	16
	3	3	171	10	6	161	172	180	19
	4	3	206	9	4	198	204	215	17
	5	3	124	5	4	119	125	129	10
	6	3	156	6	4	150	155	162	12
	7	3	187	13	7	172	191	198	26
	8	3	104	13	13	89	111	113	24
	9	3	134	4	3	131	132	139	8
	10	3	197	18	9	180	197	215	35
	11	3	54	4	7	50	56	57	7
	12	3	354	19	5	338	350	375	37

Variable	Sample	Total Count	Mean	SD	CV	Minimum	Median	Maximum	Range
B-65	1	3	590	13	2	576	594	601	25
	2	3	511	31	6	479	513	541	62
	3	3	460	36	8	420	469	491	71
	4	3	518	26	5	500	505	548	48
	5	3	330	49	15	290	316	384	94
	6	3	423	5	1	417	425	426	9
	7	3	452	33	7	415	461	479	64
	8	3	368	34	9	338	362	405	67
	9	3	409	13	3	396	409	422	26
	10	3	577	84	14	485	599	648	163
	11	3	174	22	12	150	181	192	42
	12	3	781	63	8	733	759	852	119

Variable	Sample	Total Count	Mean	SD	CV	Minimum	Median	Maximum	Range
C	1	3	248	2	1	247	248	250	3
	2	3	175	9	5	167	173	185	18
	3	3	184	10	5	177	179	195	18
	4	3	236	5	2	233	233	241	8
	5	3	201	6	3	195	202	206	11
	6	3	161	8	5	156	158	170	14
	7	3	189	10	5	181	185	200	19
	8	3	105	12	11	95	101	118	23
	9	3	112	7	6	106	110	119	13
	10	3	207	38	18	165	217	239	74
	11	3	64	5	7	60	64	69	9
	12	3	337	15	5	319	345	346	27

Variable	Sample	Total Count	Mean	SD	CV	Minimum	Median	Maximum	Range
D	1	3	131	7	5	125	130	138	13
	2	3	102	2	2	100	103	103	3
	3	3	83	5	6	79	82	88	9
	4	3	118	1	0	117	118	118	1
	5	3	33	4	12	29	33	37	8
	6	3	77	6	7	71	77	82	11
	7	3	94	3	3	92	94	97	5
	8	3	38	3	8	36	37	42	6
	9	3	59	3	5	56	60	62	6
	10	3	78	8	10	69	81	83	14
	11	3	24	3	12	21	26	26	5
	12	3	169	1	1	168	169	170	2

Variable	Sample	Total Count	Mean	SD	CV	Minimum	Median	Maximum	Range
E	1	3	4.3	0.1	2.7	4.2	4.2	4.4	0.2
	2	3	5.0	0.2	4.7	4.7	5.1	5.1	0.4
	3	3	4.9	0.3	6.6	4.5	5.0	5.1	0.6
	4	3	4.4	0.2	3.5	4.2	4.4	4.5	0.3
	5	3	5.9	0.7	11.8	5.2	6.0	6.6	1.4
	6	3	4.9	0.2	4.1	4.7	4.9	5.1	0.4
	7	3	3.9	0.1	3.0	3.8	3.8	4.0	0.2
	8	3	7.2	0.1	1.6	7.1	7.1	7.3	0.2
	9	3	5.3	0.1	1.1	5.2	5.3	5.3	0.1
	10	3	4.8	0.4	7.4	4.4	4.8	5.1	0.7
	11	3	6.1	0.3	5.0	5.8	6.2	6.4	0.6
	12	3	2.9	0.0	0.0	2.9	2.9	2.9	0.0

Variable	Sample	Total Count	Mean	SD	CV	Minimum	Median	Maximum	Range
4.9 J	1	3	57	1	2	56	57	59	3
	2	3	57	2	3	55	58	58	3
	3	3	71	2	3	68	71	73	4
	4	3	62	0	0	62	62	62	0
	5	3	106	5	4	101	106	110	9
	6	3	66	2	4	64	67	69	5
	7	3	56	2	4	54	56	59	5
	8	3	113	3	2	110	113	115	5
	9	3	91	4	5	87	93	95	8
	10	3	70	8	11	63	69	79	16
	11	3	84	1	1	83	84	84	2
	12	3	44	1	2	43	44	44	1

Variable	Sample	Total Count	Mean	SD	CV	Minimum	Median	Maximum	Range
9.8 J	1	3	153	3	2	151	153	156	5
	2	3	151	1	0	150	151	151	1
	3	3	163	6	4	158	160	170	12
	4	3	148	4	3	143	150	152	8
	5	3	171	2	1	169	172	173	4
	6	3	149	3	2	147	148	152	5
	7	3	138	4	3	134	139	142	8
	8	3	181	4	2	176	181	185	9
	9	3	174	3	1	171	175	176	5
	10	3	156	7	4	149	156	162	13
	11	3	146	1	0	145	145	146	1
	12	3	95	4	4	91	96	99	9

Variable	Sample	Total Count	Mean	SD	CV	Minimum	Median	Maximum	Range
14.7 J	1	3	220	1	1	219	220	221	2
	2	3	221	1	0	220	221	222	2
	3	3	229	1	0	228	229	230	2
	4	3	223	3	1	221	222	227	5
	5	3	232	1	1	231	231	233	3
	6	3	223	1	1	221	223	224	3
	7	3	210	5	2	204	212	214	10
	8	3	222	2	1	219	222	224	5
	9	3	220	4	2	215	221	224	9
	10	3	215	2	1	214	214	217	3
	11	3	183	10	6	174	180	194	20
	12	3	155	7	4	148	158	160	13

Variable	Sample	Total Count	Mean	SD	CV	Minimum	Median	Maximum	Range
Density	1	5	41	1	2	40	41	42	2
	2	5	72	1	1	71	71	73	3
	3	5	72	1	2	70	73	74	3
	4	5	40	2	4	39	40	43	4
	5	5	27	2	9	25	26	30	5
	6	5	49	1	2	49	49	51	2
	7	5	82	2	3	80	82	85	5
	8	5	109	3	3	103	110	112	8
	9	5	73	5	7	67	75	79	12
	10	5	65	3	4	62	65	69	7
	11	5	260	5	2	256	258	268	12
	12	5	53	1	1	53	53	54	1

proceedings

Proceedings

Efficacy of Density in Predicting the Protective Properties of Padded Clothing in Rugby [†]

Syed Imam [1,*], Heather Driscoll [2], Keith Winwood [3], Prabhuraj Venkatraman [4] and Tom Allen [1]

[1] Department of Engineering, Manchester Metropolitan University, Manchester M1 5GD, UK; T.Allen@mmu.ac.uk

[2] Advanced Manufacturing Research Centre (AMRC), University of Sheffield, Sheffield S60 5BL, UK; H.Driscoll@amrc.co.uk

[3] Department of Life Sciences, Manchester Metropolitan University, Manchester M1 5GD, UK; K.Winwood@mmu.ac.uk

[4] School of Fashion, Faculty of Arts and Humanities, Manchester Metropolitan University, Manchester M15 6BH, UK; P.Venkatraman@mmu.ac.uk

* Correspondence: Syed.A.Imam2@stu.mmu.ac.uk; Tel.: +44-759-845-7659

† Presented at the 13th Conference of the International Sports Engineering Association, Online, 22–26 June 2020.

Published: 15 June 2020

Abstract: World Rugby™ permits players to wear padded clothing meeting the requirements of Regulation-12, which limits density, thickness and impact performance. Due to non-uniform geometry, measuring the density of padding can be challenging and provides limited information on mechanical properties. This study investigated how well density could predict the impact performance of rugby padding, whilst reviewing compliance parameters as alternatives. Eleven samples of rugby padding, plus one control material, were tested for compliance, then impacted at energies of 4.9, 9.8 and 14.7 J using the setup as defined in Regulation-12, and finally cut to calculate density. The density and compliance parameters were correlated against peak impact accelerations using a Spearman's rank test. Density was not significantly correlated with peak acceleration at any energy level, with compliance tests significantly correlated with impact acceleration at only 4.9 J.

Keywords: padded clothing; Regulation 12; density; compliance; World Rugby™

1. Introduction

Rugby has grown in popularity with participation rates increasing worldwide from 7.73 to 8.5 million within 2016 [1] and has high global economic impact [2]. With the plans of World Rugby™ to expand and involve more players [3], the market for rugby personal protective equipment (PPE) is likely to increase [4]. Sinclair [4] states that while there are scientific studies on the effectiveness of rugby PPE, both to ensure the protection of players and to substantiate manufacturers' claims, much controversy remains on its ability to reduce injury risk.

To govern the equipment used, World Rugby™ have defined a set of specifications and directives in their Handbook, specifically Regulation-12 Schedule 1: *Specifications relating to Players' Dress* [5]. Regulation-12 concentrates on player clothing, providing, (i) design and construction regulations; (ii) material specifications, and (iii) performance requirements and test methods. Under these sections, Regulation-12 specifies limitations on padding thickness (10 (+2) mm), material density (45 (+15) kgm^{-3}) and impact performance (acceleration >150 g for a 14.7 J impact, referred to as impact attenuation performance in Regulation-12).

Regulation-12 does not specify a method for measuring padding density. Padding often combines foam with fabric layers, typically compressed into regular or irregular geometries (Figure 1a–c). Density measurements according to ISO:845 [6] require foam samples to be cut into a shape

such that its volume can be easily calculated. The combination of fabric and foam (typically bonded together) and the varied geometry of padding means density measurements can be challenging, and prone to uncertainty.
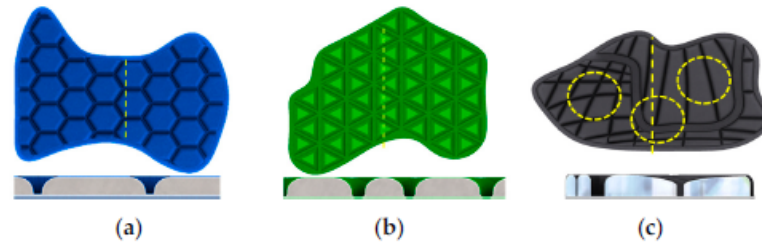

Figure 1. Computer-aided design reconstructions of approved paddings showing (a) hexagonal, (b) triangular and (c) irregular patterns with enlarged cross-sectional view showing variation within geometry.

With advances in manufacturing, the density of padding material can be tailored to enhance impact performance, as with auxetic [7] and biomimetic [8] foams. Impact testing of shin guards has shown that adding material, such as a sock, can reduce impact force [9]. Measuring the compliance of rugby padding using mechanical test methods as in ISO-2439 [10], would most likely be easier and more accurate than measuring its density. With World Rugby's intention to limit impact protection provided by padding (>150 g for a 14.7 J impact), compliance testing could complement the impact test. Compliance testing could be performed at low strain rates and prevent the use of stiffer materials, such as plastic shells, which could pass the impact test but change the nature of the game and may put players at risk of other injures, like cuts, lacerations and abrasions. This study investigated the potential of compliance tests for replacing the density criterion of padding in World Rugby Regulation-12.

2. Materials and Methods

Eleven designs of World Rugby™ approved jerseys were obtained from five manufacturers. Intact padding samples (size range: 150 × 120 mm to 280 × 220 mm) were taken from the shoulder region. A 220 × 150 mm sample of control material (Aortha White Plastazote ® -LD-60, Algeos), similar to the foam used in PPE [9], and meeting the thickness and density (LD-60 corresponds to 60 kgm^{-3}) requirements of Regulation-12, was also tested alongside the padding samples for compliance, impact performance and density.

2.1. Compliance Testing

Compliance testing was carried out according to ISO-2439 [10], using a uniaxial testing machine (Hounsfield HK10S) with a 1 kN load cell (0.5% or 5 N accuracy) and a 62 mm diameter indenter, at a compression rate of 100 mm/min. Sample thicknesses were measured using a height gauge (Dial Gauge, J.E. Baty & Co., Burgess Hill, UK, accuracy: 0.01 mm) and used to calculate compressive strain. Samples were subjected to the five testing methodologies in the standard:

- A: Force at 40% strain after a 30 s hold;
- B: Forces at 25% (B-25), 40% (B-40) and 65% (B-65) strain, after a 30 s hold at each strain;
- C: Instantaneous force at 40% strain;
- D: Force at 20% compression after a 20 s hold;
- E: Ratio of forces at 25% and 65% strain during compression cycle.

For Methods A to D, a higher force reading corresponds to a higher compliance. Method E gives a compression deflection coefficient and only provides additional information about the load bearing properties of the material and cannot be linked directly to its compliance.

2.2. Impact Testing

Samples were impacted at energies of 4.9, 9.8 and 14.7 J using a 5 kg mass (flat face, Ø 130 mm) dropped from 0.1, 0.2 and 0.3 m (Figure 2). The anvil (horizontal steel cylinder, Ø 115 mm) was fixed on four load cells (208C05-Force Sensor, PCB Piezotronics) with a sampling rate of 20 kHz and connected to an oscilloscope (PicoScope®, Version 6, Pico Technology) via two 3-Channel ICP® sensor signal conditioners (480B21, PCB®) to record impact force. To measure deformation, each impact was filmed with a High-Speed Video (HSV) Camera (Phantom Miro R111, Vision Research, Wayne, NJ, USA) with a resolution of 512 × 320 and a sample rate of 10 kHz and 99.00 µs exposure rate. The camera and load cells were synchronized using the oscilloscope.

Each sample was impacted three times at each energy with at least one minute between impacts. The sample was moved between impacts to change the impact location (as per Regulation-12: 20 mm from the periphery and minimum 30 mm apart). The voltage readings from each load cell was converted to force using the calibration factors (range: 0.2214 to 0.2399 mVN⁻¹) provided by the manufacturer. Peak force was divided by the product of the drop mass (5 kg) and the gravitational constant (9.81 ms⁻²) to give acceleration in g (as per Regulation-12).
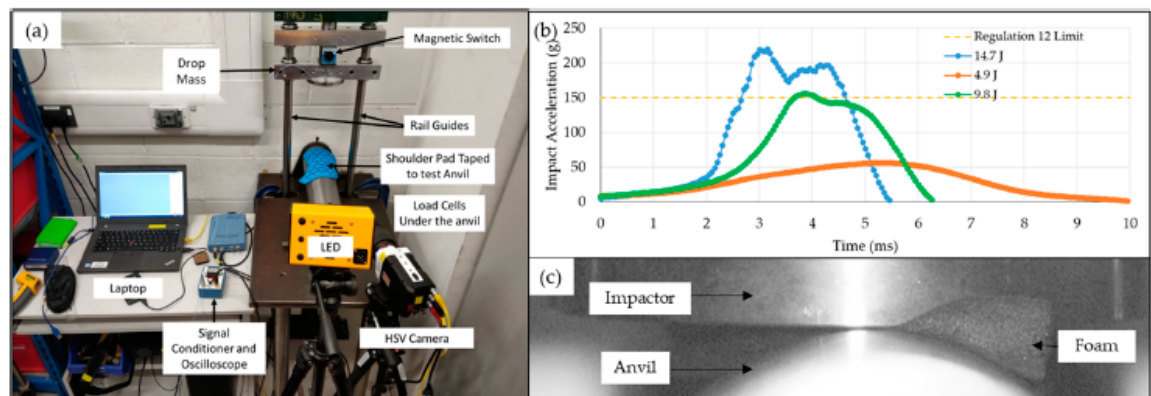

Figure 2. (a) Drop rig setup (as per Regulation-12) used for impact testing, (b) sample output graph Figure 4. 9, 9.8 and 14.7 J and (c) a High-Speed Video (HSV) image showing padding bottoming out at 4.9 J.

2.3. Density Testing

Density measurements were carried out according to ISO:845 [9]. Following impact testing, five cylindrical specimens were cut from each padding sample (at varied locations) using a wad punch (Ø 9.8 mm to accommodate padding patterns). The diameter (mean of three locations: two ends and approximate middle) and height of each specimen were measured using a Vernier caliper (Composite Digital Vernier Caliper, Silverline®) and used to calculate the volume. The mass of each cylindrical specimen was measured using a balance (ABS 220-4N, KERN®, Germany). Density of the padding was calculated as the ratio of specimen mass to volume. The mean values for thickness, compliance, density and peak acceleration for each sample were compared using a Spearman's rank correlation at a confidence level of 95% using Minitab® (V18 Statistical software, USA).

The diameter and height of one cylindrical specimen was measured five times by three operators and the resultant density values were used to estimate the intra operator error (E_{INTRA}), as the coefficient of variation (CV) (Equation (1)).

$$E_{INTRA} = \left(\frac{\sigma_{op}}{\mu_{op}}\right) \times 100 \ \% \tag{1}$$

where σ_{op} is the standard deviation and μ_{op} is the mean density for each operator.

Ten cylindrical specimens (5 from Sample 1 and 5 from Sample 6) were measured once by two additional operators (giving three total) to estimate inter-operator error E_{INTER} (Equation (2)).

$$E_{INTER} = \sqrt{(\sigma_1 + \sigma_6)} \tag{2}$$

where σ_1 and σ_6 are the CV values for the two sets of five specimens (from Sample 1 and 6) for combined density measurements for all three operators (Equation (3)).

$$\sigma_n = \left(\frac{\sigma_{sample\_n}}{\mu_{sample\_n}}\right) \times 100, \ (n = 1, 6) \tag{3}$$

where σ_{sample_n} is the standard deviation and μ_{sample_n} is the mean of all density measurements for a sample set.

The error propagation (E_{PROP}) during the density calculation was estimated using the accuracy of the measuring instruments for variables in the density equation (Equation (4)) [11].

$$E_{PROP} = \sqrt{\left(\frac{A_B}{m}\right)^2 + 2\left(\frac{A_C}{d}\right)^2 + \left(\frac{A_C}{h}\right)^2} \tag{4}$$

where A_B is balance accuracy (0.1 mg), m is the measured mass, A_C is the caliper accuracy (0.01 mm), d is the measured diameter and h is the measured height.

3. Results

Force values increased with applied strain (B-65 > B-40 > B-25), while instantaneous readings were typically higher than readings after a hold period (C > A) (Table 1). Some density values exceeded the Regulation-12 limit. For all samples, peak acceleration increased with impact energy (Table 2). All compliance methods (apart from E, which was positive) and thickness had significant negative correlation with peak impact acceleration at 4.9 J (Table 3), meaning peak acceleration decreased as sample compliance or thickness increased. Density was not significantly correlated with peak impact acceleration at any impact energy.

Table 1. Force measurements using the five different methods in ISO: 2439 and density. (mean ± SD).

S. No.	Thickness (mm)	Force Values (N)							Density (kgm⁻³)
		A	B-25	B-40	B-65	C	D	E [A]	
1	10.3 ± 0.2	220 ± 3	129 ± 2	234 ± 1	590 ± 13	248 ± 1	131 ± 7	4.3 ± 0.1	41.1 ± 0.8
2	10.5 ± 0.3	178 ± 2	97 ± 4	187 ± 8	511 ± 31	175 ± 10	102 ± 2	5.0 ± 0.2	71.5 ± 1.0 [B]
3	9.6 ± 0.2	154 ± 10	90 ± 4	171 ± 9	460 ± 36	184 ± 10	83 ± 5	4.9 ± 0.3	72.4 ± 1.3 [B]
4	10.2 ± 0.1	204 ± 2	111 ± 6	206 ± 9	518 ± 27	236 ± 4	118 ± 1	4.4 ± 0.2	40.2 ± 1.6
5	9.8 ± 0.1	96 ± 19	45 ± 6	124 ± 5	330 ± 49	201 ± 6	33 ± 4	5.9 ± 0.7	27.2 ± 2.4
6	11.0 ± 0.2	145 ± 7	76 ± 7	156 ± 6	423 ± 5	162 ± 8	77 ± 5	4.9 ± 0.2	49.4 ± 0.8
7	10.1 ± 0.3	169 ± 11	102 ± 12	187 ± 13	452 ± 33	189 ± 10	94 ± 3	3.9 ± 0.1	82.3 ± 2.5 [B]
8	7.7 ± 0.3	97 ± 9	44 ± 8	104 ± 14	368 ± 34	105 ± 12	38 ± 3	7.2 ± 0.1	109.1 ± 3.3 [B]
9	8.1 ± 0.4	128 ± 4	60 ± 4	134 ± 4	409 ± 13	112 ± 7	59 ± 3	5.3 ± 0	72.9 ± 5.0 [B]
10	11.0 ± 0.3	196 ± 41	96 ± 10	197 ± 18	577 ± 83	207 ± 38	78 ± 8	4.8 ± 0.3	65.3 ± 2.6 [B]
11	5.8 ± 0.1	46 ± 1	33 ± 1	54 ± 4	174 ± 22	64 ± 4	24 ± 3	6.1 ± 0.4	259.5 ± 4.7 [B]
12 [C]	10.2 ± 0.2	274 ± 14	202 ± 17	354 ± 19	781 ± 63	337 ± 16	169 ± 1	2.9 ± 0	53.5 ± 0.5

[A] has no unit. [B] Density outside regulation-12 limits (45 + (15) kgm⁻³). [C] Control material.

Sample deformation, measured using the HSV showed >90% compression for all samples at 9.8 and 14.7 J. When measuring samples, E_{INTRA} values were 1.8%, 2.4% and 5.9% (mean error: 4.1%), E_{INTER} was 16.9% (value range sample 1: 40.3 to 52.2 kgm⁻³, sample 6: 48.6 to 68.0 kgm⁻³), and E_{PROP} was 0.2%.

The results from the correlation testing (Table 3), although not significant, indicate that changing the impact energy changed the relationship (positive to negative) between both peak impact acceleration and density and peak impact acceleration and compliance. Figure 3 illustrates how the relationship between compliance measured using Method C and peak impact acceleration changed from negative to positive as impact energy increased.

Table 2. Peak impact acceleration at three impact energies (mean ± SD).

S No.	Peak Impact Acceleration (g)		
	4.9 J	9.8 J	14.7 J
1	57 ± 1.4	153 ± 2.6	220 ± 1.2
2	57 ± 1.5	151 ± 0.7	221 ± 0.7
3	71 ± 2.1	163 ± 6.3	229 ± 1.1
4	62 ± 0.1	148 ± 4.4	223 ± 2.9
5	106 ± 4.5	171 ± 2.0	232 ± 1.3
6	66 ± 2.3	149 ± 3.0	223 ± 1.4
7	56 ± 2.3	138 ± 4.0	210 ± 5.2
8	113 ± 2.6	181 ± 4.4	222 ± 2.3
9	91 ± 4.2	174 ± 2.5	220 ± 4.4
10	70 ± 7.9	156 ± 6.5	215 ± 7.5
11	84 ± 0.8	146 ± 0.6	183 ± 1.3
12[C]	44 ± 0.7	95 ± 4.2	155 ± 5.7

Table 3. Spearman's (rho) Correlation Matrix.

	4.9 J	9.8 J	14.7 J	Density
Thickness	−0.593 *	−0.274	−0.014	-
Density	0.224	0.042	−0.434	-
A	−0.804 *	−0.434	−0.294	−0.441
B−25	−0.881 *	−0.531	−0.280	−0.455
B−40	−0.816 *	−0.462	−0.280	−0.501
B−65	−0.748 *	−0.357	−0.280	−0.427
C	−0.601 *	−0.336	0.098	−0.713 *
D	−0.860 *	−0.483	−0.231	−0.392
E−CDC	0.862 *	0.630 *	0.371	0.378

* indicates significant correlation $p < 0.05$.

The control material was less compliant than the rugby padding samples (~100 N higher, using Method C) and had lower peak acceleration at all energy levels. At 14.7 J, the mean impact acceleration of the control material exceeded the Regulation-12 limit by 5 g. The linear relationship between compliance (Method C) and peak impact acceleration at 14.7 J is skewed due to the lower peak impact acceleration of the control sample, although this is accounted for in Spearman's correlation (which gave a positive correlation).
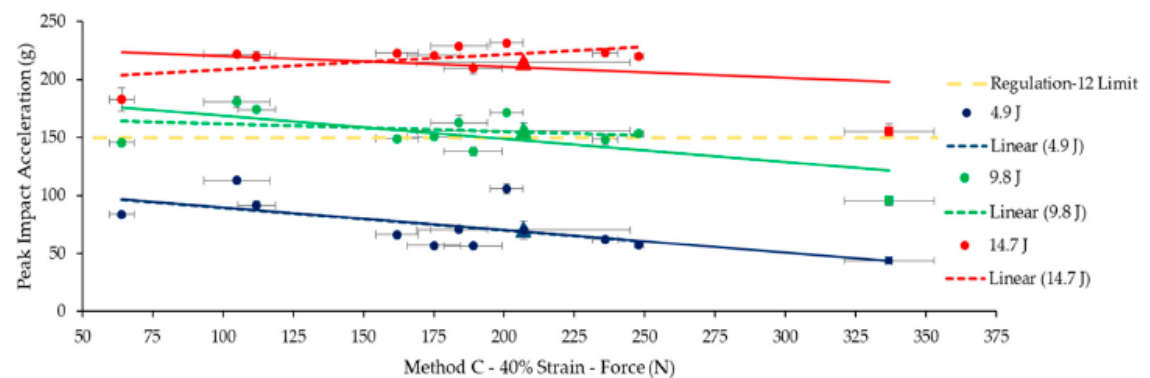

Figure 3. Peak impact acceleration vs. compliance at impact energies of 4.9, 9.8 and 14.7 J. Compliance measured using ISO-2439 Method C. The error bars indicate SD. Sample 10 (with high variance in compliance) is represented by triangles. The linear trend for padding excluding (dashed) and including (continuous) the control material (square) is shown.

4. Discussion

All compliance test methods provided a statistically significant correlation ($p < 0.05$) to the peak impact acceleration at 4.9 J impact energy only, whereas padding density had no significant correlation at any energy level. Relationships changed between density and impact peak acceleration (positive to negative), thickness or compliance and peak impact acceleration (large negative to low negative/positive) as impact energy increased. At the lowest impact energy (4.9 J), more compliant foams gave higher peak acceleration on impact, while stiffer foams tended to withstand the impact and reduce peak acceleration. In contrast, for higher energy impacts, there was no significant correlation (apart from E at 9.8 J) because the samples were bottoming out (compression > 90%) and providing little to no resistance to impact as seen on the HSV image in Figure 2c (noted in Samples 1 to 11 at 9.8 J and in all samples at 14.7 J impact).

Large variances were noticed in compliance and peak impact values for Sample 10, which may be due to the irregular geometry highlighted in Figure 1c (Sample 10). While measuring density, it was noticed that the extracted cylindrical specimens were often warped. While the E_{PROP} during density calculations accounted for only 0.2% of the error, the E_{INTER} was 17%, indicating that measuring foam density can also be prone to human error. The presence of fabric in certain samples (as it was glued to the padding) added further uncertainty to the measured density values. These limitations provide some justification to replace the density criterion in Regulation-12 with a compliance parameter that is easier to measure, although further work is needed.

When comparing the compliance testing methodologies, Methods A, B and D measure force after a period of hold. The often viscoelastic nature of padding material means that the stress can relax during this period of hold, with reducing force readings compared to the value at the end of the loading ramp. As stated in ISO:2439, the reduction in force values can be noticed when comparing values obtained from Methods A and C, with the instantaneous force values obtained using Method C being higher (or similar) for most samples.

Compliance testing can be applied to intact samples of padding (as they would be worn by rugby players), unlike density, which required the extraction of specimens. With E_{INTRA} and E_{INTER} equaling 4% and 17% respectively, measuring the density of a padding is error prone and does not appear to be a good indicator of impact performance. To improve our understanding of compliance parameters, padding materials with different density and compliance ranges, such those used in sports like ice hockey and American football, could be explored. Further research is to investigate the inter-user variances for compliance testing and inter-laboratory testing to gauge repeatability.

5. Conclusions

The compliance and densities of eleven samples of padded rugby clothing and one control material were compared against their peak acceleration for an impact test at 4.9, 9.8 and 14.7 J. Compliance parameters and thickness showed a significant negative correlation with peak impact acceleration at only 4.9 J, while density showed no significant correlation. Results at 9.8 and 14.7 J indicate that the padding materials bottomed out (as seen in HSV images) due to the rigid impactor and anvil. Compliance has shown potential to replace the density criterion in Regulation-12. Furthermore, quasi-static compliance testing could complement the impact testing methodology and prevent the use of stiff materials, such as stiff plastic shells, which may increase the risk of injuries such as cuts, lacerations and abrasions.

Conflicts of Interest: The authors declare no conflict of interest. The results are for research purposes only and do not affect the approval status of the padding.

References

1. Player Numbers-2017. World Rugby. Available online: https://www.worldrugby.org/development/player-numbers (accessed on 19 September 2019).
2. Chadwick, S.; Semens, A.; Schwarz, E.C.; Zhang, D. *Economic Impact Report on Global Rugby Part III: Strategic and Emerging Markets*; Centre for International Business of Sport, Coventry University: Coventry, UK, 2010.
3. World Rugby Press Release. 2016. Available online: https://www.world.rugby/news/203177?lang=en (accessed on 10 October 2019).
4. Sinclair, M. Protective Equipment in Rugby Literature Review. 2009. Available online: https://www.springboks.rugby/en/pages//media/project/sa%20rugby/pagecontent/boksmart/medical%20protocol/protective%20equipment%20in%20rugby/review%20%20protective%20equipment%20in%20rugby%20union (accessed on 28 September 2017).
5. *Regulation 12: Provisions Relating to Players Dress, World Rugby Handbook*; World Rugby: Dublin, Ireland, 2015; pp. 191–222.
6. International Organization for Standardization. *ISO 845: Cellular Plastics and Rubbers—Determination of Apparent Density*; International Organization for Standardization: Geneva, Switzerland, 2006.
7. Duncan, O.; Shepherd, T.; Moroney, C.; Foster, L.; Venkatraman, P.; Winwood, K.; Allen, T.; Alderson, A. Review of auxetic materials for sports applications: Expanding options in comfort and protection. *Appl. Sci.* **2018**, *8*, 941.
8. Svagan, A.J.; Samir, M.A.A.; Berglund, L.A. Biomimetic foams of high mechanical performance based on nanostructured cell walls reinforced by native cellulose nanofibrils. *Adv. Mater.* **2008**, *20*, 1263–1269.
9. Ruznan, W.S.; Laing, R.M.; Lowe, B.J.; Wilson, C.A. Impact attenuation provided by shin guards for field hockey. *Sports Eng.* **2018**, *21*, 161–175.
10. International Organization for Standardization. *ISO 2439: Flexible Cellular Polymeric Materials—Determination of Hardness (Indentation Technique)*; International Organization for Standardization: Geneva, Switzerland, 2008.
11. A Summary of Error Propagation. Instructional Physics Laboratory, Harvard University. 2013. Available online: http://ipl.physics.harvard.edu/wp-uploads/2013/03/PS3_Error_Propagation_sp13.pdf.(accessed on 21 September 2019).